

Megabranchiella gen. nov., a new mayfly genus (Ephemeroptera, Baetidae) from Thailand with description of two new species

Sirikamon Phlai-ngam¹, Boonsatien Boonsoong²,
Jean-Luc Gattolliat^{3,4}, Nisarar Tungpairajwong^{1,5}

1 Department of Biology, Faculty of Science, Khon Kaen University, Khon Kaen 40002, Thailand **2** Animal Systematics and Ecology Speciality Research Unit (ASESRU), Department of Zoology, Faculty of Science, Kasetsart University, Bangkok 10900, Thailand **3** Museum of Zoology, Palais de Rumine, Place Riponne 6, CH-1005 Lausanne, Switzerland **4** Department of Ecology and Evolution, University of Lausanne, CH-1015 Lausanne, Switzerland **5** Applied Taxonomic Research Center (ATRC), Faculty of Science, Khon Kaen University, Khon Kaen 40002, Thailand

Corresponding author: Nisarar Tungpairajwong (knisar@kku.ac.th)

Academic editor: Ben Price | Received 25 July 2022 | Accepted 15 September 2022 | Published 18 October 2022

<https://zoobank.org/F4ACDB4D-5BC1-415C-B098-5D494A15263A>

Citation: Phlai-ngam S, Boonsoong B, Gattolliat J-L, Tungpairajwong N (2022) *Megabranchiella* gen. nov., a new mayfly genus (Ephemeroptera, Baetidae) from Thailand with description of two new species. ZooKeys 1125: 1–31. <https://doi.org/10.3897/zookeys.1125.90802>

Abstract

Megabranchiella gen. nov. (Ephemeroptera: Baetidae) is established as a new baetid mayfly genus from northern Thailand. Two new species, *Megabranchiella scutulata* sp. nov. and *Megabranchiella longusa* sp. nov., are described. This genus is distinguished from other Baetidae by abdominal segment I, bearing a pair of enlarged, ventrally oriented single gills, covering abdominal sternites II–V; other gills have normal size and are dorsolaterally oriented. The two new species *Megabranchiella longusa* sp. nov. and *Megabranchiella scutulata* sp. nov. can be differentiated by the setation of femur dorsal margin and the shape of abdominal gill I. This mayfly genus was found in flowing water with cobble microhabitats in headwater streams of northern Thailand.

Keywords

Baetidae mayflies, enlarged gills, South East Asia, taxonomy

Introduction

Baetidae is a common family of mayflies with a worldwide distribution, except for Antarctica and New Zealand. The family comprises ca. 1,070 species assigned to 110 genera; it comprises approximately one-third of the global mayfly diversity and is therefore the most diversified mayfly family (Sartori and Brittain 2015; Jacobus et al. 2019; Kaltenbach et al. 2020). The generic diversity of Baetidae is the highest in the Afrotropical realm (ca. 40 genera), followed by the Oriental and Neotropical realms (ca. 28 and 27 genera, respectively), and finally the Nearctic and Palearctic realms (ca. 20 genera and 17 genera, respectively), while the lowest diversity is in the Australasian realm (ca. 12 genera) (Gattolliat and Nieto 2009; Kaltenbach et al. 2020). Although the Oriental realm has several regions with high potential diversity (e.g. the Indian subcontinent, Sunda islands and the Philippines), the apparent low diversity most certainly reveals a lack of data and poor sampling (Kaltenbach et al. 2021). The knowledge of the diversity in the Oriental realm, including South-east Asia has been gradually improved in the last two decades. New genera and new species have been described and reported from many islands, including Indonesia, New Guinea, Philippines, and Malaysia (Sabah) (Kaltenbach et al. 2020, 2021). Despite these recent improvements, the real extent of the diversity remains only partially known and the distribution of most species underestimated (Suttinun et al. 2020).

Three new genera have been described from Southeast Asia in recent times. A new genus, *Procerobaetis* Kaltenbach & Gattolliat, and four new species, *P. leptobranchius* Kaltenbach & Gattolliat, 2020 *P. petersorum* Kaltenbach & Gattolliat, 2020 *P. fretagi* Kaltenbach & Gattolliat, 2020 and *P. totuspinosus* Suttinun, Kaltenbach & Boonsoong were, 2021 reported from Indonesia (Sumatra), Philippines and Thailand (Kaltenbach et al. 2020; Suttinun et al. 2021). *Philibaetis* Kaltenbach & Gattolliat, a new baetid mayfly genus, was also reported from the Philippines with two species, *P. luzonensis* (Müller-Liebenau, 1982) and *P. realonae* (Müller-Liebenau 1982) (Kaltenbach et al. 2021). Since the last decade, the trend in species diversity of the Baetidae has also been increasing in Thailand, due to recording of new taxa or distribution extension. Approximately nine genera and 13 species have been reported and described from Thailand (Suttinun et al. 2021). The newest genus, *Cymbalcloeon* Suttinun, Gattolliat & Boonsoong, with a new species, *Cymbalcloeon sartorii* Suttinun, Gattolliat & Boonsoong, 2020 was reported as a Thai endemic (Suttinun et al. 2020). The present work describes a new genus of Baetidae from Thailand. This new genus was collected during a large survey of Baetidae from Northern Thailand. It was collected in headwater streams. Herein, the new genus and two new species were described at the larval stage. The comparison with the larval morphology of other genera is also provided.

Materials and methods

Larval specimens were collected by hand-picking from all stream orders in Northern Thailand. Sampling sites are located in various natural conditions. *Megabranchiella* larval specimens were found and collected from headwater streams in the northern region only (Table 1; Fig. 15).

The specimens were preserved in 95% ethanol. The larvae were dissected in glycerin under a Nikon SMZ745 stereomicroscope, with subsequent mounting on slides by glycerin. The micro-characters were observed with a Nikon Eclipse E200LED MV J compound microscope. Drawings were prepared using a camera lucida attached to an Olympus CH30 compound microscope, and they were scanned for illustration with the Procreate application (iOS application). Photographs of larvae were taken with a Canon EOS 700D camera and edited with Adobe Lightroom (<http://www.adobe.com>). The habitus photographs and measurements (given in mm) were obtained using NIS-Elements software with a Nikon SMZ25 stereomicroscope. Final plates were prepared and processed with Adobe Photoshop (<http://www.adobe.com>). For scanning electron microscopy (SEM), specimens were preserved in 95% ethanol and transferred to absolute ethanol for dehydration. The specimens were then dissected and transferred to microtubes and covered with a fine mesh net (mesh size 60 μm) for drying in a Critical Point Dryer (CPD). The dried specimens were set on stubs and coated with a 20 nm layer of gold with a Cressington sputter Coater. SEM images were obtained by Field Emission Scanning Electron Microscopy (FESEM; Fei Model: Helios NanoLab G3 CX). The examined material was deposited in the Collection of Aquatic Insect of Department of Biology at Khon Kaen University in Khon Kaen, Thailand (KKU-AIC), the collection of the Zoological Museum at Kasetsart University in Bangkok, Thailand (ZMKU) and the Museum of Zoology in Lausanne, Switzerland (MZL).

This research has been reviewed and approved by the Institutional Animal Care and Use Committee of Khon Kaen University, based on the Ethic of Animal Experimentation of National Research Council of Thailand (Record No. IACUC-KKU-65/63) for collecting the baetid mayfly specimens.

Table 1. GPS coordinates of locations of examined specimens.

Species	Provinces	GPS coordinates	Altitudes (m a.s.l.)
<i>M. scutulata</i> sp. nov.	Chiang Mai	18°52'01.65N, 99°19'20.83E	779
	Chiang Rai	20°00'39.60N, 99°48'14.47E	476
<i>M. longusa</i> sp. nov.	Chiang Mai	18°32'50.02N, 98°30'49.79E	1,359
	Nan	19°09'19.09N, 101°10'12.96E	995

Results

Taxonomy

Order Ephemeroptera Hyatt & Arms, 1891

Family Baetidae Leach, 1815

Genus *Megabranchiella* Phlai-ngam & Tungpairojwong, gen. nov.

<https://zoobank.org/A9F66B30-FEDB-46FA-B8E7-D6A338E10D63>

Type species. *Megabranchiella scutulata* sp. nov., by present designation.

Included species. *Megabranchiella longusa* sp. nov.

Megabranchiella scutulata sp. nov.

Diagnosis. *Larva* (Figs 1–3). Larval body ventrally flattened (Fig. 4). Margins of head capsule relatively densely covered with fine, long setae. Antenna without process on scape, margins of scape and pedicel densely covered with long, fine, simple setae; flagellum short, covered with scattered long, fine, simple setae. Mouthparts relatively compact. Labrum (Fig. 5A) broadly rounded, dorsally with one central seta and a row of setae reduced in number. Mandibles with smooth margin between mola and prosthema, without setae, right and left prosthema comb-shaped. Maxilla (Fig. 5H) with 2-segmented palp, with a small tip at apex. Labium compact (Fig. 5K), glossa and paraglossa covered with stout setae, labial palp 3-segmented, terminal segment rounded. Thorax broad; forewing pad broad, large, divergent; hindwing pad highly reduced. Femur with a regular row of long, stout, setae on dorsal margin, surface covered with scattered tiny spine-like setae anteromedially, ventral femoral patch present. Tibia with long feathered setae on dorsal margin, covered with scattered fine setae and short, pectinate setae. Tarsus without preapical setae, tarsal claw with one row of denticles. Abdominal tergites covered with scattered long, fine setae; posterior margin smooth. Abdominal gills segment I (Fig. 6D) ventrally oriented, enlarge covering abdominal sternites II to V; gill margin smooth without setae. Abdominal gills segment II–VII dorsolaterally oriented, gill margins with densely covered with long fine setae. Gonostily under larval cuticle *Acentrella*-type (Fig. 6E). Paraproct surface with notched scales and long setae; distal margin smooth without prolongation. Caudal filaments with swimming setae; median filament reduced to shorter than 0.4× of cerci length.

Winged stage. Unknown.

Etymology. *Megabranchiella* is a combination of *Mega-* in reference to the enlarged, *-branchio-* in reference to gills and *-iella* in reference to the genera *Liebebiella* and *Acentrella* which are most certainly the closely related genera. The “*Megabranchiella*” refers to the remarkable enlarged abdominal gill segment I of baetid mayfly. The gender is feminine.

Description. *Larva* (Figs 1–3). **Body** Relatively short and ventrally flattened (Fig. 4), covered with scattered long, fine setae; head and thorax in lateral view rounded.

Head. Antenna. ca. 2 × as long as head length; scape, pedicel and flagellum without process, without scale bases and spines, covered with scattered long, fine setae; flagellum covered with scattered long, fine setae in each segment.



Figure 1. *Megabranchiella scutulata* sp. nov., male larva **A** early larval stage **B** last larval instar.



Figure 2. *Megabranchiella scutulata* sp. nov., female larva. **A** early larval stage **B** last larval instar.

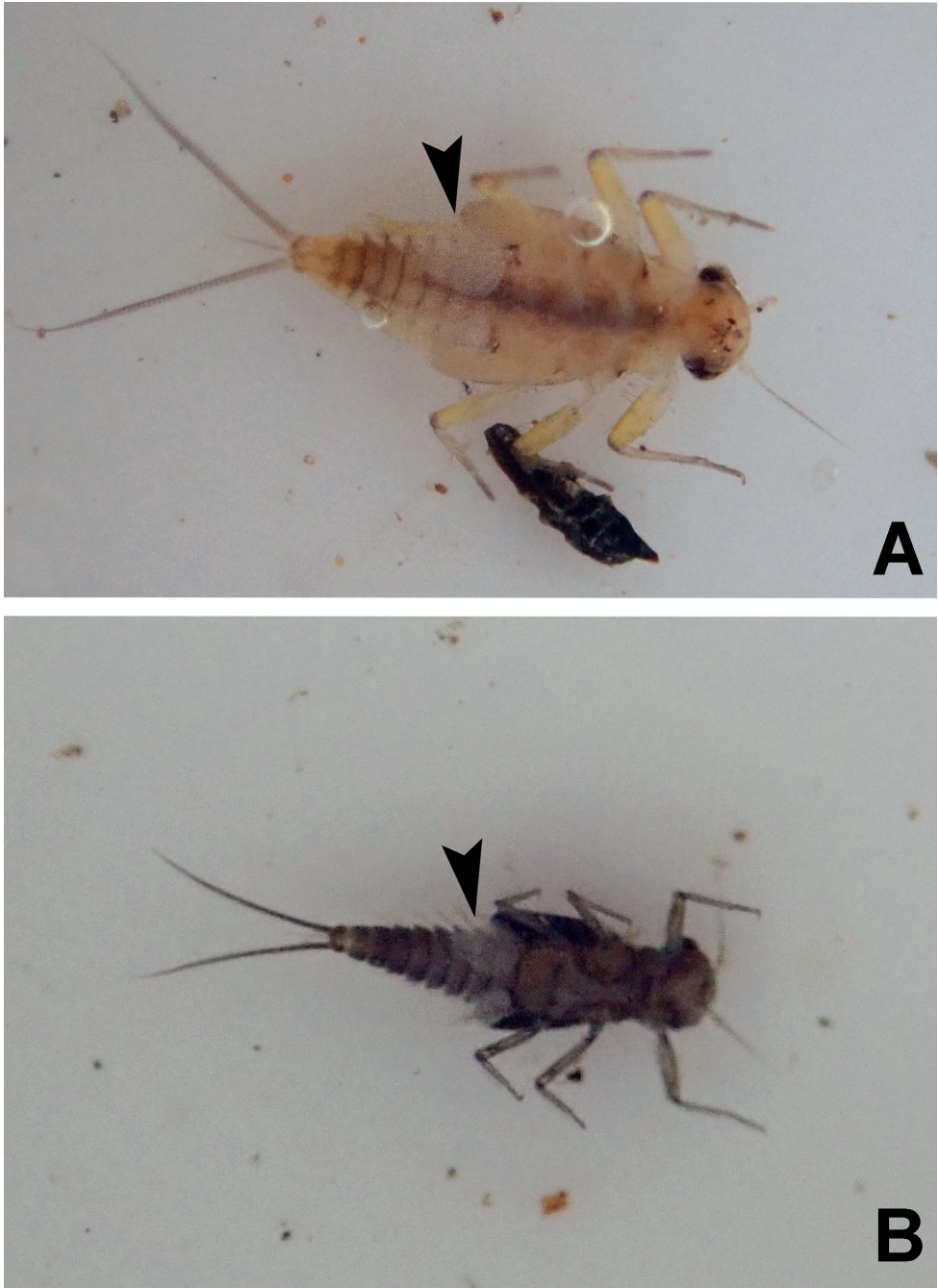


Figure 3. *Megabranchiella scutulata* sp. nov., ventral view **A** early larval stage **B** last larval instar. (arrow: gills I).

Labrum (Fig. 5A). Broadly rounded; wider than long; dorsal surface with one central seta and a row of setae reduced in number, long scattered simple setae along dorsal margin, scattered simple, hairlike setae; distal margin with anteromedian notch shallow, disterolateral margin with long feathered setae; distomedial margin with a row of small, short, feathered setae.

Right mandible (Fig. 5B–D). Canine with almost completely fused outer and inner incisors, incisors well developed, apically rounded; prostheca robust, apically with small denticles and comb-shaped structure; edge between mola and prostheca smooth, without setae; molar area with numerous small, apically rounded teeth; apex of mola with tuft of spines like setae.

Left mandible (Fig. 5E–G). Canine with almost completely fused outer and inner incisors, well developed incisors, apically rounded; prostheca robust, apically with small denticles; margin between mola and prostheca smooth, without setae; molar area with numerous small, round teeth, apex of mola with tuft of thin setae.

Maxilla (Fig. 5H). Short and compact; galea-lacinia (Fig. 5I) with long, robust, simple setae under crown. Inner dorsal row of setae with three denti-setae, distal denti-seta tooth-like, middle denti-seta slender, bifid and pectinate (Fig. 5J), proximal denti-seta slender, pectinate; innermost denticles with a row of robust, simple setae; medially with one seta and four short to long, simple setae. Short, stocky, 2-segmented maxillary palp, with scattered small setae; distal segment with distinct, small tip.

Labium (Fig. 5K). Short and compact; glossa basally broad, narrower toward apex, slightly shorter than paraglossa; paraglossa sub-rectangular, broader than glossa, apically curved inward, apical margin with three rows of medium stout setae; labial palp 3-segmented, segment II with small distolateral expansion, segment III rounded, ventral surface covered with scattered setae.

Hypopharynx (Fig. 5M). Lingua subequal to superlingua, apically rounded, with apical tuft of fine, long, simple setae; superlingua with distal margin slightly incurved, margin covered with fine simple setae.

Thorax. Forewing pads. Highly developed related to body size; clearly divergent.

Hindwing pads. Highly reduced.

Forelegs (Figs 7A, 12A). Dorsal margin of femur with a row of long, simple setae; short, stout, lanceolate, laterally pectinate setae and scattered fine hair-like setae along dorsal and ventral margins; femora patch present; dorsal surface with scattered tiny spine-like setae anteromedially; scattered long translucent scales present; dorsal margin of tibia with a row of long, simple setae; several broad, lanceolate, laterally pectinate setae and scattered hair-like setae along dorsal and ventral margins, patella-tibial suture present; tarsus dorsally with a row of spine-like simple setae, ventral margin bare or with a row of spine-like simple setae, surface covered with scattered fine hair-like setae; tarsal claw with one row of denticles increasing in length toward apex, subapical setae absent. **Midlegs and hindlegs.** As forelegs.

Abdomen (Fig. 6B). **Tergites.** Posterior margin smooth, posterior marginal spines reduced to absent, tergal surface with scattered stout, fine, hair-like setae and scattered long translucent scales distally. Gonosyli under larval cuticule *Acentrella*-type (Fig. 6E).

Gills. Seven pairs of gills present on abdominal tergites I–VII; gills I enlarged to covered abdominal sternites II–V, oriented ventrally (Fig. 6D), gill margin smooth,

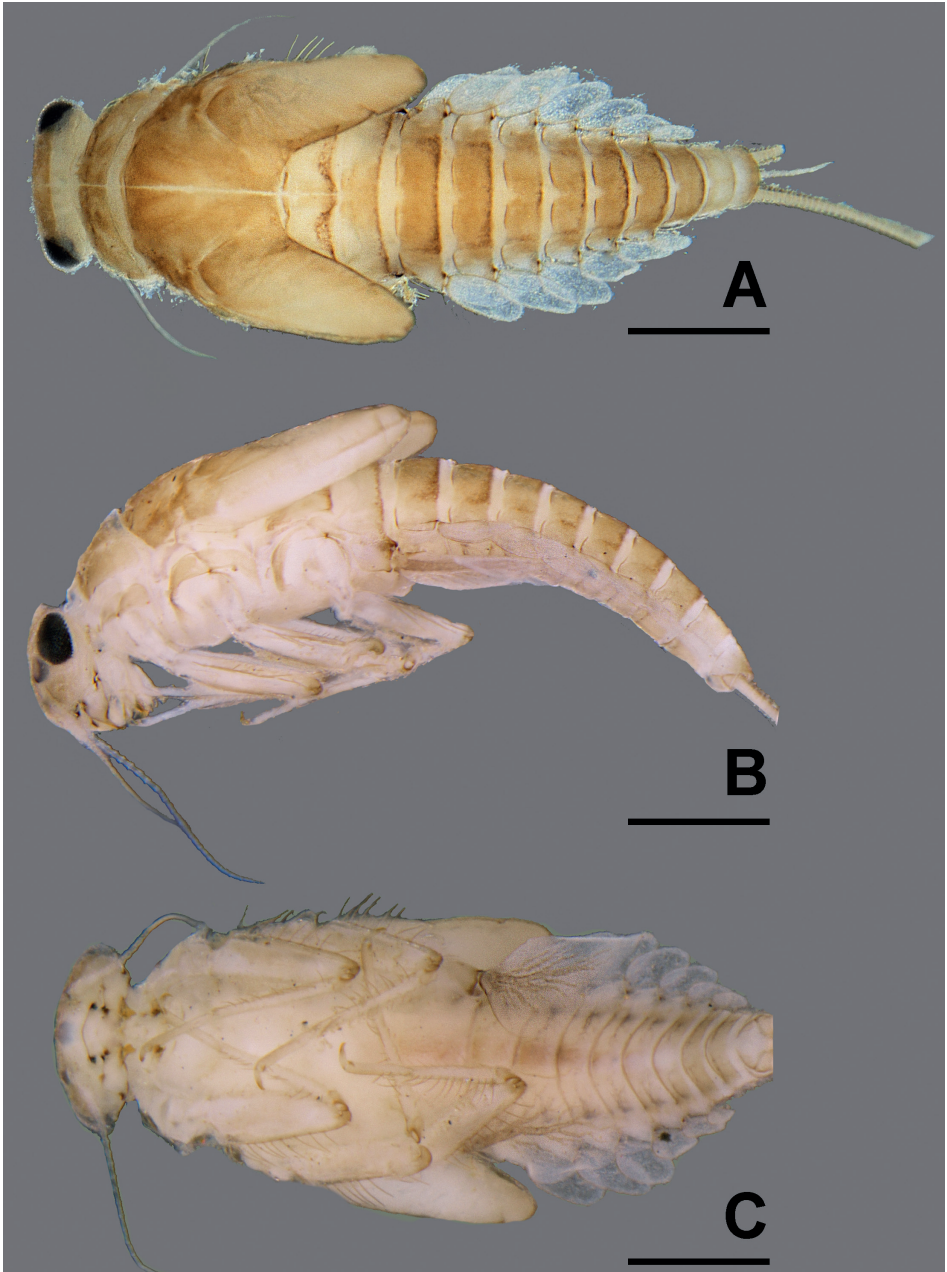


Figure 4. *Megabranchiella scutulata* sp. nov., larval habitus **A** dorsal view **B** lateral view **C** ventral view. Scale bars: 0.5 mm.

without fine hair-like setae; gills II–VII slightly oval, oriented dorsolaterally, gills margin smooth with scattered, long, fine hair-like setae.

Paraproct (Fig. 7E). Margin smooth without marginal spines and without prolongation at posterior margin.

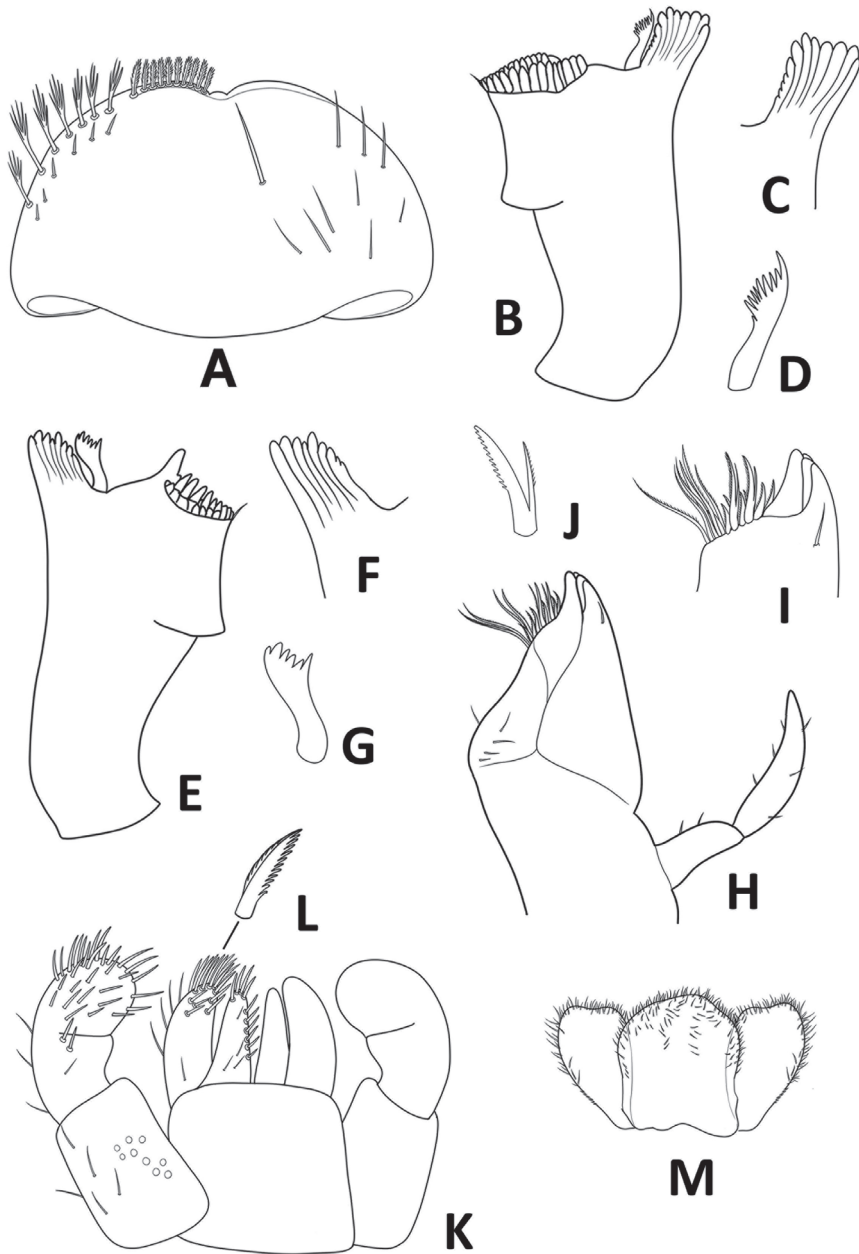


Figure 5. *Megabranchiella scutulata* sp. nov., larval morphology **A** labrum **B** right mandible **C** right incisor **D** right prosthema **E** left mandible **F** left incisor **G** left prosthema **H** maxilla **I** apex of galea-lacinia **J** denti-seta **K** labium **L** long, robust, pectinate setae **M** hypopharynx.

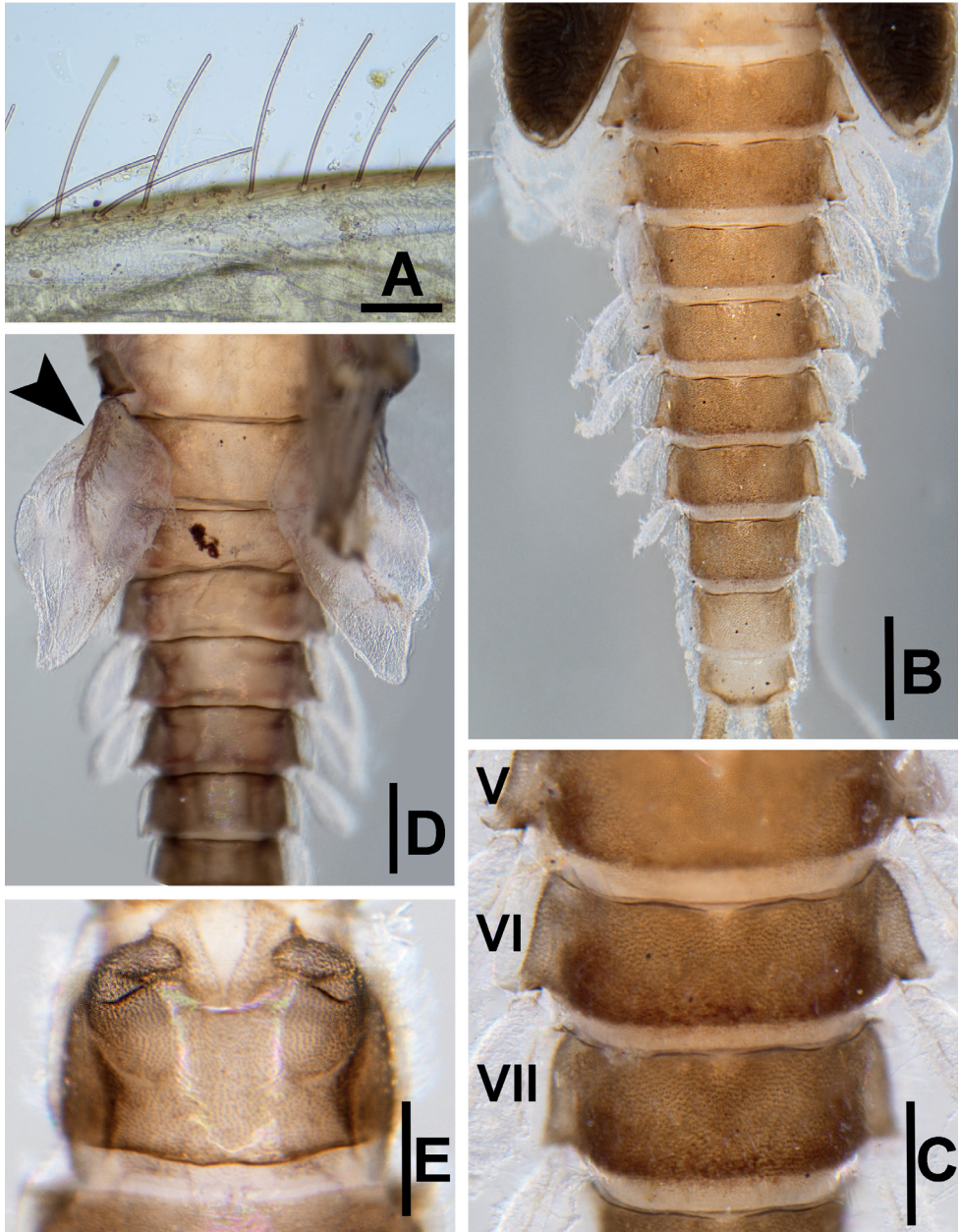


Figure 6. *Megabranchiella scutulata* sp. nov., larval morphology **A** dorsal margin of femur **B** dorsal view of abdomen **C** enlargement of abdominal tergites V–VII **D** ventral view of abdominal gills I (arrow) **E** ventral view of gonostyli. Scale bars: 0.15 mm (**A**); 0.5 mm (**B**); 0.25 mm (**C**); 0.4 mm (**D**); 0.3 mm (**E**).

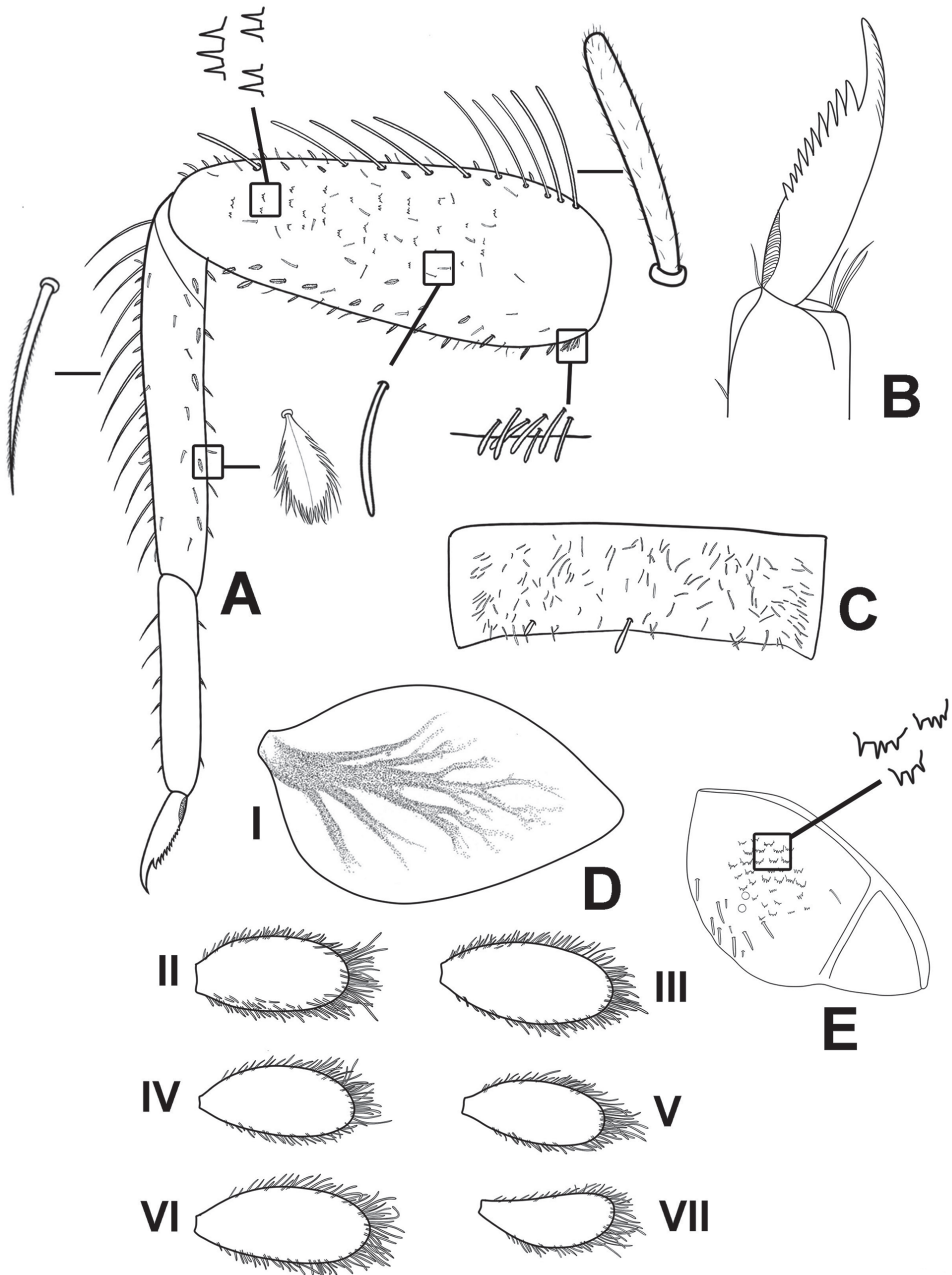


Figure 7. *Megabranchiella scutulata* sp. nov., larval morphology **A** foreleg **B** tarsal claw **C** tergite V **D** abdominal gills I–VII **E** Paraproct and notched scales on surface.

Caudal filaments. Inner margin of cerci with very thin, long setae; median filament reduced shorter than $0.4\times$ of cerci length, lateral margins with very thin, long setae.

Winged stage. Unknown.

***Megabranchiella scutulata* Phlai-ngam & Tungpairojwong, sp. nov.**
<https://zoobank.org/9DBB55FF-E63C-4DDA-9235-D825D0A0C08E>

Materials examined. *Holotype.* THAILAND, One male larva on slide (KKU-AIC), Chiang Mai, Mae On district, Mae Kampong, The Royal Project of Teen Tok, 18°52'01.65N, 99°19'20.83E, 779 m, 21.12.2020, S. Phlai-ngam leg.

Paratypes. One larva on slide (KKU-AIC), same data as holotype; 21 larvae in alcohol, same data as holotype; Four larvae in alcohol (MZL), same data as holotype.

Other materials. Two larvae in alcohol (ZMKU), Thailand, Chiang Rai, Muang district, Pong Phra Baht waterfall, 20°00'39.60N, 99°48'14.47E, 476 m, B. Boonsoong and C. Sutthinun leg.

Description. *Coloration* (Figs 1–2). Head dorsally yellow to brownish, with a darker brown pattern between ocelli. Thorax dorsally brown; pronotum with dark brown pattern laterodorsally, mesonotum with longitudinally dark brown pattern medially. Abdomen dorsally brownish; tergite I light brown; tergites I–VIII brown with reddish brown pattern posterolaterally, tergites IV and V slightly lighter; tergites IX and X light brown with or without pale markings. Head and thorax ventrally light brown to yellow; abdomen ventrally light brown; sternites I–V light brown; sternites V–X medium to dark brown (Fig. 3). Legs light brown; dorsal, ventral, and apical femur margins dark brown; claws distally dark brown. Caudal filaments brownish.

Body (Fig. 4). Relatively short and ventrally flattened (Fig. 4B), body length 3.6 mm, covered with scattered long, hair-like setae.

Head (Fig. 4B). Lateral view rounded, head width ca. 1.5 × as long as head length.

Antenna. ca. 2 × as long as head length (Fig. 4B); scape without process, subequal in width and length, pedicel length, ca. 2 × as long as width, scape and pedicel almost bare, without scales bases and spines, covered with scattered long fine setae; flagellum covered with scattered long fine setae in each segment.

Labrum (Fig. 5A). Broadly rounded; wider than long, width ca. 1.75 × as long as length; dorsal surface with submarginal row composed of one long, point, simple seta medially plus three medium, simple setae anterolaterally, dorsal surface with scattered simple, hairlike setae; distal margin with shallow anteromedian notch. Ventrally with submarginal row of setae composed of lateral and anterolateral long, feathered setae and medial long, pectinate setae; ventral surface with six short, spine-like setae near lateral and anterolateral margin.

Right mandible (Fig. 5B). Canine with 4 + 4 apically rounded denticles (Fig. 5C), largely fused outer and inner incisors, inner margin of inner incisor with small denticulation; prostheca robust (Fig. 5D), apically with small denticles and comb-shaped structure; margin between mola and prostheca smooth, without setae; mola with well-developed denticulation; apex of mola with tuft of spines like setae.

Left mandible (Fig. 5E). Canine with 4 + 3 apically rounded denticles (Fig. 5F), largely fused outer and inner incisors, outer and inner incisors separated by a small, rounded tooth; prostheca robust (Fig. 5G), apically with small denticles and comb-

shaped structure; margin between mola and prostheca smooth, without setae; mola with reduced denticulation, apex of mola with tuft of spines like setae.

Maxilla (Fig. 5H). Short and compact; galea-lacinia (Fig. 5I) with long, robust, simple seta under crown; inner dorsal row of setae with three denti-setae, distal denti-seta tooth-like, middle denti-seta slender, bifid and pectinate (Fig. 5J); proximal denti-seta slender, pectinate; inner ventral row of seven robust, simple setae; medially with one seta and four short to long, simple setae. Maxillary palp 2-segmented, with scattered small, blunt setae; distal segment with distinct, small tip at apex.

Labium (Fig. 5K). Glossa basally broad, narrower toward apex, slightly shorter than paraglossa; inner margin with medium, pointed, simple setae; apex with four long, robust, pectinate setae; basal area with fine scattered setae. Paraglossa sub-rectangular, broader than glossa, apically curved inward, apical margin with three rows of long, robust, apically pectinate setae (Fig. 5L), ventrally with 4–5 long, spine-like setae near inner margin, with an arch of 4–5 long, simple setae on outer margin; basal area with a single medium seta. Labial palp 3-segmented, segment I rectangular and broad, covered with scattered fine, setae and several micropores; segment II with small distolateral expansion, with a few scattered, simple setae and row of setae reduced to two large, blunt, robust, simple setae near distal margin; segment III rounded, covered with long, robust, simple setae.

Hypopharynx (Fig. 5M). Lingua subequal to superlingua, apically rounded, with apical tuft of fine, simple setae; superlingua with distal margin slightly incurved, margin covered with fine simple setae.

Thorax. Hindwing pads (Fig. 8A). Highly reduced.

Forelegs (Fig. 7A). Ratio of foreleg segments 0.58: 0.48: 0.22. *Femur*. Length ca. 2.5× maximum width. Dorsal margin of femur (Figs 6A, 8B–C) with a row of 11–13 long, robust, apically rounded, simple setae; short stout, lanceolate, laterally pectinate setae and scattered fine hair-like setae along dorsal and ventral margins (Fig. 8D); femora patch present; surface with scattered tiny spines anteromedially (Fig. 8E); scattered long translucent scales present; dorsal margin of tibia with a row of long, simple setae; several short stout, lanceolate, laterally pectinate setae and scattered hair-like setae along dorsal and ventral margins, patella-tibial suture present; tarsus dorsally with a row of fine, spine-like, simple setae, ventral margin bare or with a row of fine, spine-like, simple setae, surface covered with scattered fine hair-like setae; tarsal claw (Fig. 7B) with one row of about 12 denticles increasing in length toward apex, subapical setae absent. **Midlegs and hindlegs**. As forelegs.

Abdomen (Fig. 6B). **Tergites**. Posterior margin smooth, posterior marginal spines extremely reduced to absent, tergal surface with scattered stout, fine, hair-like setae and scattered long translucent scales distally (Figs 6C, 7C, 8F); abdominal sternites without posterior marginal spines; sternal surface with loose scattered fine, hair-like setae.

Gills (Fig. 7D). Seven pairs of gills present on abdominal tergites I–VII; gills I (Fig. 6D) enlarged to covered abdominal sternites II–V, ventrally oriented, relatively rhombus shape, length approximately 1.4× of width, medially part broad, tracheation extending from main trunk to outer margin, gill margin smooth, surface and gill

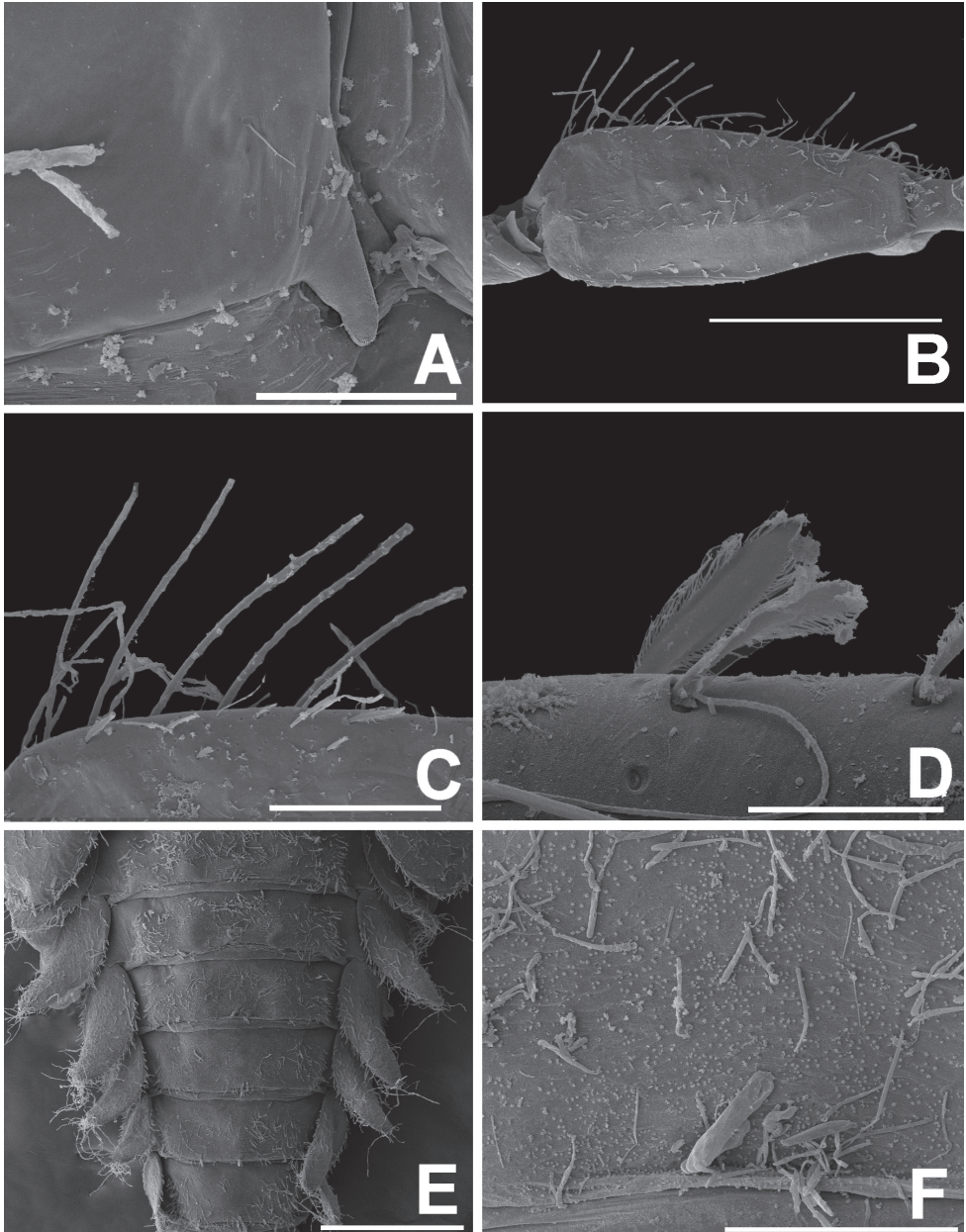


Figure 8. *Megabranchiella scutulata* sp. nov., larval morphology (SEM) **A** hindwing pad **B** forefemur (dorsal view) **C** setae on dorsal margin of forefemur **D** setae on ventral margin of forefemur **E** abdominal tergites **F** tergite V. Scale bars: 50 μ m (**A**); 100 μ m (**B–C, F**); 20 μ m (**D**); 500 μ m (**E**).

margin without long, fine hair-like setae; gills II–VII oriented dorsolaterally, slightly oval length approximately 2.1 \times of width, gill margin smooth, surface and gill margin covered with scattered long, fine hair-like setae.

Gonostyli bud (Fig. 6E). *Acentrella*-type, three-segmented, segment I very short, $0.3 \times$ of segment II length, segment III relatively short and broad, rounded at apex.

Paraproct (Fig. 7E). Margin smooth without marginal spines and without prolongation at posterior margin. Surface without scale bases, with micropores and fine, stout, simple setae and scattered fine, hair-like setae, and with a patch of notch scales.

Caudal filaments. Cerci $0.4 \times$ of body length, inner margin of cerci with very thin, long setae; median filament $0.5 \times$ of cerci length, lateral margins with very thin, long setae.

Winged stages. Unknown

Etymology. The name of the species “scutula” refers to the outline of abdominal gill I which is rhombus-shaped.

Distribution. Northern part of Thailand (Chiang Mai and Chiang Rai Provinces) (Fig. 15).

Ecological notes. The larvae were collected in headwater stream (Mae Kampong River) (Fig. 14A) and Pong Phra Baht waterfall (Fig. 14B). The sampling sites were located with altitudes of 475–780 m a.s.l. Both stream and waterfall were situated in forest areas with relatively complete canopy cover on mountains in the northern part of Thailand. The stream was in The Royal Project of Teen Tok area which has some human disturbances resulting from touristic attractions and resorts. The substrates were dominated by 50% cobbles, 20% pebble, 20% boulders, 10% gravels respectively with sand bottom. The waterfall was located upstream. The larvae were found on the surface of cobbles in fast-flowing water (Fig. 14C).

***Megabranchiella longusa* Phlai-ngam & Tungpairojwong, sp. nov.**

<https://zoobank.org/65816410-4304-459F-85AF-5C372989F48A>

Holotype. One male larva on slide and SEM stubs (KKU-AIC), Thailand, Chiang Mai, Chom Thong district, Ban Luang, Siribhum waterfall, $18^{\circ}32'50.02\text{N}$, $98^{\circ}30'49.79\text{E}$, 1,359 m, 11.03.2021, B. Boonsoong and C. Suttinun leg.

Paratype. One larva in alcohol (ZMKU), same data as holotype.

Other materials. One larva in alcohol (MZL), Thailand, Nan, Bo Kluea district, Kluea district Tai, Sapan River, $19^{\circ}09'19.09\text{N}$, $101^{\circ}10'12.96\text{E}$, 995 m, B. Boonsoong and C. Suttinun leg.

Description. Coloration (Fig. 9A–B). Head dorsally brownish, darker brown along frontal suture. Thorax dorsally brown; pronotum with dark brown pattern medially, mesonotum with longitudinally darker brown pattern medially. Abdomen light brown with dark brown pattern; tergites I–VIII brownish, with darker brown marks laterally to posterior margin, tergites II–III with a paired of pale dots medially, tergites IV–VIII with distinct paired of pale, oblique streak, and with a pale, longitudinal pattern medially, tergites IX–X paler than other tergites, with the same pattern as tergites IV–VIII; abdomen ventrally light brown (Fig. 9C). Legs light brown; dorsal, ventral, and apical femur margins dark brown; claws distally dark brown. Caudal filaments brownish.

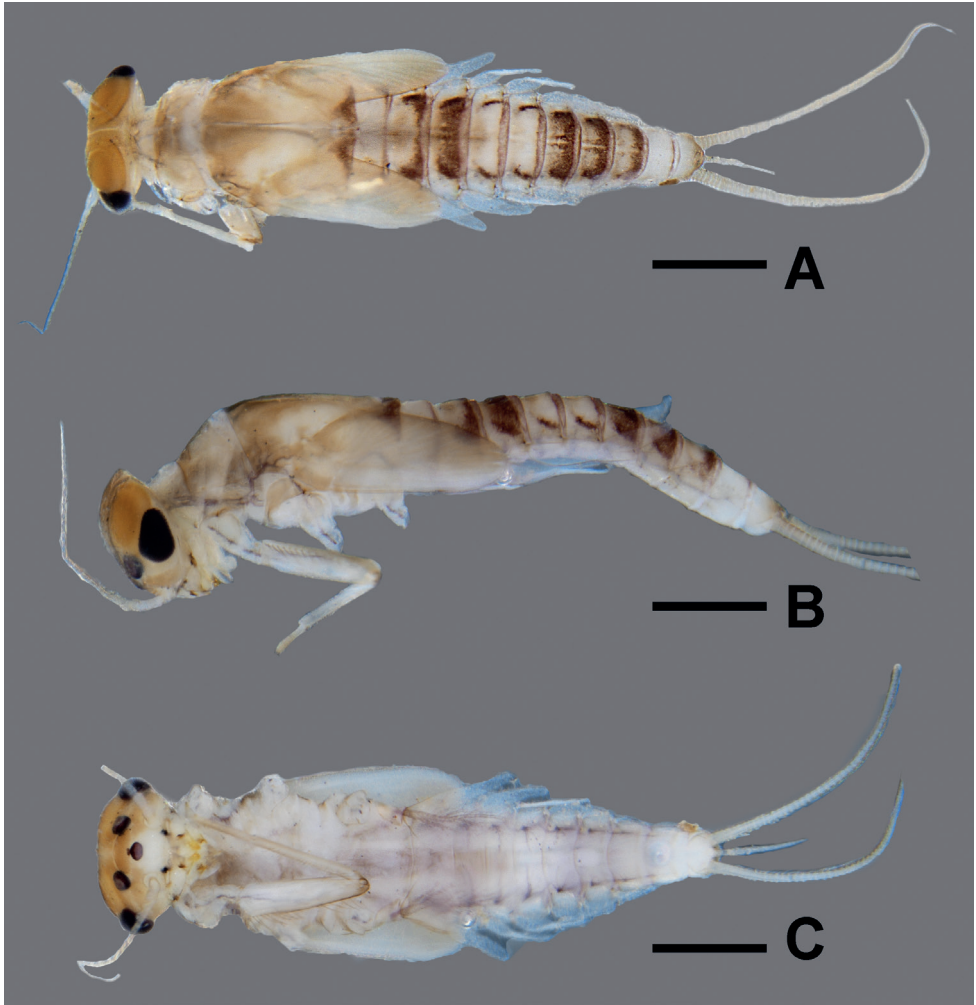


Figure 9. *Megabranchiella longusa* sp. nov., larval habitus: **A** dorsal view **B** lateral view **C** ventral view. Scale bars: 1 mm.

Body (Fig. 9). Ventrally flattened (Fig. 9C), body length 3.5 mm, covered with scattered long, hair-like setae.

Head (Fig. 9B). Lateral view rounded, head width ca. $1.2 \times$ as long as head length.

Antenna. Ca. $2 \times$ as long as head length (Fig. 9B); scape without process, subequal in width and length, slightly shorter than pedicel, pedicel ca. $2 \times$ as long as width, scape and pedicel almost bare, without scales bases, covered with scattered long, fine setae; flagellum covered with scattered long, fine setae.

Labrum (Fig. 10A). Broadly rounded; wider than long, width ca. $1.17 \times$ as long as length; dorsal surface with submarginal row composed of one long, point, simple seta medially plus three long, point, simple setae anterolaterally, dorsal surface with scattered simple, hairlike setae; distal margin with anteromedian notch shallow. Ventrally

with submarginal row of setae composed of lateral and anterolateral long, feathered setae and medial long, pectinate setae; ventral surface with five short, spine-like setae near lateral and anterolateral margin.

Right mandible (Fig. 10B). Canine (Fig. 10C) with 4 + 4 apically rounded denticles, largely fused outer and inner incisors; inner margin of inner incisor with small denticulation; prosthema robust (Fig. 10D), apically with small denticles and comb-shaped structure; mola between mola and prosthema smooth, without setae; mola with well-developed denticulation; apex of mola with tuft of spines like setae.

Left mandible (Fig. 10E). Canine (Fig. 10F) with 4 + 4 apically rounded denticles, largely fused outer and inner incisors; inner margin of inner incisor with small denticulation; prosthema robust, apically with small denticles and comb-shaped structure (Fig. 10G); mola between mola and prosthema smooth, without setae; mola with reduced denticulation, molar area with numerous small, round teeth, apex of mola with tuft of spines like setae.

Maxilla (Fig. 10H). Short and compact; galea-lacinia (Fig. 10I) with long, robust, simple setae under crown; inner dorsal row of setae with denti-setae; distal denti-seta tooth-like, middle denti-seta (Fig. 10J) slender, bifid and pectinate; proximal denti-seta slender, pectinate; inner ventral row of six robust, simple setae; medially with one seta and four simple setae. Maxillary palp 2-segmented, with scattered small, blunt setae; distal segment with distinct, small tip at apex.

Labium (Fig. 10K). Short and compact; glossa basally broad, narrower toward apex, slightly shorter than paraglossa; inner margin with medium, pointed, simple setae; apex with four long, robust, pectinate setae. Paraglossa sub-rectangular, broader than glossa, apically curved inward, apical margin with three rows of long, robust, apically pectinate setae (Fig. 10L), ventrally with 2–3 long, spine-like setae near inner margin, with an arch of 4–5 long, simple setae on outer margin. Labial palp 3-segmented, segment I rectangular and broad, covered with scattered fine, setae and several micropores; segment II with small distolateral expansion, with a few scattered, simple setae and a row of setae reduced to two large, blunt, robust, simple setae near distal margin; segment III rounded, covered with long, robust, simple setae.

Hypopharynx (Fig. 10M). Lingua subequal to superlingua, apically rounded, with apical tuft of fine, short simple setae; superlingua with distal margin rounded, with fine, short simple setae along margin.

Thorax. Hindwing pads (Fig. 13A). Highly reduced.

Forelegs (Fig. 12A). Ratio of foreleg segments 0.68: 0.59: 0.25. **Femur** (Fig. 13B). Length ca. 3× maximum width. Dorsal margin of femur (Figs 11A, 13C–D) with a row of 18–20 long, robust, apically pointed, laterally pectinated setae; short stout, lanceolate, laterally pectinate setae and scattered fine hair-like setae along dorsal and ventral margins; femora patch present; surface with scattered tiny spines anteromedially (Fig. 13E); dense long, fine, small apically blunt, hair-like setae present; dorsal margin of tibia with a row of long, apically pointed, pectinate setae; several short stout, lanceolate, laterally pectinate setae and scattered short, apically pointed, hair-like setae along dorsal and ventral margins, patella-tibial suture present; tarsus dorsally with a row of fine, simple

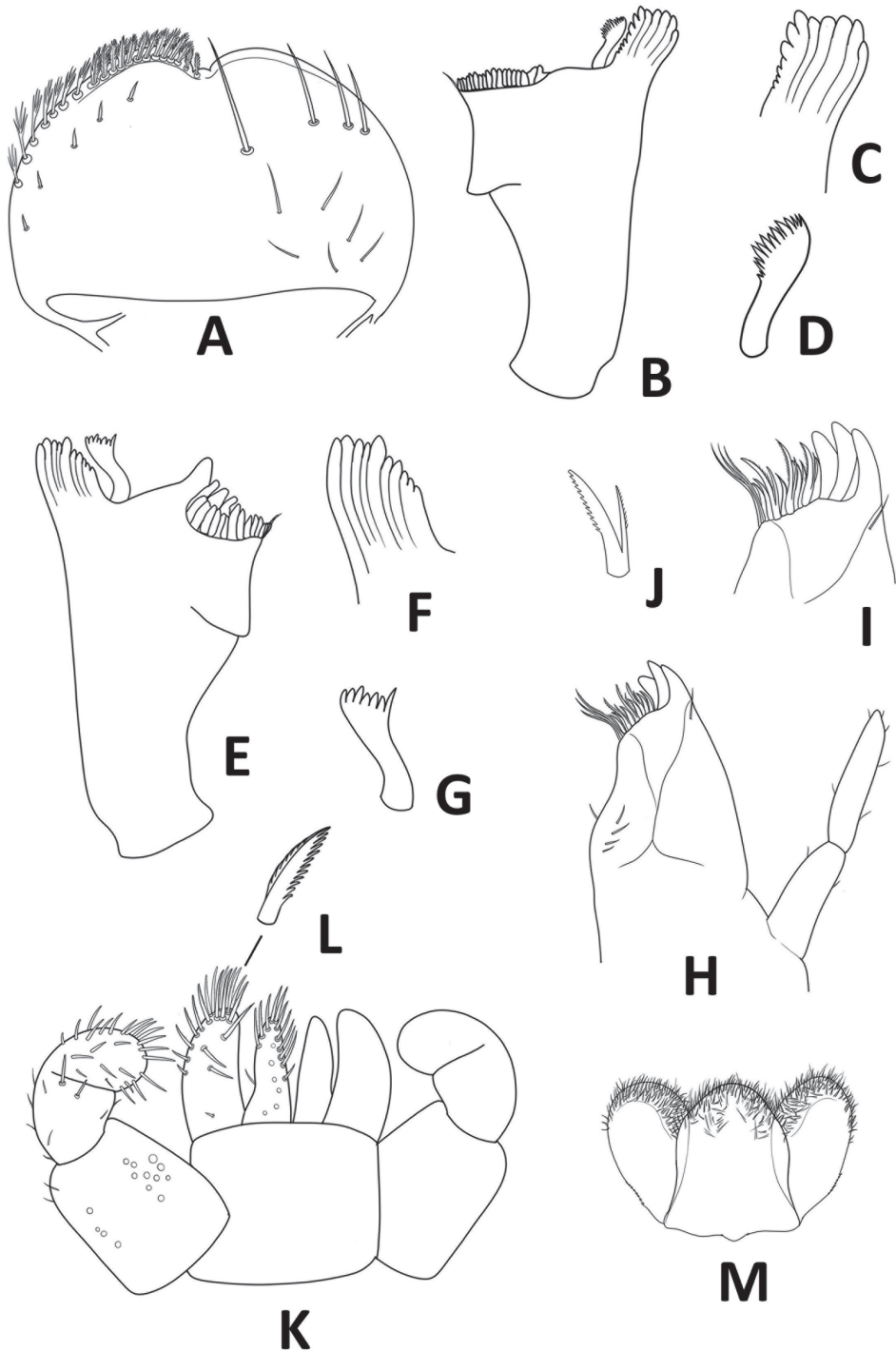


Figure 10. *Megabranchiella longusa* sp. nov., larval morphology **A** labrum **B** right mandible **C** right incisor **D** right prosthema **E** left mandible **F** left incisor **G** left prosthema **H** maxilla **I** apex of galea-lacinia **J** denti-seta **K** labium **L** long, robust, pectinate setae **M** hypopharynx.

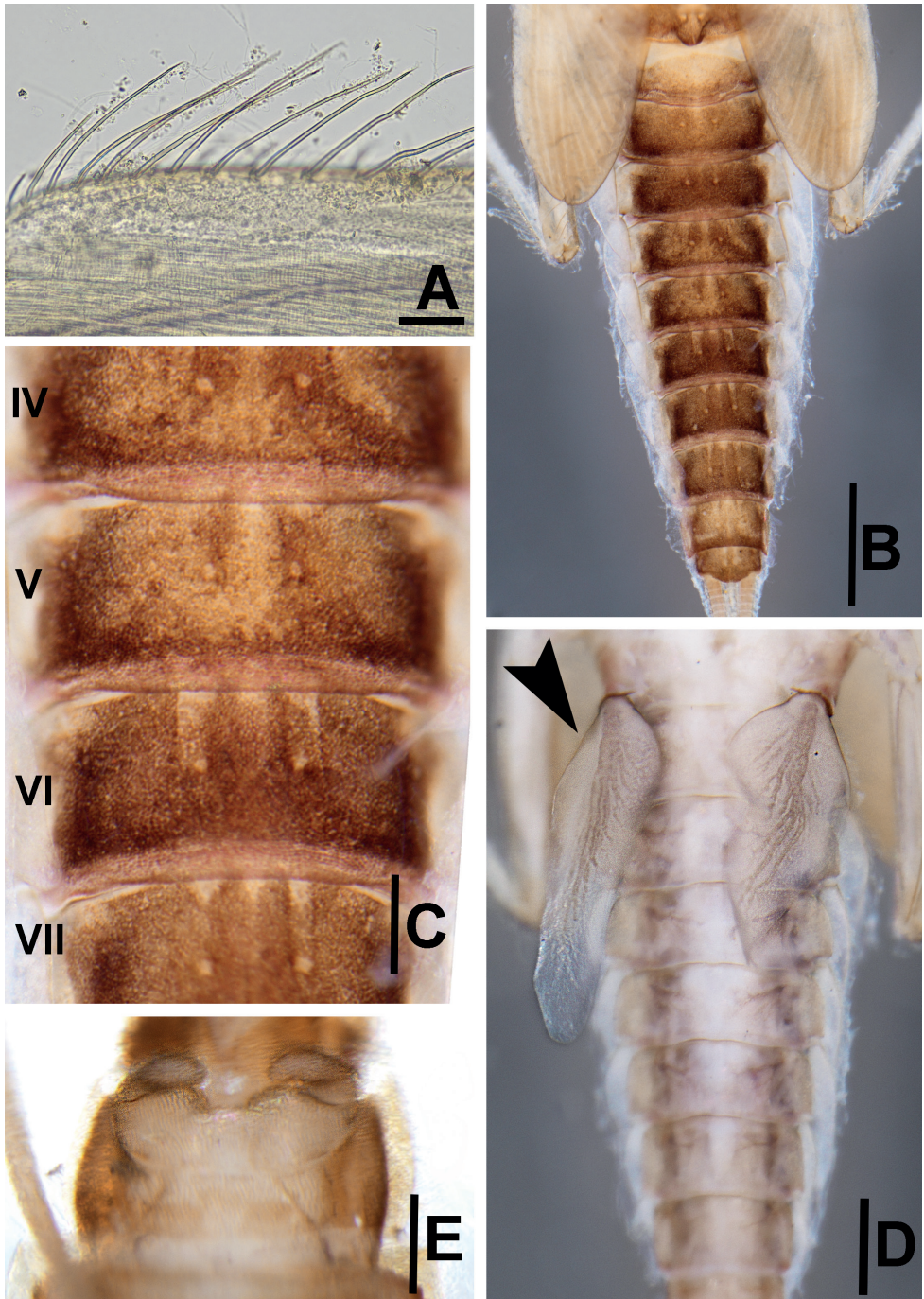


Figure 11. *Megabranchiella longusa* sp. nov., larval morphology **A** dorsal margin of femur **B** dorsal view of abdomen **C** enlargement of abdominal tergites IV–VII **D** ventral view of abdominal gills I (arrow) **E** ventral view of gonostyli. Scale bars: 0.1 mm (**A**); 0.8 mm (**B**); 0.2 mm (**C**); 0.4 mm (**D**); 0.3 mm (**E**).

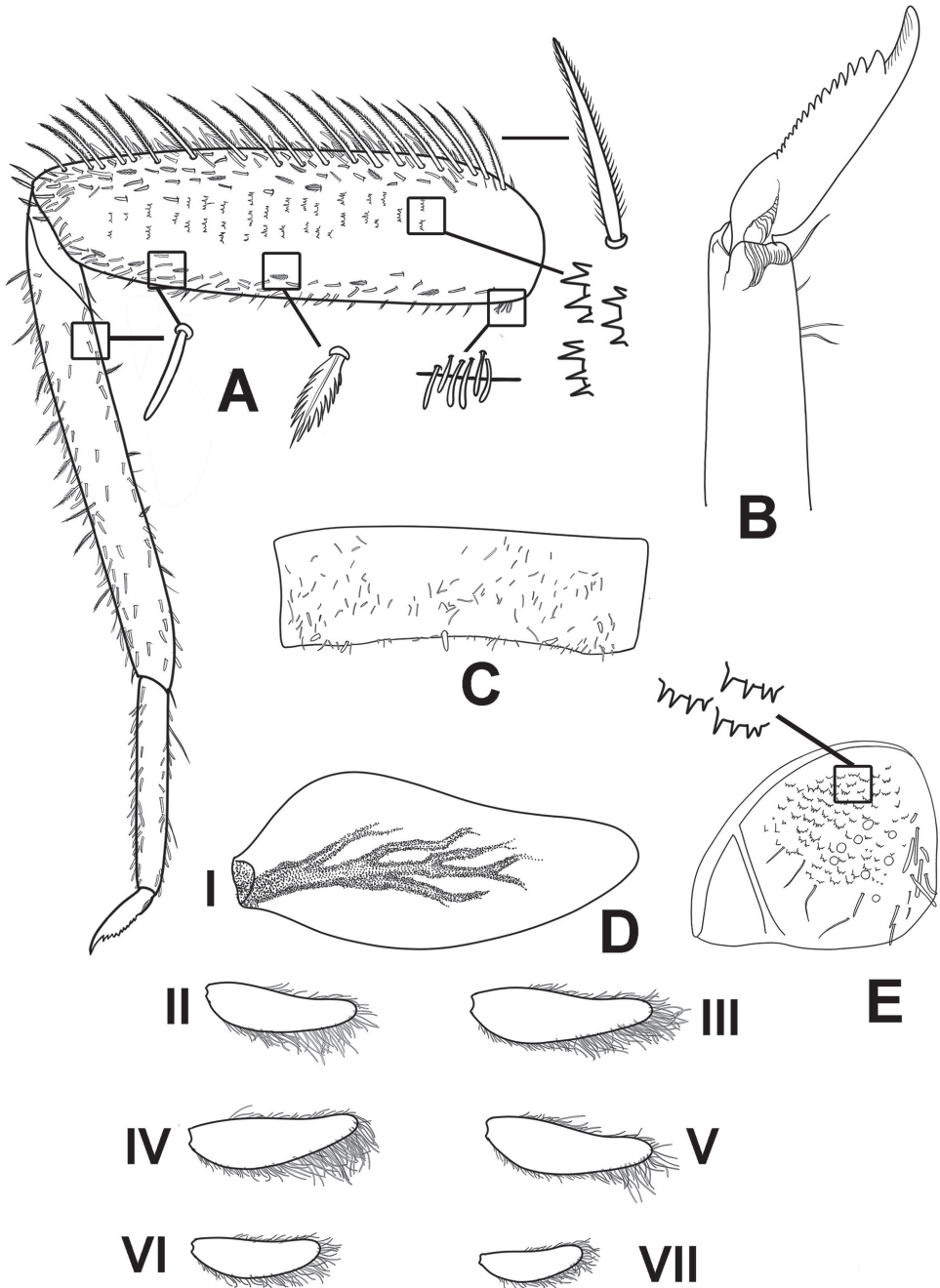


Figure 12. *Megabranchiella longusa* sp. nov., larval morphology **A** foreleg **B** tarsal claw **C** tergite **D** abdominal gills I–VII **E** paraproct and notched scales on surface.

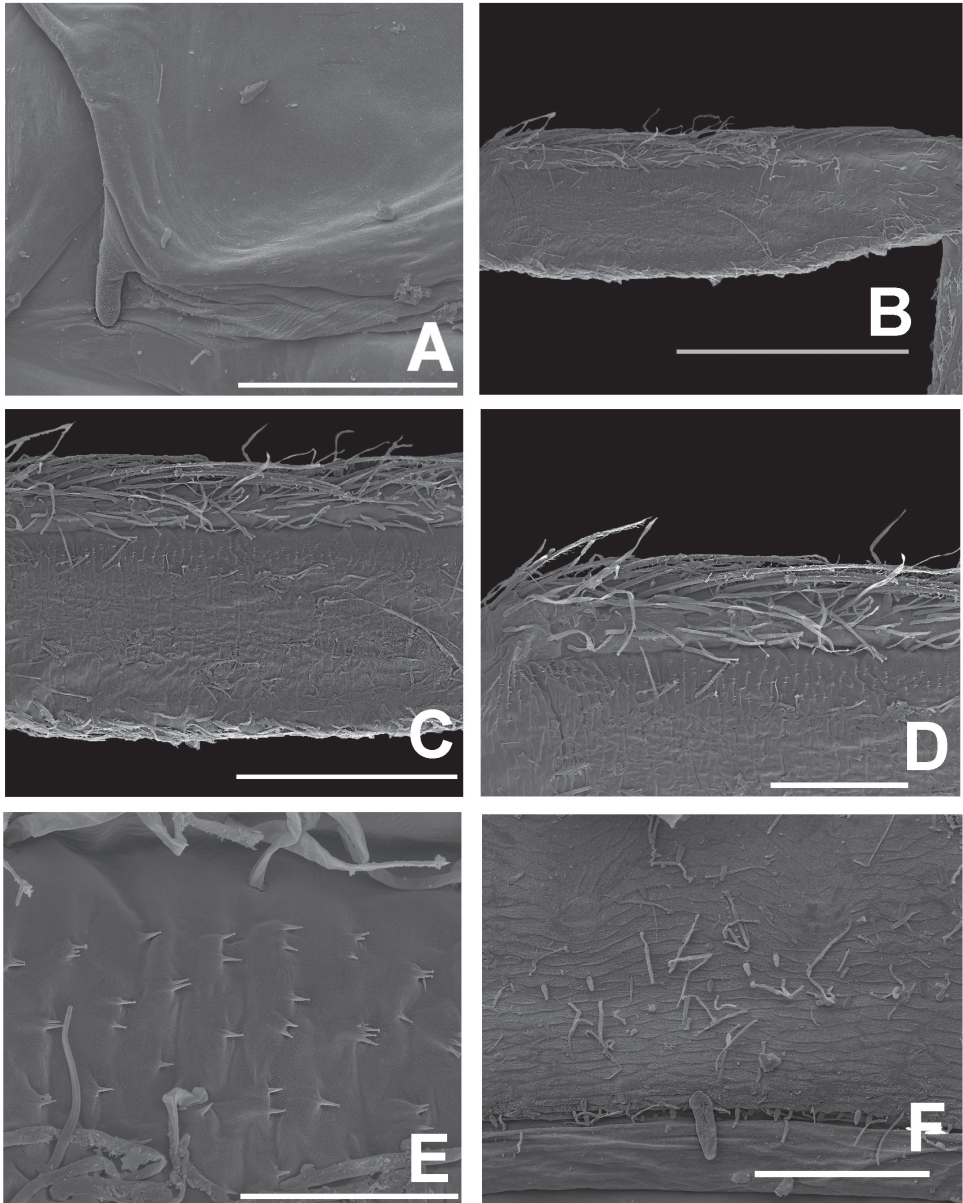


Figure 13. *Megabranchiella longusa* sp. nov., larval morphology (SEM) **A** hindwing pad **B** forefemur (dorsal view) **C–D** setae on dorsal margin of forefemur **E** spines on dorsal surface of forefemur **F** tergite V. Scale bars: 100 μ m (**A, D, F**); 400 μ m (**B**); 200 μ m (**C**); 30 μ m (**E**).

setae; ventral margin with a row of fine, simple setae; surface covered with scattered fine hair-like setae. Tarsal claw (Fig. 12B) with one row of about 16 denticles increasing in length toward apex, subapical setae absent. **Midlegs and hindlegs.** As forelegs.

Abdomen (Fig. 11B). **Tergites.** Posterior margin smooth, posterior marginal spines extremely reduced to absent (Figs 11C, 12C, 13F), tergal surface with scattered fine,

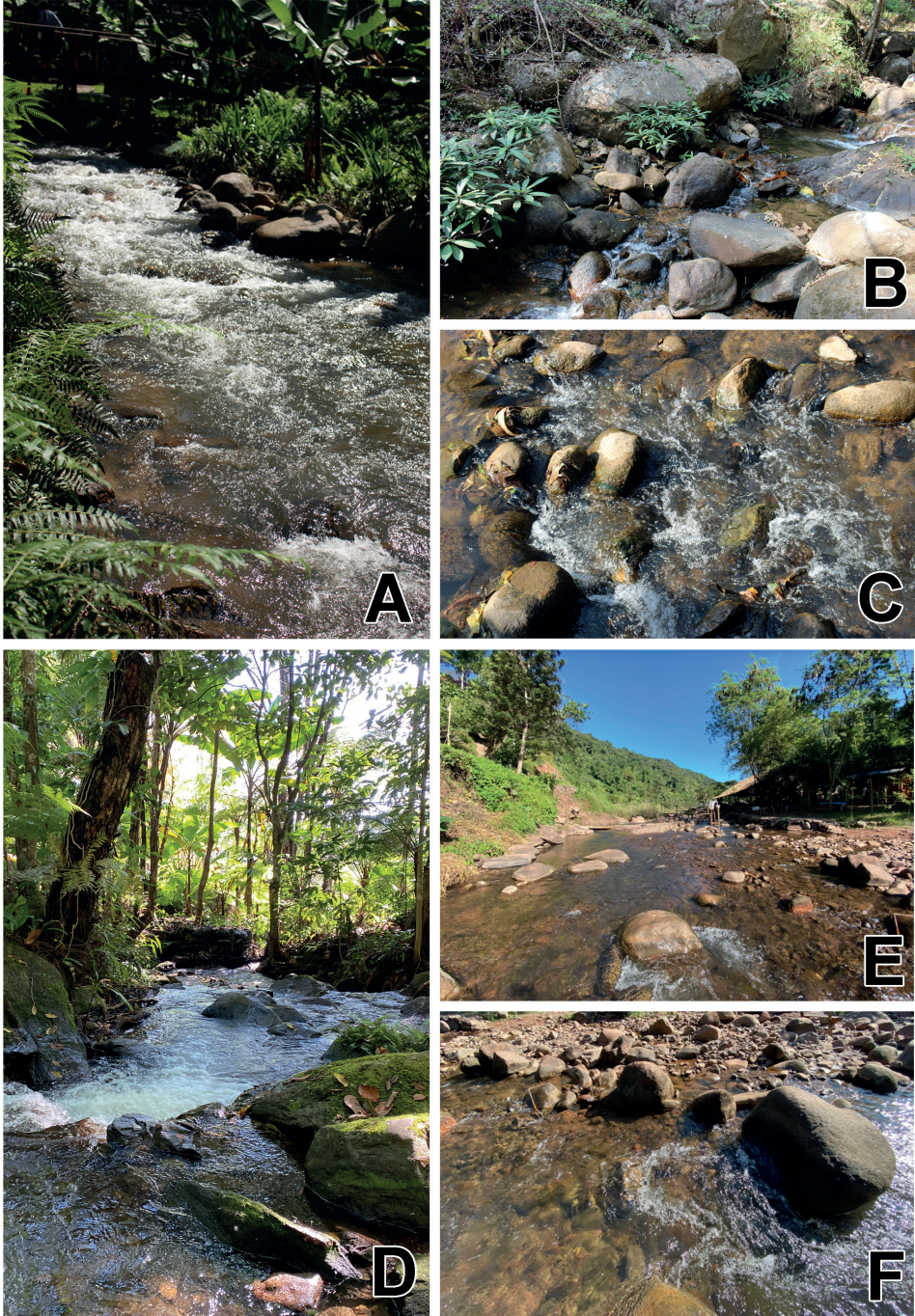


Figure 14. Type locality and larval habitats of *Megabranchiella* gen. nov. **A–C** type locality and larval habitats of *M. scutulata* sp. nov. **A** Mae Kampong stream, The Royal Project of Teen Tok, Chiang Mai Province **B** Pong Phra Baht Waterfall, Chiang Rai Province **C** fast-flowing water with pebble and cobble habitats (**D–F**) type locality and larval habitats of *M. longusa* sp. nov. **D** Siribhum waterfall, Chiang Mai Province **E** Sapan River, Bor Kluea district, Nan Province **F** fast-flowing water with boulder, cobble, and pebble habitats.

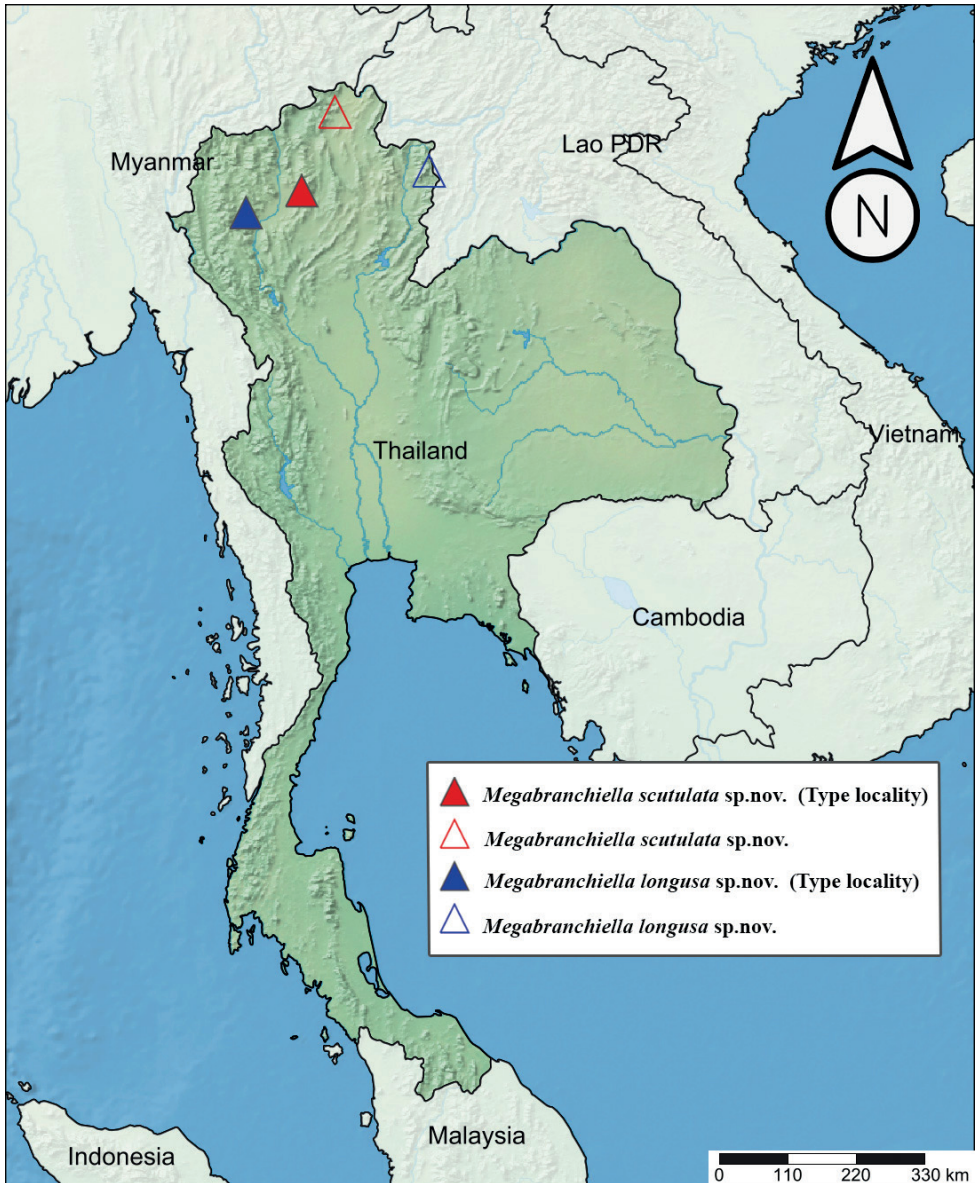


Figure 15. Distribution of genus *Megabranchiella* gen. nov. in Thailand **A** distribution of *M. scutulata* sp. nov. (red triangle) **B** distribution of *M. longusa* sp. nov. (blue triangle).

hair-like setae and scattered long translucent scales distally; abdominal sternites without posterior marginal spines, sternal surface with loose scattered, fine, hair-like setae.

Gills (Fig. 12D). Seven pairs of gills present on abdominal tergites I–VII, slender and elongated; gills I (Fig. 11D) enlarged to covered abdominal sternites II–V, oriented ventrally, relatively elongated shape with length approximately 2.5× of width, medially part broad, tracheation extending from main trunk and outer margin, gill margin

smooth, surface and gill margin without long, fine hair-like setae; gills II–VII oriented dorsolaterally, slightly oval and slender with length approximately 3.3× of width, gill margin smooth, surface and gill margin covered with scattered long, fine hair-like setae.

Gonostyli bud (Fig. 11E). Acentrella-type, three-segmented, segment I very short, 0.3 × of segment II length, segment III relatively short and broad, rounded at apex.

Paraproct (Fig. 12E). Margin smooth without marginal spines and without prolongation at posterior margin, surface without scale bases, with micropores and fine, stout, simple setae and scattered fine, hair-like setae, and with a patch of notch scales.

Caudal filaments. Cerci 0.4× of body length, inner margin of cerci with very thin, long setae; median filament 0.5 × of cerci length, lateral margins with very thin, long setae.

Winged stage. Unknown.

Etymology. The name of the species “longusa” refers to the outline of abdominal gill I which is elongate-shaped.

Distribution. Northern part of Thailand (Chiang Mai and Nan Provinces) (Fig. 15).

Ecological notes. The larvae were collected in Siribhum waterfall (Fig. 14D) and headwater stream (Sapan River River) (Fig. 14E). The sampling sites were located at high altitudes of 995–1,360 m a.s.l. in forest areas on mountains in the northern part of Thailand. The waterfall was in the upper stream of the Ping River, and the substrate types were dominated by boulders, cobbles, pebbles, gravel, and a sand bottom. The stream was in the Sapan River and located near the resort which can be disturbed by touristic attractions. The larvae were found on the surface and underside of cobbles in fast-flowing water (Fig. 14F).

Discussions

Generic affinities

The morphological characters of *Megabranchiella* gen. nov. clearly confirm that it belongs to the family Baetidae. These include a Y-shaped epicranial suture reaching ventrally of the lateral ocelli, relatively long antennae originating anterolaterally on the head, the developing turbinate eyes of late instar male larvae, a labrum with a median incision, the shape of the glossa, widen basally, and the shape of the right and left prostheca of the mandibles. This genus can be assigned to the clade Anteropatellata due to the presence of a patella-tibial suture on the foreleg and referred to Baetofemorata. The taxon Baetofemorata or Baetis/fg8 sensu Kluge & Novikova, 2011 includes the lineages Baetinae and Acentrella/fg1. As other members of this taxon, *Megabranchiella* gen. nov. is characterized by a ventral femoral patch (villopore) on the fore femur of larva.

Despite the presence of this femoral patch, which has been used to assign taxonomic status, the position within Baetofemorata remains unclear. Taxon Acentrella/fg1 is a mayfly group assigned to the Baetofemorata. This taxon is composed of the genera

Acentrella Bengtsson, 1912, *Acerobiella* Gattolliat, 2012, *Asiobaetodes* Gattolliat, 2012, *Jubabaetis* Müller - Liebenau, 1980, *Liebebiella*, and *Platybaetis* Müller-Liebenau, 1980 and *Tanzaniops* McCafferty & Barber-James, 2005 (Kluge and Novikova 2011). The *Megabranchiella* gen. nov. larvae seem intimately related to *Acentrella*/fg1 by the following larval characters: (i) labial palp 2nd segment without large inner-apical projection, 3rd segment widened and rounded; (ii) short body, with ventrally flattened, thorax enlarged, abdomen diminished; (iii) head hypognathous, shortened or compact mouthparts; (iv) leg bases widely separated, femur with a row of long, dense setae along dorsal margin, tibia with a similar setal row; and (v) cerci long, with reduced paracercus (Sroka and Arnekleiv 2010; Kluge and Novikova 2011). Therefore, this study assigned this new genus to *Acentrella*/fg1 Kluge & Novikova, 2011, along with two closely related genera of *Acentrella*/fg1: *Acentrella* (*Acentrella*/fg1 Kluge & Novikova, 2011) and *Liebebiella* (*Liebebiella*/g1 Kluge & Novikova, 2011).

Megabranchiella gen. nov. has a ventrally flattened body with compact mouthparts, as in *Acentrella* (Bengtsson, 1912) and *Liebebiella* (Waltz & McCafferty, 1987). The labial palps have a weakly developed inner lobe with a rounded terminal segment. The maxillary palps are 2-segmented, while the 2nd segment with the apical tip is distinct in *Megabranchiella* gen. nov. The hind wing pads are reduced to absent in all genera (Waltz and McCafferty 1987; Kluge and Novikova 2011). The dorsal margin of the femur has a regular row of long, dense setae and distinct multiciliate setae in *Liebebiella*. The dorsal margin of the tibia has two rows of relatively long, dense, multiciliate setae in *Liebebiella*, while it can be present with 1 or 2 rows in *Acentrella* (Waltz and McCafferty 1987; Kluge et al. 2013). *Megabranchiella* gen. nov. has only one row of regular, long, simple setae on the dorsal margin of the tibia. The preapical tarsal seta is highly developed in *Liebebiella* but absent in *Acentrella* and *Megabranchiella* gen. nov. The subapical setae of the tarsal claw show are present in some species of *Acentrella* (Waltz and McCafferty, 1987; Kluge et al. 2013) and absent in *Megabranchiella* gen. nov. Seven pairs of abdominal gills are present in *Acentrella* and *Liebebiella*; these gills are simple, dorsally oriented, and smooth margined, with scattered fine, hair-like setae. The genus *Megabranchiella* gen. nov. can be distinguished from other genera by its gill I ventrally oriented, enlarged to cover abdominal sternites II–V, and the gill margins are smooth, with scattered fine, hair-like setae. Gills II–V are dorsally oriented and have smooth margins with long scattered fine, hair-like setae. The posterior marginal spines of the abdomen are varied and poorly developed in *Acentrella* and *Megabranchiella* gen. nov. but are distinct in *Liebebiella*. The gonostyli buds of these genera are of *Acentrella* type; the paracercus is reduced or vestigial (Table 2).

Abdominal gill segment I

The gills allow a straightforward identification of the genus: the position of the larval abdominal gills of *Megabranchiella* gen. nov., specifically the ventral orientation of gill I, is an important character. Ventrally oriented gills are also present in the genera

Table 2. Larval character comparisons of *Megabranchiella* gen. nov. and related genera.

Characters	<i>Acentrella</i>	<i>Liebebiella</i>	<i>Megabranchiella</i> gen. nov.
Body	Body ventrally flattened	Body ventrally flattened	Body ventrally flattened
Mouthpart	Compact, the 2 nd segment of labial palp with weakly developed inner lobe, the 3 rd segment evenly rounded to slightly truncate	Compact, the 2 nd segment of labial palp with weakly developed inner lobe, the 3 rd segment rounded, weakly tapered, or flattened apically	Compact, the 2 nd segment of labial palp with weakly developed inner lobe, the 3 rd segment relatively rounded
Maxillary palp	2-segmented, terminal segment with or without apical tip	2-segmented, terminal segment usually with apical tip	2-segmented, terminal segment with apical tip
Hindwing pad	Present, reduced or absent	Absent	Highly reduced
Femur	Dorsal margin of femur usually with a row of relatively long setae	Dorsal margin of femur with relatively long, dense multiciliate setae	Dorsal margin of femur with a regular row of long, simple setae
Ventral femoral patch	Present	Present	Present
Tibia	Dorsal margin of tibia with 1 or 2 regular rows of long, simple setae	Dorsal margin of tibia usually with 1 or 2 rows of dense, long, multiciliate setae	Dorsal margin of tibia with a row of long, simple setae
Tarsus	Without a preapical seta	With a preapical seta	Without a preapical seta
Tarsal claw	Generally without subapical setae (presence in a few species)	Without subapical setae	Without subapical setae
Abdominal gills	Usually 7 pairs (8 pairs in <i>A. joosti</i>), dorsally oriented; gill margin smooth with a few scattered fine hair-like setae	Seven pairs, dorsally oriented; gill margin smooth with a few scattered fine hair-like setae	Seven pairs; gill I enlarged to cover sternites II–V, ventrally oriented, gill margin smooth without dense long fine hair-like setae; gill II–VII dorsally oriented, gill margin with dense long fine hair-like setae
Posterior marginal spines	Poorly developed, often spiculate or multidentate	Well developed	Reduced to absent
Paracercus	Generally reduced (sometimes to a segment)	Reduced to a few segments (generally 10–14 segments)	Reduced to a few segments (Approximately 12–15 segments)
Distribution	Palaearctic, Nearctic and Oriental realms	Oriental realm	Northern Thailand (Chiang Mai, Chiang Rai and Nan Provinces)
References	Waltz and McCafferty (1987); Sroka and Arnekleiv (2010); Kluge and Novikova (2011)	Waltz and McCafferty (1987); Kluge and Novikova (2011); Kluge et al. (2013)	Present study

Afrobaetodes (Demoulin, 1970) and *Baetodes* (Needham & Murphy, 1924), but they differ from *Megabranchiella* by the following features: the number of ventrally oriented gills, the number of rows of denticles on the tarsal claws, and the presence of accessories' gills (Gattolliat and Sartori 1999). *Megabranchiella* gen. nov. cannot be assigned to the same group as these genera. The genus *Cymbalcloeon* also has ventrally oriented gills but is defined to a non-Baetovectata taxon, apart from *Afrobaetodes* and *Baetodes*. Even though *Cymbalcloeon* and *Megabranchiella* have ventrally inserted gills, morphological characters assign them to different lineages. *Cymbalcloeon* has strong characters such as absence of gills on segments I–IV, and modified gills on abdominal segments V–VII (Suttinun et al. 2020). The genus *Asiobaetodes* Gattolliat, 2012 also possesses ventrally oriented gills; moreover this genus belongs to *Acentrella*/fg1. *Megabranchiella* and *Asiobaetodes* can be easily separated by the position of the gills II to VII and the presence/absence of a subapical setae on the ventral margin of tarsi (Gattolliat 2012).

Larval body and movement

The larval body of *Megabranchiella* gen. nov. was comparable to *Acentrella*/g1 (including *Acentrella* and *Liebebiella*), as the larvae are adapted for inhabitation on stones in rapid flowing water. *Megabranchiella* gen. nov. larvae have the same general *Acentrella*-type body, which is dorso-ventrally flattened. They have lost the primary siphonouroid swimming specialization and lost the ability for normal swimming, similarly to *Acentrella*/g1 larvae. The legs of *Acentrella*/g1 and *Megabranchiella* gen. nov. larvae are widely separated and cannot be stretched backward and pressed to the body. The abdomen is too short, with relatively long cerci, so the larvae cannot make undulating movements and cannot serve as a swimming flipper. In the natural conditions, they do not swim but crawl on the stone surfaces. When the larvae try to swim, they make poorly effective dorso-ventral movements with the abdomen. They swim upward, then stop and slowly fall passively, with their legs kept in lateral position, the abdomen bent dorsally, and the cerci diverging (see Kluge and Novikova 2011 for detailed description of swimming movements in other genera of *Acentrella*/g1).

Species diversity of *Megabranchiella*

Surprisingly, two species of this new genus were found in the northern part of Thailand. *Megabranchiella scutulata* nov. sp. was found in Chiang Mai and Chiang Rai provinces, while *Megabranchiella longusa* sp. nov. was collected in Chiang Mai and Nan provinces. These two *Megabranchiella* larvae can be separated by the following diagnostic characters: i) the dorsal pattern of the body; ii) the number of spine-like setae near the lateral and anterolateral margins of labrum; iii) the number of canines of the mandible; iv) the shape of the setae on the dorsal margin of the femur; these setae are long, apically rounded, simple in *Megabranchiella scutulata* nov. sp. while they are dense long, robust, apically pointed, pectinate in *Megabranchiella longusa* sp. nov., vi) number of denticles of the tarsal claw, and vii) the shape of the abdominal gills, which are more elongated and slenderer in *Megabranchiella longusa* sp. nov. (Table 3).

Ecological notes and adaptation

Megabranchiella gen. nov. larvae were found in fast-flowing water in headwater streams and a waterfall. They live on stone surfaces of cobble and sand microhabitats in shallow water streams. Their habitat may possibly explain why *Megabranchiella* larvae have a ventrally oriented gill I. This feature might be important to *Megabranchiella* larvae for adaptation to fast-flowing shallow water streams. It is likely an adaptation to shallow fast streams as in *Afrobaetodes* and *Baetodes* (Gattolliat & Sartori, 1999). *Cymbalocleon*, another genus with a ventral gill insertion, is also found in shallow streams, but occurs in slow-flowing water. Conceivably, ventral gill insertion could be a useful adaptation that allows mayflies to survive in shallow streams under various conditions.

The enlarged abdominal gill I is a remarkable morphological adaptation of *Megabranchiella* larvae. As in *Cymbalocleon* larvae, a single pair of gills is enlarged.

Table 3. Larval character comparisons of two new species of *Megabranchiella* gen. nov.

Characters		<i>M. scutulata</i> sp. nov.	<i>M. longusa</i> sp. nov.
Hindwing pads		Highly reduced	
Femur	Dorsal margin	Regular row of long, apically rounded, simple setae	Regular row of dense long, robust, apically pointed, pectinate setae
	Number of dorsal setae	11–13	18–20
	Dorsal surface	with scattered tiny spines and some long, apically blunt, fine, hair-like setae	with scattered tiny spines and dense long, apically blunt, fine, hair-like setae
Tibia	Dorsal margin	A regular row of long, apically pointed, pectinate setae	A regular row of long, apically pointed, pectinate setae
Abdominal gills	Gill I	Enlarged to covered abdominal sternites II–V, oriented ventrally, relatively rhombus shape, gill margin smooth	Enlarged to covered abdominal sternites II–V, oriented ventrally, relatively rhombus shape, gill margin smooth
	Length/width gill I	1.4×	2.5×
	Gill II–VII	Oriented dorsally, slightly oval, gill margin smooth, surface and gill margin covered with scattered long, fine hair-like setae	Oriented dorsally, slightly oval and slender, gill margin smooth, surface and gill margin covered with scattered long, fine hair-like setae
	Length/width gill II–VII	2.1×	3.3×
Gonostyli bud		<i>Acentrella</i> -type, 3-segmented	
Terminal filament	Paracercus	Reduced to several segments; approximately 0.4× cerci length	Reduced to several segments; approximately 0.3× cerci length
Distribution		Northern Thailand (Chiang Mai and Chiang Rai Provinces)	Northern Thailand (Chiang Mai and Nan Provinces)

Because of the reductions of abdominal gills I–IV in *Cymbalocleon*, this feature might be used for active respiration in slow-flowing water, whereas *Megabranchiella* larvae prefer fast-flowing water. The abdominal gills of mayflies have been revealed to perform various functions, such as respiration, osmoregulation, locomotion, water circulation, protection, and attachment (Zhou 2010; Kluge 2004). Why *Megabranchiella* larvae have modified their abdominal gill I to expand ventrally is unclear. However, considering their microhabitat and morphology (tracheation and margin), one possibility is that gill I can perform a role of attachment in addition to respiration. In fast-flowing water, the larvae have to maintain a body position that avoids friction against the stone surface, similar to the function of the adhesive disks of some species of *Rhithrogena* Eaton, 1881 and *Epeorus* Eaton, 1881 (Heptageniidae) (Ditsche-Kuru et al. 2010; Zhou 2010).

In conclusion, *Megabranchiella* gen. nov. from Thailand can be assigned to *Acentrella*/g1 Kluge & Novikova, 2011 based on the diagnostic morphological characters of the taxon. However, the complex taxonomy of *Acentrella*/g1 creates difficulties in deciding the position of this new genus within the clade. Molecular work can resolve and clarify the taxonomic status according to the evolutionary relationship with *Acentrella*/g1. The ecology and habit of this new genus make its association with *Acentrella*/g1 quite likely, in view of their similar habitats, behaviors, and morphology. A clearer picture of the adaptation and modifications of the gill morphological characteristics of this genus should be studied intensively in future work.

Acknowledgements

The research was supported by the Fundamental Fund of Khon Kaen University, fiscal year 2022. This research has received funding support from the National Science, Research and Innovation Fund (NSRF). This work was partially financially supported by Academic Affairs Promotion Fund, Faculty of Science, Khon Kaen University, fiscal year 2022 (RAAPF), Research and Graduated Studies, Khon Kaen University and a Science Achievement Scholarship of Thailand (SAST). We are deeply indebted to Dr. Chanaporn Suttinun, who provided part of the *Megabranchiella* specimens to this project. We are thankful to our colleagues for their kindness and support throughout field trips. We would like to thank the Department of Biology, Faculty of Science at Khon Kaen University for facility support.

References

- Ditsche-Kuru P, Koop JHE, Gorb SN (2010) Underwater attachment in current: The role of setose attachment structures on the gills of the mayfly larvae *Epeorus assimilis* (Ephemeroptera, Heptageniidae). *The Journal of Experimental Biology* 213(11): 1950–1959. <https://doi.org/10.1242/jeb.037218>
- Gattolliat J-L (2012) Two new genera of Baetidae (Ephemeroptera) from Borneo (East Kalimantan, Indonesia). *Annales de Limnologie-International Journal of Limnology* 48(2): 187–199. <https://doi.org/10.1051/limn/2012012>
- Gattolliat J-L, Nieto C (2009) The family Baetidae (Insecta: Ephemeroptera): synthesis and future challenges. *Aquatic Insects* 31(sup1): 41–62. <https://doi.org/10.1080/01650420902812214>
- Gattolliat J-L, Sartori M (1999) A new species of *Afrobaetodes* (Ephemeroptera: Baetidae) and first report of this genus from Madagascar. *Annales de Limnologie – International Journal of Limnology* 35(3): 179–184. <https://doi.org/10.1051/limn/1999025>
- Jacobus LM, Macadam CR, Sartori M (2019) Mayflies (Ephemeroptera) and their contributions to ecosystem services. *Insects* 10(6): 1–26. <https://doi.org/10.3390/insects10060170>
- Kaltenbach T, Garces JM, Gattolliat J-L (2020) A new genus of Baetidae (Insecta, Ephemeroptera) from Southeast Asia. *European Journal of Taxonomy* 612(612): 1–32. <https://doi.org/10.5852/ejt.2020.612>
- Kaltenbach T, Garces JM, Gattolliat J-L (2021) *Philibaetis* gen. nov., a new genus from the Philippines (Ephemeroptera, Baetidae). *Deutsche Entomologische Zeitschrift* 68(1): 1–20. <https://doi.org/10.3897/dez.68.59462>
- Kluge NJ (2004) *The phylogenetic system of Ephemeroptera*. Kluwer Academic Publishers, Dordrecht, 442 pp. <https://doi.org/10.1007/978-94-007-0872-3>
- Kluge NJ, Novikova EA (2011) Systematics of the mayfly taxon *Acentrella* (Ephemeroptera: Baetidae), with description of new Asian and African species. *Russian Entomological Journal* 20(1): 1–56. <https://doi.org/10.15298/rusentj.20.1.01>

- Kluge NJ, Kumbakonam G, Selvakumar C, Kubendran T (2013) Notes about *Acentrella* (*Liebebiella*) *vera* (Müller-Liebenau, 1982) (= *Pseudocloeon difficile* Müller-Liebenau, 1982 syn. n.= *Platybaetis arunachalae* Selvakumar, Sundar and Sivaramakrishnan, 2012 syn. n.) (Ephemeroptera: Baetidae). *Oriental Insects* (35): 63–70. <https://doi.org/10.1080/01650424.2014.980272>
- Sartori M, Brittain JE (2015) Order Ephemeroptera. In: Thorp J, Rogers DC (Eds) *Ecology and General Biology: Thorp and Corvich's Freshwater Invertebrates: 873–891*. [Academic Press, Boston] <http://doi.org/10.3897/dez.68.59462>
- Sroka P, Arnekleiv J (2010) Two new species of *Acentrella* Bengtsson, 1912 (Ephemeroptera, Baetidae) from Kazakhstan with notes on the Palaearctic fauna. *Zootaxa* 2693(1): 1–20. <https://doi.org/10.11646/zootaxa.2693.1.1>
- Suttinun C, Gattolliat JL, Boonsoong B (2020) *Cymbalocloeon* gen. nov., an incredible new mayfly genus (Ephemeroptera: Baetidae) from Thailand. *PLoS ONE* 15(10): e0240635. <https://doi.org/10.1371/journal.pone.0240635>
- Suttinun C, Kaltenbach T, Gattolliat J-L, Boonsoong B (2021) A new species and first record of the genus *Procerobaetis* Kaltenbach & Gattolliat, 2020 (Ephemeroptera, Baetidae) from Thailand. *ZooKeys* 1023: 13–28. <https://doi.org/10.3897/zookeys.1023.61081>
- Waltz RD, McCafferty WP (1987) Systematics of *Pseudocloeon*, *Acentrella*, *Baetiella* and *Liebebiella*, new genus (Ephemeroptera: Baetidae). *Journal of the New York Entomological Society* 95(4): 553–568.
- Zhou CF (2010) Accessory gills in mayflies (Ephemeroptera). *Stuttgarter Beiträge zur Naturkunde A* 3: 79–84.

Description and phylogenetic analysis of two new *Episinus* (Araneae, Theridiidae) species from China

Fengjie Liu^{1,2}, Ingi Agnarsson^{2,3}, Jie Liu^{1,2,4}, Yang Zhu^{1,5}

1 Hubeiate Key Laboratory of Regional Development and Environmental Response, Faculty of Resources and Environmental Science, Hubei University, Wuhan 430062, China **2** State Key Laboratory of Biocatalysis and Enzyme Engineering, School of Life Sciences, Hubei University, Wuhan 430062, Hubei, China **3** Faculty of Life and Environmental Sciences, University of Iceland, Sturlugata 7, 102 Reykjavik, Iceland **4** School of Nuclear Technology and Chemistry and Biology, Hubei University of Science and Technology, Xianning 437100, Hubei, China **5** Wuhan Lujia Technology Co., Ltd, Wuhan 430114, Hubei, China

Corresponding author: Yang Zhu (zhu@hubu.edu.cn)

Academic editor: Shuqiang Li | Received 11 July 2022 | Accepted 8 October 2022 | Published 19 October 2022

<https://zoobank.org/021F82C7-5C47-4491-BB36-E3D95F395FEE>

Citation: Liu F, Agnarsson I, Liu J, Zhu Y (2022) Description and phylogenetic analysis of two new *Episinus* (Araneae, Theridiidae) species from China. ZooKeys 1125: 33–46. <https://doi.org/10.3897/zookeys.1125.90212>

Abstract

The spider genus *Episinus* Walckenaer, 1809 currently contains 66 species worldwide, mostly in warm temperate to tropical areas. This paper describes two new Chinese *Episinus* species: *E. ornithorrhynchus* **sp. nov.** (♂♀) and *E. papilionaceus* **sp. nov.** (♀). We add these two new and one known *Episinus* species to the phylogenetic data matrix of Liu et al. 2016 and reanalyze the data. The new phylogeny recovers the monophyly of *Episinus* and supports its division into two groups, a finding also supported by morphology.

Keywords

New species, phylogenetic, taxonomy

Introduction

Currently, the Theridiidae Sundevall, 1833, constitutes one of the largest families of spider, with 2539 described species in 125 genera distributed worldwide. In China, there are 380 species of Theridiidae, and they belong to 54 genera (World Spider Catalog 2022). The theridiid subfamily Spintharinae currently consists of 10 genera: *Brunepisinus* Yoshida & Koh, 2011; *Chrosiothes* Simon, 1894; *Episinus* Walckenaer

in Latreille, 1809; *Moneta* O. Pickard-Cambridge, 1870; *Pycnoepisinus* Wunderlich, 2008; *Spintharus* Hentz, 1850; *Thwaitesia* O. Pickard-Cambridge, 1881; *Stemmops* O. Pickard-Cambridge, 1894; *Neopisinus* Marques, Buckup & Rodrigues, 2011; *Janula* Strand, 1932 (Agnarsson 2004; Arnedo et al. 2004; Marques et al. 2011; Durán-Barron et al. 2013; Liu et al. 2016; Vanuytven 2021; Rodrigues et al. 2022).

At present, the genus *Episinus* has 66 described species and of which only 10 have been reported in China (World Spider Catalog 2022). More than half of these species are widespread and also recorded in the Nearctic, Japan, Europe, and Africa (Levi 1955; Yoshida 1985; Okuma 1994; Zhu 1998; Song et al. 1999). *Episinus* differs from other genera of the Spintharinae by the straight shape of the opisthosoma in lateral view, and in dorsal view with median or posterior humps (Durán-Barron et al. 2013; Rodrigues et al. 2022). Rodrigues et al. 2022 provided a phylogenetic framework based on a morphological analysis, which suggested that *Janula* and some species of *Episinus* belong to the same group, and the genus *Episinus* appeared polyphyletic. The genus *Moneta* is similar to *Episinus*, but according to Okuma (1994) can be separated by the alignment of the eyes, the length ratio of the metatarsus to the tarsus, and the structure of the male palp. Our phylogenetic results clearly differentiate between these genera and strongly support the monophyly of the genus *Episinus* (Fig. 6).

We describe herein two new *Episinus* species from China, *E. ornithorrhynchus* sp. nov. and *E. papilionaceus* sp. nov. We add these species, as well as *E. nubilus* Yaginuma, 1960, to the data matrix of Liu et al. (2016) and rerun phylogenetic analyses.

Materials and methods

All specimens were kept in absolute ethanol and examined with an Olympus SZX7 stereomicroscope; details were further investigated with an Olympus BX51 compound microscope. Male palps and female genitalia were examined and photographed after dissection from the spider bodies, epigynes were cleared with Proteinase K, and palps were studied after immersion in KOH; habitus photos were obtained using a Leica 205C digital microscope. Left palps are illustrated. All specimens are deposited at the Centre for Behavioural Ecology and Evolution, College of Life Sciences, Hubei University, Wuhan, China (CBEE).

Leg measurements are shown as total length (femur, patella, tibia, metatarsus, tarsus). The number of spines is listed for each segment in the following order: prolateral, dorsal, retrolateral, and ventral (in femora and patellae ventral spines are absent, and the fourth digit is omitted in the spination formula). The terminology used in the text, figure legends, and palp homologies follow Agnarsson (2004) and Agnarsson et al. (2007). All measurements are given in millimeters.

Molecular data

We used the dataset from Liu et al. (2016) and added to it *E. ornithorrhynchus* sp. nov. and *E. papilionaceus* sp. nov., as well as *E. nubilus* Yaginuma, 1960. The final

dataset includes 62 theridiid genera and two outgroups representing Nesticidae and Synotaxidae. Sequences for two mitochondrial genes: cytochrome c oxidase subunit I (COI) and ribosomal RNA16S (16S), and three nuclear genes, ribosomal RNAs 18S (18S) and 28S (28S) and histone (H3), were collected for the newly added species. The phylogenetic data collection and analytical methods used conform to Liu et al. (2016).

The appropriate models for the Bayesian analysis were selected with jModelTest2 on XSEDE (2.1.6) (Darriba et al. 2012) using the Akaike information criterion (AIC) (Posada 2008). Bayesian analysis for morphology was carried out using MrBayes 3.2.7a on XSEDE (Huelsenbeck and Ronquist 2001) and maximum likelihood with IQ-Tree stable release 1.6.12 (Chernomor et al. 2016; Nguyen et al. 2015) of individual gene trees as well as concatenated matrices. All large analyses were run in parallel on the CIPRES cluster at the San Diego Supercomputing Center (Miller et al. 2010).

Abbreviations used

ALE—anterior lateral eyes, **AME**—anterior median eyes, **Atr**—atrium, **C**—conductor, **CD**—copulatory duct, **CY**—cymbium, **E**—embolus, **FD**—fertilization duct, **MA**—median apophysis, **MS**—medium septum, **PLE**—posterior lateral eyes, **PME**—posterior median eyes, **I–IV**—1st to 4th leg, **S**—spermathecae, **Teg**—tegulum, **CBEE**—Centre for Behavioural Ecology and Evolution, College of Life Sciences, Hubei University, Wuhan, China.

Results

Taxonomy

Family Theridiidae Sundevall, 1833

Genus *Episinus* Walckenaer in Latreille, 1809

Type species. *Episinus truncates* Latreille, 1809.

Episinus ornithorrhynchus sp. nov.

<https://zoobank.org/D15231DB-9F9B-4A5D-A517-40A941EA92B6>

Figs 1A–D, 2A–E, 3A, B, 5

Type material. **Holotype:** ♂, CHINA, **Yunnan Province:** Mengsong Town, Mengsong Township Central Primary School, (22°4'12"N, 100°33'36"E, 1340 m alt.), 1 August 2020, Z.C. Li, R. Zhong, W.Z. Deng, W. Zhang, and Y.T. Zhang leg. **Paratypes:** 1♂2♀, same data as holotype; **Yunnan Province:** 2♀, Menglun Town, Baka Xiaozhai, (22°4'12"N, 101°12'0"E, 810 m alt.), 24 July 2020, Z.C. Li, R. Zhong, W.Z. Deng, W. Zhang, and Y.T. Zhang leg.

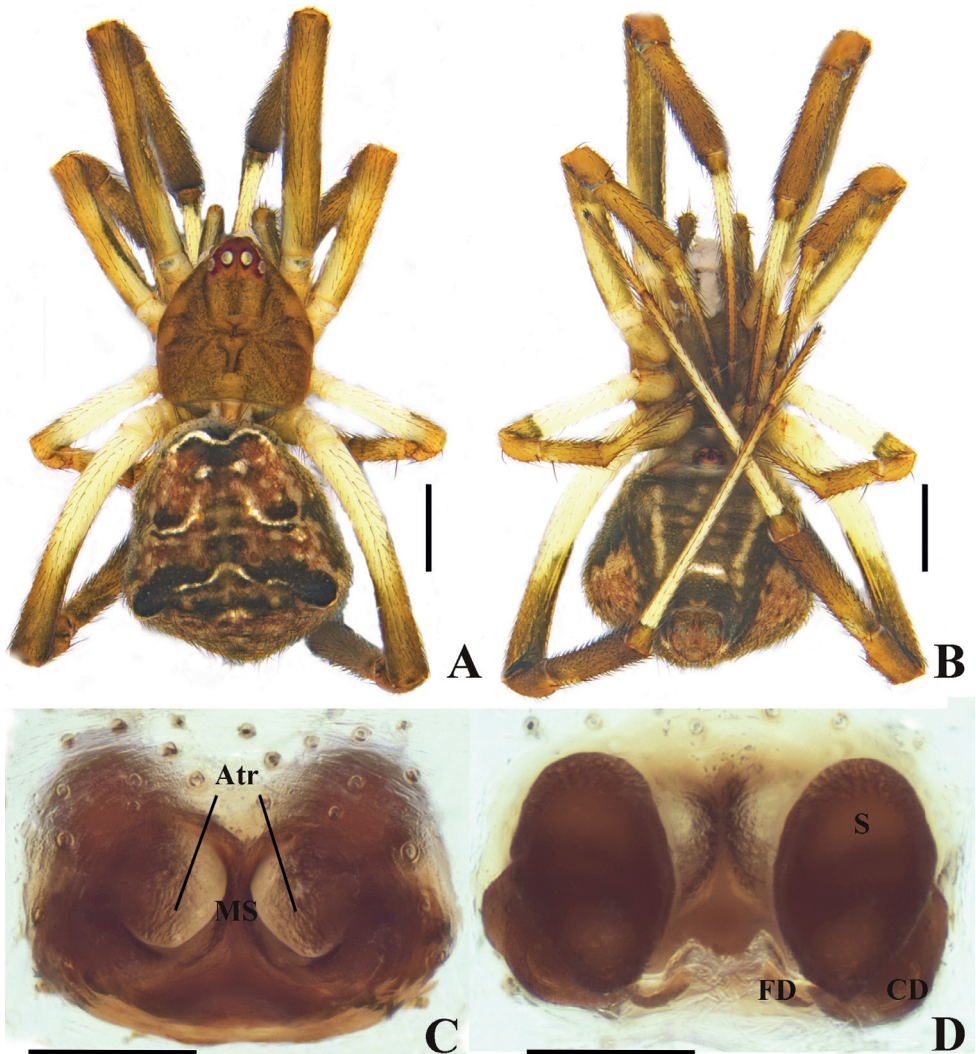


Figure 1. *Episinus ornithorhynchus* sp. nov. **A, B** female habitus **A** dorsal **B** ventral **C, D** epigynum in alcohol **C** ventral **D** dorsal. Abbreviations: Atr—atrium, CD—copulatory duct, FD—fertilization duct, MS—medium septum, S—spermathecae. Scale bars: 1 mm (**A, B**); 0.1 mm (**C, D**).

Diagnosis. Males are similar to *E. baoshanensis* Liu et al. (2019) but can be distinguished from them by the palpal structure: 1) embolus extends along the left lower lateral aspect of the genital bulb to the posterior margins, but the embolus mainly encircles the left upper lateral and anterior margins of the bulb in *E. baoshanensis* (Figs 2C, D, 3A, B); 2) conductor with a sharp tip in ventral view and not bifurcated, but conductor sclerotized and tip bifurcated in *E. baoshanensis* (Figs 2C, 3A). Females are similar to *E. nubilus* but can be distinguished from them by the direction of the copulatory duct: fertilization ducts are slightly shorter in the new species, but long and C-shaped in *E. nubilus* (Fig. 1D).

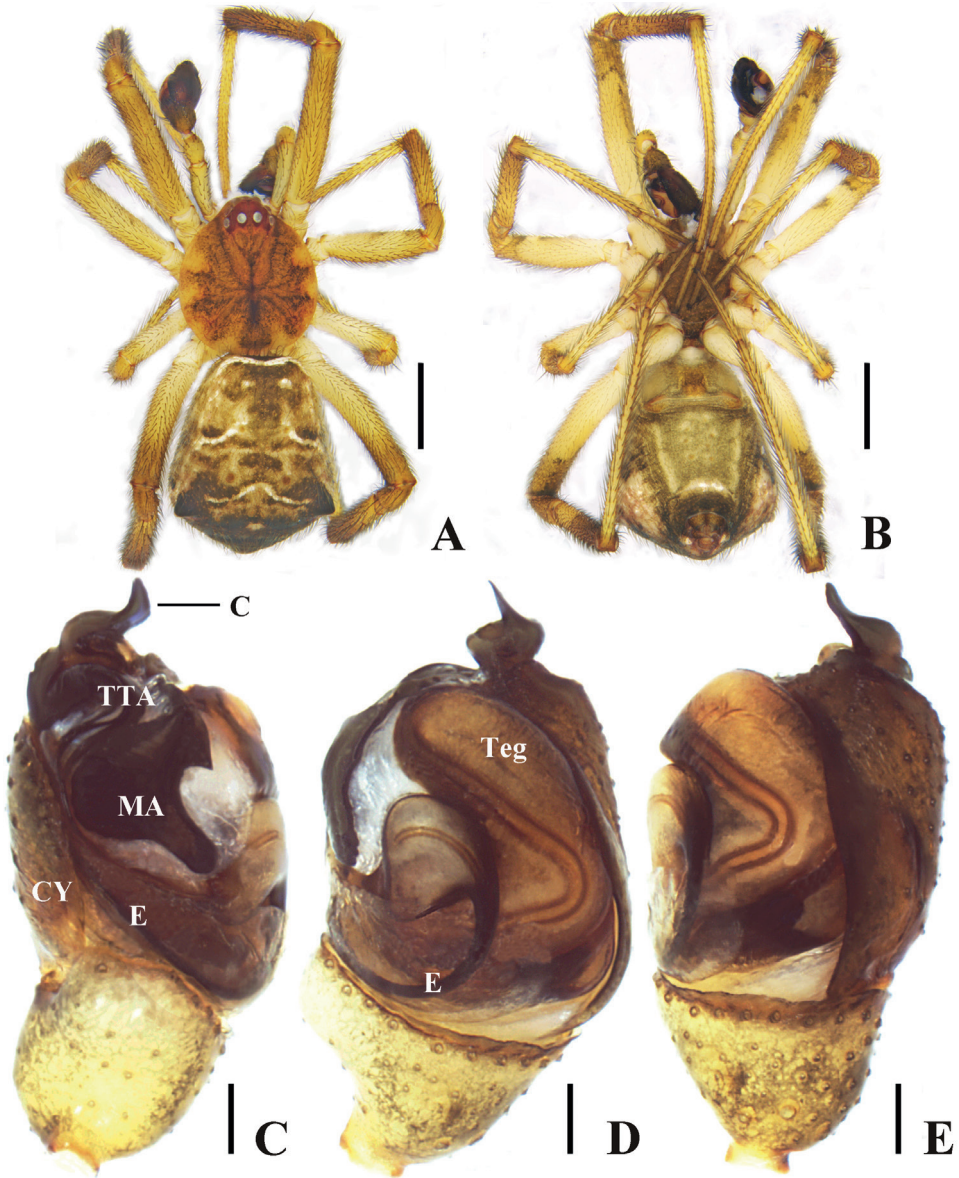


Figure 2. *Episinus ornithorrhynchus* sp. nov. **A, B** male habitus **A** dorsal **B** ventral **C–E** palp in alcohol **C** prolateral **D** ventral **E** retrolateral. Abbreviations: C—conductor, CY—cymbium, E—embolus, MA—Median apophysis, Teg—tegulum. Scale bars: 1 mm (**A, B**); 0.1 mm (**C–E**).

Etymology. The specific name is derived from the Latin adjective *ornithorrhynchus*, meaning bird's beak, referring to the shape of the conductor; adjective.

Description. Male (paratype): total length 3.79; prosoma length 1.60, width 1.39; opisthosoma length 2.19, width 1.67; eye diameters: ALE 0.10, AME 0.10, PLE 0.10, PME 0.10; eye interdistances: AME–AME 0.10, AME–ALE 0.05, PME–PME

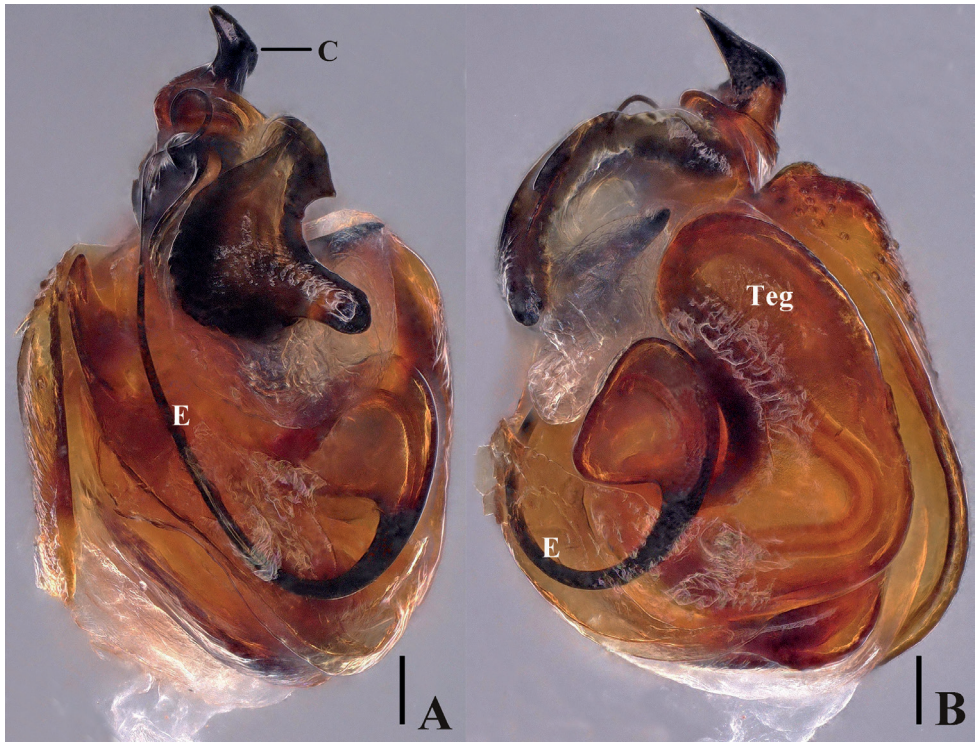


Figure 3. *Episinus ornithorrhynchus* sp. nov. **A, B** male palp (previously soaked with KOH) in alcohol. **A** prolateral **B** ventral. Abbreviations: C—conductor, E—embolus, Teg—tegulum. Scale bars: 0.1 mm.

0.10, PME–PLE 0.05; clypeus height 0.24; leg measurements: I 6.84 (1.83, 0.41, 2.11, 1.78, 0.71), II 5.04 (1.46, 0.39, 1.14, 1.35, 0.70), III 3.72 (1.11, 0.35, 0.73, 0.96, 0.57), IV 7.76 (2.28, 0.52, 1.70, 2.40, 0.86). Leg formula: IV, I, II, III. Overall, the color was slightly lighter and as in females (Fig. 2A, B).

Palp (Figs 2C–E, 3A, B). Subtegulum mostly covered by tegulum. Embolus originates at center of palp, a slightly triangular basement that curves upward clockwise. Conductor sclerotized, with a sharp tip extending over apex of cymbium.

Female (holotype): total length 4.25; prosoma length 1.70, width 1.49; opisthosoma length 2.55, width 2.05; eye diameters: ALE 0.10, AME 0.10, PLE 0.10, PME 0.10; eyes interdistances: AME–AME 0.10, AME–ALE 0.06, PME–PME 0.08, PME–PLE 0.08; clypeus height 0.25; leg measurements: I 7.44 (2.05, 0.61, 1.79, 2.23, 0.76), II 5.06 (1.52, 0.50, 1.06, 1.30, 0.68), III 3.91 (1.28, 0.33, 0.68, 0.93, 0.69), IV 8.25 (2.36, 0.80, 1.65, 2.46, 0.98). Leg formula: IV, I, II, III. Carapace yellowish to reddish brown, with a deep transverse depression. Sternum gray-black, slightly longer than wide. Femur and tibia to tarsus yellowish white, and distal patella reddish brown (Fig. 1A, B). Opisthosoma yellowish to orange-brown, with longitudinal white stripes in ventral view, extending posteriorly and short humps on each side. Opisthosoma dorsally grayish black, with a rectangular dark spot (Fig. 1B).

Epigyna (Fig. 1C–D). Atria separated by median septum. Spermathecae slightly oval with two parallel stripes on middle part; fertilization ducts shorter.

Variation. Total length male 3.75–3.79 ($n = 2$), female 4.10–4.25 ($n = 4$).

Distribution. China (Yunnan Province) (Fig. 5).

***Episinus papilionaceus* sp. nov.**

<https://zoobank.org/83AD0CDA-5904-4EC9-8BB7-5E14133D2CC6>

Figs 4A–D, 5

Type material. Holotype: ♀, CHINA, **Hunan Province:** Zhangjiajie City, Badagong Mountain National Nature Reserve (29°47'24"N, 110°6'0"E, 1395 m alt.), 2 June 2018, F.X. Liu and Z.C. Li leg.

Diagnosis. This new species is similar to *E. xiushanicus* Zhu, 1998 in having a peach-shaped structure at the posterior part of the epigynal field but can be distinguished from them by the following characteristics: 1) abdomen without spinous process in ventral view, but the ventral protuberance is spinous in *E. xiushanicus* (Fig. 4A); 2) spermathecae slightly S-shaped in the new species but W-shaped in *E. xiushanicus* (Fig. 4D).

Etymology. The specific name is derived from the Latin adjective *papilionaceus*, meaning butterfly-shaped, referring to the shape of the epigynum; adjective.

Description. Male unknown. Female (holotype): total length 4.29. Prosoma length 1.55, width 1.44; opisthosoma length 2.74, width 2.55; eye diameters: ALE 0.11, AME 0.11, PLE 0.09, PME 0.09; eye interdistances: AME–AME 0.10, AME–ALE 0.05, PME–PME 0.15, PME–PLE 0.08; clypeus height 0.50; leg measurements: I 8.00 (2.48, 0.61, 1.83, 2.47, 0.61), II 5.46 (1.78, 0.41, 1.17, 1.42, 0.68), III 4.77 (1.43, 0.34, 0.76, 1.83, 0.41), IV 8.57 (2.75, 0.69, 2.09, 2.34, 0.70). Leg formula: IV, I, II, III. Carapace yellowish brown, with two parallel elongate yellowish-white markings posterior to eyes, and submarginal black markings laterally. Posterior median eyes slightly mound-shaped and surrounding area black. Sternum grayish yellow, slightly longer than wide. Legs yellow, with brown markings. Opisthosoma yellowish black, with irregular black stripes in ventral view and extending posteriorly. Opisthosoma dorsally yellowish black, with tiny white to black dots (Fig. 4A, B).

Epigyna (Fig. 4C, D). Ventral view wider than long, with a peach-shaped structure at posterior margin. Copulatory ducts thick and curved. Fertilization ducts arising medially.

Distribution. China (Hunan Province) (Fig. 5).

Phylogenetic analyses

Our phylogeny tree supports the fundamental findings of prior studies, the monophyly of Theridiidae and seven subfamilies of Theridiidae: Latrodectinae, Pholcommatinae, Argyroderinae, Hadrotarsinae, Spintharinae, Anelosiminae, and Theridiinae.

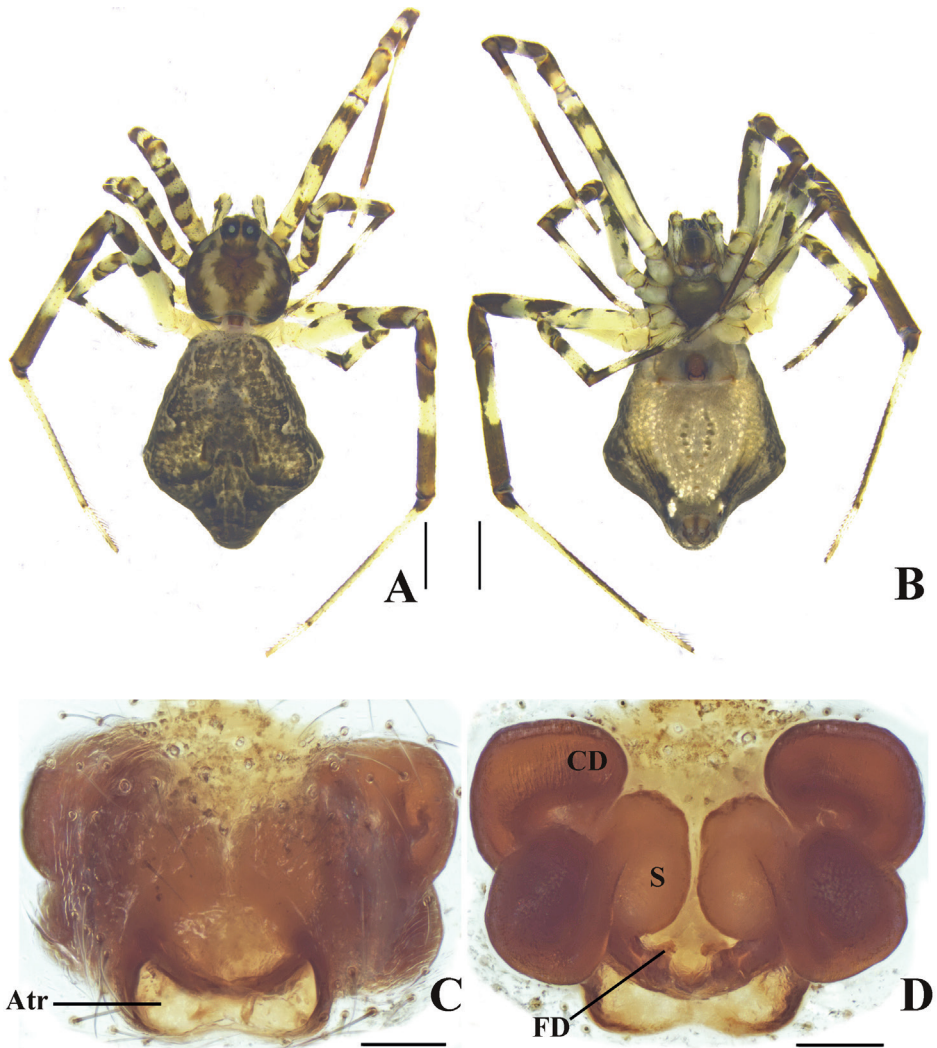


Figure 4. *Episinus papilionaceus* sp. nov. **A, B** female habitus **A** dorsal **B** ventral **C, D** epigynum in alcohol **C** ventral **D** dorsal. Abbreviations: Atr—atrium, CD—copulatory duct, FD—fertilization duct, S—spermathecae. Scale bars: 1 mm (**A, B**); 0.1 mm (**C, D**).

From the results (Fig. 6), the Latrodectinae is the earliest branching subfamily. Pholcommatinae is polyphyletic and redefined by removing *Styposis* and *Phoroncidia* that must be placed in insertae sedis until further data become available. Argyrodinae is in the same monophyletic group as the *Phoroncidia*, and these are sisters to Spintharinae and Hadrotarsinae. Our results strongly support the sister relationship between Spintharinae and Hadrotarsinae, two specialized groups with most of their species either building reduced webs or having abandoned web building and hunting ants as prey. Anelosiminae is recovered as a monophyletic sister to Theridiinae.

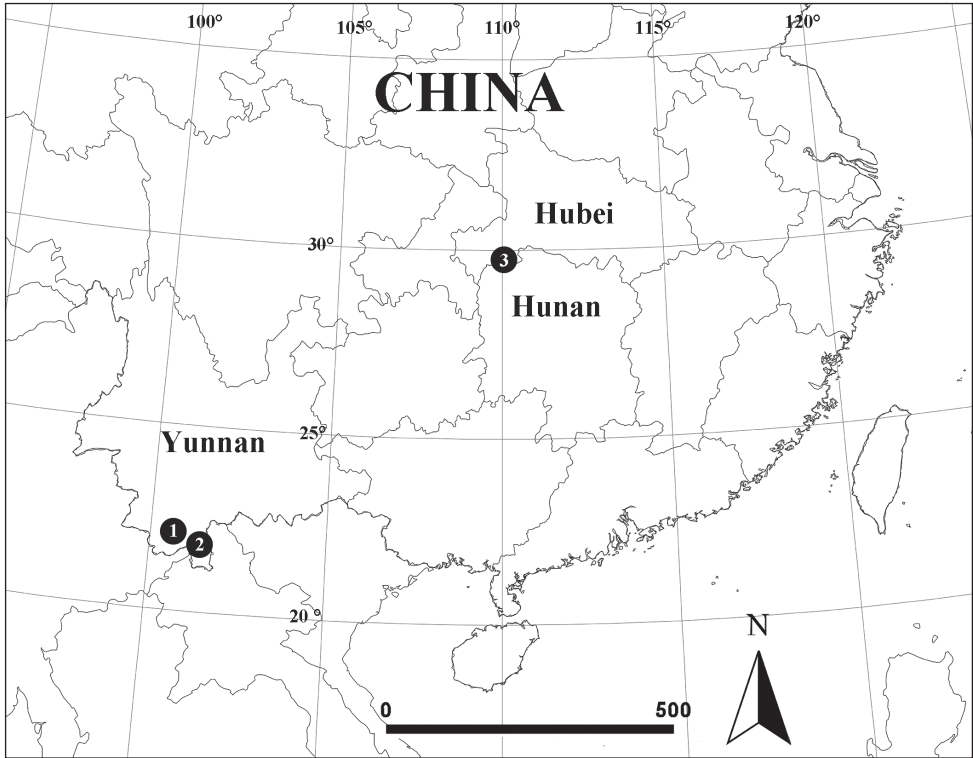


Figure 5. Locality records for two species of *Episinus*: 1 = *Episinus ornithorrhynchus* sp. nov., 2 = *Episinus papilionaceus* sp. nov.

Our results strongly support the monophyly of the subfamily Spintharinae. We have also found compelling evidence to support the monophyly of the genus *Episinus*, although this is weak due to the lack of data for the most-related genera: *Janula*, *Neopisinus*, and *Brunepisinus*. Regardless, we found evidence for the first time for the division of the genus *Episinus* into two groups. The “angulatus” group to which *E. ornithorrhynchus* sp. nov., belongs is characterized by the male embolus, and the “nubilus” group to which *E. papilionaceus* sp. nov. belongs is characterized by female atria. These two groups can be clearly diagnosed based on the following morphological traits: in the “angulatus” group, the male embolus originates at the center of the palp and is close to the cymbium; in the “nubilus” group, female atria are separated by a medium septum. *Episinus nubilus* Yaginuma, 1960, here newly added to the phylogenetic matrix, was found to be closely related to *E. ornithorrhynchus* sp. nov. Our findings suggest that the genus *Moneta* O. Pickard-Cambridge, 1871 which is morphologically similar to *Episinus*, is unrelated to it, but instead related to the genus *Stemmops* O. Pickard-Cambridge, 1894. The genus *Thwaitesia* O. Pickard-Cambridge, 1881 was recovered as sister to *Episinus*, with strong support (Bayesian PP 97.4%, ML bootstrap 95%). This is similar to the morphological phylogeny of Durán-Barron et

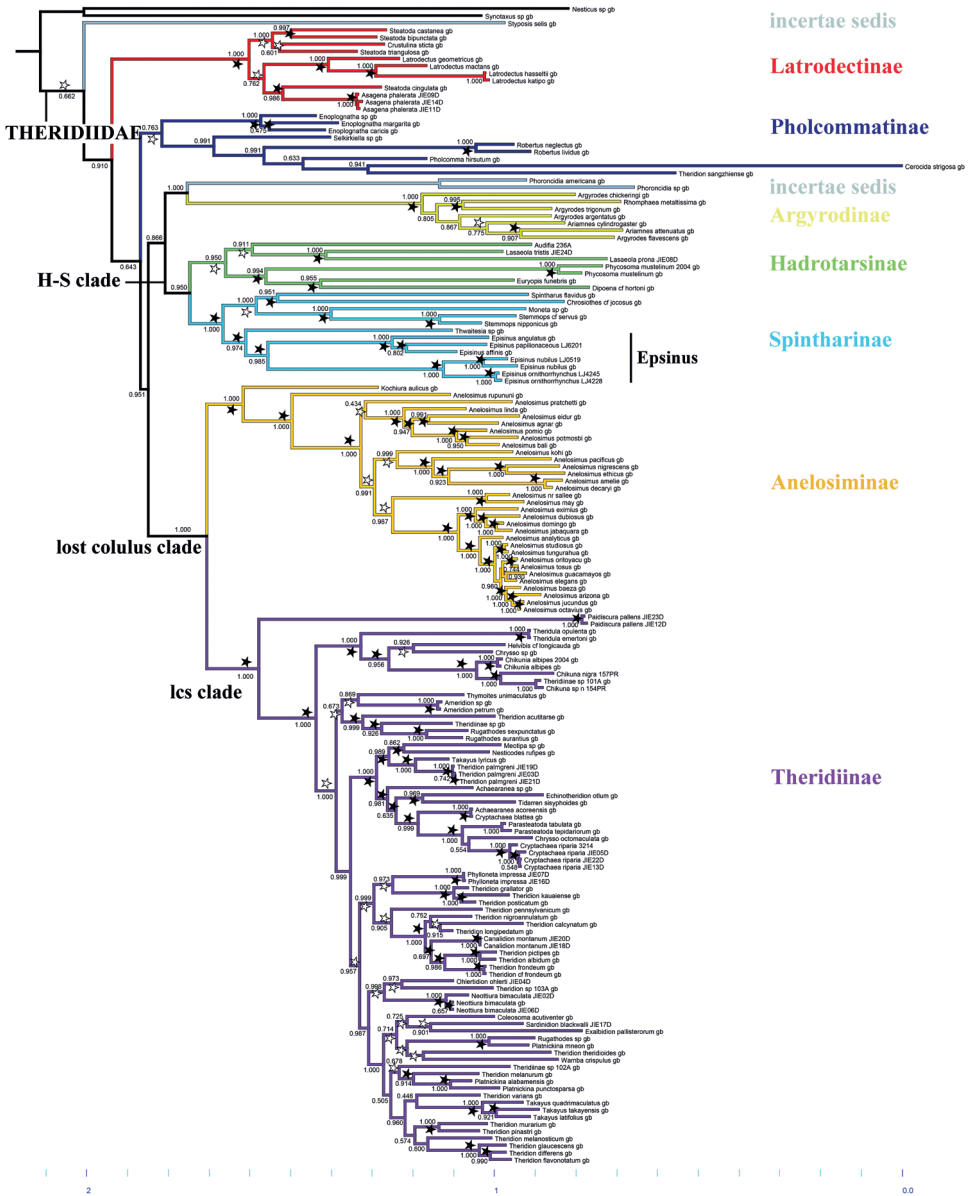


Figure 6. Bayesian analysis of molecular and morphological data of the focal dataset, a matrix excluding all taxa with over 70% missing data. Numbers on nodes are posterior probabilities; bootstrap support from ML analyses is indicated: solid stars indicate bootstrap support values >95%, the gray stars >50–95%, and nodes with less than 50% support lack stars.

al. (2013) but in stark contrast with the morphological phylogeny of Rodrigues et al. (2022), which places *Thwaitesia* far from *Episimus* and *Moneta*. Unlike our study, which contains both molecular and morphological data, the relationship between the genera was discussed more from an evolutionary perspective.

Discussion

Based on the combination of molecular and morphological data, our knowledge of the phylogeny of Theridiidae is rapidly growing (Agnarsson 2004; Liu et al. 2016). The phylogeny serves as a useful tool for comparative studies and as a guide to improved classification. Our phylogeny (Fig. 6) refined that of Liu et al. (2016) by focusing on the genus *Episinus*. Our results offer the strongest test of the monophyly of *Episinus* to date and indicate that the genus can be clearly divided into two groups, supported independently by molecular and morphological evidence.

Our results also have implications for the broader phylogeny of Theridiidae in as much as they differ from Liu et al. (2016). As found previously, the placement of the “orphan” pholcommatines *Styposis* and *Phoroncidia* is unstable across different analyses, with the current results indicating *Styposis* is close to Latrodectinae and *Phoroncidia* is close to Argyrodinae. Latrodectinae includes some of the largest species and of which the genus *Steatoda* Sundevall, 1833 is polyphyletic. *Theridion sangzhiense* Zhu, 1998 is here again placed within Pholcommatinae, most likely indicating an error in species identification of GenBank materials. Different from previous studies, we recovered Argyrodinae (plus *Phoroncidia*) as a sister to Spintharinae plus Hadrotarsinae. If this group is true, these taxa may be united by extreme reduction or loss of webs. Importantly, we recovered *Audifia* as a member of Hadrotarsinae, as expected based on morphology, but in contrast to Liu et al. (2016). This result indicates the monophyly of Hadrotarsinae, although this subfamily has strong morphological diversity (including two pairs of spermathecae and modifications of spinnerets and palpal claws). The undisputed sister relationship of Anelosiminae and Theridiinae was again supported.

Our study focuses mainly on the subfamily Spintharinae and confirmed its monophyly. The genera *Spintharus*, *Thwaitesia*, and *Episinus* all tend to build an H-shaped web with the animal facing downwards and holding onto parts of the web with its feet, presumably specializing on pedestrian prey such as ants (Agnarsson 2004; Eberhard et al. 2008). A close relationship between *Thwaitesia* and *Episinus* was proposed by Durán-Barron et al. (2013) based on morphology. However, also based on morphology, Rodrigues et al. (2022), found that *Thwaitesia* is unrelated to *Episinus*, and morphological evidence showed that humps are present on the abdomen in *Episinus* but absent in *Thwaitesia*. Further evidence for the relationship between *Thwaitesia* and *Episinus* may come from the structure of the egg sac (Eberhard et al. 2008). Most theridiid egg sacs have a densely spun outermost layer, while the outermost fibers are loosely woven in *Episinus* and *Thwaitesia* (Agnarsson 2004). However, there are insufficient data available on egg sacs of other spintharines.

We found support for the monophyly of *Episinus* and its division into two morphologically well-defined branches. The “angulatus” group includes *E. angulatus* (Blackwall, 1836), *E. papilionaceus* sp. nov., and *E. affinis* Bösenberg & Strand, 1906. This group differs from the “nubilus” group, which includes *E. nubilus* Yaginuma, 1960 and *E. ornithorrhynchus* sp. nov., in the origin of the male embolus and the ventral view of female epigynal. The “angulatus” group can be characterized by the male embolus originating closer to the cymbium at the lateral edge of the palp, whereas in

the “nubilus” group the embolus arises in clockwise direction upward bending in the middle of the palp. The “angulatus” group presents only one large atrium in the ventral view of the female epigynal, but the “nubilus” group has two atria separated by the medium septum. The medium septum is a projection in the middle of the atrium and has a guiding function (Yin et al. 2012). In future studies of *Episinus* and Spintharinae, it will be critical to include other spintharine genera, especially those previously included in *Episinus*, such as *Janula*, *Neopisinus*, and *Brunepisinus*.

Acknowledgements

This research was funded by the National Natural Sciences Foundation of China (NSF C-31970406/31772420/31573236) and National Science & Technology Fundamental Resources Investigation Program of China (grant no. 2019FY101800).

References

- Agnarsson I (2004) Morphological phylogeny of cobweb spiders and their relatives (Araneae, Araneoidea, Theridiidae). *Zoological Journal of the Linnean Society* 141(4): 447–626. <https://doi.org/10.1111/j.1096-3642.2004.00120.x>
- Agnarsson I, Maddison WP, Avilés L (2007) The phylogeny of the social *Anelosimus* spiders (Araneae: Theridiidae) inferred from six molecular loci and morphology. *Molecular Phylogenetics and Evolution* 43(3): 833–851. <https://doi.org/10.1016/j.ympev.2006.09.011>
- Arnedo MA, Coddington JA, Agnarsson I, Gillespie RM (2004) From a comb to a tree: Phylogenetic relationships of the comb-footed spiders (Araneae, Theridiidae) inferred from nuclear and mitochondrial genes. *Molecular Phylogenetics and Evolution* 31(1): 225–245. [https://doi.org/10.1016/S1055-7903\(03\)00261-6](https://doi.org/10.1016/S1055-7903(03)00261-6)
- Chernomor O, Haeseler AV, Minh BQ (2016) Terrace aware phylogenomic inference from supermatrices. *Quantitative Biology* 65: 997–1008. <https://doi.org/10.1093/sysbio/syw037>
- Darriba D, Taboada GL, Doallo R, Posada D (2012) JModelTest 2: More models, new heuristics and parallel computing. *Nature Methods* 9(8): 772. <https://doi.org/10.1038/nmeth.2109>
- Durán-Barron CG, Rosas MV, Contreras-Ramos A (2013) Phylogenetic relationships of the comb-footed spider subfamily Spintharinae (Araneae, Araneoidea, Theridiidae), with generic diagnoses and a key to the genera. *Zootaxa* 3666(2): 171–193. <https://doi.org/10.11646/zootaxa.3666.2.4>
- Eberhard WG, Agnarsson I, Levi HW (2008) Web forms and the phylogeny of theridiid spiders (Araneae: Theridiidae): chaos from order. *Systematics and Biodiversity* 6(4): 415–475. <https://doi.org/10.1017/S1477200008002855>
- Huelsenbeck JP, Ronquist F (2001) MRBAYES: Bayesian inference of phylogenetic trees. *Bioinformatics* 17(8): 754–755. <https://doi.org/10.1093/bioinformatics/17.8.754>

- Levi HW (1955) The spider genera *Episinus* and *Spintharus* from North America, Central America and the West Indies (Araneae: Theridiidae). *Journal of the New York Entomological Society* 62: 65–90.
- Liu J, May-Collado LJ, Pekár S, Agnarsson I (2016) A revised and dated phylogeny of cobweb spiders (Araneae, Araneoidea, Theridiidae): A predatory Cretaceous lineage diversifying in the era of the ants (Hymenoptera, Formicidae). *Molecular Phylogenetics and Evolution* 94: 658–675. <https://doi.org/10.1016/j.ympev.2015.09.023>
- Liu F, Irfan M, Peng XJ (2019) Two new species of Theridiidae (Arachnida, Araneae) from Yunnan province, China. *Journal of Asia-Pacific Biodiversity* 12(3): 394–399. <https://doi.org/10.1016/j.japb.2019.01.012>
- Marques MAL, Buckup EH, Rodrigues ENL (2011) Novo gênero neotropical de Spintharinae (Araneae, Theridiidae). *Iheringia, Série Zoologia* 101(4): 372–381. <https://doi.org/10.1590/S0073-47212011000300011>
- Miller MA, Pfeiffer W, Schwartz T (2010) Creating the CIPRES science gateway for inference of large phylogenetic trees. In: *Gateway Computing Environments Workshop (GCE) 2010*, 1–8. <https://doi.org/10.1109/GCE.2010.5676129>
- Nguyen LT, Schmidt HA, von Haeseler A, Minh BQ (2015) IQ-TREE: A fast and effective stochastic algorithm for estimating maximum likelihood phylogenies. *Molecular Biology and Evolution* 32(1): 268–274. <https://doi.org/10.1093/molbev/msu300>
- Okuma C (1994) Spiders of the genera *Episinus* and *Moneta* from Japan and Taiwan, with descriptions of two new species of *Episinus* (Araneae: Theridiidae). *Acta Arachnologica* 43(1): 5–25. <https://doi.org/10.2476/asjaa.43.5>
- Posada D (2008) JModelTest: Phylogenetic model averaging. *Molecular Biology and Evolution* 25(7): 1253–1256. <https://doi.org/10.1093/molbev/msn083>
- Rodrigues ENL, Rodrigues PES, Brescovit AD, Koh JKH (2022) An update on the phylogeny of Spintharinae with analysis based on morphological characters and taxonomy of *Janula* (Araneae, Theridiidae). *Organisms, Diversity & Evolution* 22(3): 749–787. <https://doi.org/10.1007/s13127-022-00547-x>
- Song DX, Zhu MS, Chen J (1999) *The Spiders of China*. Hebei Science and Technology Publishing House, Shijiazhuang, 640 pp.
- Vanuytven H (2021) The Theridiidae (Araneae) of the world. A key to the genera with the diagnosis and a study of the body length of all known species. *Arachnological Contributions. Newsletter Belgian Arachnological Society* 35(suppl.): 1–363.
- World Spider Catalog (2022) *World Spider Catalog, Version 23.0*. Natural History Museum Bern. <http://wsc.nmbe.ch> [Accessed on: 2022-6-10]
- Yaginuma T (1960) *Spiders of Japan in Colour*. Hoikusha, Osaka, 186 pp.
- Yin CM, Peng XJ, Yan HM, Bao YH, Xu X, Tang G, Zhou QS, Liu P (2012) *Fauna Hunan: Araneae in Hunan, China*. Hunan Science and Technology Press, Changsha, 1590 pp.
- Yoshida H (1985) A new spider of the genus *Episinus* (Araneae, Theridiidae) from Nagano Prefecture, central Japan. *Nihon Seibutsu Chiri Gakkai Kaiho* 40: 25–30.
- Zhu MS (1998) *Fauna Sinica: Arachnida: Araneae: Theridiidae*. Science Press, Beijing, 436 pp.

Supplementary material I

Table S1

Authors: Fengjie Liu, Ingi Agnarsson, Jie Liu, Yang Zhu

Data type: Genomic.

Explanation note: Phylogenetic analysis of the spider genus *Episinus* (Araneae: Theridiidae) and description of the two new species from China.

Copyright notice: This dataset is made available under the Open Database License (<http://opendatacommons.org/licenses/odbl/1.0/>). The Open Database License (ODbL) is a license agreement intended to allow users to freely share, modify, and use this Dataset while maintaining this same freedom for others, provided that the original source and author(s) are credited.

Link: <https://doi.org/10.3897/zookeys.1125.90212.suppl1>

Triplophysa daryoae, a new nemacheilid loach species (Teleostei, Nemacheilidae) from the Syr Darya River basin, Central Asia

Bakhtiyor Sheraliev¹, Yorkinoy Kayumova², Zuogang Peng¹

1 Key Laboratory of Freshwater Fish Reproduction and Development (Ministry of Education), Southwest University, School of Life Sciences, Chongqing 400715, China **2** Fergana State University, Faculty of Life Sciences, Fergana 150100, Uzbekistan

Corresponding author: Zuogang Peng (pzg@swu.edu.cn)

Academic editor: Sven Kullander | Received 17 April 2022 | Accepted 12 September 2022 | Published 19 October 2022

<https://zoobank.org/D5DC2DA5-4217-4C97-A1D5-165E87B66D10>

Citation: Sheraliev B, Kayumova Y, Peng Z (2022) *Triplophysa daryoae*, a new nemacheilid loach species (Teleostei, Nemacheilidae) from the Syr Darya River basin, Central Asia. ZooKeys 1125: 47–67. <https://doi.org/10.3897/zookeys.1125.85431>

Abstract

Triplophysa daryoae, new species, is described from the Sokh River, a former tributary of Syr Darya that today fails to reach the river, in the Sokh District, an exclave of Uzbekistan, surrounded by Kyrgyzstan. *Triplophysa daryoae* is distinguished from other species of *Triplophysa* in Central Asia by a truncate caudal fin with 13 or 14 branched rays, body without obvious mottling, dorsal-fin origin opposite to pelvic-fin insertion, and absence of the posterior chamber of the air bladder. Molecular data suggest that *Triplophysa daryoae* is closely related to *T. ferganaensis* from the Shakhimardan stream, a small tributary of Syr Darya in the Yordon village, another exclave of Uzbekistan in Kyrgyzstan. The two species were separated by a Kimura 2-parameter genetic distance of 2.8% in the mitochondrial DNA cytochrome *c* oxidase subunit I barcode region; they are also distinguished morphologically. A key to the species of *Triplophysa* in the Syr Darya basin and adjacent regions is provided.

Keywords

Fergana Valley, freshwater fish, ichthyofauna, phylogeny, taxonomy

Introduction

The genus *Triplophysa* Rendahl, 1933, comprises approximately 160 species (Fricke et al. 2022). The genus is widespread in western and central Asian waters, inland drainages of Balochistan, northwest to western Mongolia, and from the Qinghai-Tibet Plateau to the Yunnan-Guizhou Plateau in China (Zhu 1989; Wu and Wu 1992; Prokofiev 2017).

Syr Darya is the longest river in Central Asia and the second largest in volume after Amu Darya. It originates in the Fergana Valley at the confluence of the Naryn and Kara Darya, which flow from the Tian Shan Mountains and drain into the Aral Sea after passing through Uzbekistan, Tajikistan, and Kazakhstan. To date, eight species of *Triplophysa* species have been reported from the Syr Darya basin (Berg 1949; Turdakov 1963; Mitrofanov 1989; Sheraliev and Peng 2021a, b). The Fergana Valley is a mountainous region and its fish fauna differs from that of other regions in Uzbekistan. *Triplophysa dorsalis* (Kessler, 1872), *T. elegans* (Kessler, 1874), *T. ferganaensis* Sheraliev & Peng, 2021, and *T. strauchii* (Kessler, 1874) have been recorded from the rivers of the Fergana Valley (Turdakov 1963; Sheraliev and Peng 2021b). The occurrence of *T. stolickai* (Steindachner, 1866) in the Fergana Valley is controversial and requires additional in-depth taxonomic research (Sheraliev and Peng 2021b; Sheraliev and Kayumova 2022).

The Sokh River is a tributary of the Syr Darya. It flows through the Sokh exclave of Uzbekistan, which is surrounded by Kyrgyzstan, and enters the Fergana Region. At present, the river fails to reach Syr Darya because its water is used for irrigation. The ichthyofauna of the Sokh River is almost unexplored. Here we report a new species of loach from the Sokh River.

Materials and methods

Specimen sampling, preservation, and morphological analysis

Handling of specimens was consistent with the Republic of Uzbekistan Animal Welfare Laws (No. 545-I 26.12.1997; <https://lex.uz/docs/-31719>), guidelines, and policies approved by the Southwest University Local Ethics Committee for Animal Experiments. After euthanasia, specimens were fixed in 10% formalin and stored in 70% ethanol. The right-side pectoral fin was preserved in 95% ethanol for molecular analysis. Counts and measurements were performed following the procedures of Kottelat and Freyhof (2007) and, whenever possible, on the left side of the specimen. Measurements to the nearest 0.01 mm were acquired using digital calipers and performed point-to-point rather than based on projections. The nomenclature of the head pores follows Kottelat (1984). Standard length was measured from the tip of the upper jaw to the end of the hypural complex, whereas the length of the caudal peduncle was measured from the base of the last ray of the anal fin to the end of the hypural complex at the mid-height of the base of the caudal fin. The last two branched rays in the dorsal and

anal fins articulated on a single pterygiophore and were counted as single rays. Caudal-fin rays were counted separately in the upper and lower lobes; segmented unbranched and rudimentary rays were not counted. Cephalic lateral-line pores and gill rakers (four specimens) were counted under a stereo microscope (Nikon SMZ25, Tokyo, Japan). Vertebral counts (two specimens), including the four Weberian vertebrae, were obtained from x-radiographs. The specimens examined in the present study were deposited in the collections of the School of Life Sciences, Southwest University (SWU) in Beibei, Chongqing, China, and the private Bakhtiyor Sheraliev Fish Collection (BSFC) in Fergana, Uzbekistan.

Data on *Triphophysa paradoxa* (Turdakov, 1955), *T. ulacholica* (Anikin, 1905), and *T. coniptera* (Turdakov, 1954) were obtained from Turdakov (1963), *T. sewerzowi* (Nikolskii, 1938) from Mitrofanov (1989), *T. dorsonotata* (Kessler, 1879) and *T. lacusnigri* (Berg, 1928) from Prokofiev (2007), and *T. kungessana* (Kessler, 1879) from Zhao (1984). For *Triphophysa* species from the Tarim basin, data on *T. laterimaculata* Li, Liu & Yang, 2007, *T. papillosolabiata* (Kessler, 1879), *T. bombifrons* (Herzenstein, 1888), *T. zamegacephala* (Zhao, 1985), *T. moquensis* Ding, 1994, *T. orientalis* (Herzenstein, 1888), *T. microphysa* (Fang, 1935), and *T. incipiens* (Herzenstein, 1888) were obtained from Li et al. (2007). Data on *T. herzensteini* (Berg, 1909), *T. microphthalmia* (Kessler, 1879), *T. kaznakowi* Prokofiev, 2004, and *T. waisihani* Cao & Zhang, 2008 were obtained from Cao and Zhang (2008). Other species used for comparative purposes were examined at BSFC, FSU, ICIZ, NWIPB, and SWU.

Abbreviations: **CPD**, caudal-peduncle depth; **CPL**, caudal-peduncle length; **HL**, head length; **K2P**, Kimura 2-parameter; **SL**, standard length.

Collection codes: **BSFC**, Bakhtiyor Sheraliev Fish Collection, Fergana, Uzbekistan; **FSU**, Fergana State University, Faculty of Life Sciences, Fergana, Uzbekistan; **ICIZ**, Ichthyological Collection of the Institute of Zoology, Academy of Sciences of Uzbekistan, Tashkent, Uzbekistan; **NWIPB**, Northwest Institute of Plateau Biology, Chinese Academy of Sciences, Qinghai, China; **SWU**, Southwest University, School of Life Sciences, Chongqing, China.

DNA extraction, PCR amplification, and sequencing

DNA was extracted from the right-side pectoral fin using proteinase K digestion followed by a standard phenol-chloroform method (Sambrook and Russell 2001). The mitochondrial cytochrome *c* oxidase subunit 1 (COI) barcode region (652 bp) was amplified using primers VF2_t1 (5'-TGT AAA ACG GCC AGT CAA CCA ACC ACA AAG ACA TTG GCA C-3') and FR1d_t1 (5'-CAG GAA ACA GCT ATG ACA CCT CAG GGT GTC CGA ARA AYC ARA A-3'), as designed by Ivanova et al. (2007). The PCR assay was performed in a reaction volume of 25 μ L containing 10 ng template DNA, 1 μ L each primer, 12.5 μ L 2 \times *Taq* Master Mix (Novoprotein, Guangdong, China), and double distilled water. Thermal cycling consisted of an initial step at 94 $^{\circ}$ C for 3 min, followed by 35 cycles at 94 $^{\circ}$ C for 20 s, 54 $^{\circ}$ C for 45 s, and 72 $^{\circ}$ C for 1 min 10 s, and a final extension step at 72 $^{\circ}$ C for 7 min. The PCR products were sent to TsingKe Biological Technology Co., Ltd (Chongqing, China) for sequencing.

Phylogenetic reconstruction

The 652 bp COI gene sequence was used for phylogenetic analysis. Molecular analysis was conducted using three new COI sequences (*T. daryoae*; ; *T. elegans*; ; and *T. uranoscopus* (Kessler, 1872),), as well as 29 previously published sequences retrieved from the National Center for Biotechnology Information (NCBI) GenBank (Table 1) database (<https://www.ncbi.nlm.nih.gov>). The COI sequences were aligned using the Clustal_W algorithm in MEGA7 (Kumar et al. 2016), with manual checks for inconsistencies. The distances between different groups were determined using MEGA7, with 1000 bootstrap replicates calculated using the best-selected K2P model. For phylogenetic reconstruction, the datasets were analyzed based on Bayesian inference (BI) using MrBayes ver.3.2 (Ronquist et al. 2012) and maximum likelihood (ML) using MEGA7. MrBayes was run with six substitution types (nst = 6), considering a general

Table 1. List of mitochondrial COI sequences retrieved from GenBank with information on drainage and country of origin.

Species	Drainage	Country	GenBank Accession No.	Voucher ID	Reference
<i>Barbatula barbatula</i>	Helge	Sweden		NRM:44850	Norén et al. (2017)
<i>Barbatula toni</i>	Yenisey	Russia		Tuva-38FB	Freyhof et al. (2016)
<i>Triplophysa alticeps</i>	Qihai Lake	China		NWIPB1206002	Wang et al. (2016)
<i>Triplophysa anterodorsalis</i>	Yangtze	China		IHB-Tran-001	Shen et al. (2019)
<i>Triplophysa bleekeri</i>	Anning	China		–	Li et al. (2016)
<i>Triplophysa bleekeri</i>	Danling	China		–	Tang et al. (2013)
<i>Triplophysa chondrostoma</i>	Tiangeli	China		CH3	Li et al. (2017)
<i>Triplophysa chondrostoma</i>	Tiangeli	China		NWIPB1006052	Wang et al. (2016)
<i>Triplophysa daryoae</i> sp. nov.	Sokh	Uzbekistan		SWU540	This study
<i>Triplophysa dorsalis</i>	Irtys	China		–	Lei et al. (2016)
<i>Triplophysa dorsonotata</i>	Kegen	Kazakhstan		Kaz-2-1	Freyhof et al. (2016)
<i>Triplophysa elegans</i>	Chirchik	Uzbekistan		SWU634	This study
<i>Triplophysa ferganaensis</i>	Shakhimardan	Uzbekistan		SWU209	Sheraliev and Peng (2021b)
<i>Triplophysa leptosoma</i>	Ganzi	China		NWIPB1109002	Wang et al. (2016)
<i>Triplophysa leptosoma</i>	Heihe	China		LZUTL12022	Zhang et al. (2017)
<i>Triplophysa markehenensis</i>	Sichuan	China		SCU1010706	Wang et al. (2016)
<i>Triplophysa moquensis</i>	Ruoergai	China		SCU20130901	Wang et al. (2016)
<i>Triplophysa obscura</i>	Jialing	China		GS0629	Wang et al. (2020)
<i>Triplophysa orientalis</i>	Tagong	China		TG5	Li et al. (2017)
<i>Triplophysa orientalis</i>	–	China		–	Ma and Yang (unpublished)
<i>Triplophysa scleroptera</i>	Baijia	China		IHB201306600	Wang et al. (2016)
<i>Triplophysa sellaefer</i>	Juma	China		IHB20151303	Feng et al. (2019b)
<i>Triplophysa sewerzovi</i>	Kegen	Kazakhstan		Kaz-2-2	Freyhof et al. (2016)
<i>Triplophysa stoliczcai</i>	Zequ	China		SST-2	Li et al. (2017)
<i>Triplophysa stoliczcai</i>	–	China		–	Li et al. (2013)
<i>Triplophysa stoliczcai</i>	Yangtze	China		IHB-Trst-024	Shen et al. (2019)
<i>Triplophysa strauchii</i>	Chirchik	Uzbekistan		SWU625	Sheraliev and Peng (2021b)
<i>Triplophysa tenuis</i>	Dang	China		IHB201307126	Wang et al. (2016)
<i>Triplophysa ulacholica</i>	Mulei	China		IHB201305179	Wang et al. (2016)
<i>Triplophysa uranoscopus</i>	Zeravshan	Uzbekistan		SWU524	This study
<i>Triplophysa wuweiensis</i>	Jinchuanxia	China		IHB201307124	Wang et al. (2016)
<i>Triplophysa xichangensis</i>	Anning	China		IHB201306572	Wang et al. (2016)

time-reversible model with gamma-distributed rate variation and proportion of invariable sites (GTR+G+I) for the COI datasets. For BI analysis, we ran four simultaneous Monte Carlo Markov chains for 3,000,000 generations, with sampling every 1000 generations. The chain temperature was set as 0.2. Log-likelihood stability was determined after 10,000 generations, and the first 1000 trees were excluded as burn-in. The remaining trees were used to compute a 50% majority-rule consensus tree. For ML analysis, we conducted heuristic searches (1000 runs) also using the GTR+G+I model (nst = 6). Phylogenetic trees were visualized and edited using FigTree ver.1.4.2 (Rambaut 2014). *Barbatula barbatula* (Linnaeus, 1758), (), and *B. toni* (Dybowski, 1869) () were used as outgroup.

Results

Triphophysa daryoae sp. nov.

<http://zoobank.org/8CE5BCB5-F671-4270-BFA3-7884DEF0BED7>

Figs 1–3

English common name: Sokh stone loach

Uzbek common name: So‘x yalangbalig‘i

Russian common name: Сохский голец

Holotype. SWU 20211207001, male, 78.5 mm SL; Uzbekistan, Fergana Region, Sokh District, Sokh River, near Limbur village, an exclave of Uzbekistan surrounded by Kyrgyzstan, Syr Darya basin, 40°3.1528'N, 71°5.8195'E, altitude 1054 m, December 07, 2021, collected by B. Sheraliev and Y. Kayumova.

Paratypes. SWU 20211207002-011, 10, 49.0–94.0 mm SL; BSFC 0023, 4, 62.1–82.4 mm SL; Uzbekistan, Fergana Region, Sokh District, Sokh River, near the Limbur village, exclave of Uzbekistan, Syr Darya basin, 40°2.7387'N, 71°6.288'E, altitude 1054 m, April 12, 2021, collected by Y. Kayumova. BSFC 0024, 3, 74.1–81.3 mm SL, same data as holotype.

Diagnosis. *Triphophysa daryoae* is distinguished from congeners by a combination of characters. It is distinguished from *T. ferganaensis* by possessing a truncate caudal fin with 13–14 branched rays (vs emarginate, 16 rays), 9 pores in the pre-opercular mandibula (vs 7–8), and a slenderer body (body depth at dorsal-fin origin 1.4–1.8 times the HL vs 1.2–1.4). It is distinguished from *T. strauchii* by absence of the posterior chamber of the air bladder (vs developed, with a long tube), possessing 9–10 inner gill rakers on the first gill arch (vs 12–16), and no obvious skin mottling (vs mottling). *Triphophysa daryoae* is also distinguished from *T. dorsalis*, *T. dorsonotata*, and *T. elegans* by having a truncate caudal fin (vs emarginate) and lacking a posterior chamber of the air bladder (vs developed in *T. dorsalis* and *T. elegans*). It is distinguished from *T. sewerzowi*, *T. tenuis*, and *T. ulacholica* by the dorsal-fin origin opposite to the pelvic-fin insertion (vs anterior to vertical line of pelvic fin origin).

Description. Morphometric data of *T. daryoae* are given in Table 2. Dorsal-fin rays iii, 6(2) or 7(16); anal-fin rays ii, 5; pectoral-fin rays i, 9(1), 10(16), or 11(1); pelvic-fin



Figure 1. Lateral **a** dorsal **b** and ventral **c** views of *Triplophysa daryoae*, holotype, SWU 20211207001, male, 78.5 mm SL; Uzbekistan: Sokh River.

rays i, 6; caudal-fin rays, 13–14 (6+7 [5]; 7+7 [13]); vertebrae, 4+35 ($N = 2$); gill rakers, 9–10 in the inner row of first gill arch ($N = 4$). Cephalic lateral-line system, 2 supratemporal, 6 supraorbital, 4+10–11 infraorbital, and 9 pre-operculum mandibular pores.

Body elongate; posterior portion gradually compressed from dorsal fin to caudal-fin origin. Dorsal profile slightly convex from the snout to the insertion of the anterior dorsal fin (Fig. 1). Deepest point of body slightly anterior to dorsal-fin origin; body depth at dorsal-fin origin 12.4–15.3% of SL. Head compression, maximum width always greater than depth; head maximum width 63.2–73.2% of HL. Snout slightly pointed, length shorter, equal, or slightly longer than postorbital length; snout length 34.9–47.3% of HL. Anterior and posterior nostrils adjacent; anterior nostril as short tube with elongated barbel-like tip; tip of nostril barbel not reaching the anterior mar-

Table 2. Morphometric data of *Triplophysa daryovae* (holotype SWU 202111207001, paratypes SWU 202111207002–011, $N = 10$; BSFC 0023, $N = 4$; BSFC 0024, $N = 3$) and closely related and occurred two loach species.

	<i>Triplophysa daryovae</i> sp. nov.			<i>Triplophysa ferganaensis</i>			<i>Triplophysa srauchii</i>		
	holotype	holotype, paratypes ($N = 18$)	SD	holotype	holotype, paratypes, non-types ($N = 33$)	SD	range	range	SD
	range	mean	SD	range	mean	SD	range	range	mean
Standard length (mm)	78.54	49.00–94.04		42.85–109.17			83.63–155.86		
In percent of standard length									
Lateral head length	21.80	20.10–23.01	21.71	20.21–24.53	22.12	1.21	22.84–24.36	23.64	0.55
Body depth at dorsal-fin origin	15.33	12.37–15.33	13.91	14.57–17.39	15.85	0.72	19.23–19.91	19.63	0.27
Body width at dorsal-fin origin	11.85	10.84–12.72	11.81	11.99–15.93	13.37	0.87	16.72–18.43	17.44	0.62
Pre-dorsal length	55.03	51.32–55.03	53.52	49.35–56.80	53.36	1.56	51.51–53.62	52.51	0.82
Post-dorsal length	37.08	34.73–40.96	37.53	33.75–39.56	36.64	1.15	35.00–38.62	36.50	0.47
Pre-pelvic length	53.50	50.74–55.49	53.01	49.80–54.19	51.93	1.10	53.21–54.80	54.24	0.47
Prenasal length	71.68	69.30–73.75	71.42	66.41–73.45	70.36	1.55	69.65–72.68	71.09	1.05
Prenasus length	65.58	64.33–68.73	66.67	62.27–68.74	65.71	1.52	66.01–69.08	67.81	1.05
Dorsal-fin depth	16.51	14.85–18.54	16.22	13.61–19.08	16.88	1.48	17.07–19.80	18.10	0.83
Dorsal-fin base length	11.08	9.61–11.85	10.58	12.13	10.84–13.23	12.04	12.18–13.98	12.98	0.62
Anal-fin depth	16.68	13.09–16.68	14.66	12.67–18.27	15.17	1.35	13.38–15.81	14.33	0.89
Anal-fin base length	7.89	7.22–8.25	7.75	7.47–10.51	8.69	0.80	7.70–9.15	8.16	0.46
Pectoral-fin length	17.93	15.37–19.74	17.28	18.77	15.64–21.52	18.22	15.42–18.93	16.75	1.09
Pelvic-fin length	14.65	13.68–17.04	15.04	16.58	13.47–17.49	15.65	15.19–16.84	16.05	0.57
Caudal-fin length	21.86	18.98–23.60	20.91	21.99	19.62–25.25	22.07	19.30–22.80	20.69	1.27
Caudal-peduncle length (CPL)	23.07	19.12–23.07	20.80	20.50	18.45–23.11	20.72	18.70–23.39	20.85	1.35
Caudal-peduncle depth (CLD)	7.93	7.56–9.16	8.18	8.19	7.42–9.67	8.60	6.67–7.68	7.32	0.31
Pectoral-pelvic distance	32.77	30.37–34.18	32.09	30.92	28.80–35.29	31.62	31.09–33.84	32.48	0.84
Pelvic-anal distance	17.35	17.35–20.66	18.96	20.23	16.80–21.37	18.97	16.84–19.59	17.77	0.90
Vent – anal-fin origin distance	5.46	3.72–5.80	4.81	4.77	3.64–5.54	4.63	3.16–4.54	3.84	0.40
CPL/CPD	2.91	2.20–2.91	2.55	2.50	2.06–2.76	2.42	2.49–3.11	2.85	0.17
In percent of head length									
Head depth at nape	56.19	52.06–60.64	56.53	53.34	52.21–65.53	57.42	56.57–65.04	61.07	3.01
Head depth at eye	44.22	36.31–49.48	44.05	44.62	42.39–54.73	47.51	42.87–48.64	45.39	1.90
Maximum head width	70.74	63.20–73.16	67.78	68.68	59.87–79.24	68.84	63.36–70.59	67.70	2.32
Snout length	44.51	34.88–47.34	41.28	38.94	32.83–42.79	39.05	37.62–43.57	40.27	2.08
Eye diameter	13.26	12.49–17.08	14.07	13.73	10.33–17.03	13.86	12.49–16.28	14.04	1.30
Interorbital width	30.61	29.51–35.60	32.15	30.58	27.40–35.69	31.45	30.56–35.42	33.05	1.66
Postorbital distance	44.22	41.40–47.78	44.54	43.11	42.60–48.35	45.45	39.01–44.65	42.30	1.80
Maxillary barbel length	25.99	22.04–37.40	30.54	29.54	22.65–37.37	30.42	30.93–38.20	34.25	2.41
Inner rostral barbel length	22.55	19.82–30.17	24.18	25.37	19.31–27.62	23.63	23.06–30.14	26.63	2.27
Outer rostral barbel length	32.71	22.71–42.04	33.03	36.64	24.45–42.34	34.48	32.78–43.43	38.99	3.36

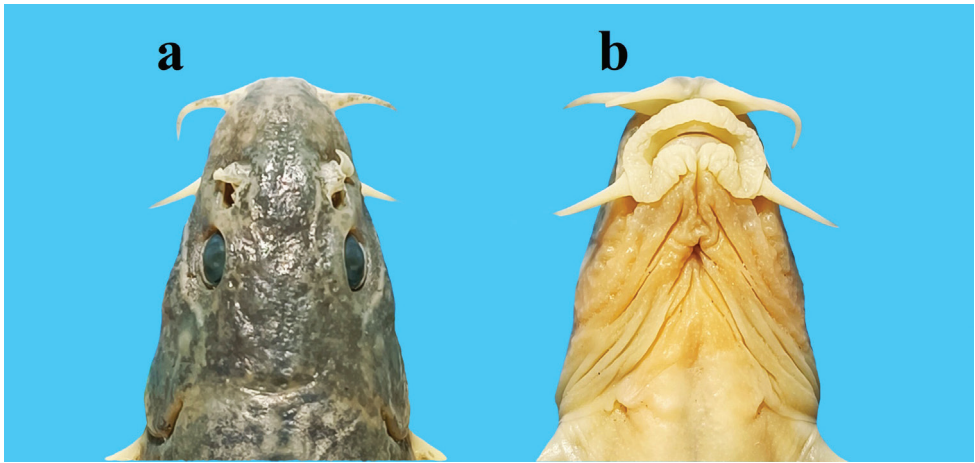


Figure 2. Dorsal **a** and ventral **b** views of the head of *Triplophysa daryoae*, SWU 20211207001, holotype, male, 78.5 mm SL.

gin of eyes. Eyes normal; diameter 12.5–17.1% of HL (Fig. 2). Mouth inferior, gape arched; mouth width 16.1–24.3% of HL. Rictus situated below the anterior nostril. Lips thick with furrows and papillae; upper lip pectinate, without medial notch; lower lip wide, interrupted in middle, with mental lobes and two highly developed ridges. Upper jaw covered by the upper lip; processus dentiformis absent. Three pairs of barbels: inner rostral barbel reaching rictus, length 19.8–30.2% of HL; outer rostral barbel reaching anterior margin of eye, length 22.7–42.0% of HL; maxillary barbel reaching posterior margin of eye, length 22.0–37.4% of HL.

Dorsal fin convex, origin opposite to pelvic-fin insertion, situated slightly posterior to midpoint between snout tip and caudal-fin base; upper margin slightly convex; second branched ray longest; depth of dorsal fin always shorter than lateral head length; depth 14.9–18.5% of SL. Anal fin short-based, posterior margin convex; length 13.1–16.7% of SL. Pectoral fins developed; 46.6–61.6% of pectoral-pelvic distance. Tips of depressed pelvic fins reaching the anus and anus separated from the anal-fin origin by a short distance. Caudal peduncle compressed laterally; length 2.2–2.9 times the peduncle depth. Caudal fin truncate, tips rounded; length 86.2–119.9% of caudal-peduncle length.

Body smooth and scaleless; cephalic lateral-line system well developed. Infraorbital and supraorbital canals stretching from the outer rostral barbel base and ethmoid, respectively, uniting in the posterior orbital region and extending posteriorly before converging with the supratemporal canal on the back of the head, and uniting with the lateral canal. Complete lateral line ending at caudal-fin base. Intestine moderately long, with two coils. Stomach U-shaped. Posterior chamber of the air bladder degenerated.

Coloration. Dorsal profile grayish-brown to pale green without regular blotches in live individuals, and dark gray-brown in preserved specimens. Ventral side of the body ivory with gray tint. Dorsal side of head with small irregular dark melanophores;



Figure 3. From top: *Triplophysa daryoae*, holotype SWU 20211207001, male, 78.5 mm SL, photographed alive immediately upon capture, Uzbekistan: Sokh River; *T. daryoae*, paratype, BSFC 0024, 72.8 mm SL, Uzbekistan: Sokh River; *T. ferganaensis*, BSFC 0025, 66.2 mm SL, Uzbekistan: Shahimardan stream; *T. trauchii*, not preserved, about 110 mm SL, Uzbekistan: Oltiariqsoy stream.

dorsal side of caudal peduncle with four or five irregular dark brown blotches. All fin membranes hyaline and light gray, without obvious mottling (Figs 1, 3).

Sexual dimorphism. Mature males presenting granular tubercles on each side of the preorbital region and broadened and thickened external branched pectoral-fin rays dorsally covered by small and condensed epidermal breeding tubercles. Females without tubercles on the head and pectoral-fin rays.

Distribution and habitat. *Triplophysa daryoae* sp. nov. is known only from its type locality, the Sokh River, which originates in the Alay mountains and Turkestan range

(Fig. 4). Presently, Sokh River water is primarily used for irrigation and does not reach Syr Darya. The river is located at an altitude of 700–1500 m and is constantly flowing rapidly; the water is clear and cold (the water temperature was 7.3 °C when the holotype was caught), and the bottom consists of gravel and stone (Fig. 5). *Triplophysa daryoae* cohabited with *Cottus spinulosus* Kessler, 1872 and *Schizothorax eurystomus* Kessler, 1872, which are high-altitude fish species.

Etymology. *Triplophysa daryoae* is dedicated to Daryo Sheralieva, the lovely daughter of the first author. The specific name is a noun in the genitive case.

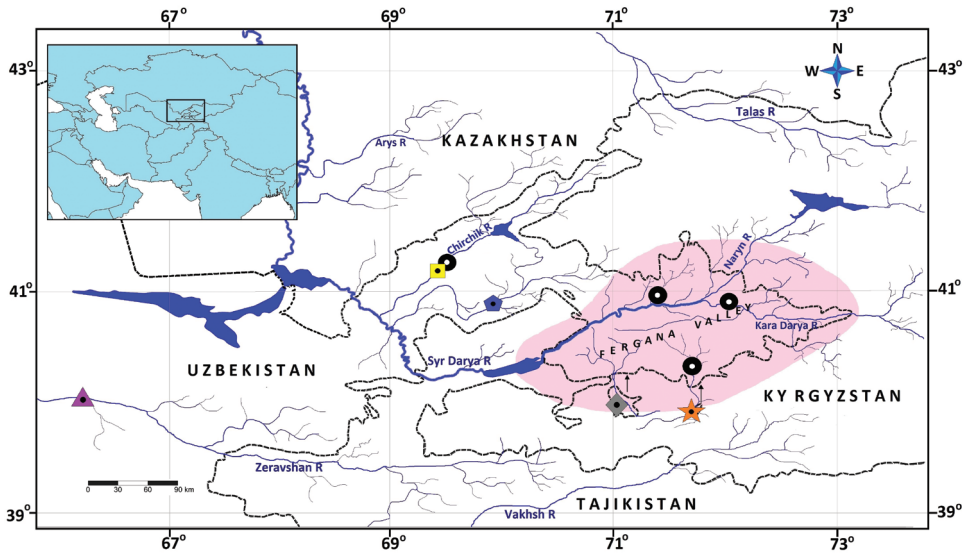


Figure 4. Map of the distribution of *Triplophysa* species in Uzbekistan: *T. daryoae* (grey diamond); *T. ferganaensis* (orange star); *T. trauchii* (black circle); *T. dorsalis* (blue pentagon); *T. elegans* (yellow rectangle); and *T. uranoscopus* (purple triangle).



Figure 5. Sampling locality of the holotype (SWU 20211207001) of *Triplophysa daryoae* in the Sokh River left tributary of the Syr Darya, in Sokh District, the exclave of Uzbekistan, surrounded by Kyrgyzstan, photograph taken on December 7, 2021.

Molecular analysis

COI sequence data (Fig. 6) showed that *Triplophysa daryoae* belongs to a group of species with a wide distribution in the Syr Darya, Tarim, and Ili-Balkhash river drainages, an endorheic basin in Central Asia. This group is defined here as the *T. dorsalis* species group, and our molecular data suggest that it includes *T. chondrostoma* (Herzenstein, 1888), *T. dorsalis*, *T. dorsonotata*, *T. elegans*, *T. ferganaensis*, *T. sewerzowi*, *T. strauchii*, *T. tenuis* (Day, 1877), and *T. ulacholica*. The minimum K2P distances between *T. daryoae* and its closest relatives *T. ferganaensis* and *T. tenuis* were 2.8% and 4.5%, respectively (Table 3). *Triplophysa daryoae* was distinguished from its most closely related congener, *T. ferganaensis*, by 18 unique and diagnostic nucleotide substitution sites in the COI barcode region (652 bp) (Table 4).

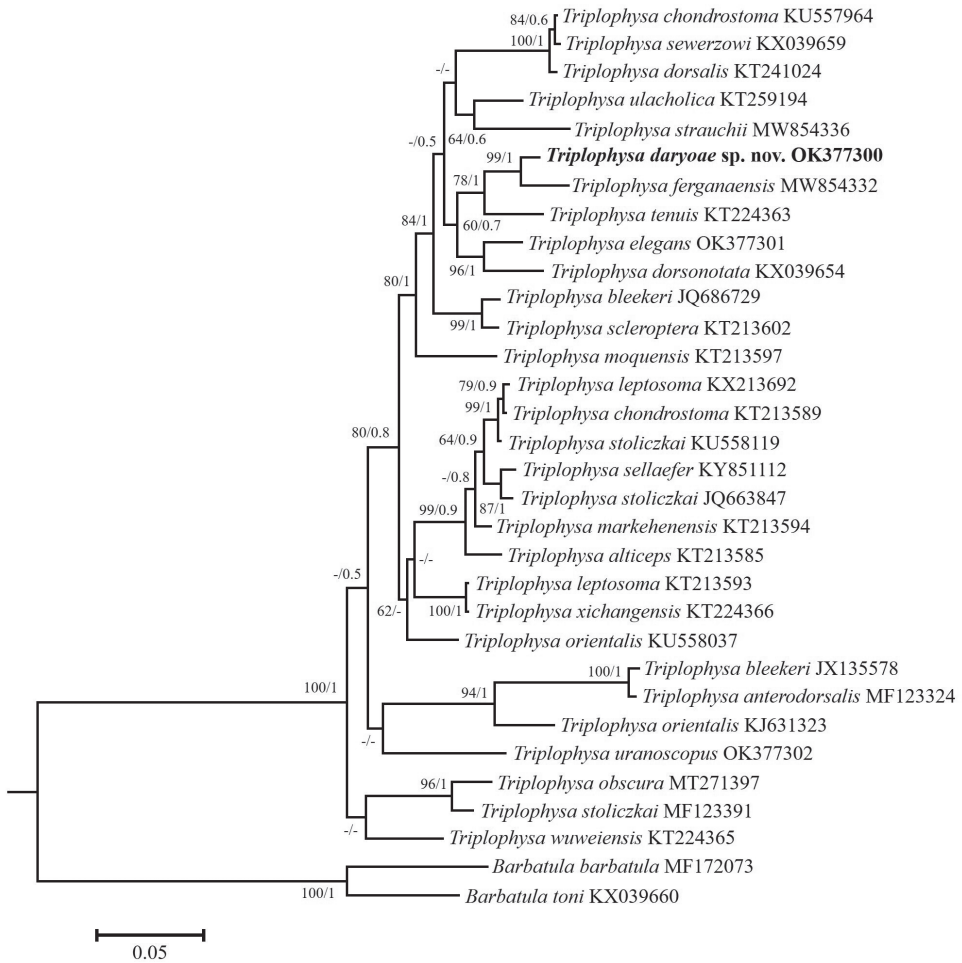


Figure 6. Bayesian inference tree based on mitochondrial COI gene sequences of 24 *Triplophysa* species. Maximum likelihood and Bayesian inference analyses resulted in congruent trees. Bootstrap and posterior probability values are shown above nodes on tree if 50% or higher.

Table 3. The Kimura’s 2-parameter distance of mitochondrial COI dataset within *Triplophysa dorsalis* species group based on 1000 bootstrap replications.

	1	2	3	4	5	6	7	8	9
1 <i>T. chondrostoma</i>									
2 <i>T. daryoae</i> sp. nov.	0.065								
3 <i>T. dorsalis</i>	0.003	0.065							
4 <i>T. dorsonotata</i>	0.081	0.062	0.077						
5 <i>T. elegans</i>	0.065	0.056	0.062	0.041					
6 <i>T. ferganaensis</i>	0.079	0.028	0.079	0.070	0.061				
7 <i>T. sewerzowi</i>	0.002	0.067	0.005	0.083	0.067	0.081			
8 <i>T. strauchii</i>	0.074	0.068	0.074	0.081	0.074	0.084	0.075		
9 <i>T. tenuis</i>	0.073	0.045	0.077	0.065	0.060	0.056	0.075	0.077	
10 <i>T. ulacholica</i>	0.053	0.063	0.056	0.062	0.060	0.075	0.055	0.058	0.061

Table 4. Diagnostic nucleotide substitutions in the 652 base pairs long mitochondrial COI barcoding region of *Triplophysa daryoae* and its closest two species.

Species	Variable Nucleotide Positions*																			
	90	117	120	123	129	153	210	249	255	264	267	270	273	279	288	291	306	315	318	334
<i>T. daryoae</i>	G	T	G	A	G	C	G	T	A	A	T	A	T	A	T	G	C	A	C	C
<i>T. ferganaensis</i>	A	T	G	G	G	T	G	T	G	A	C	A	T	A	T	G	C	G	T	T
<i>T. tenuis</i>	G	C	A	G	A	T	A	C	A	G	C	G	C	C	A	A	T	A	G	C

Species	Variable Nucleotide Positions																			
	375	411	453	462	465	468	471	510	547	558	561	570	582	585	589	603	606	666	678	699
<i>T. daryoae</i>	A	C	C	T	A	A	C	C	T	G	T	G	A	A	T	C	G	T	G	C
<i>T. ferganaensis</i>	G	T	C	T	A	G	C	C	T	G	C	A	G	A	C	C	G	A	A	T
<i>T. tenuis</i>	A	C	T	C	G	A	T	T	C	A	T	G	A	C	C	T	A	T	G	T

* The nucleotide position number was provided relative to the first nucleotide base of the complete COI gene of *T. tenuis* (KT224363).

Discussion

Triplophysa differs from other Nemacheilidae genera by presenting sexual dimorphism (Zhu 1989). The presence of specific aggregations of breeding tubercles on the dorsal surfaces of the pectoral fin and from the lower edge of the eye to the base of the outer barbel in mature males can be regarded as an autapomorphy and is the unique diagnostic character of *Triplophysa* (Prokofiev 2010). These tubercles are present in *T. daryoae* males.

This study added three species (*T. daryoae*, *T. elegans*, and *T. uranoscopus*) to the previously published molecular reconstructions (Wang et al. 2016; Feng et al. 2019a; Wu et al. 2020). Our phylogenetic analysis was consistent with the results of previous molecular and morphological studies. Overemphasis on some characteristics with eco-phenotypic variation, such as body color, color patterns, barbel length, and mouth structure, when identifying *Triplophysa* species may be misleading (Ren et al. 2018). Therefore, it is advisable to employ a combination of morphological and molecular approaches to distinguish between loach species (Chen et al. 2021; Sheraliev and Peng 2021b; Deng et al. 2022; Lu et al. 2022).

Triplophysa dorsalis is recorded from the middle and upper reaches of Kara Darya, whereas *T. elegans* is only recorded from the upper reaches (Baltabaev 1971). *Triplophysa trauchii* occurs in all waters of the Fergana Valley, whereas *T. ferganaensis* has only been recorded from its type locality, the Shakhimardan stream (Sheraliev and Peng 2021b). These species are more similar to *Triplophysa daryoae* than to other congeners. Nevertheless, they can be easily distinguished from the new species based on morphology.

Triplophysa daryoae can be distinguished from *T. ferganaensis*, which is the most similar species in terms of morphometric characteristics and habitat conditions, using the following characteristics: caudal fin truncate with 13 or 14 branched rays (vs emarginated with 16 branched rays), 6 branched pelvic-fin rays (vs 7 or 8), 9–11 (modally 10) branched pectoral-fin rays (vs 11–13, modally 12); cephalic lateral-line system with 6 suborbital and 9 pre-operculo mandibular pores (vs 7 and 7 or 8, respectively), dorsal and caudal fins almost hyaline, and spots imperceptible (vs spots on dorsal and caudal fins clearly visible). *Triplophysa daryoae* is distinguished from *T. trauchii*, which is the most common species of *Triplophysa* in the waters of Fergana Valley, by the small number of vertebrae (4+35 vs 4+37–38); a smaller number of gill rakers in the inner row of the first gill arch (9 or 10 vs 12–16); absent posterior chamber of air bladder (vs developed, with a long tube); shorter body depth and width at dorsal-fin origin (12.4–15.3% and 10.8–12.7% of SL vs 19.2–19.9% and 16.7–18.4% of SL, respectively); dorsal-fin origin equal to pelvic-fin insertion (vs anterior to vertical line of pelvic fin); and upper and lower lobes of caudal fin equal (vs upper lobe slightly longer than lower lobe). *Triplophysa daryoae* differs from *T. dorsalis* and *T. elegans*, which are rare species in the Fergana Valley, according to the following characteristics: dorsal-fin origin equal to pelvic-fin insertion (vs anterior to vertical line of pelvic fin in both); 9 or 10 gill rakers in the inner row of the first gill arch (vs 13–16 in *T. dorsalis*); wider interorbital width (29.5–35.6% of HL vs 23.9–27.6% of HL in *T. dorsalis*); longer pectoral-pelvic distance (30.4–34.2% of SL vs 24.6–28.7% of SL in *T. dorsalis*); shorter dorsal-fin depth (14.9–18.5% of SL vs 19.8–22.8% of SL in *T. dorsalis* and 18.9–24.1% of SL in *T. elegans*); caudal peduncle equal to HL (vs usually shorter in *T. dorsalis*); caudal-peduncle depth 7.6–9.2% of SL (vs 6.6–7.1% of SL in *T. elegans*); posterior chamber of air bladder degenerated (vs developed in both); lips thick with furrows (vs smooth lips in *T. dorsalis*); and caudal-peduncle depth 2.2–2.9 times its length (vs 3.2–3.5 times in *T. elegans*). Moreover, the genetic distance between the *Triplophysa daryoae*, *T. dorsalis*, *T. elegans*, *T. ferganaensis*, and *T. trauchii* (6.5%, 5.6%, 2.8%, and 6.8%, respectively), based on the mitochondrial COI barcoding region, is consistent with the species-level divergence in other fish taxa (Ward et al. 2005; Rosso et al. 2012; Abdulmalik-Labe and Quilang 2019; Freyhof et al. 2021).

Another ten species of *Triplophysa* occur in the Syr Darya basin and adjacent area of the Fergana Valley (Berg 1949; Turdakov 1963; Sheraliev and Peng 2021b). Among them, *T. tenuis* is similar to *T. daryoae* in its general body structure, especially in the caudal-fin shape. However, *T. daryoae* is distinguished from *T. tenuis* by presenting 9–10 gill rakers in the inner row of the first gill arch (vs 12–15); dorsal fin slightly posterior to the midpoint between the tip of the snout and caudal-fin origin (vs anterior to the midpoint

between the tip of the snout and caudal-fin origin); caudal-peduncle depth 7.6–9.2% of SL (vs 5.2–5.7% of SL), head depth 52.1–60.6% of HL (vs 47.8–51.2% of HL); and caudal-peduncle depth 2.2–2.9 times its length (vs 4.1–4.3 times). *Triplophysa daryoae* is distinguished from *T. paradoxa* by the absence of scales (vs covered by scales), dorsal-fin origin opposite to pelvic-fin insertion (vs anterior to vertical line trough pelvic-fin origin), and dorsal-fin origin closer to the caudal-fin base than to the snout tip (vs closer to the snout tip). *Triplophysa daryoae* is distinguished from *T. ulacholica* by the shorter average caudal-peduncle length ($20.8 \pm 1.11\%$ of SL vs $27.0 \pm 0.24\%$ of SL), deeper caudal peduncle (7.6–9.2% of SL vs 4.9–6.8% of SL), caudal-peduncle depth 2.2–2.9 times its length (vs 4.0–5.3 times), and smaller eye diameter (12.5–17.1% of HL vs 18.5–23.3% of HL). The new species can be distinguished from *T. coniptera* by the rounded edge of the pectoral fin (vs pointed); caudal fin truncate (vs deeply forked); snout length 7.4–10.0% of SL (vs 10.1–11.8% of SL); caudal-peduncle depth 7.6–9.2% of SL (vs 5.2–7.3% of SL); and caudal-peduncle depth 2.2–2.9 times its length (vs 3.4–4.5 times). *Triplophysa daryoae* is distinguished from *T. sewerzowi* by the following characteristics: dorsal-fin origin opposite to pelvic-fin insertion (vs anterior to vertical line of pelvic-fin origin), second branched ray of dorsal fin the longest (vs third or fourth), and degenerated posterior chamber of the air bladder (vs developed). It is also distinguished from *T. dorsonotata* by its smaller eye diameter (7.2 times of HL vs approximately 6 times), pre-dorsal length longer than post-dorsal length (vs pre-dorsal length slightly shorter than post-dorsal length), cephalic lateral-line system with 6 suborbital pores (vs 7 or 8), and caudal fin truncate (vs emarginated). The new species can be distinguished from *T. kungessana* by its thick lips with furrows and papillae (vs almost thin and smooth, without clear fringes or papillae) and pelvic fin reaching the anus (vs not reaching the anus). *Triplophysa daryoae* can be distinguished from *T. herzensteini* by having 4+35 vertebrae (vs 4+39–41) and a caudal-peduncle depth 7.6–9.2% of SL (vs 5.9–6.8% of SL). *Triplophysa daryoae* can be distinguished from *T. uranoscopus* by its caudal-peduncle depth measuring 2.2–2.9 times its length (vs. 2.7–4.1 times); caudal-peduncle depth 7.6–9.2% of SL (vs 5.4–7.0% of SL); dorsal-fin origin opposite to pelvic-fin insertion (vs anterior to vertical line of pelvic-fin origin). It differs from *T. lacusnigri* by a shorter head length (4.3–5.0 times SL vs 3.4–4.5 times SL) and non-oblique head profile in front of the eye (vs strongly oblique); the tip of the pectoral fin is usually formed by 4 branched rays (vs 2 or 3).

Triplophysa dorsonotata, *T. elegans*, *T. lacusnigri*, *T. tenuis*, and *T. uranoscopus* from different water bodies in Central Asia have long been synonymized with *T. stolicikai* due to their morphological resemblance (Berg 1949; Turdakov 1963; Zhu 1989; Wu and Wu 1992, Prokofiev 2010). We were unable to find *T. stolicikai* in inland waters of Uzbekistan (Sheraliev and Peng 2021a). To confirm the existence of *T. stolicikai* in the waters of Uzbekistan, further morphological and genetic taxonomic revisions of *Triplophysa* from this region, previously synonymized with *T. stolicikai*, are required. However, Feng et al. (2019a) reported that *T. stolicikai* from the Qinghai-Tibet Plateau represents an interesting case of morphological convergence and consists of distinct four lineages that are not closely related. In the phylogenetic tree presented here, *T. stolicikai* nested in three lineages with genetic distances (K2P) from *T. daryoae* of 6.3%, 6.8%, and 9.7% (Fig. 6). Despite the high morphological diversity of *T. stolicikai*, the new spe-

cies differs from it by its caudal-peduncle depth (7.6–9.2% of SL vs 5.9–7.1% of SL in Ili River, 5.4–7.3% of SL in Tarim and Indus rivers, and 6.2–6.5% of SL in Yangtze River); interorbital width being 29.5–35.6% of HL (vs 20.8–26.2% of HL); head depth at nape 52.1–60.6% of HL (vs 46.1–51.5% of HL in Ili River); caudal-peduncle depth 2.2–2.9 times its length (vs 3.2–3.9 times in Ili River; 2.9–4.6 times in Tarim and Indus rivers; 3.6–3.8 times in Yangtze River); vertebrae 4+35 (vs 4+38–41); body without obvious mottling (vs. with mottling); supraorbital sensory canal always connected with the infraorbital canal (vs usually not connected); and 2 supratemporal pores (vs 3 or 4).

Berg (1905:243) noted that the rivers of the Syr Darya and Tarim basins originate on a flat marshy plateau in the Tian Shan, where water streams periodically change their direction and is difficult to distinguish between waters in separate basins. On this basis, he explained the similarity of ichthyofauna in the highlands of Central Asia (Berg, 1905). *Triplophysa daryoae* is similar to some species of *Triplophysa* from the Tarim basin and adjacent regions, with normal eyes, scaleless body, body color, color patterns, and slightly laterally compressed caudal peduncle (Li et al. 2007; Cao and Zhang 2008). However, it can be distinguished from *T. bombifrons*, *T. laterimaculata*, *T. moquensis*, *T. papillosolabiata*, and *T. zamegacephala* by the posterior chamber of its air bladder being degenerated (vs developed); 9 or 10 gill rakers in the inner row of the first gill arch (vs 12–14, 12, 13–15, 12–15, and 15–19, respectively); dorsal fin inserted opposite to vertical through pelvic-fin origin (vs dorsal-fin origin anterior to pelvic-fin insertion); pelvic fin reaching the anus (vs not reaching in *T. kaznakowi*); pre-pelvic length 50.7–55.5% of SL (vs 56.3–60.5% of SL in *T. laterimaculata*); caudal-peduncle length 19.1–23.1% of SL (vs. 28.6–31.3% of SL in *T. bombifrons* and 23.3–29.4% of SL in *T. papillosolabiata*); caudal-peduncle depth 7.6–9.2% of SL (vs. 4.5–6.7% of SL in *T. waisihani*); and 4+35 vertebrae (vs 4+38–43 in *T. moquensis* and 4+39–41 in *T. waisihani*). *T. daryoae* can be distinguished from other *Triplophysa* species by the following characteristics: 39 vertebrae (vs 41–47 in *T. orientalis*); caudal-peduncle depth 2.2–2.9 times its length (vs 3.3 times in *T. microphysa*, and 6.7–8.7 times in *T. incipiens*); and posterior chamber of air bladder degenerate (vs developed in *T. microphthalmia*).

A *Triplophysa dorsalis* species group is proposed here based on the molecular data and phylogenetic reconstruction obtained. The proposed species (see above) have also been nested in a single clade in previous phylogenetic studies of *Triplophysa* (Wang et al. 2016; Li et al. 2017; Feng et al. 2019a; Wu et al. 2020). However, no unique morphological synapomorphies that diagnose the *T. dorsalis* species group have been identified. In-depth morphological studies may clarify this issue in the future. Regarding biogeographical distribution, we hypothesize that species such as *T. coniptera* (Talas River), *T. dorsonotata* (Ili River), *T. herzensteini* (Ili River basin), *T. kungessana* (Künes River), *T. paradoxa* (Talas River basin) and *T. salari* (Chirchik River) also belong to this species group. In contrast, *T. uranoscopus*, which is widely distributed in the Zeravshan River, was not nested in this clade (Fig. 6). This result suggests that loaches from Amu Darya have evolved separately from the *Triplophysa* of Syr Darya. A comprehensive study of this situation by examination of other species of *Triplophysa* (e.g., *T. lacusnigri* and *T. kafirnigani*) in the Amu Darya basin may serve as an important key to understanding how *Triplophysa* species have evolved in Central Asia.

Key to *Triplophysa* species occurring in the Syr Darya basin and adjacent regions

- 1 The posterior chamber of the air bladder developed, clearly visible2
 – The posterior chamber of the air bladder degenerated, directly connecting with the bony capsule4
- 2 The caudal peduncle compressed at the base, its width less than its depth
 *T. dorsalis* (Syr darya basin)
 – The caudal peduncle not compressed at the base, its width greater than or equal to its depth3
- 3 Branched dorsal-fin rays usually 8, caudal-fin emarginated and upper lobe longer than lower, maximum body depth fits to the origin of dorsal-fin
 *T. strauchii* (Balkhash and upper Syr Darya basin)
 – Branched dorsal-fin rays usually 7, caudal-fin truncate, upper and lower lobes equal, maximum body depth significantly anterior to the origin of dorsal-fin
 *T. ulacholica* (Issyk Kul Lake and its tributaries)
- 4 Caudal-fin truncate5
 – Caudal-fin emarginated or forked7
- 5 Standard length not exceeding 100 mm; brush-like agglomerations on the sides of the head are absent *T. sewerzowi* (Ili River basin)
 – Standard length exceeding 100 mm; brush-like agglomerations on the sides of the head are present6
- 6 Gill rakers in the inner row on the first gill arch 9–10; caudal peduncle depth 3 times less than its length *T. daryoae* sp. nov. (Sokh River)
 – Gill rakers in the inner row on the first gill arch 12–15; caudal peduncle depth 4 times more than its length *T. tenuis* (Yarkand River)
- 7 Vertebrae number exceeds 408
 – Vertebrae number does not exceed 4011
- 8 Branched pectoral-fin rays 10 or more; intestine not too long, with less than 6 loops9
 – Branched pectoral-fin rays 10 or less; intestine too long, with 10 loops
 *T. chondrostoma* (Qaidam basin)
- 9 Caudal-fin forked; caudal peduncle depth more than 6% of SL10
 – Caudal-fin emarginated; caudal peduncle depth less than 6% of SL
 *T. dorsonotata* (Ili River basin)
- 10 Branched dorsal-fin rays usually 8; cephalic lateral-line system with more than 14 infraorbital pores *T. stenura* (Yangtze River basin)
 – Branched dorsal-fin rays usually 7; cephalic lateral-line system with less than 14 infraorbital pores *T. coniptera* (Talas River basin)
- 11 Caudal peduncle depth more than 8% of SL; 8–9 light-brown irregular blotches on dorsum and 10–12 dark-grey spots on side
 *T. ferganaensis* (Shakhimardan River)
 – Caudal peduncle depth less than 7% of SL; 6–15 transverse stripes on side and back and brindle colored *T. elegans* (Chirchik River)

Comparative materials

- T. dorsalis*: FSU uncatalogued, 6, 56.2–83.5 mm SL; Kara Darya, Andijan Region, Uzbekistan; ICIZ 2200016, 11, 51.6–88.8 mm SL; Achangaran River, Tashkent Region, Uzbekistan.
- T. elegans*: SWU 20190818630–634, 5, 47.9–69.1 mm SL; Chirchik River, Tashkent Region, Uzbekistan.
- T. ferganaensis*: SWU 20190813001, holotype, 87.5 mm SL; Shakhimardan stream in Yordon village, Syr Darya basin, Fergana District, Fergana Region, Uzbekistan. SWU 20190813002–021, FSU 082019650–654, 25 paratypes, 49.5–109.2 mm SL; Shakhimardan stream in Yordon village, Syr Darya basin, Fergana District, Fergana Region, Uzbekistan. BSFC 0025, 2, 42.9–66.2 mm SL; Shakhimardan stream in Yordon village, Syr Darya basin, Fergana District, Fergana Region, Uzbekistan.
- T. stoliczkai*: NWIPB 1305044, 1305046–48, 1305052, 1305056, 1305060, 7, 56.0–102.5 mm SL; Kashi River, Nilka County, Ili River System, Xinjiang Province, China. NWIPB 1305111, 1305113–115, 4, 67.6–91.0 mm SL; Künes River, Xinyuan County, Ili River System, Xinjiang Province, China. NWIPB 1305131, 1305141–142, 3, 64.0–75.4 mm SL; Tekes River, Tekes County, Ili River System, Xinjiang Province, China. NWIPB 1307006–007, 1307014, 3, 58.3–79.5 mm SL; Zhaqu River, Chindu County, Yangtze River System, Qinghai Province, China. NWIPB 1407013–018, 6, 62.7–84.2 mm SL; Changchuan River, Rutog County, Indus River System, Tibet Autonomous Region, China. NWIPB 1007083, 1, 97.5 mm SL; Yarkand River, Yecheng County, Tarim River System, Xinjiang Province, China. NWIPB 1007084, 1, 73.9 mm SL; Qaraqash River, Pishan County, Tarim River System, Xinjiang Province, China.
- T. strauchii*: SWU 20190820642–644, 3, 74.0–110.5 mm SL; unnamed stream, Syr Darya River System, Fergana District, Fergana Region, Uzbekistan. SWU 20190809551, 1, 69.5 mm SL; Kara Darya, Andijan Region, Uzbekistan. SWU 20190818617–642, 26, 45.9–98.7 mm SL; Chirchik River, Tashkent Region, Uzbekistan. BSFC 0022, 8, 83.6–155.9 mm SL; Great Fergana Canal, Syr Darya River System, Uzbekistan District, Fergana Region, Uzbekistan.
- T. tenuis*: NWIPB1250170–174, 5, 83.2–111.2 mm SL; Heihe River, Zhangye city, Heihe River System, Gansu Province, China.
- T. uranoscopis*: SWU 20190802503–504, 2, 78.0–80.2 mm SL; Zeravshan River, Samarkand Region, Uzbekistan; BSFC 0041, 8, 51.5–96.1 mm SL; Karadarya River, Zeravshan River System, Oqdaryo District, Samarkand Region, Uzbekistan.

Acknowledgements

Our sincere thanks go to Dr Barno Bakhromova (Fergana State University) and biology students of Fergana State University for their assistance in the field work and Akbarjon Rozimov (National University of Uzbekistan) for help with the morphological

analysis. We thank Davronbek Rustamov for preparing photos in Figs 1, 2. This work was funded by the grant from the National Natural Science Foundation of China (No. 32170457).

References

- Abdulmalik-Labe OP, Quilang JP (2019) DNA barcoding of fishes from Lake Lanao, Philippines. *Mitochondrial DNA Part B* 4(1): 1890–1894. <https://doi.org/10.1080/23802359.2019.1614890>
- Baltabaev A (1971) Ichthyofauna of the Kara Darya River basin. Doctoral thesis, Tashkent State University, Tashkent, Uzbekistan. <http://diss.natlib.uz/ru-RU/Download/OnlineView/35478>
- Berg LS (1905) Fishes of Turkestan. Printing house of Isidor Goldberg, Sankt-Peterburg, 260 pp. [in Russian]
- Berg LS (1949) Fishes of Fresh Waters of the USSR and Adjacent Countries. Vol. 2. Academy of Sciences USSR Press, Moscow, Leningrad, 467–925. [in Russian]
- Cao L, Zhang E (2008) *Triplophysa waisihani*, a new species of nemacheiline loach from Northwest China (Pisces: Balitoridae). *Zootaxa* 1932(1): 33–46. <https://doi.org/10.11646/zootaxa.1932.1.4>
- Chen S, Sheraliev B, Shu L, Peng Z (2021) *Triplophysa wulongensis*, a new species of cave-dwelling loach (Teleostei, Nemacheilidae) from Chongqing, Southwest China. *ZooKeys* 1026: 179–192. <https://doi.org/10.3897/zookeys.1026.61570>
- Deng SQ, Wang XB, Zhang E (2022) *Triplophysa qini*, a new stygobitic species of loach (Teleostei: Nemacheilidae) from the upper Chang-Jiang Basin in Chongqing, Southwest China. *Ichthyological Exploration of Freshwaters* IEF-1178: 1–11. <https://doi.org/10.23788/IEF-1178>
- Feng C, Tang Y, Liu S, Tian F, Zhang C, Zhao K (2019a) Multiple convergent events created a nominal widespread species: *Triplophysa stoliczkae* (Steindachner, 1866) (Cobitoidea: Nemacheilidae). *BMC Evolutionary Biology* 19(1): e177. <https://doi.org/10.1186/s12862-019-1503-3>
- Feng X, Chen Y, Sui X, Chen Y (2019b) The complete mitochondrial genome of *Triplophysa sellaefer* (Cypriniformes: Balitoridae). *Mitochondrial DNA Part B* 4(1): 536–537. <https://doi.org/10.1080/23802359.2018.1553512>
- Freyhof J, Geiger MF, Goltzarianpour K, Patimar R (2016) *Sasanidus*, a new generic name for *Noemacheilus kermanshahensis* Bănărescu & Nalbant, with discussion of *Ilamnemacheilus* and *Schistura* (Teleostei; Nemacheilidae). *Zootaxa* 4106(2): 065–080. <https://doi.org/10.11646/zootaxa.4107.1.3>
- Freyhof J, Yoğurtçuoğlu B, Kaya C (2021) *Oxynoemacheilus sarus*, a new nemacheilid loach from the lower Ceyhan and Seyhan in southern Anatolia (Teleostei: Nemacheilidae). *Zootaxa* 4964(1): 123–139. <https://doi.org/10.11646/zootaxa.4964.1.6>
- Fricke R, Eschmeyer WN, Van der Laan R (2022) Eschmeyer's Catalog of Fishes: genera, species, references. Electronic Version. <http://researcharchive.calacademy.org/research/ichthyology/catalog/fishcatmain.asp> [accessed 05 April 2022]
- Ivanova NV, Zemlak TS, Hanner RH, Hebert PDN (2007) Universal primer cocktails for fish DNA barcoding. *Molecular Ecology Notes* 7(4): 544–548. <https://doi.org/10.1111/j.1471-8286.2007.01748.x>

- Kottelat M (1984) Revision of the Indonesian and Malaysian loaches of the subfamily Noemacheilinae. *Japanese Journal of Ichthyology* 31(3): 225–260.
- Kottelat M, Freyhof J (2007) Handbook of European freshwater fishes. Kottelat, Cornol & Freyhof, Berlin, 646 pp.
- Kumar S, Stecher G, Tamura K (2016) MEGA7: Molecular Evolutionary Genetics Analysis Version 7.0 for Bigger Datasets. *Molecular Biology and Evolution* 33(7): 1870–1874. <https://doi.org/10.1093/molbev/msw054>
- Lei D, Conteh Kanu U, Zhao G, Xie P, Yuan H, Li Y, Niu J, Ma X (2016) The complete mtDNA genome of *Triplophysa dorsalis* (Cypriniformes, Balitoridae, Cobitoidea): Genome characterization and phylogenetic analysis. *Mitochondrial DNA, Part A, DNA Mapping, Sequencing, and Analysis* 27(5): 3745–3746. <https://doi.org/10.3109/19401736.2015.1079886>
- Li JL, Liu NF, Yang JX (2007) A brief review of *Triplophysa* (Cypriniformes: Balitoridae) species from the Tarim Basin in Xinjiang, China, with description of a new species. *Zootaxa* 1605(1): 47–58. <https://doi.org/10.11646/zootaxa.1605.1.3>
- Li J, Si S, Guo R, Wang Y, Song Z (2013) Complete mitochondrial genome of the stone loach, *Triplophysa stoliczkae* (Teleostei: Cypriniformes: Balitoridae). *Mitochondrial DNA* 24(1): 8–10. <https://doi.org/10.3109/19401736.2012.710225>
- Li J, Yang K, Si S, Zhang X, Song Z (2016) Complete mitochondrial genome of *Triplophysa bleekeri* (Cypriniformes: Balitoridae: Nemacheilinae), and analysis of mitochondrial genetic variability among *Triplophysa* species. *Mitochondrial DNA, Part A* 27(6): 4132–4133. <https://doi.org/10.3109/19401736.2014.1003878>
- Li J, Wang Y, Jin H, Li W, Yan Ch, Yan P, Zhang X, He S, Song Z (2017) Identification of *Triplophysa* species from the Qinghai-Tibetan Plateau (QTP) and its adjacent regions through DNA barcodes. *Gene* 605: 12–19. <https://doi.org/10.1016/j.gene.2016.11.045>
- Lu Z, Li X, Lu W, Huang J, Xu T, Huang G, Qian F, Yang P, Chen S, Moa W, Zhao Y (2022) *Triplophysa xuanweiensis* sp. nov., a new blind loach species from a cave in China (Teleostei: Cypriniformes: Nemacheilidae). *Zoological Research* 43(2): 221–224. <https://doi.org/10.24272/j.issn.2095-8137.2021.310>
- Mitrofanov VP (1989) Genus *Noemacheilus* van Hasselt, 1823 - Charr. In: Mitrofanov VP, Dukravets GM (Eds) Fishes of Kazakhstan. Vol. 4. Cobitidae, Siluridae, Atherinidae, Gadidae, Gasterosteidae, Syngnathidae, Percidae, Gobiidae, Cottidae. Nauka, Alma-Ata, 6–63. [in Russian]
- Norén M, Kullander S, Nydén T, Johansson P (2017) Multiple origins of stone loach, *Barbatula barbatula* (Teleostei: Nemacheilidae), in Sweden based on mitochondrial DNA. *Journal of Applied Ichthyology* 34(1): 58–65. <https://doi.org/10.1111/jai.13507>
- Prokofiev AM (2007) Materials towards the revision of the genus *Triplophysa* Rendahl, 1933 (Cobitoidea: Balitoridae: Nemacheilinae): A revision of nominal taxa of Herzenstein (1888) described within the species “*Nemachilus*” *stoliczkae* and “*N.*” *dorsonotatus*, with the description of the new species *T. scapanognatha* sp. nova. *Journal of Ichthyology* 47(1): 1–20. <https://doi.org/10.1134/S0032945207010018>
- Prokofiev AM (2010) Morphological classification of loaches (Nemacheilinae). *Journal of Ichthyology* 50(10): 827–913. <https://doi.org/10.1134/S0032945210100012>
- Prokofiev AM (2017) Loaches of the subfamily Nemacheilinae of the World. Filigran, Yaroslavl, 315 pp. [in Russian]

- Rambaut A (2014) FigTree 1.4.2 software. Institute of Evolutionary Biology, Univ. Edinburgh, Edinburgh. [software]
- Ren Q, Yang JX, Chen XY (2018) Phylogeographical and Morphological Analyses of *Triplophysa stenura* (Cypriniformes: Nemacheilidae) from the Three Parallel Rivers Region, China. *Zoological Studies* 57: 26.
- Ronquist F, Teslenko M, van der Mark P, Ayres DL, Darling A, Höhna S, Larget B, Liu L, Suchard MA, Huelsenbeck JP (2012) MrBayes 3.2: Efficient bayesian phylogenetic inference and model choice across a large model space. *Systematic Biology* 61(3): 539–542. <https://doi.org/10.1093/sysbio/sys029>
- Rosso JJ, Mabragaña E, González Castro M, Díaz de Astarloa JM (2012) DNA barcoding Neotropical fishes: Recent advances from the Pampa Plain, Argentina. *Molecular Ecology Resources* 12(6): 999–1011. <https://doi.org/10.1111/1755-0998.12010>
- Sambrook J, Russell DW (2001) *Molecular cloning: a laboratory manual*. Vol. 2. Cold Spring Harbor Press, New York, 2100 pp.
- Shen Y, Hubert N, Huang Y, Wang X, Gan X, Peng Z, He S (2019) DNA barcoding the ichthyofauna of the Yangtze River: Insights from the molecular inventory of a mega-diverse temperate fauna. *Molecular Ecology Resources* 19(5): 1278–1291. <https://doi.org/10.1111/1755-0998.12961>
- Sheraliev B, Kayumova Y (2022) Issue of taxonomic status and conservation of loach species (Teleostei: Cobitoidei) in inland waters of Uzbekistan. *Uzbek Biological Journal* 2: 35–40.
- Sheraliev B, Peng Z (2021a) Molecular diversity of Uzbekistan's fishes assessed with DNA barcoding. *Scientific Reports* 11(1): e16894. <https://doi.org/10.1038/s41598-021-96487-1>
- Sheraliev B, Peng Z (2021b) *Triplophysa ferganaensis*, a new loach species from Fergana Valley in Central Asia (Teleostei: Nemacheilidae). *Journal of Fish Biology* 99(3): 807–817. <https://doi.org/10.1111/jfb.14764>
- Tang Q, Huang Y, Wang J, Huang J, Wang Z, Peng Z (2013) The complete mitochondrial genome sequence of *Triplophysa bleekeri* (Teleostei, Balitoridae, Nemacheilinae). *Mitochondrial DNA* 24(1): 25–27. <https://doi.org/10.3109/19401736.2012.716050>
- Turdakov FA (1963) *Fishes of Kirghizia*. Academy of Sciences of the Kyrgyz SSR Press, Frunze, 283 pp. [in Russian]
- Wang Y, Shen Y, Feng C, Zhao K, Song Z, Zhang Y, Yang L, He S (2016) Mitogenomic perspectives on the origin of Tibetan loaches and their adaptation to high altitude. *Scientific Reports* 6(1): e29690. <https://doi.org/10.1038/srep29690>
- Wang T, Zhang Y, Yang Z, Liu Z, Du Y (2020) DNA barcoding reveals cryptic diversity in the underestimated genus *Triplophysa* (Cypriniformes: Cobitidae, Nemacheilinae) from the northeastern Qinghai-Tibet Plateau. *BMC Ecology and Evolution* 20: e151. <https://doi.org/10.1186/s12862-020-01718-0>
- Ward RD, Zemlak TS, Innes HB, Last RP, Hebert PDN (2005) DNA barcoding Australia's fish species. *Philosophical Transactions of the Royal Society of London: Series B Biological Sciences* 360(1462): 1847–1857. <https://doi.org/10.1098/rstb.2005.1716>
- Wu YF, Wu CZ (1992) *The Fishes of the Qinghai-Xizang Plateau*. Sichuan Publishing House of Science & Technology, Chengdu, 599 pp. [in Chinese]

- Wu H, Gu Q, Zhou Ch, Tang Y, Husemann M, Meng X, Zhang J, Nie G, Li X (2020) Molecular phylogeny and biogeography of *Triplophysa* stone loaches in the Central Chinese Mountains Biological Journal of the Linnean Society 130(3): 563–577. <https://doi.org/10.1093/biolinnean/blaa060>
- Zhang F, Zhu L, Zhang L, Wang W, Sun G (2017) Phylogeography of freshwater fishes of the Qilian Mountains area (*Triplophysa leptosoma*, Cobitidae: Cypriniformes). Environmental Biology of Fishes 100(11): 1383–1396. <https://doi.org/10.1007/s10641-017-0650-x>
- Zhao TQ (1984) Taxonomic problems of some *Nemachilus* fishes. Zoological Research 5: 341–346. [in Chinese]
- Zhu SQ (1989) The loaches of the Subfamily Nemacheilinae in China (Cypriniformes: Cobitidae). Jiangsu Science and Technology Publishing House, Nanjing, 150 pp. [in Chinese]

Chimena gen. nov., a new spider genus (Araneae, Mysmenidae) from China, with descriptions of two new species and a new combination

Yucheng Lin^{1,2}, Shuqiang Li³

1 Key Laboratory of Bio-resources and Eco-environment (Ministry of Education), College of Life Sciences, Sichuan University, Chengdu 610065, China **2** The Sichuan key Laboratory for Conservation Biology of Endangered Wildlife, Sichuan University, Chengdu 610065, China **3** Institute of Zoology, Chinese Academy of Sciences, Beijing 100101, China

Corresponding authors: Yucheng Lin (linyucheng@scu.edu.cn), Shuqiang Li (lisq@ioz.ac.cn)

Academic editor: Dimitar Dimitrov | Received 24 April 2022 | Accepted 30 September 2022 | Published 20 October 2022

<https://zoobank.org/BC000963-14DB-433C-B517-ED05918968CF>

Citation: Lin Y, Li S (2022) *Chimena* gen. nov., a new spider genus (Araneae, Mysmenidae) from China, with descriptions of two new species and a new combination. ZooKeys 1125: 69–86. <https://doi.org/10.3897/zookeys.1125.85741>

Abstract

A new mysmenid genus, *Chimena* **gen. nov.**, is reported from China. Two new species: *C. qiong* **sp. nov.** (Hainan, ♂♀, the type species) and *C. nantou* **sp. nov.** (Taiwan, ♀) are illustrated and described in detail. A new combination is suggested: *Chimena taiwanica* (Ono, 2007) **comb. nov.** (Taiwan, ♂♀, transferred from *Mysmena* Simon, 1894). The molecular phylogeny and morphological characters were used to discuss the taxonomy and circumscription of the newly erected genus.

Keywords

Diagnosis, Hainan, mysmenids, new genus, symphytognathoids, Taiwan, taxonomy

Introduction

The spider family Mysmenidae Petrunkevitch, 1928 includes 158 extant species in 14 genera (WSC 2022), making it the second most species-rich spider family of the symphytognathoids. Known species of Mysmenidae are recorded mainly in Asia and South America (Brescovit and Lopardo 2008; Lin and Li 2008, 2013, 2014, 2016; Miller et al. 2009; Feng et al. 2019; Li and Lin 2019; Dupérré and Tapia 2020). Lopardo et al.

(2011) suggested that this family is distributed worldwide, and its diversity is grossly underestimated due to their small size and cryptic lifestyle.

In Asia, nearly 50 species of nine genera have been recorded. Simon (1895a, b) first reported three species from Sri Lanka and the Philippines. Baert (1988) described three species from Sulawesi, Indonesia. The Vietnamese mysmenids were first reported by Lin and Li (2014), and three species were recorded. Nearly 40 species from South China have been described in the past 20 years, more than half of them from Yunnan Province (Lin and Li 2008, 2013; Miller et al. 2009). However, the extraordinary species diversity of Mysmenidae in China and surrounding areas needs to be further investigated.

The aim of this paper is to expand the knowledge about the species diversity of Chinese mysmenid spiders by describing a new genus and two new species and proposing one new combination.

Materials and methods

Material

The mysmenid specimens in this study were collected in Taiwan and Hainan, China, between June 2011 and July 2013. All the specimens were collected by sifting leaf litter or by hand and stored in 95% ethanol at -20°C .

Molecular data

We selected seven specimens from two new species and used the prosoma and all of the legs to extract genomic DNA to amplify COI, H3, 16S, 18S, and 28S. DNA was extracted with the TIANamp Micro DNA Kit (**TIANGEN**) following the manufacturer's protocol for animal tissues. The five gene fragments were amplified in $25\mu\text{L}$ reactions. Primer pairs and PCR protocols are given in Table 1. Raw sequences were edited and assembled using BioEdit v.7.2.5 (Hall 1999). New sequences from this study were deposited in GenBank, and the accession numbers are reported in Table 2. All molecular vouchers and material are stored in the Natural History Museum of Sichuan University in Chengdu (**NHMSU**), China.

We analysed data from 50 species of symphytognathoids including members of the families Theridiosomatidae Simon, 1881, Mysmenidae, Anapidae Simon, 1895, and Symphytognathidae Hickman, 1931. We used the MAFFT v.7.450 online server (<https://mafft.cbrc.jp/alignment/server/>) with default parameters to align the sequences of *Chimena* and *Chanea* species involved in this study. All sequences were concatenated in SequenceMatrix v.1.7.8 (Vaidya et al. 2011). PartitionFinder2 (Lanfear et al. 2017) was used to identify the best-fit models of molecular evolution for each locus. GTR+I+G was selected for COI, H3, 18S, and 28S, and GTR+G was selected for 16S.

We analysed the data using both maximum parsimony (MP) and Bayesian Inference (BI). The MP tree was constructed using MEGA X (Kumar et al. 2018) with TBR (Tree-Bisection-Reconnection) branch swapping and 2000 bootstrap replicates

Table 1. The loci, primer pairs, and PCR protocols used in this study.

Locus	Annealing temperature/ time	Direction	Primer	Sequence 5'→3'	Reference
16S	46.45°/30s	F	16sb2_12864	CTCCGGTTTGAAGCTCAGATCA	Hormiga et al. 2003
		R	LR-J-13360	GTAAGGCCTGCTCAATGA	Feng et al. 2019
	47°/30s	F	16S-A	CGCCTGTTTATCAAAAACAT	Palumbi et al. 1991
		R	16S-B	CTCCGGTTTGAAGCTCAGATCA	
18S	52.1°/30s	F	18s_1F	TACCTGGTTGATCCTGCCAGTAG	Giribet et al. 1996
		R	18s_1000R	GTGGTGCCCTTCCGTCAATT	Balczun et al. 2005
28SD2	54.9°/30s	F	28sa	GACCCGTCTTGAAACACGGA	Rix et al. 2008
		R	LSUR	GCTACTACCACCAAGATCTGCA	
COI	48.95°/30s	F	LCO1490	GGTCAACAAATCATAAAGATATTGG	Folmer et al. 1994
		R	HCO2198	TAAACTTCAGGGTGACCAAAAAATCA	
	46°/30s	F	LCO1490	GGTCAACAAATCATAAAGATATTGG	Simon et al. 1994
		R	COI-Nancy	CCCGGTAAAAATAAAATATAAACTTC	
H3	48°/30s	F	H3af	ATGGCTCGTACCAAGCAGACVGC	Colgan et al. 1998
		R	H3ar	ATATCCTTRGGCATRATRGTGAC	
	50°/30s	F	H3nf	ATGGCTCGTACCAAGCAGAC	
		R	H3nr	ATRTCCTTGGGCATGATTGTTAC	

Table 2. GenBank accession numbers for newly generated DNA sequences.

Species	Identifier	16S	18S	28S	COI	H3
<i>Chimena taiwanica</i>	TW02					
<i>Chimena qiong</i> sp. nov.	HN01					
	HN02					
	HN05					
	HN08				–	
	HN09					
	HN10		–			–
<i>Chanea suukyii</i>	GlgMY01					
	GlgMY02					
	GlgMY03					
	GlgMY04					
	GlgMY05					
	GlgMY80					
	GlgMY98					
<i>Chanea voluta</i>	XZ01					
	XZ02					
	XZ03					
	XZ04					
<i>Chanea</i> sp.	MS_261_MYA					
<i>Chanea</i> sp.	MS_263_MYA	–				
<i>Chanea</i> sp.	MS_250_INN					
<i>Chanea</i> sp.	MS_251_INN					
<i>Chanea</i> sp.	INNE02					
<i>Chanea</i> sp.	INNE03					

with all other parameters set to default. BI was performed using MrBayes v.3.2.7 (Ronquist et al. 2012) on the Cipres Science Gateway (Miller et al. 2010), with four Markov Chains (MCMCs) with default heating parameters for 50,000,000 genera-

tions until the average standard deviation of split frequencies was less than 0.01. The Markov chains were sampled every 1000 generations, and the first 25% of sampled trees were burn-in.

Morphological data

Specimens were examined and measured under a Leica M205 C stereomicroscope. Further details were examined using an Olympus BX51 compound microscope. Male palps and epigynes were examined and photographed after dissection. They were treated in lactic acid for several minutes, and subsequently embedded in Hoyer's Solution before photographing. Photos were made with a Canon EOS 60D wide zoom digital camera (8.5 megapixels) mounted on the Olympus BX51 compound microscope. Images were combined using Helicon Focus v.3.10 software (Khmelik et al. 2006). All measurements are in millimetres. Leg measurements are given as follows: total length (femur, patella, tibia, metatarsus, and tarsus). Abbreviations of institutions and morphological terminology are given in Table 3. References to figures in cited papers are listed in lowercase (fig. or figs), and figures in this paper are noted with an initial capital (Fig. or Figs).

Table 3. List of abbreviations used in the text or figures.

Morphological terminologies			
AER	anterior eye row	FD	fertilization ducts
ALE	anterior lateral eyes	MN	male metatarsal nodule at distal-prolaterally
AME	anterior median eyes	MS	male metatarsal clasping spine
BH	basal haematodocha	PC	paracymbium
CD	copulatory ducts	PER	posterior eye row
CS	cheliceral spines rooted at base	PLE	posterior lateral eyes
CyC	cymbial conductor	PME	posterior median eyes
CyF	cymbial fold	S	spermathecae
CyFs	setae on cymbial fold	SD	spermatid duct
CyP1	process on cymbial conductor	SP	scape
CyP2	process on paracymbium	St	subtegulum
E	embolus	Ti	palpal tibia
Institutions			
FRIT	Forestry Research Institute of Taipei, Taipei, China		
IZCAS	Institute of Zoology, Chinese Academy of Sciences, Beijing, China		
NSMT	Department of Zoology, National Science Museum, Tokyo, Japan		
NHMSU	Natural History Museum of Sichuan University, Chengdu, China		

Results

Phylogenetic analysis

The topologies from both the MP and BI analyses (Figs 1, 2) showed mysmenids and theridiosomatids were highly supported as monophyletic in both analyses, although the

position of theridiosomatids was not consistent between analyses. Symphytognathidae was rendered polyphyletic by three anapid species. The monophyly of Anapidae is not strongly supported and is rendered paraphyletic due to the placement of the theridiid *Steatoda borealis* (Hentz, 1850). In the BI tree anapids are divided into two highly supported clades that we refer to as “Anapidae 1” and “Anapidae 2” (Fig. 2), but Anapidae 2 is rendered polyphyletic by the theridiid *Steatoda borealis* and the linyphiid *Linyphia triangularis* (Clerck, 1757).

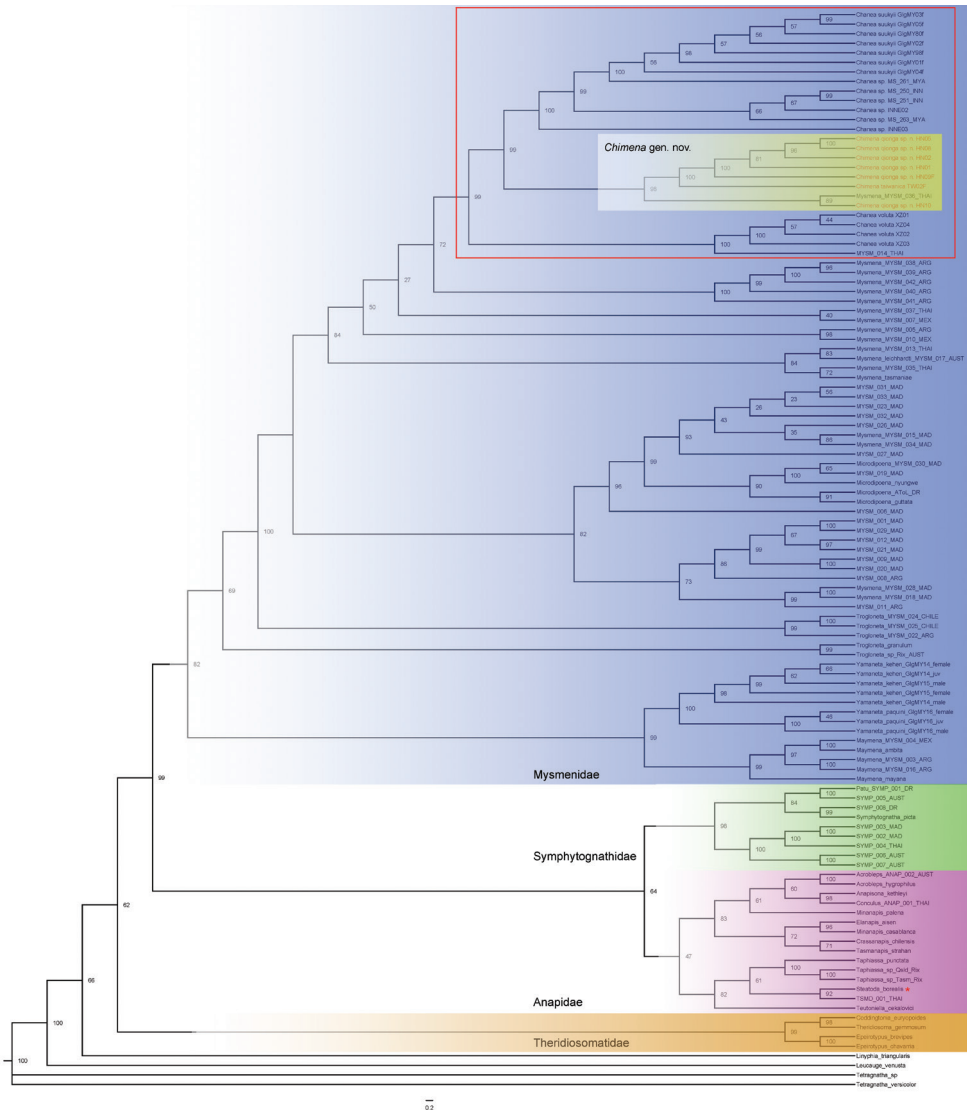


Figure 1. Tree topology obtained by maximum likelihood. Numbers at nodes are bootstrap values. The clade of *Chimena* gen. nov. (yellow) + *Chanea* is nested within Mysmenidae (blue). Further clades are Symphytognathidae (green), Anapidae (pink) and Theridiosomatidae (orange).

Etymology. The generic name is a combination of the first three letters of China and the latter half of *Mysmena*. The gender is feminine.

Diagnosis. *Chimena* gen. nov. differs from other mysmenid genera by the presence of strong spines on the chelicerae of males (as in some Chinese species of *Gaoligonga* Miller, Griswold & Yin, 2009 and *Mysmena* Miller, Griswold & Yin, 2009; see fig. 38A in Miller et al. 2009, fig. 8C in Lin and Li 2014, and figs 5E, 6A, 7E in Lin and Li 2008); a very long embolus spiralling around the bulb at least 5 times; and the spermathecae near the posterior margin of the epigyne; the copulatory ducts are highly coiled and extend anteriorly. *Chimena* gen. nov. is morphologically similar to *Chanea* Miller, Griswold & Yin, 2009 in having an extremely coiled embolus (cf. Figs 3A, 5A; figs 49A–B, 51A–B in Miller et al. 2009; figs 3A in Lin and Li 2016) and a membranous, translucent, wrinkled scape (Figs 4J, 6J, 7F; fig. 4D in Lin and Li 2016). Males can be distinguished by the presence of a cymbial process (CyP1, CyP2), which is absent in *Chanea* (Figs 3D, 3F, 5B, 5G vs. 49A, 49B in Miller et al. 2009 and figs 2C, 3C in Lin and Li 2016). Females differ by having the spiral rod-shaped spermathecae close to the posterior margin of the epigyne, versus globular spermathecae located anteriorly in *Chanea*, as well as the copulatory ducts not being entwined with the fertilization ducts [intertwined in *Chanea* (Figs 4I, J, 6I, J, 7E–F vs. fig. 49C in Miller et al. 2009 and fig. 4C–D in Lin and Li 2016)].

Description. Carapace pear-shaped, cephalic part distinctly raised in male; clypeus slightly concave. Ocular area black, AME black, others white; AER procurved, PER recurved or straight; ALE adjoined to AME and PLE, AMEs separated by at least its diameter; further separated in males than in females. Two or three pairs of strong spines on anterior surface of male chelicerae (Figs 4E, 6E). Labium fused to sternum. Sternum triangular, slightly plump, posteriorly truncated, light colour anteriorly and centrally. Each leg segment proximally pale yellow, distally darkish grey. Male with a mesal clasping spine and a distal, small nodule prolaterally on metatarsus I (Fig. 3C), female with weakly sclerotized spot on femur I. Abdomen dorsally rounded, surrounded by stripe of white pigmentation laterally and posteriorly. Venter black between epigastric furrow and spinnerets (Figs 4B, D, 6B, D, 7B).

Male palp. Tibia swollen, proximally narrow and distally broad, larger number of long setae on dorsally than ventrally (Figs 3F–G, 5G–H). Cymbium translucent, encloses ventral and prolateral sides of bulb (Figs 3G, 5E, H). Paracymbium flat, wide, with a few long setae and a horn-shaped process (CyP2) distally (Figs 3D, F, 5B, D). Distal part of cymbium extends to form an apical cymbial conductor (CyC), with horn-shaped or dentoid process (CyP1) attached to lateral margin of cymbial conductor (Figs 3E, F, 5B–D, G–H). Tegulum flat, without any process or projection (Figs 3F, 5D, F). Embolus slender, filiform, elongate, encircles the bulb multiple times, end extends to apex of cymbial conductor (Figs 3F, 5E, G–H).

Epigyne and vulva. Genital area covered with sparse setae, sclerotized spermathecae faintly visible through tegument (Figs 4H, 6H, 7D). Scape wrinkled, membranous, finger-like, short. Spermathecae rod-shaped, spiral, near epigynal posteromargin, separated from one another by about their length. Most of copulatory ducts membranous, extending anteriorly, coiled, overlapped with anterior end of spermathecae.

Fertilization ducts relatively long, wide, originating at distal part of spermathecae, middle and proximal parts entwined with spermathecae, distal part thins gradually, inflexed (Figs 4I–J, 6I–J, 7E–F).

Composition. *Chimena qiong* sp. nov., *C. taiwanica* (Ono, 2007) comb. nov., and *C. nantou* sp. nov.

Distribution. China (Hainan, Taiwan).

***Chimena qiong* sp. nov.**

<https://zoobank.org/B9AAA398-0B07-4F88-8477-643064500729>

Figs 3, 4, 8

Type material. *Holotype* ♂ (IZCAS) and *paratypes* 2♀ (IZCAS), CHINA: Hainan Province, Limushan Township, Limushan Natural Reserve, Yinhe Protected Station, 19°12.002'N, 109°43.710'E, 591±20 m, 25.III.2012, Z. Chen leg.; *paratypes* 2♀ (IZCAS), CHINA: Hainan Province, Changjiang Township, Bawangling Natural Reserve, near the Yaga Convention Centre, 19°04.828'N, 109°07.369'E, 567±20 m, 13.IV.2012, Z. Chen leg.; *Paratypes* 1♂ (IZCAS); CHINA: Hainan Province, Lingshui County, Diaolushan Natural Reserve, 18°43.505'N, 108°52.104'E, 920 m, 18.VI.2011, Y. Zhou leg.

Etymology. The species epithet, a noun in apposition, refers to 'qiong', which is short for Hainan Province.

Diagnosis. Males and females are similar to *Chimena taiwanica* comb. nov. in having a long, coiled embolus and the configuration of the vulva, but they can be distinguished by having three pairs of cheliceral spines (two pairs in the latter) (Fig. 4E vs. Fig. 6E) and a horn-shaped process (CyP1) on the cymbial conductor (tooth-shaped in the latter) (Fig. 3E, G vs. Fig. 5C, H). The female differs from congeners by the strongly spiralled, longer spermathecae (moderately spiralled in *C. taiwanica* comb. nov., and shorter in *C. nantou* sp. nov.) (Fig. 4I, J vs. Figs 6I, J, 7E, F).

Description. Male. Habitus as in Fig. 4A, B, E, F. Total length 0.63. Carapace 0.23 long, 0.24 wide. Clypeus 0.11 high. Sternum 0.20 long, 0.19 wide. Abdomen 0.45 long, 0.44 wide. Length of legs: I 0.92 (0.29, 0.13, 0.18, 0.14, 0.18); II 0.80 (0.27, 0.09, 0.17, 0.12, 0.15); III 0.60 (0.17, 0.08, 0.12, 0.11, 0.12); IV 0.73 (0.21, 0.08, 0.15, 0.14, 0.15). Carapace pale yellow, black on cephalic area, pear-shaped. Cephalic area strongly raised. AER procurved, PER straight. Mouthparts pale brown. Chelicerae bearing 3 pairs of strong spines anteriorly (Fig. 4E). Sternum subtriangular, slightly plump, pale, anterior-centrally and laterally black, posteriorly truncated. Legs pale, gradually darkening to grey at each segment distally. Patella with distodorsal seta, proximal seta on tibia. Mesal clasping spine and distal, small nodule on metatarsus I (Figs 3C, 4B). Abdominal dorsum rounded, darkish grey, with paired light speckles, white stripe laterally and posteriorly. Posterior area of epigastric furrow and spinnerets black. Colulus black, long, tongue shaped.

Palp (Fig. 3A, B, D–G): weakly sclerotized. Femur equal to 2.2× length of patella, patella approximately half of tibial width. Tibia cup-shaped, with dense, long setae

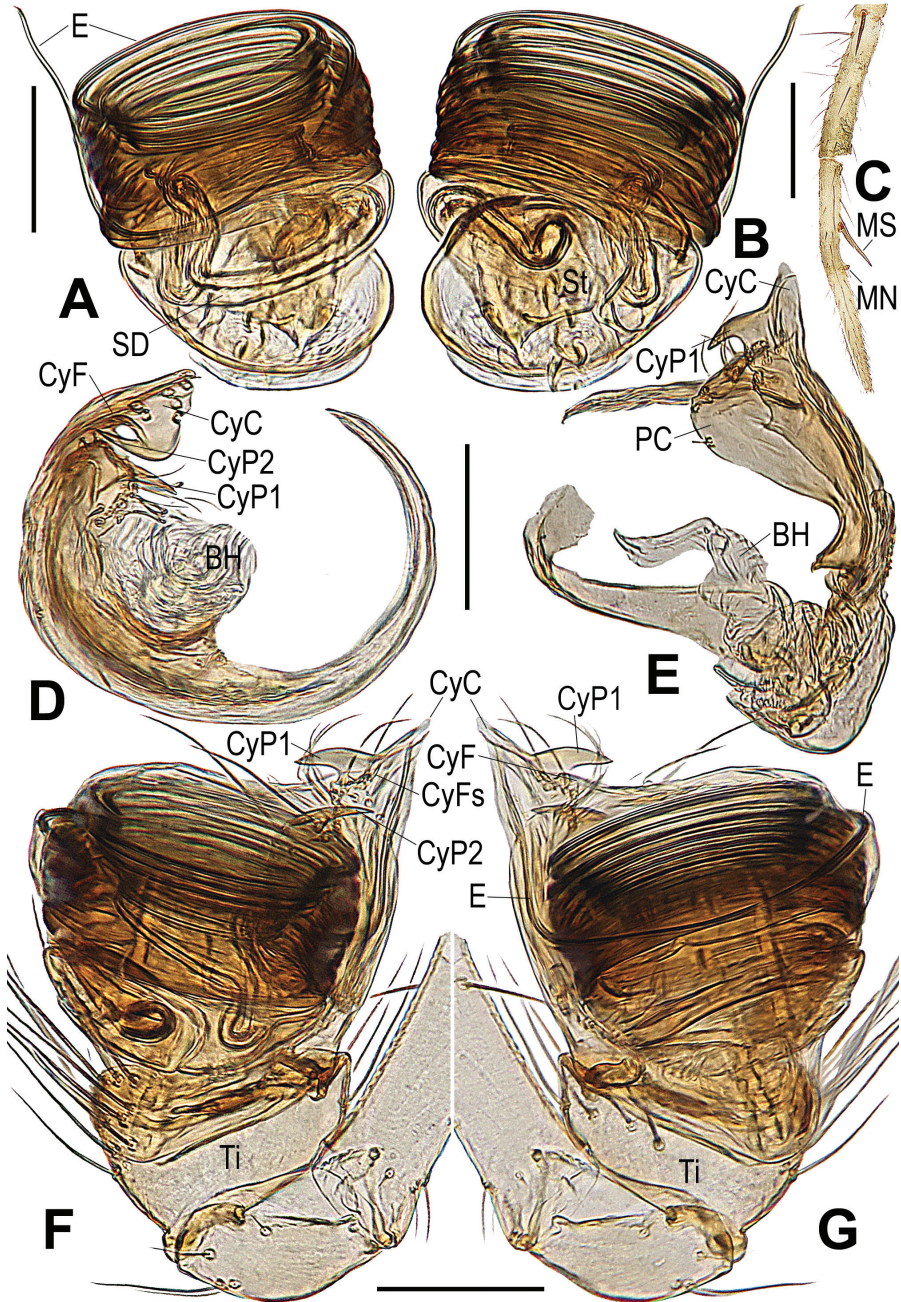


Figure 3. *Chimena qiong* sp. nov., male **A** left palpal bulb, retrolateral **B** palpal bulb, prolateral **C** distal segments of right leg I, prolateral **D** cymbium, apical **E** cymbium, retrolateral **F** left palp, retrolateral **G** left palp, prolateral. Abbreviations: BH basal haematodocha; CyC cymbial conductor; CyF cymbial fold; CyFs setae on cymbial fold; CyP1 process on cymbial conductor; CyP2 process on paracymbium; PC paracymbium; E embolus; MN male metatarsal nodule at distal-prolaterally; MS male metatarsal clasp spine; SD spermatheca; St subtegulum; Ti palp tibia. Scale bars: 0.10 mm.

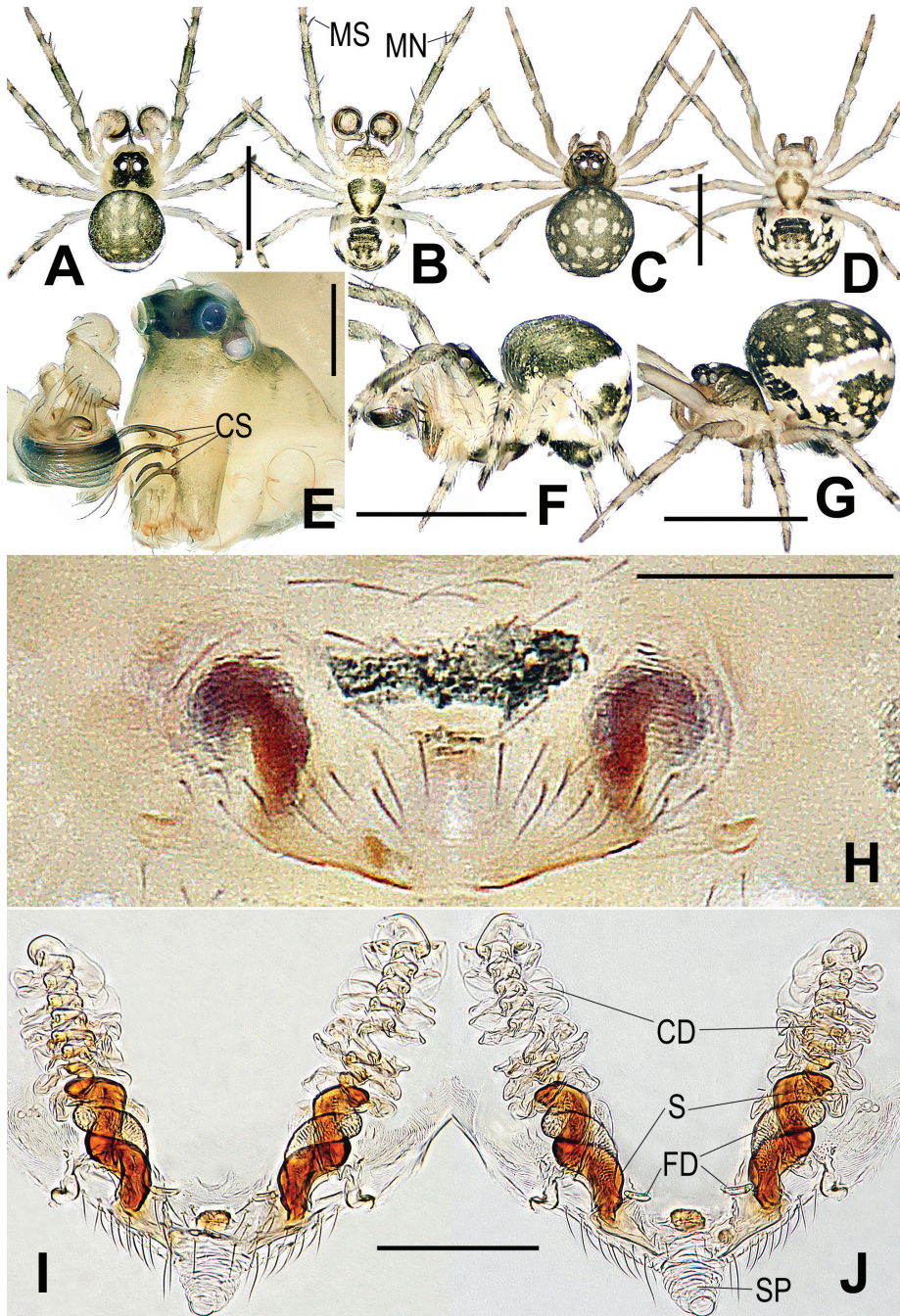


Figure 4. *Chimena qiong* sp. nov., male (A, B, E, F) and female (C, D, G–J) A, C habitus, dorsal B, D habitus, ventral E prosoma, front-lateral, F, G habitus, lateral H epigyne, ventral I vulva, ventral J vulva, dorsal. Abbreviations: CD copulatory ducts; CS cheliceral spines rooted at base; FD fertilization ducts; MN male metatarsal nodule at distal-prolaterally; MS male metatarsal clasp spine; S spermathecae; SP scape. Scale bars: 0.50 mm (A–D, F, G); 0.20 mm (E); 0.10 mm (H–J).

dorsally. Cymbium narrow basally, wrapped around bulb ventrally and retrolaterally; distal cymbial conductor triangular, lamellar, a sub-distal tooth-shaped process (CyP1) at medial margin; paracymbium wide, earlobe shaped, bearing a few long setae and a sharp process (CyP2) distally. CyP1 almost same length as CyP2. Cymbial fold located at base of CyP1, with a few short setae (CyFs). Tegulum flat, smooth; subtegulum translucent, inner spermathecal duct faintly visible. Embolus very long, filiform, tightly coiled around entire tegulum at least 10 times, distal end extending to cymbial conductor (CyC).

Female. Habitus as in Fig. 4C, D, G. Total length 0.72. Carapace 0.23 long, 0.25 wide. Clypeus 0.06 high. Sternum 0.19 long, 0.17 wide. Abdomen 0.48 long, 0.43 wide. Length of legs: I 0.90 (0.28, 0.12, 0.18, 0.15, 0.17); II 0.82 (0.25, 0.10, 0.18, 0.13, 0.15); III 0.63 (0.18, 0.09, 0.12, 0.11, 0.13); IV 0.76 (0.22, 0.09, 0.15, 0.14, 0.16). Cephalic area moderately raised, chelicerae unmodified, femur I with weak sclerotized spot; other features as in male.

Epigyne (Fig. 4H–J): genital area bears sparse setae, with central dark speckle. Scape tongue shaped, protruded, rugose, membranous. Spermathecae long, claviform, separated by about their length, base near epigynal posterior margin. Copulatory ducts membranous, translucent, distal part overlapping and convoluted at spermathecae anteriorly. Fertilization ducts long, middle and proximal parts entwined with spermathecae, distal part extends horizontally to atrium.

Distribution. China (Hainan) (Fig. 8).

***Chimena taiwanica* (Ono, 2007) comb. nov.**

Figs 5, 6, 8

Mysmena taiwanica Ono, in Ono et al. 2006: 73, figs 8–19 (♂♀).

Type material. *Holotype* ♂ (FRIT) and *paratypes* 2 ♀ (NSMT), CHINA: southern Taiwan, Kaohsiung Hsien, Shanping Work Station of Liukuei Research Center, ca 700 m, by sifting soil litter in a forest, 9.III.2005, H. Ono leg. Not examined.

Examined materials. 6♂13♀ (IZCAS), CHINA: central Taiwan, Nantou County, Ren'ai Township, Xinsheng Village, Huisun Farm, 24°05.279'N, 121°02.078'E, 788 m, 1.VII.2013, G. Zheng leg.

Diagnosis. *Chimena taiwanica* comb. nov. is similar to *C. qiong* sp. nov. in having strong, modified cheliceral spines in the males (cf. Figs 6E, 4E), a long and multi-coiled embolus (cf. Figs 5A, 3A), and in females, the similar configuration of the vulva, as in that of *C. nantou* sp. nov. (cf. Figs 6J, 4J, 7F). Males of *C. taiwanica* can be distinguished by having 2 pairs of cheliceral spines (3 pairs in *C. qiong* sp. nov.) (Fig. 6E vs. Fig. 4E and figs 8, 10 in Ono et al. 2006) and a tooth-shaped process (CyP1) (process horn-shaped in *C. qiong*) (Fig. 5C, H vs. Fig. 3E, G). The female differs from *C. qiong* sp. nov. by the moderately spiralled, thinner spermathecae tapered at the base (strongly spiralled, thicker and blunt at the base in *C. qiong* sp. nov.) (Fig. 6I, J vs. Fig. 4I, J); and from *C. nantou* sp. nov. by the longer spermathe-

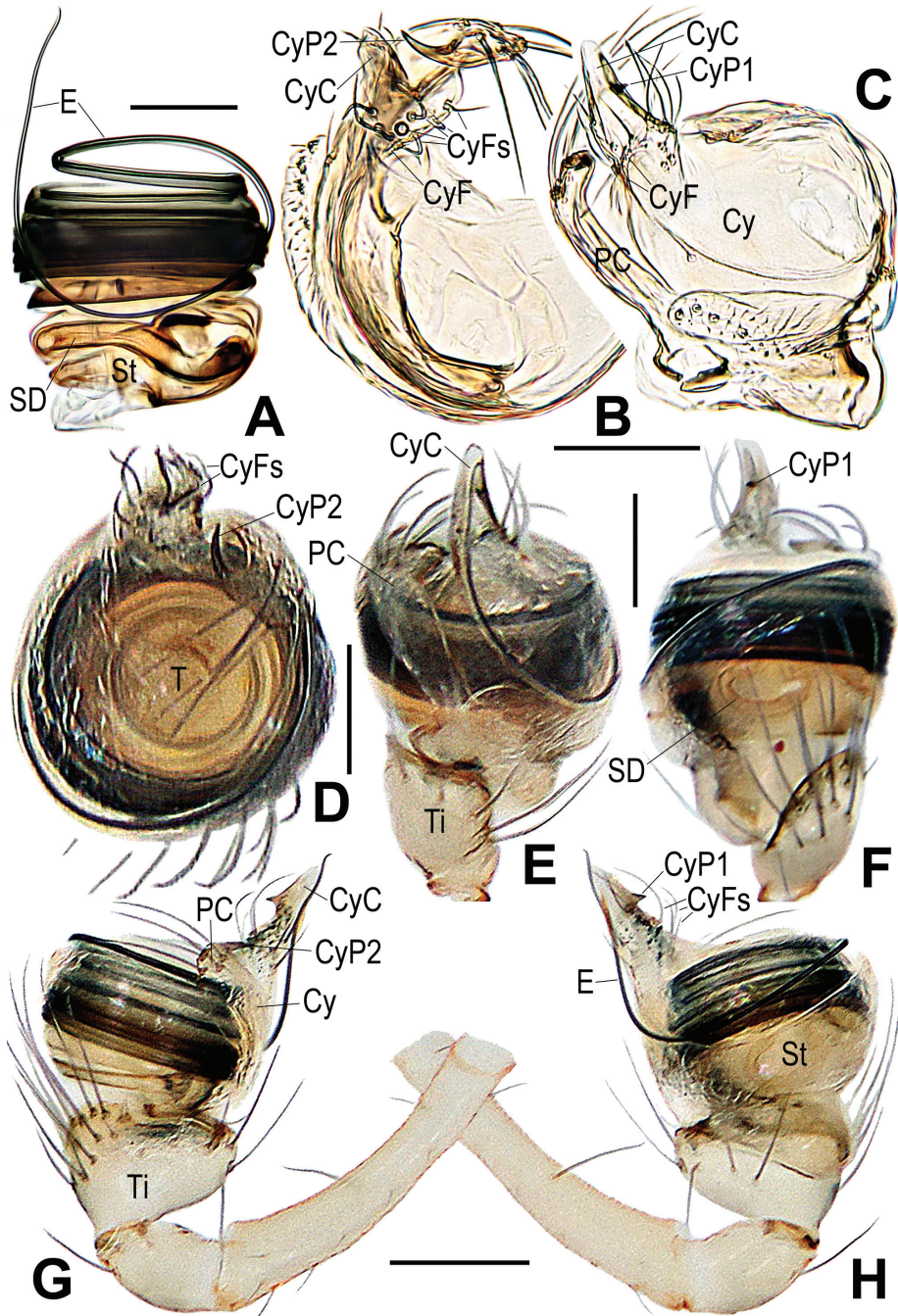


Figure 5. *Chimena taiwanica* (Ono, 2007) comb. nov., male **A** left palpal bulb, retrolateral **B** cymbium, apical **C** cymbium, dorsal-retrolateral **D** left palp, apical **E** left palp, ventral **F** left palp, dorsal **G** left palp, retrolateral **H** left palp, retrolateral. Abbreviations: Cy cymbium; CyC cymbial conductor; CyF cymbial fold; CyFs setae on cymbial fold; CT cymbial tooth; CyP2 process on paracymbium; PC paracymbium; E embolus; SD spermatheca; St subtegulum; T tegulum; Ti palpal tibia. Scale bars: 0.10 mm.

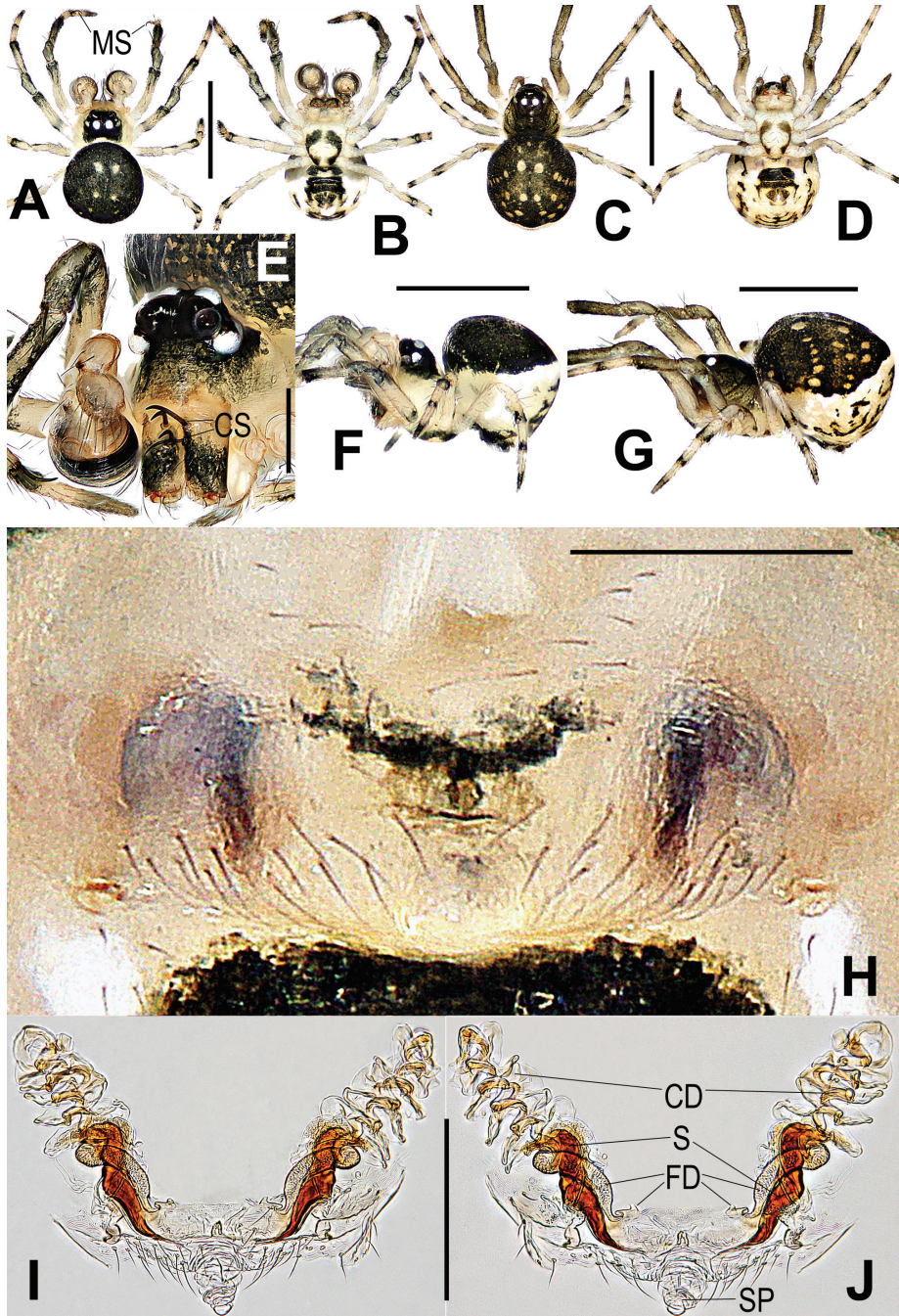


Figure 6. *Chimena taiwanica* (Ono, 2007) comb. nov., male (A, B, E, F) and female (C, D, G–J) A, C habitus, dorsal B, D habitus, ventral E prosoma, front-lateral F, G habitus, lateral H epigyne, ventral I vulva, ventral J vulva, dorsal. Abbreviations: CD copulatory ducts; CS cheliceral spines rooted at base; FD fertilization ducts; MS male metatarsal clasp spine; S spermathecae; SP scape. Scale bars: 0.50 mm (A–D, F, G); 0.20 mm (E); 0.10 mm (H–J).

cae narrowed in the middle (shorter and wider at the middle in *C. nantou* sp. nov.) (Fig. 6I, J vs. Fig. 7E, F).

Description. Male. Habitus as in Fig. 6A, B, E, F. Total length 0.65. Carapace 0.24 long, 0.24 wide. Clypeus 0.12 high. Sternum 0.22 long, 0.20 wide. Abdomen 0.43 long, 0.43 wide. Length of legs: I 0.96 (0.30, 0.13, 0.19, 0.14, 0.20); II 0.84 (0.27, 0.11, 0.17, 0.13, 0.16); III 0.62 (0.17, 0.09, 0.12, 0.11, 0.13); IV 0.74 (0.22, 0.09, 0.15, 0.14, 0.16). Features same as in *C. qiong* sp. nov., except for 2 paired spines on chelicerae and darker body colouration.

Palp (Fig. 5A–H): weakly sclerotized. Femur equal to 2.4× length of patella, patella about half of tibial width. Tibia cup-shaped in prolateral view, slightly wider than long, bearing long setae with more dorsally than ventrally. Cymbium constricted basally, enwrapping bulb ventrally and retrolaterally; distal cymbial conductor (CyC) triangular, lamellar, tooth-shaped process (CyP1) at medial margin (Fig. 5G). Paracymbium long, with sharp distal process (CyP2), a few long setae (Fig. 5C, G). CyP1 smaller and shorter than CyP2. Cymbial fold at base of CyP1 (Fig. 5B), with a few short setae (CyFs). Tegulum flat, smooth, button-shaped (Fig. 5D); subtegulum translucent, spermathecal duct faintly visible. Embolus very long, filiform, strongly sclerotized, tightly coiled around entire tegulum ca 8 times, distal end extended slightly beyond cymbial conductor (CyC) (Fig. 5G, H).

Female. Habitus as in Fig. 6C, D, G. Total length 0.78. Carapace 0.24 long, 0.22 wide. Clypeus 0.06 high. Sternum 0.24 long, 0.20 wide. Abdomen 0.46 long, 0.44 wide. Length of legs: I 1.00 (0.30, 0.13, 0.20, 0.15, 0.22); II 0.86 (0.27, 0.12, 0.17, 0.13, 0.18); III 0.68 (0.18, 0.09, 0.14, 0.14, 0.15); IV 0.78 (0.23, 0.10, 0.16, 0.14, 0.17). Cephalic area lower than in male, chelicerae unmodified, femur I with weak sclerotized spot; other features as in male.

Epigyne (Fig. 6H–J): vulval configuration similar to *C. qiong* sp. nov. Spermathecae narrow, proximally base tapering, separated by more than their length.

Distribution. China (Taiwan) (Fig. 8).

Remarks. Although the type specimens of *Chimena taiwanica* comb. nov. (= *Mysmena taiwanica* Ono, 2007) have not been examined for this study, the modified strong spines on the male chelicerae, the very long, multiply coiled embolus around the bulb, the paracymbium with two processes (CyP1, CyP2), the shape of epigyne, and the protruded scape depicted in the original illustrations (see figs 8, 10, 12–15, 18–19 in Ono et al. 2006: 74–76) leave little doubt that our identification is correct. Additionally, the specimens examined here were also collected from Taiwan, not too far from the type locality.

***Chimena nantou* sp. nov.**

<https://zoobank.org/DCD77110-6568-4DBA-9B03-8063C16EBC41>

Figs 7, 8

Type material. Holotype ♀ (IZCAS), CHINA: Taiwan, Nantou County, Ren'ai Township, Songgang Village, 24°05.222'N, 121°10.335'E, 2067 m, 2.VII.2013, G. Zheng leg.

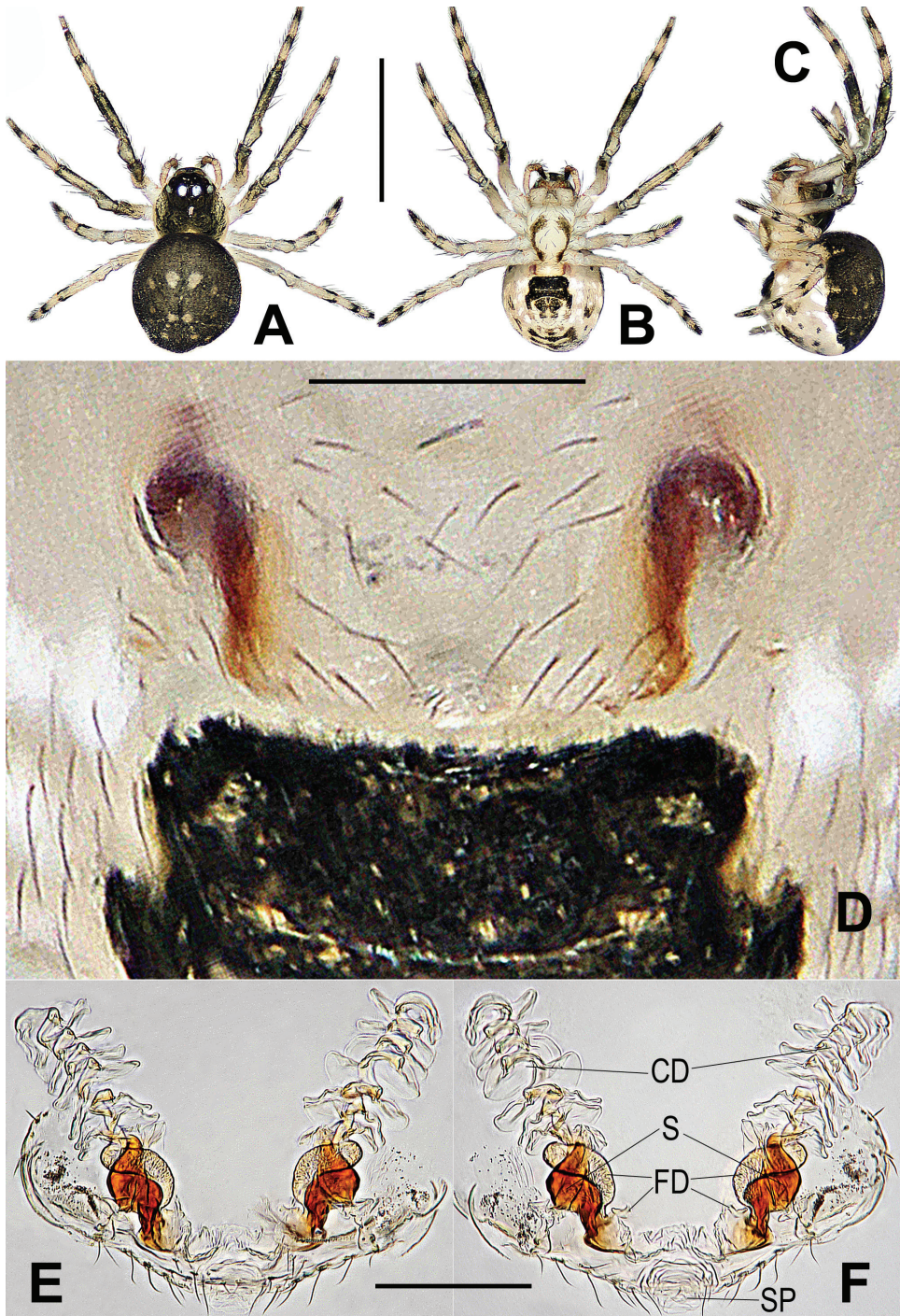


Figure 7. *Chimena nantou* sp. nov., holotype female **A** habitus, dorsal **B** habitus, ventral **C** habitus, lateral **D** epigyne, ventral **E** vulva, ventral **F** vulva, dorsal. Abbreviations: CD copulatory ducts; FD fertilization ducts; S spermathecae; SP scape. Scale bars: 0.50 mm (**A–C**); 0.10 mm (**D–F**).

Etymology. The new species is named after the type locality; noun in apposition.

Diagnosis. *Chimena nantou* sp. nov. shares a similar configuration of the vulva to *C. qiong* sp. nov. and *C. taiwanica* comb. nov., but differs from the former by the shorter spermathecae with fewer spirals (longer and with more spirals in *C. qiong*) (cf. Fig. 7E, F vs. Fig. 4I, J), and from the latter by the more compact spermathecae (elongated in the latter) (cf. Fig. 7E, F vs. Fig. 6I, J).

Description. Female: Habitus as in Fig. 7A–C. Total length 0.75. Carapace 0.25 long, 0.23 wide. Clypeus 0.07 high. Sternum 0.24 long, 0.22 wide. Abdomen 0.45 long, 0.42 wide. Length of legs: I 0.98 (0.30, 0.13, 0.19, 0.14, 0.22); II 0.87 (0.27, 0.12, 0.17, 0.14, 0.18); III 0.66 (0.19, 0.09, 0.14, 0.14, 0.16); IV 0.80 (0.23, 0.10, 0.16, 0.15, 0.18). Somatic features as in female of *C. taiwanica* comb. nov.

Epigyne (Fig. 7D–F): vulval configuration similar to *C. qiong* sp. nov. and *C. taiwanica* comb. nov. Genital area bears sparse setae, without a dark speckle. Spermathecae short, tapering at distal end and proximal base, separated by ca 1.1× their length. Scape knob shaped, rugose, membranous. Copulatory ducts translucent. Most of fertilization ducts intertwined with spermathecae, distal part of fertilization ducts thin, inflected.

Male. Unknown.

Distribution. China (Taiwan) (Fig. 8).

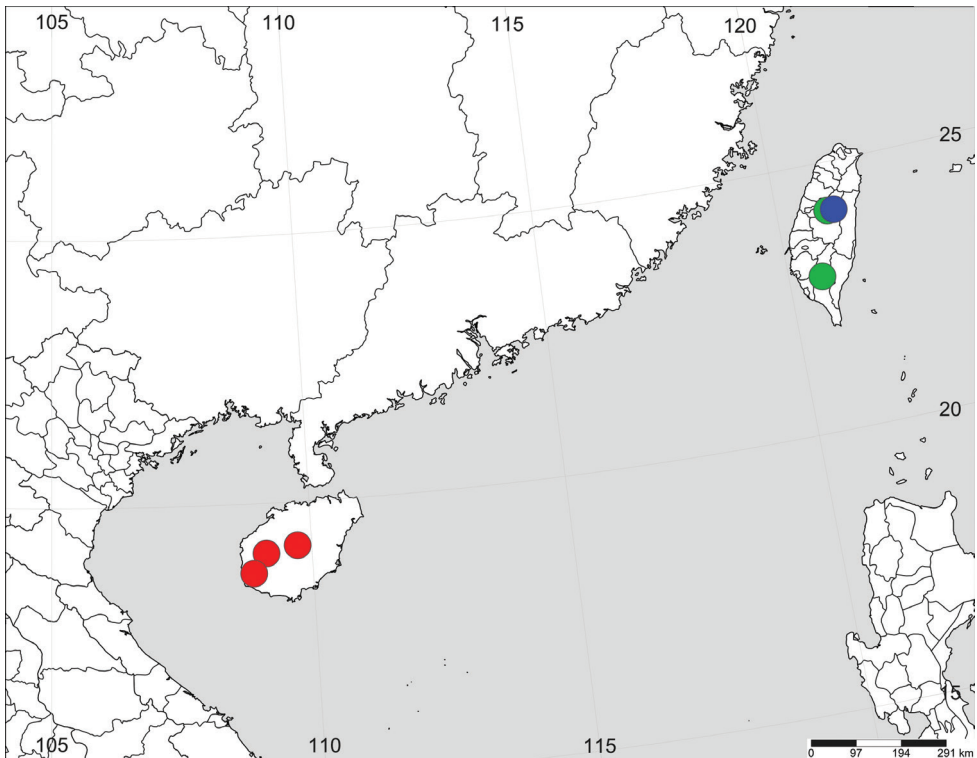


Figure 8. Distribution records of three *Chimena* spp.: *C. qiong* sp. nov. (red dot), *C. taiwanica* (green dot) and *C. nantou* sp. nov. (blue dot).

Discussion

We tested the phylogenetic and taxonomic position of *Chimena* gen. nov. based on molecular data and unique morphological evidence. The results of our analyses indicate that *Chimena* gen. nov. is highly supported. However, further detailed phylogenetic analysis based on more mysmenid specimens will help better place the mysmenid species and genera.

Acknowledgements

We thank Yuri M. Marusik (Magadan, Russia) and an anonymous referee for insightful comments, and are especially grateful to Dimitar Dimitrov (Bergen, Norway), the subject editor of this manuscript, for his kind help. Danni Sherwood (UK) and Sarah Crews (San Francisco, USA) kindly checked the English of the final draft. This study was supported by the National Natural Foundation of China (NSFC-31972870, 31772410, 31750002).

References

- Baert L (1988) The Ochyroceratidae and Mysmenidae from Sulawesi (Araneae). *Indo-Malayan Zoology* 5: 9–22.
- Brescovit AD, Lopardo L (2008) The first record on the spider genus *Trogloneta* Simon in the southern hemisphere (Araneae, Mysmenidae), with descriptions of three new species from Brazil and remarks on the morphology. *Acta Zoologica, Stockholm* 89(2): 93–106. <https://doi.org/10.1111/j.1463-6395.2007.00296.x>
- Dupérré N, Tapia E (2020) Megadiverse Ecuador: A review of *Mysmenopsis* (Araneae, Mysmenidae) of Ecuador, with the description of twenty-one new kleptoparasitic spider species. *Zootaxa* 4761(1): 1–81. <https://doi.org/10.11646/zootaxa.4761.1.1>
- Feng C, Miller JA, Lin Y, Shu Y (2019) Further study of two Chinese cave spiders (Araneae, Mysmenidae), with description of a new genus. *ZooKeys* 870: 77–100. <https://doi.org/10.3897/zookeys.870.35971>
- Hall TA (1999) BioEdit: A user-friendly biological sequence alignment editor and analysis program for Windows 95/98/NT. *Nucleic Acids Symposium Series* 41: 95–98. <https://10.1021/bk-1999-0734.ch008>
- Khmelik VV, Kozub D, Glazunov A (2006) Helicon Focus 3.10.3. <http://www.heliconsoft.com/heliconfocus.html> [accessed on 10 September 2018]
- Kumar S, Stecher G, Li M, Knyaz C, Tamura K (2018) MEGA X: Molecular evolutionary genetics analysis across computing platforms. *Molecular Biology and Evolution* 35(6): 1547–1549. <https://doi.org/10.1093/molbev/msy096>
- Lanfear R, Frandsen PB, Wright AM, Senfeld T, Calcott B (2017) Partitionfinder 2: New methods for selecting partitioned models of evolution for molecular and morphological

- phylogenetic analyses. *Molecular Biology and Evolution* 34(3): 772–773. <https://doi.org/10.1093/molbev/msw260>
- Li Y, Lin Y (2019) Taxonomic review of the Asian *Trogloneta* species (Araneae, Mysmenidae). *ZooKeys* 817: 41–60. <https://doi.org/10.3897/zookeys.817.30468>
- Lin Y, Li S (2008) Mysmenid Spiders of China (Araneae: Mysmenidae). *Annales Zoologici* 58(3): 487–520. <https://doi.org/10.3161/000345408X364337>
- Lin Y, Li S (2013) Two new species of the genera *Mysmena* and *Trogloneta* (Mysmenidae, Araneae) from southwestern China. *ZooKeys* 303: 33–51. <https://doi.org/10.3897/zookeys.303.4808>
- Lin Y, Li S (2014) Mysmenidae (Arachnida, Araneae), a spider family newly recorded from Vietnam. *Zootaxa* 3826(1): 169–194. <https://doi.org/10.11646/zootaxa.3826.1.5>
- Lin Y, Li S (2016) Mysmenidae, a spider family newly recorded from Tibet (Arachnida, Araneae). *ZooKeys* 549: 51–69. <https://doi.org/10.3897/zookeys.549.6046>
- Lopardo L, Giribet G, Hormiga G (2011) Morphology to the rescue: Molecular data and the signal of morphological characters in combined phylogenetic analyses – a case study from mysmenid spiders (Araneae, Mysmenidae), with comments on the evolution of web architecture. *Cladistics* 27(3): 278–330. <https://doi.org/10.1111/j.1096-0031.2010.00332.x>
- Miller JA, Griswold CE, Yin CM (2009) The symphytognathoid spiders of the Gaoligongshan, Yunnan, China (Araneae, Araneoidea): Systematics and diversity of micro-orbweavers. *ZooKeys* 11: 9–195. <https://doi.org/10.3897/zookeys.11.160>
- Miller MA, Pfeiffer WT, Schwartz T (2010) Creating the CIPRES Science Gateway for inference of large phylogenetic trees. Gateway Computing Environments Workshop (GCE), 1–8. <https://doi.org/10.1109/gce.2010.5676129>
- Ono H, Chang YH, Tso IM (2006) Three new spiders of the families Theridiidae and Anapidae (Araneae) from southern Taiwan. *Memoirs of the National Science Museum, Tokyo* 44: 71–82. <https://doi.org/10.2476/asjaa.44.71>
- Ronquist F, Teslenko M, van der Mark P, Ayres DL, Darling A, Höhna S, Larget B, Liu L, Suchard MA, Huelsenbeck JP (2012) MrBayes 3.2: Efficient Bayesian phylogenetic inference and model choice across a large model space. *Systematic Biology* 61(3): 539–542. <https://doi.org/10.1093/sysbio/sys029>
- Simon E (1895a) Etudes arachnologiques. 26e. XLI. Descriptions d'espèces et de genres nouveaux de l'ordre des Araneae. *Annales de la Société Entomologique de France* 64: 131–160.
- Simon E (1895b) Histoire naturelle des araignées. Deuxième édition, tome premier. Roret, Paris, 761–1084.
- Vaidya G, Lohman DJ, Meier R (2011) SequenceMatrix: Concatenation software for the fast assembly of multi-gene datasets with character set and codon information. *Cladistics* 27(2): 171–180. <https://doi.org/10.1111/j.1096-0031.2010.00329.x>
- WSC (2022) World Spider Catalog. Version 23.0. Natural History Museum Bern. [accessed April 21, 2022]

Three new species of the genus *Tetragnatha* Latreille, 1804 (Araneae, Tetragnathidae) from China

Song-lin Li¹, Ping Liu¹, Xian-jin Peng¹

¹ College of Life Sciences, Hunan Normal University, Changsha, Hunan 410081, China

Corresponding author: Ping Liu (pingzi129@126.com)

Academic editor: Yuri Marusik | Received 27 May 2022 | Accepted 27 September 2022 | Published 20 October 2022

<https://zoobank.org/8B173267-C53A-4018-BFF2-E8397DD6EA1F>

Citation: Li S-l, Liu P, Peng X-j (2022) Three new species of the genus *Tetragnatha* Latreille, 1804 (Araneae, Tetragnathidae) from China. ZooKeys 1125: 87–101. <https://doi.org/10.3897/zookeys.1125.86905>

Abstract

Three new species of *Tetragnatha* Latreille, 1804 are described from China: *T. bifurcata* Li & Liu, **sp. nov.** (♂♀) and *T. tortilis* Li & Liu, **sp. nov.** (♂♀) from Yunnan Province, and *T. bimaculata* Li & Liu, **sp. nov.** (♂♀) from Hubei and Hunan provinces. Detailed descriptions, photographs of somatic features and copulatory organs, and a distribution map of these three species are provided.

Keywords

Araneoidea, long-jawed spider, taxonomy, Tetragnathinae

Introduction

Tetragnatha Latreille, 1804 is the largest genus of the family Tetragnathidae, currently comprising 322 species distributed worldwide, of which 51 species are known from China (Li and Lin 2016; WSC 2022). The Chinese species of *Tetragnatha* are relatively well studied by Zhu et al. (2003), who reviewed the Chinese fauna comprising 36 species. Since 2003, an additional seven species have been reported from this country (Zhao and Peng 2010; Barrion et al. 2011, 2013). However, approximately half of the species recorded or described from China are only known from a single sex (Li and Lin 2016).

While examining specimens collected from the Gaoligong and Wuling mountains, three new species of *Tetragnatha* were recognized and are described here.

Materials and methods

Specimens were collected by beating shrubs and hand picking, and were stored in 75% ethanol. The epigyne were cleaned with trypsin solution before examination and photography. Left male palps and chelicerae were used for description and photography. Specimens were examined and measured with a Leica M205C stereomicroscope. Photographs were taken with a Kuy Nice E3IS PM digital camera mounted on an Olympus BX53 compound microscope and focus-stacked images were generated using Helicon Focus v. 7.6.1 and then modified in Adobe Photoshop CS2. The map was created by the online mapping software SimpleMappr (Shorthouse 2010). All measurements are given in millimeters (mm). Leg measurements are given in the following order: total length (femur, patella + tibia, metatarsus, tarsus). All specimens are deposited in the College of Life Sciences, Hunan Normal University, Changsha City, China (HNU). The terminology follows Castanheira and Baptista (2020).

Abbreviations used in the text and figures

Eyes:

ALE	anterior lateral eye;
AME	anterior median eye;
AME–AME	distance between AME;
AME–ALE	distance between AME and ALE;
PLE	posterior lateral eye;
PME	posterior median eye;
PME–PME	distance between PME;
PME–PLE	distance between PME and PLE;
MO	median ocular quadrangle.

Chelicera:

AXI	auxiliary guide tooth of the lower row of chelicera;
AXu	auxiliary guide tooth of the upper row of chelicera, above Gu;
Ds	dorsal spur of chelicera;
Gl	guide tooth of the lower row of chelicera;
Gu	guide tooth of the upper row of chelicera;
L2–n	teeth on the lower row of chelicera numbered from the distal end after Gl;
OC	outer cusp;
rsu	remaining proximal teeth on the upper row of male chelicera after ‘T’;
sl	first major tooth after Gu in the upper row of male chelicera;
T	elongated tooth in the upper row of male chelicera;
U2–n	teeth on the upper row of chelicera numbered from the distal end after Gu.

Palps and epigyne:

C	conductor;	P	paracymbium;
E	embolus;	Sp	spermatheca;
F	fold;	TL	translucent lobe;
K	knob;	Y	cymbium.

Taxonomic account

Family Tetragnathidae Menge, 1866

Genus *Tetragnatha* Latreille, 1804

Type species. *Aranea extensa* Linnaeus, 1758 from Sweden.

***Tetragnatha bifurcata* Li & Liu, sp. nov.**

<https://zoobank.org/27CEAEB3-4814-4DFD-AAB4-745CE7C240A1>

Figs 1, 2, 7

Type material. *Holotype* ♂: CHINA, Yunnan Province: Tengchong County, Houqiao Township, Zhaobitang Village, 25.5378°N, 98.2094°E, 2480 m, 29.V.2006, X.P. Wang & P. Hu leg. (Wang060529-1). *Paratypes*: 2♂♂ 3♀♀, same data as holotype (Wang060529-1); 5♂♂, Tengchong County, Houqiao Township, Zhaobitang Village, 25.3986°N, 98.3053°E, 2374 m, 27.V.2006, X.P. Wang & P. Hu leg. (Wang060527-2); 1♂ 1♀, Lushui County, Luzhang Township, Yaojiaping River 25.9772°N, 98.7109°E, 2527 m, 19.V.2005, D. Kavanaugh et al. leg. (2005-015A).

Etymology. The specific epithet is derived from the Latin adjective *bifurcus*, referring to the bifurcate distal end of the conductor.

Diagnosis. The new species resembles *T. tortilis* sp. nov. (Figs 5, 6). Males of the two species are similar in having a tapered dorsal spur on the chelicera, and the conductor with 2 folds, but can be distinguished by: (1) the distal portion of conductor bifurcated in *T. bifurcata* sp. nov. (Fig. 1L) (vs. not bifurcated; Fig. 5K); (2) the paracymbium with a pointed tip and terminal part located beyond the tegulum in ventral view (Fig. 1I) (vs. with blunt tip and terminal part located at the middle part of the tegulum; Fig. 5I). Females of the two species are similar in the shape of the epigynal fold and the absence of a central membranous sac in the vulva, but can be distinguished by: (1) the distance between the guide tooth and the second tooth of the upper row of chelicera slightly longer than the distance between the second tooth and the third tooth of the upper row of chelicera in *T. bifurcata* sp. nov. (Fig. 2E) (vs. the distance between the guide and the second tooth of the upper row of chelicera 3×

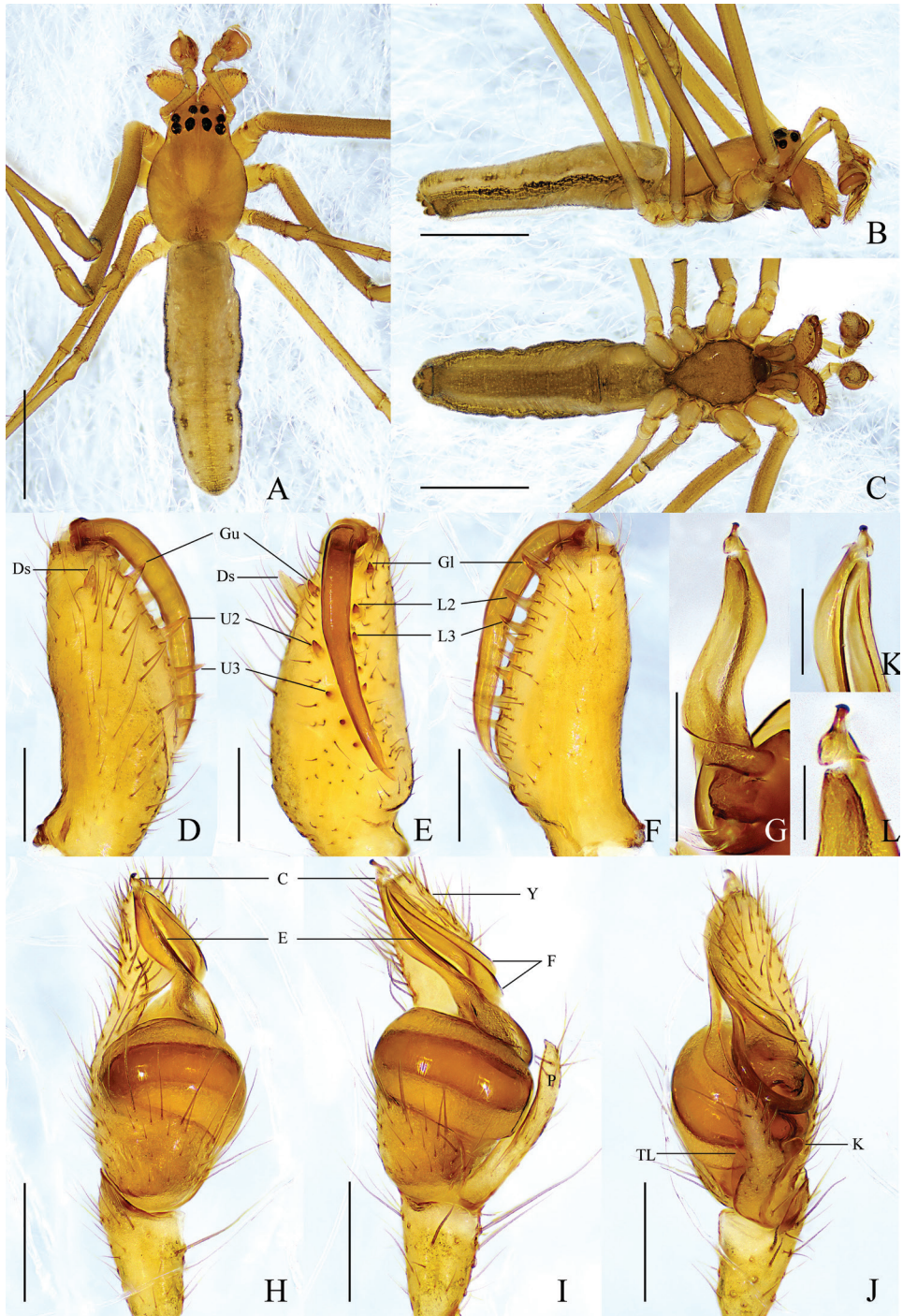


Figure 1. *Tetragnatha bifurcata* sp. nov., holotype ♂ **A–C** habitus **A** dorsal view **B** lateral view **C** ventral view **D–F** left chelicera **D** upper view **E** inner view **F** lower view **G, K, L** conductor and embolus detail **G** dorsal view **H–J** left palp **H** prolateral view **I** ventral view **J** retrolateral view. Scale bars: 1 mm (**A–C**); 0.5 mm (**D–F**); 0.1 mm (**G**); 0.2 mm (**H–J**); 0.05 mm (**K, L**).

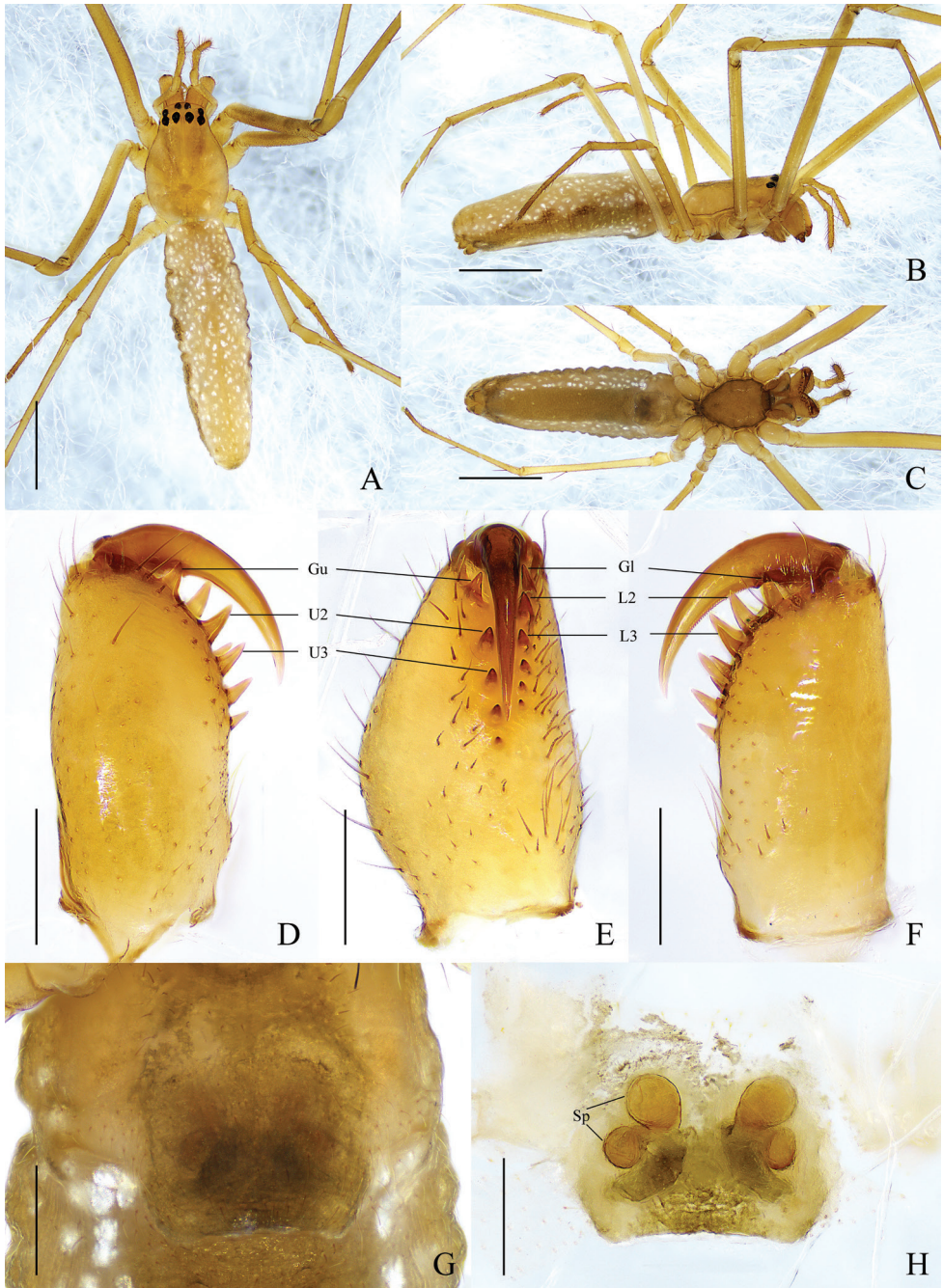


Figure 2. *Tetragnatha bifurcata* sp. nov., paratype ♀ **A–C** habitus **A** dorsal view **B** lateral view **C** ventral view **D–F** left chelicera **D** upper view **E** inner view **F** lower view **G, H** female genitalia **G** epigynal fold, ventral view **H** vulva, dorsal view. Scale bars: 1 mm (**A–C**); 0.5 mm (**D–F**); 0.2 mm (**G, H**).

longer than the distance between the second tooth and the third tooth of the upper row of chelicera; Fig. 6E); (2) the spherical anterior spermathecae are $\sim 1.5\times$ larger than the posterior spermathecae (Fig. 2H) (vs. anterior spermathecae oval and $\sim 5\times$ larger than the posterior spermathecae; Fig. 6H).

Description. Male (holotype) (Fig. 1A–F). Total length 3.60. Carapace 1.31 long, 0.92 wide, yellowish brown, fovea and cervical and radial grooves distinct. Eye sizes and interdistances: AME 0.06, ALE 0.12, PME 0.12, PLE 0.10; AME–AME 0.08, AME–ALE 0.12, PME–PME 0.12, PME–PLE 0.10. MO anterior width 0.17, posterior width 0.24, length 0.22. Clypeus 0.08 high. Labium dark brown, with thickened edge. Sternum brown with dark edge. Legs yellowish brown, with sparse spines. Leg measurements: I, 11.45 (3.12, 3.84, 3.23, 1.26); II, 8.15 (2.38, 2.72, 2.19, 0.86); III, 3.73 (1.32, 1.04, 0.91, 0.46); IV, 7.16 (2.42, 2.21, 1.86, 0.67). Chelicera: $\sim 1/2$ carapace length; dorsal spur tapered, with blunt tip; *AXu* absent; upper row with 5 teeth: *Gu* slightly smaller than *U2*, *U2* almost equal to *U3* in size, distance between *U2* and *Gu* longer than distance between *U2* and *U3*, other teeth decreasing in size gradually; *AXl* absent; lower row with 5 teeth: *Gl* slightly smaller than *L2*, *L2* largest, other teeth decreasing in size gradually. Abdomen 2.26 long, 0.72 wide, dorsum yellowish brown, with 5 pairs of dark spots laterally and brown longitudinal line medially, both lateral sides with longitudinal dark band throughout entire abdomen; venter yellowish brown, median band brown.

Palp (Fig. 1G–L). Paracymbium with pointed tip, notch shallow, translucent lobe elongated, $\sim 1/3$ width of paracymbium, knob thumb-shaped. Tegulum oval, $\sim 2\times$ as wide as long. Conductor with 2 folds, distal portion bifurcated, upper branch thicker with slightly swollen tip, lower branch thinner with blunt tip. Embolus partly enveloped by conductor.

Female (Wang060529-1) (Fig. 2A–F). Total length 4.02. Carapace 1.38 long, 0.91 wide. Eye sizes and interdistances: AME 0.06, ALE 0.06, PME 0.07, PLE 0.07; AME–AME 0.05, AME–ALE 0.10, PME–PME 0.09, PME–PLE 0.09. MO anterior width 0.17, posterior width 0.24, length 0.20. Clypeus 0.04 high. Leg measurements: I, 10.31 (2.85, 3.50, 2.92, 1.04); II, 7.13 (2.13, 2.30, 1.92, 0.78); III, 3.24 (1.09, 0.94, 0.80, 0.41); IV, 6.39 (2.20, 1.98, 1.63, 0.58). Chelicera: *AXu* absent; upper row with 5 teeth: *Gu* slightly smaller than *U2*, *U2* largest, other teeth almost equidistant and decreasing in size gradually; *AXl* absent; lower row with 6 teeth: *Gl* slightly smaller than *L2*, *L2* largest, other teeth decreasing in size gradually. Abdomen 2.71 long, 0.85 wide, dorsum without dark spots but with dispersed pale spots; venter with pale spots on both sides. Color paler than that in male.

Epigyne (Fig. 2G, H). Fold $\sim 3\times$ wider than long. Vulva composed of 2 pairs of spherical spermathecae, diameter of anterior pair $\sim 1.5\times$ of posterior pair, anterior pair spaced by 1 diameter of anterior spermatheca, posterior pair spaced by 3 diameters of posterior spermatheca. Central membranous sac absent.

Distribution. Known only from the type locality (Fig. 7).

***Tetragnatha bimaculata* Li & Liu, sp. nov.**

<https://zoobank.org/928B67AD-F5F6-47BC-8DEB-CD5B30C282B0>

Figs 3, 4, 7

Type material. *Holotype* ♂: CHINA: Hubei Province, Xuanen County: Shadaogou Township, Yuquan River, 29.7114°N, 109.7278°E, 805 m, 1.V.2016, W. Liu et al. leg. (HNU-HB-IV-1610). *Paratypes*: 4♂♂ 4♀♀, same data as holotype (HNU-HB-IV-1610); 1♂, Sidaoshui Village, 29.6846°N, 109.5791°E, 602 m, 2.V.2016 (HNU-HB-IV-1611), 6♂♂, Wanzhai Township, Dongping Dam, 30.1470°N, 109.6127°E, 519 m, 4.V.2016 (HNU-HB-IV-1613), W. Liu et al. leg. Hunan Province, Shimen County, Huping Township: 2♀♀, Quanping Village, Zhipeng River, 30.0131°N, 110.5980°E, 611 m, 15.VI.2014 (HPS140615), 2♀♀, Jinbanshan Village, Yanshan Road, 30.0066°N, 110.5653°E, 520 m, 13.VI.2014 (HPS140613), 1♀, Quanping Village, 30.0123°N, 110.5432°E, 935 m, 18.VI.2014 (HPS140618), J.H. Gan et al. leg.

Etymology. The specific epithet is the combination of the prefix *bi-* (two) and the Latin adjective *maculatus* (with spot), referring to the two dark spots on the posterior part of the abdomen.

Diagnosis. The males of this new species resemble those of *T. tanigawai* Okuma, 1988 (Okuma 1988: fig. 3A–G) in the elongate and curved dorsal spur of chelicera, the fang with an outer cusp, and the expanded proximal part of the conductor, but can be distinguished by: (1) the distance between the guide tooth and the second tooth of the upper row of chelicera almost equal to the distance between the second and third teeth of the upper row of chelicera in males of *T. bimaculata* sp. nov. (Fig. 3D) (vs. the distance between the guide tooth and the second tooth of the upper row of chelicera > 3× longer than the distance between the second and third teeth of the upper row of chelicera; fig. 3A in Okuma [1988]); (2) the conductor is ~ 3× longer than tegulum (Fig. 3I) with proximal 2/3 expanded (Fig. 3H) (vs. the conductor is ~ 2× longer than the tegulum (fig. 3G in Okuma [1988]) with proximal 1/2 part expanded; fig. 3D in Okuma [1988]); (3) the distal portion of conductor is almost rounded (Fig. 3G, H) (vs. with notch; fig. 3E, G in Okuma [1988]). The females of this new species resemble that of *T. esakii* Okuma, 1988 (Zhu et al. 2003: fig. 62A–F) in the shape of epigynal fold, the presence of a pair of spermathecae, and the absence of a central membranous sac in the vulva, but can be distinguished by the spermathecae that are bean-shaped and ~ 2× longer than wide in *T. bimaculata* sp. nov. (Fig. 4H) (vs. almost claviform and ~ 4× longer than wide; fig. 62F in Zhu et al. [2003]).

Description. Male (holotype) (Fig. 3A–F). Total length 5.85. Carapace 1.59 long, 1.20 wide, yellow, fovea and cervical and radial grooves distinct. Eye sizes and interdistances: AME 0.11, ALE 0.08, PME 0.08, PLE 0.09; AME–AME 0.10, AME–ALE 0.17, PME–PME 0.15, PME–PLE 0.15. MO anterior width 0.28, posterior width 0.30, length 0.29. Clypeus 0.16 high. Labium yellow. Sternum pale yellow. Legs yellow, with sparse spines. Leg measurements: I, 20.04 (5.24, 6.43, 6.56, 1.81);

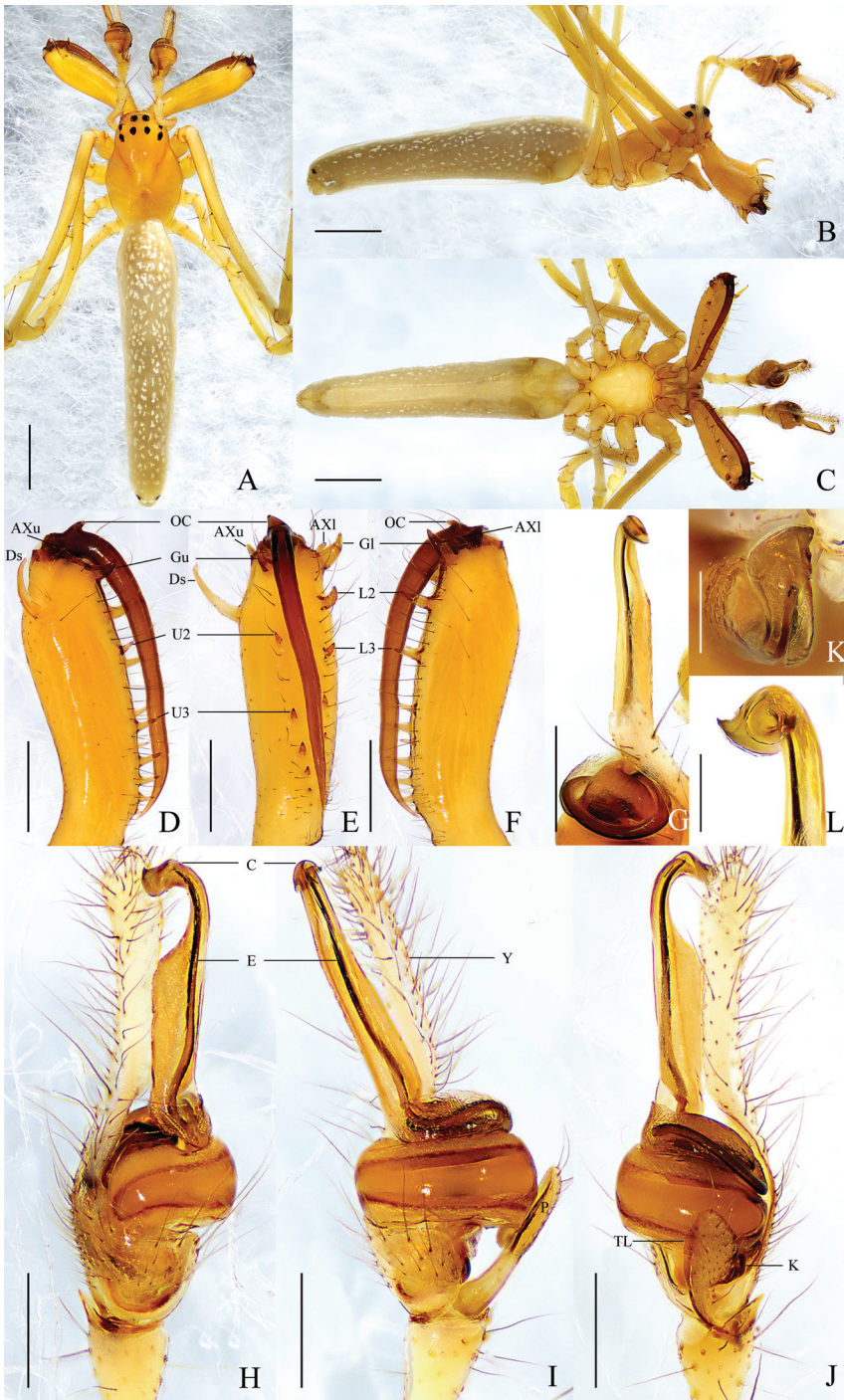


Figure 3. *Tetragnatha bimaculata* sp. nov., holotype ♂ **A–C** habitus **A** dorsal view **B** lateral view **C** ventral view **D–F** left chelicera **D** upper view **E** inner view **F** lower view **G, K, L** conductor and embolus detail **H–J** left palp **H** prolateral view **I** ventral view **J** retrolateral view. Scale bars: 1 mm (**A–C**); 0.3 mm (**D–J**); 0.1 mm (**K, L**).

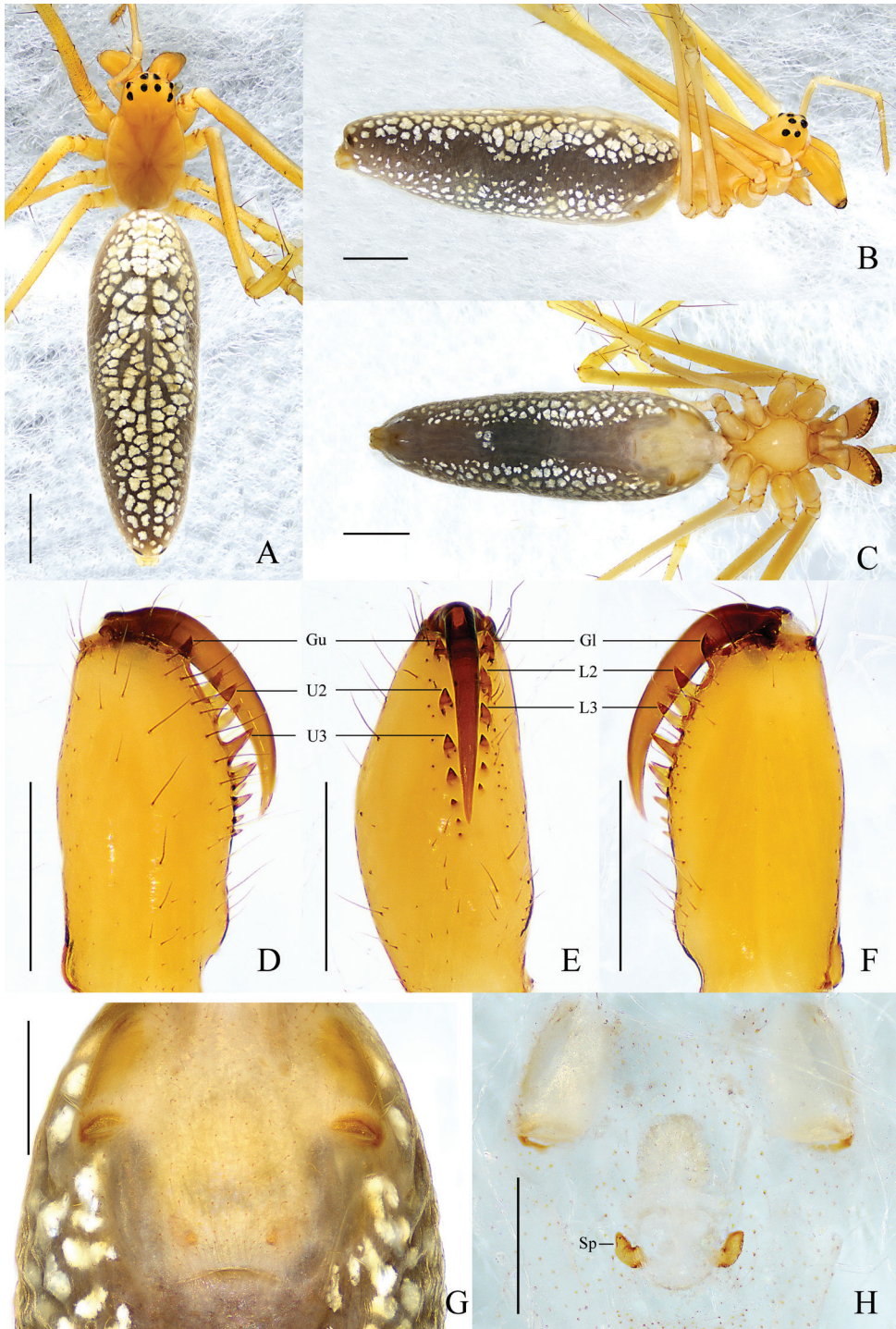


Figure 4. *Tetragnatha bimaculata* sp. nov., paratype ♀ **A–C** habitus **A** dorsal view **B** lateral view **C** ventral view **D–F** left chelicera **D** upper view **E** inner view **F** lower view **G, H** female genitalia **G** epigynal fold, ventral view **H** vulva, dorsal view. Scale bars: 1 mm (**A–C**); 0.5 mm (**D–H**).

II, 14.25 (4.16, 4.69, 4.24, 1.16); III, 7.53 (2.70, 2.21, 1.99, 0.63); IV, 12.23 (4.18, 3.80, 3.49, 0.76). Chelicera: almost as long as carapace; dorsal spur elongated, with pointed and curved tip; *AXu* present, with blunt tip; upper row with 7 teeth: *Gu* largest, distance between *U2* and *Gu* almost equal to distance between *U2* and *U3*, *U2–U4* almost equal in size, other teeth decreasing in size gradually; *AXI* present, thumb-shaped; lower row with 5 teeth: *Gl* largest, with widened base, other teeth gradually decreasing in size; fang with an outer cusp at base. Abdomen 4.27 long, 0.94 wide, dorsum pale yellow with serried pale spots and single pair of dark spots posteriorly; venter pale yellow, with paler spots on both sides.

Palp (Fig. 3G–L). Paracymbium with blunt tip, notch inconspicuous, translucent lobe elongate, $\sim 1/6$ of width of paracymbium, knob with a truncated tip. Tegulum oval, $\sim 2\times$ wider than long. Conductor without fold, proximal $2/3$ of conductor expanded dorsally, distal portion twisted and curved towards dorsal side. Embolus completely enveloped by conductor.

Female (paratype HNU-HB-IV-1610) (Fig. 4A–F). Total length 6.82. Carapace 1.75 long, 1.16 wide. Eye sizes and interdistances: AME 0.10, ALE 0.08, PME 0.09, PLE 0.10; AME–AME 0.12, AME–ALE 0.16, PME–PME 0.14, PME–PLE 0.15. MO anterior width 0.27, posterior width 0.28, length 0.28. Clypeus 0.12 high. Leg measurements: I, 18.40 (4.78, 5.92, 6.07, 1.62); II, 13.39 (3.83, 4.32, 3.98, 1.26); III, 6.89 (2.35, 2.03, 1.87, 0.64); IV, 11.77 (4.14, 3.54, 3.34, 0.75). Chelicera: *AXu* absent; upper row with 7 teeth: *Gu* much smaller than *U2*, *U2* largest, other teeth decreasing in size gradually; *AXI* absent; lower row with 6 teeth: *Gl* largest, other teeth decreasing in size gradually. Abdomen 5.06 long, 1.7 wide, dark grey, pattern same as in male.

Epigyne (Fig. 4G, H). Fold slightly longer than wide. Vulva with 1 pair of bean-shaped spermathecae, $\sim 2\times$ longer than wide, and spaced by $\sim 5\times$ width. Central membranous sac absent.

Distribution. Known only from the type locality (Fig. 7).

***Tetragnatha tortilis* Li & Liu, sp. nov.**

<https://zoobank.org/FD801E2B-0F51-44B4-84A0-C57EF7519B93>

Figs 5, 6, 7

Type material. *Holotype* ♂: CHINA, Yunnan Province, Tengchong County: Jietou Township, Datang Village: 25.4277°N, 98.4129°E, 1952 m, 18.V.2006, P. Hu leg. (Hu060518). *Paratypes*: 1♂ 1♀, same data as holotype (Hu060518); 1♀, 25.7456°N, 98.6963°E, 2030 m, 20.V.2006, X.J. Peng & P. Hu leg. (Peng060520); 1♂, 25.4202°N, 98.4095°E, 1870 m, 17.V.2006 (Peng060517), 2♂♂, 25.7456°N, 98.6963°E, 2030 m, 15.V.2006 (Peng060515), 3♂♂ 2♀♀, 25.7572°N, 98.6946°E, 2078 m, 16.V.2006 (Peng060516), 1♂, 25.4202°N, 98.4095°E, 1878 m, 19.V.2006 (Peng060519), X. J. Peng et al. leg.; 1♂, Houqiao Township: 25.3539°N, 98.2549°E, 1785 m, 28.V.2006 (Wang060528-1), 1♀, Gaoshidong Village, 25.3986°N, 98.3053°E, 2374 m, 27.V.2006 (Wang060527-2), 3♀♀, Zhaobitang Village, 25.5380°N, 98.2094°E,

2480 m, 29.V.2006 (Wang060529-1), X.P. Wang & P. Hu leg.; 2♂♂ 1♀, Mingguang Township: Zizhi Village, Cizhu River, 25.7666°N, 98.6174°E, 2120 m, 21.V.2006, C.M. Yin & J.F. Hu leg. (YHY09).

Etymology. The specific epithet is derived from the Latin adjective *tortilis* (twisted), referring to the twisted distal end of conductor.

Diagnosis. The new species resembles *T. pinicola* L. Koch, 1870 (Zhu et al. 2003: figs 87A–G, 88A–G; Marusik 2010: fig. 7). Males of the two species are similar in the presence of an elongated tooth in the upper row of the chelicera in males (*T.*), the conductor having 2 folds, and the shape of paracymbium, but can be distinguished by: (1) the dorsal spur of chelicera is straight in ventral view in *T. tortilis* sp. nov. (Fig. 5E) (vs. distal end curved; fig. 88C in Zhu et al. [2003]); (2) the absence of an auxiliary guide tooth of the lower row of the chelicera (Fig. 5E, F) (vs. present; fig. 88C in Zhu et al. [2003]); (3) the distal portion of conductor is twisted and has a small knot (Fig. 5G) (vs. hook-shaped; fig. 7 in Marusik [2010]). Females of the two species are similar in the presence of 2 pairs of spermathecae and the absence of a central membranous sac in the vulva, but can be distinguished by the anterior spermathecae 4× larger than posterior in *T. tortilis* sp. nov. (Fig. 6H) (vs. anterior spermathecae ~ 1/2× posterior spermathecae; fig. 87G in Zhu et al. [2003]). Both sexes of the two species can be distinguished by the sternum which is yellowish brown and without a stripe in *T. tortilis* sp. nov. (vs. dark brown with yellow stripe).

Description. Male (holotype) (Fig. 5A–F). Total length 4.97. Carapace 1.72 long, 1.05 wide, yellowish brown, fovea, cervical, and radial grooves distinct. Eye sizes and interdistances: AME 0.06, ALE 0.07, PME 0.08, PLE 0.09; AME–AME 0.10, AME–ALE 0.14, PME–PME 0.15, PME–PLE 0.13, MO anterior width 0.24, posterior width 0.31, length 0.27. Clypeus 0.10 high. Labium brown, with thickened edge. Sternum yellowish brown with dark edge. Legs yellowish brown, with sparse spines. Leg measurements: I, 15.59 (4.04, 5.27, 4.87, 1.41); II, 9.96 (2.90, 3.10, 2.98, 0.98); III, 4.46 (1.50, 1.24, 1.12, 0.60); IV, 8.96 (2.93, 2.64, 2.66, 0.73). Chelicera: yellow, ~ 2/3 length of carapace; dorsal spur tapered; *AXu* absent; upper row with 7 teeth: *Gu* curved and almost equal to *sl* in size, *T* present, 4 *rsu* decreasing in size gradually; *AXl* absent; lower row with 7 teeth: *Gl* tiny, *L2* slightly smaller than *L3*, *L3* largest, all other teeth smaller than *L2* and almost equal in size. Abdomen 3.23 long, 0.85 wide, dorsum grayish yellow, dark folium covering almost complete dorsum, with scattered pale spots and a brown longitudinal line medially, 2 pairs of sigillae; venter grayish yellow, anterior part with sparse pale spots.

Palp (Fig. 5G–K). Paracymbium with blunt distal end, notch inconspicuous, translucent lobe elongated, extended to the end, ~ 1/3 of the width of paracymbium, knob spherical. Tegulum oval, ~ 2× wider than long. Conductor with 2 folds, distal portion twisted considerably, and directed to dorsal side. Embolus partially enveloped by conductor.

Female (paratype Hu060518) (Fig. 6A–F). Total length 5.70. Carapace 1.77 long, 1.24 wide. Eye sizes and interdistances: AME 0.07, ALE 0.07, PME 0.08, PLE 0.08; AME–AME 0.10, AME–ALE 0.18, PME–PME 0.12, PME–PLE 0.14. MO anterior

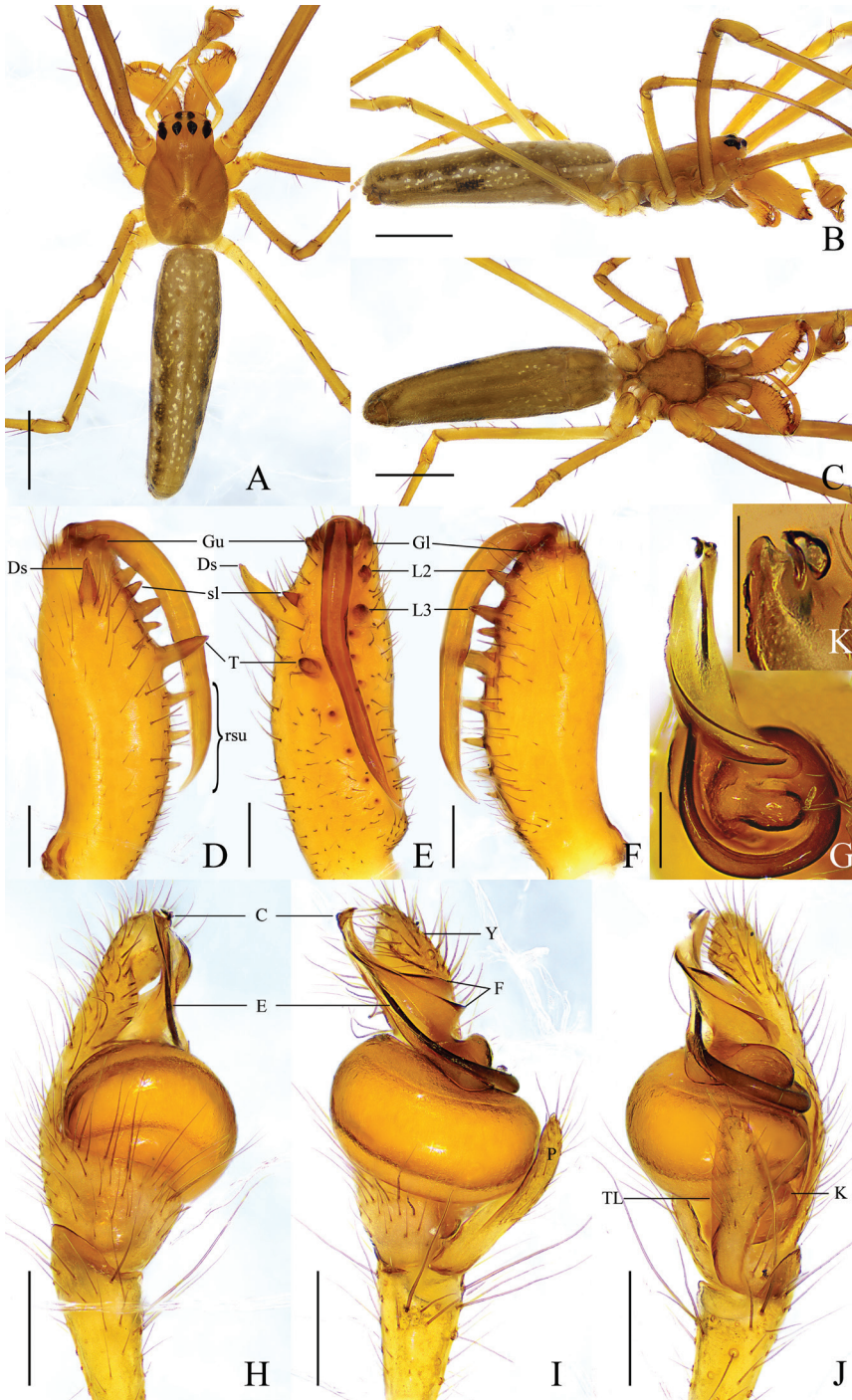


Figure 5. *Tetragnatha tortilis* sp. nov., holotype ♂ **A–C** habitus **A** dorsal view **B** lateral view **C** ventral view **D–F** left chelicera **D** upper view **E** inner view **F** lower view **G, K** conductor and embolus detail **H–J** left palp **H** prolateral view **I** ventral view **J** retrolateral view. Scale bars: 1 mm (**A–C**); 0.2 mm (**D–F, H–J**); 0.1 mm (**G, K**).

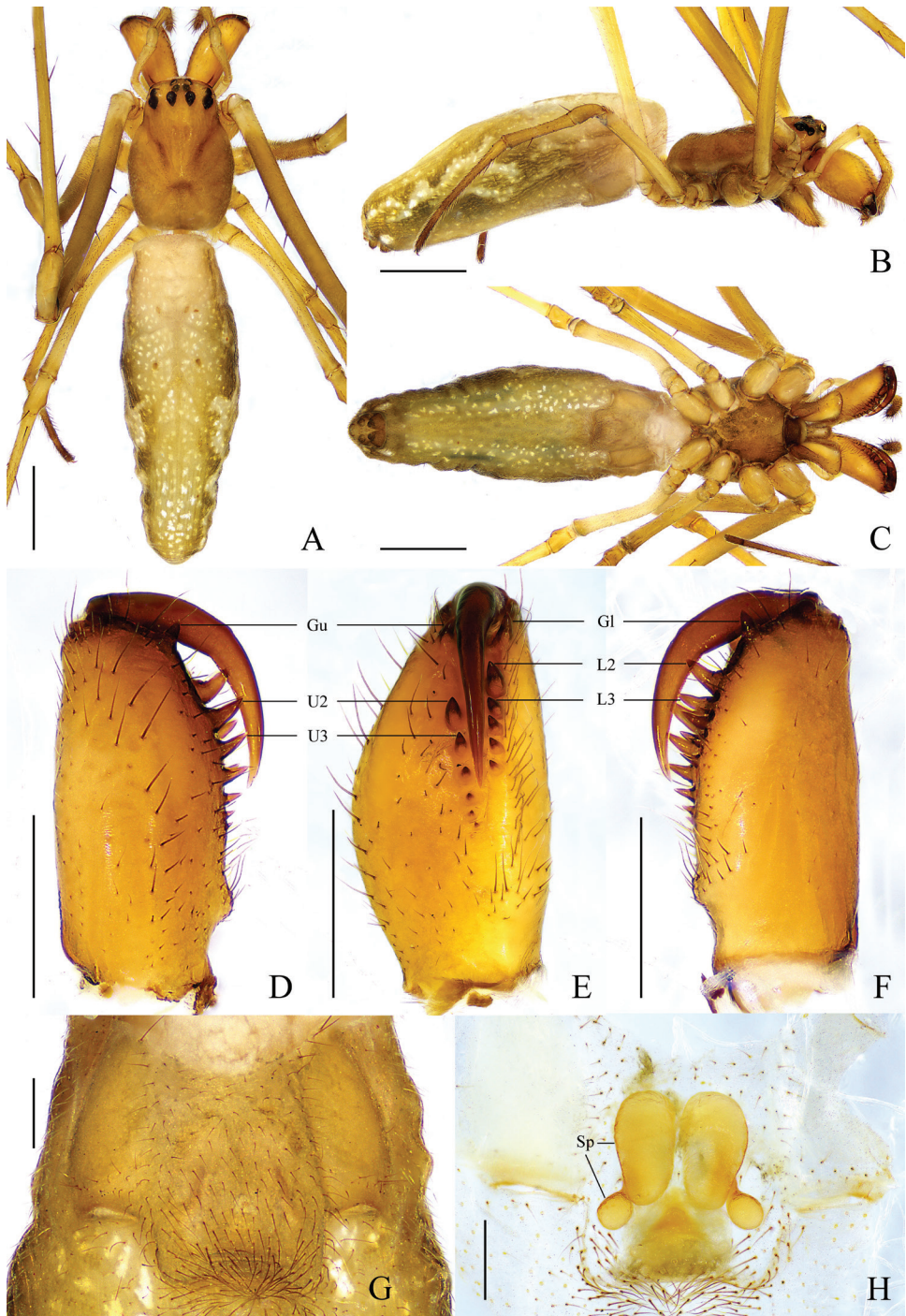


Figure 6. *Tetragnatha tortilis* sp. nov., paratype ♀ **A–C** habitus **A** dorsal view **B** lateral view **C** ventral view **D–F** left chelicera **D** upper view **E** inner view **F** lower view **G, H** female genitalia **G** epigynal fold, ventral view **H** vulva, dorsal view. Scale bars: 1 mm (**A–C**); 0.5 mm (**D–F**); 0.2 mm (**G, H**).



Figure 7. Collection localities for *Tetragnatha bifurcata* sp. nov., *Tetragnatha bimaculata* sp. nov., and *Tetragnatha tortilis* sp. nov. in China.

width 0.25, posterior width 0.33, length 0.3. Clypeus 0.07 high. Leg measurements: I, 15.33 (4.21, 5.05, 4.73, 1.34); II, 9.48 (2.91, 2.94, 2.70, 0.93); III, 4.4 (1.48, 1.25, 1.00, 0.67); IV, 8.25 (2.72, 2.50, 2.28, 0.75). Chelicera: *AXu* absent; upper row with 7 teeth: *Gu* curved, *U2* largest, other teeth decreasing in size gradually; *AXI* absent; lower row with 6 teeth: *L1* almost equal to *L3* in size, *L2* largest, other teeth decreasing in size gradually. Abdomen 3.92 long, 1.32 wide, dorsum pale yellow; venter with pale spots on both sides; otherwise, remaining pattern same as in male.

Epigyne (Fig. 6G, H). Fold ~ 3× wider than long. Vulva composed of 2 pairs of spermathecae, anterior pair larger, oval and almost touched each other, posterior pair smaller, spherical, and spaced by 3 diameters. Central membranous sac absent.

Distribution. Known only from the type locality (Fig. 7).

Acknowledgements

We are grateful to Yuri Marusik and two reviewers for their high quality and constructive reviews. We also thank Stephanie F. Loria (American Museum of Natural History, New York, USA), Junxia Zhang (Zootaxa editor, Araneae: Salticidae, Hebei, China)

and Nathalie Yonow (Wales, UK) for reviewing the English of manuscript, and Xinping Wang (New York, USA); Hongbin Liang (Beijing, China); Peng Hu, Wang Liu, Chen Zeng, Tian Tian, Cheng Wang, Bing Zhou, Jiahui Gan, Yuhui Gong, Yi Huang and Mingyong Liao (all at Hunan, China); and David Kavanaugh and Charles Griswold (San Francisco, USA) for collecting the specimens. This research was sponsored by the Scientific Research Projects of Hunan Education Department (no. 21B0055).

References

- Barrion AT, Barrion-Dupo ALA, Villareal SS, Ducheng C (2011) *Tetragnatha heongi*, a new species of long-jawed orb spider (Araneae: Tetragnathidae: Tetragnathinae) from Hainan Island, China. *Asia Life Sciences* 20: 385–394.
- Barrion AT, Barrion-Dupo ALA, Catindig JLA, Villareal MO, Cai D, Yuan QH, Heong KL (2013) New species of spiders (Araneae) from Hainan Island, China. *UPLB Museum Publications in Natural History* 3: 1–103. <https://doi.org/10.5281/zenodo.269136>
- Castanheira P de S, Baptista RLC (2020) Notes on slender species of the long-jawed spider genus *Tetragnatha* (Araneae, Tetragnathidae) with description of three new species. *Zootaxa* 4768(1): 43–75. <https://doi.org/10.11646/zootaxa.4768.1.4>
- Li SQ, Lin YC (2016) *Species Catalogue of China. Volume 2. Animals Invertebrates (I): Arachnida: Araneae*. Science Press, Beijing, 549 pp.
- Marusik YM (2010) A new species of *Tetragnatha* Latreille, 1904 (Aranei: Tetragnathidae) from western Kazakhstan. *Arthropoda Selecta* 19(3): 199–202. <https://doi.org/10.15298/arth-sel.19.3.07>
- Okuma C (1988) Five new species of *Tetragnatha* from Asia (Araneae: Tetragnathidae). *Esakia* 26: 71–77. <https://doi.org/10.5109/2506>
- Shorthouse DP (2010) SimpleMappr, an online tool to produce publication-quality point maps. <https://www.simplmappr.net> [Accessed on 28 April 2022]
- WSC [World spider catalog] (2022) World Spider Catalog, Natural History Museum Bern. Version 23.5. <http://wsc.nmbe.ch/> [Accessed 23 June 2022]
- Zhao LP, Peng XJ (2010) Two new spider species of the genus *Tetragnatha* from Yunnan province, China (Araneae, Tetragnathidae). *Acta Arachnologica Sinica* 19(1): 7–10.
- Zhu MS, Song DX, Zhang JX (2003) *Fauna Sinica: Invertebrata Vol. 35, Arachnida: Araneae: Tetragnathidae*. Science Press, Beijing, 418 pp.

Schievitermes globicornis, a new genus and species of Termitinae (Blattodea, Termitidae) from French Guiana

Yves Roisin¹

¹ *Université Libre de Bruxelles, Evolutionary Biology and Ecology, 50 avenue F.D. Roosevelt, 1050 Brussels, Belgium*

Corresponding author: Yves Roisin (yves.roisin@ulb.be)

Academic editor: Eliana Canello | Received 1 August 2022 | Accepted 10 October 2022 | Published 20 October 2022

<https://zoobank.org/4E1FBE4F-E1C9-46C2-89AE-28794DD229F7>

Citation: Roisin Y (2022) *Schievitermes globicornis*, a new genus and species of Termitinae (Blattodea, Termitidae) from French Guiana. ZooKeys 1125: 103–114. <https://doi.org/10.3897/zookeys.1125.91124>

Abstract

Asymmetrical snapping mandibles have evolved several times in termites. In the Neotropics, asymmetrical snapping mandibles are found in soldiers of four genera: *Neocapritermes*, *Planicapritermes*, *Cornicapritermes* and *Diboplotermes*. Here, I describe *Schievitermes globicornis*, new genus and species, from French Guiana. This genus is characterized by an absence of a frontal prominence and slightly asymmetrical mandibles in the soldier caste. The morphology and anatomy of the worker reveal a wood-based diet, and suggest that *Schievitermes*, *Planicapritermes* and *Neocapritermes* constitute a monophyletic group, which is consistent with mtDNA data.

Keywords

Isoptera, *Neocapritermes*, Neotropical region, new species, *Planicapritermes*, termite

Introduction

Soldiers with snapping mandibles are commonplace in termites, and there is growing evidence that this defensive device evolved several times in the family Termitidae (Inward et al. 2007), as well as once in Kalotermitidae (Scheffrahn et al. 2018). When the soldier presses its mandibles against each other, they accumulate elastic energy, which is converted into kinetic energy as soon as the mandible shafts slip past each other, delivering a very quick and powerful strike (Seid et al. 2008). Although termite

mandibles always display some degree of asymmetry, some snapping soldiers can be catalogued as symmetrical because their mandibles both show a similar elongated shape and can deliver a symmetrical blow (Deligne 1971). In asymmetrical snappers, the left mandible is bent outwards in its basal part before straightening apically, whereas the right mandible is almost straight, or slightly bent inwards. When mandibles are pressed against each other, the curved part of the left mandible functions as a spring, concentrating elastic energy in preparation for an asymmetrical blow (Deligne 1971).

Snappers are especially diverse in the Oriental region, but several genera are known from the Neotropics: *Termes* (also present in the Old World tropics), *Cavitermes*, *Palmitermes*, *Crepititermes* and *Inquilinitermes* are symmetrical snappers, whereas *Neocapritermes*, *Planicapritermes*, *Cornicapritermes* and *Dihoplotermes* are asymmetrical ones (Krishna 1968). Asymmetrical snappers appeared separately in the Old World (*Pericapritermes* and related genera), in Madagascar (*Capritermes*) and in the Neotropics, where Inward et al. (2007) suggested that they evolved independently twice, once in *Planicapritermes* and once in *Neocapritermes*. Although more recent studies have established a close relationship between *Planicapritermes* and *Neocapritermes*, forming the sister clade to the symmetrical snapper *Crepititermes* (Bourguignon et al. 2017), it remains that asymmetrical snapping must also have evolved independently in the neotropical *Termes* group (*Dihoplotermes* and probably *Cornicapritermes*). Bourguignon et al.'s (2017) study included a taxon from French Guiana provisionally labelled “G683 *Neocapritermes* sp. H”, which displayed only slightly asymmetrical snapping mandibles and whose mtDNA appeared closer to *Planicapritermes* than to *Neocapritermes*. Reexamination of this sample with more recent collections from French Guiana revealed that this species does not fit into any of the abovementioned genera. I describe it hereunder as *Schievitermes globicornis*, gen. nov., sp. nov., and discuss its relationships.

Material and methods

Dissections were made in alcohol. Guts *in situ* were drawn with a camera lucida. Detached pieces such as mandibles or enteric valves were directly mounted on microscope slides in PVA medium (BioQuip Products Inc.).

Images of entire specimens are multi-layer compilations obtained with a Zeiss Discovery V12 stereomicroscope equipped with an AxioCam ICc3 camera and controlled by AxioVision release 4.8.3 software. Images are compilations of series of successive stepwise focused photographs. Images of microscope slide preparations were taken with a Leica DFC450C camera mounted on a Leica DM5500B microscope and operated with Leica Application Suite v.4.12.0 software. Enteric valves and hindgut wall sections were observed under phase-contrast illumination.

Terminology follows that of Sands (1972) for mandible dentition and that of Noirot (1995, 2001) for gut anatomy. Measurements, as described in Roonwal (1969), were taken to the nearest 0.005 mm with a Wild MMS 235 length-measuring set fitted to a Wild M6 stereomicroscope.

Taxonomy

Schievitermes gen. nov.

<https://zoobank.org/9B8C1A8B-047A-4CEC-A182-0288A0593CF4>

Remark. This genus is presently monotypic.

Type species. *Schievitermes globicornis* sp. nov.

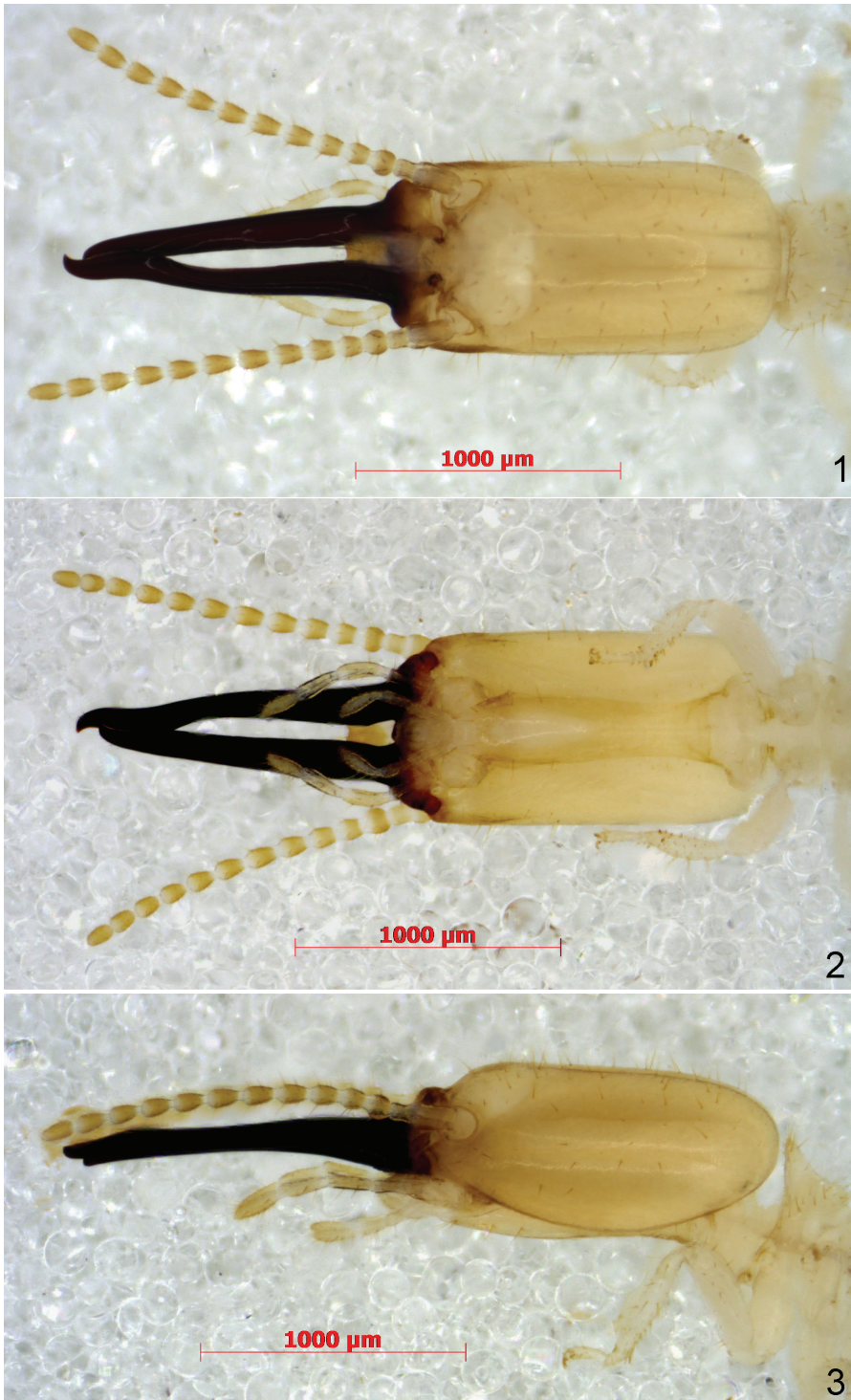
Description. Imago: only known from a single queen. See species description.

Soldier (Figs 1–4): Head capsule (Figs 1–3) subquadrangular with rounded corners, about twice as long as broad, bearing numerous (~100) setae. Mandibles approximately as long as head capsule, rather thick, of the snapping type. Right mandible almost straight, only slightly curved inwards. Left mandible slightly but distinctly sinuous: outer margin slightly concave near base, convex in middle, then concave again at level of contact with right mandible, then curved inwards at tip. Tips of both mandibles hooked, turned about 60° inwards. Antennae of 13 articles, apical article reaching beyond left mandible tip; article 3 distinctly globular, as broad as article 1 and broader than all other articles. Labrum (Fig. 4) with nearly parallel sides, anterior margin sinuous, convex in middle, bearing a few long bristles, anterior corners rounded. Frons without projection.

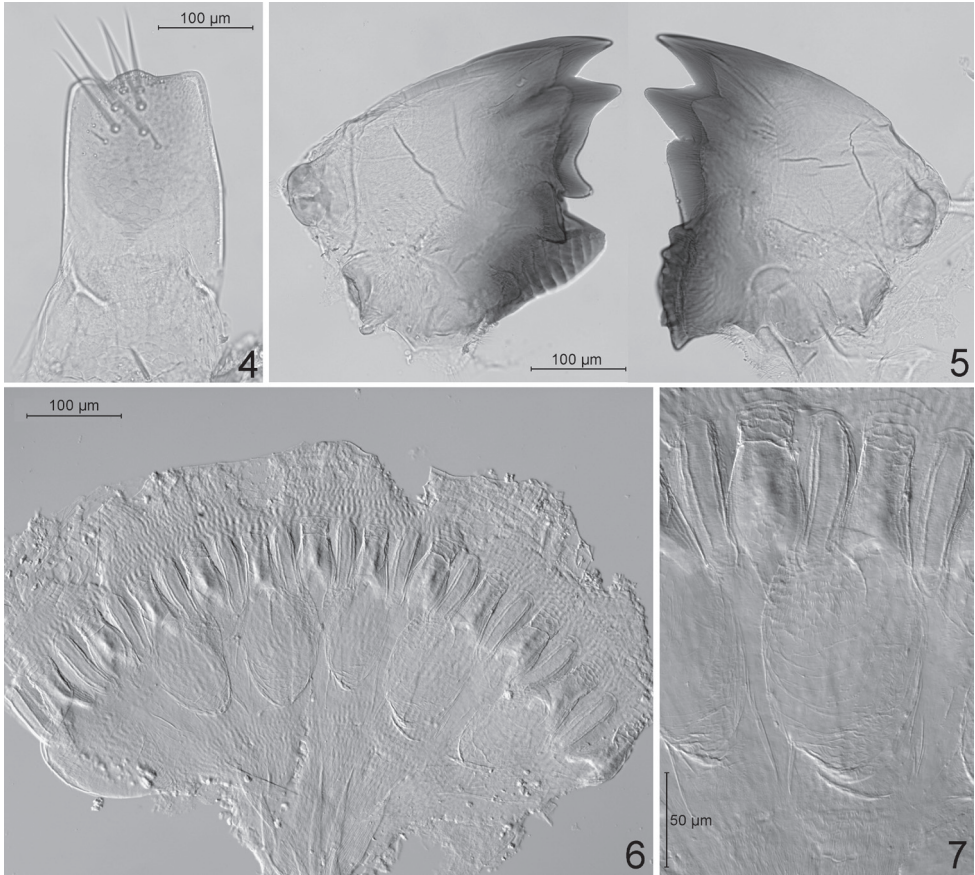
Worker (Figs 5–9, 12–13, 15–17): Monomorphic. Head capsule whitish, bearing many setae. Mandibles (Fig. 5) of the wood-feeding type. Left mandible: distance between teeth A– M_{1+2} approximately half the distance M_{1+2} – M_3 . M_3 well-marked, premolar tooth (sensu Deligne 1999) blade-like, molar ridges well developed. Right mandible: distance between teeth A– M_1 short, M_2 well-marked, molar ridges well developed. Crop moderately developed, gizzard (Figs 6, 7) of the generalized type (Noirot 2001), cuticular armature limited to small pectinated scales on the pulvilli (Fig. 7). Mixed segment long, mesenteric tongue bilobate distally (Fig. 8). Ileum (P1) slightly dilated, narrowing into P2. Enteric valve (P2) funnel-like, conical at end of P1, becoming a narrow tube at junction with P3. Enteric valve armature (Fig. 9) consisting in two rings of spine-bearing areas, the proximal one in the conical section of P2, formed by three ovoid cushions alternating with elongated ones, all bearing small triangular spines; distal ring within the narrow tubular section, formed by six alternating short and long cushions bearing thin, curved spines. Paunch (P3) voluminous, with wall bearing numerous small spines, longer in rounded posterior section near entrance of P2 (Fig. 12), short and often pectinated in anterior section narrowing towards P4 (Fig. 13).

Etymology. From local Brussels dialect *schieve* = not straight, askew, and Latin *termes* = termite. The name refers to the slight grade of asymmetry displayed by soldier mandibles.

Diagnosis. Soldier: Among neotropical snappers, the absence of a frontal projection distinguishes *Schievitermes* from *Termes*, *Inquilinitermes*, *Cavitermes*, *Palmitermes*, *Dihoplotes*, and *Cornicapritermes*. *Planicapritermes* has a characteristic flattened head capsule and strongly asymmetrical mandibles. *Schievitermes* differs from *Crepititermes* by its thicker mandibles with a slight, but distinct asymmetry, and globular third antennal article. *Neocapritermes* species are consistently larger (head width > 1 mm), have more



Figures 1–3. *Schievitermes globicornis* sp. nov.: soldier head **1** from above **2** from below **3** from left.



Figures 4–7. *Schievitermes globicornis* sp. nov.: **4** labrum of soldier **5** worker mandibles, from above **6** gizzard of worker, complete, spread on slide (phase-contrast illumination) **7** gizzard of worker, detail of pulvillus (phase-contrast illumination).

antennal articles (15–16 vs 13) and their mandible asymmetry is always more pronounced (Krishna and Araujo 1968; Constantino 1991; Bandeira and Canello 1992).

Worker: Mandibles are of the wood-feeding type, as in *Neocapritermes* and *Planicapritermes*, with a short space between apical and anterior marginal teeth, and well-developed molar ridges. *Termites* (with the exception of the wood-feeding species, *T. hispaniolae* (Banks, 1918)), *Crepititermes*, *Inquilinitermes*, *Cavitermes*, *Palmitermes*, *Dihoplotermes* and *Cornicapritermes* have mandibles of the soil feeding type, with a broad space between apical and anterior marginal teeth, and reduced molar ridges. The digestive tube of *Schievitermes* is similar to that of *Planicapritermes*, but the bilobed apex of the mesenteric part of the mixed segment is distinctive. *Neocapritermes* also possesses two mesenteric lobes, but the mixed segment is shorter and the mesenteric lobes are larger and more widely separated (Constantino 1998; Almeida-Azevedo et al. 2021). The enteric valve armature of *Schievitermes* is similar to that of *Planicapritermes*

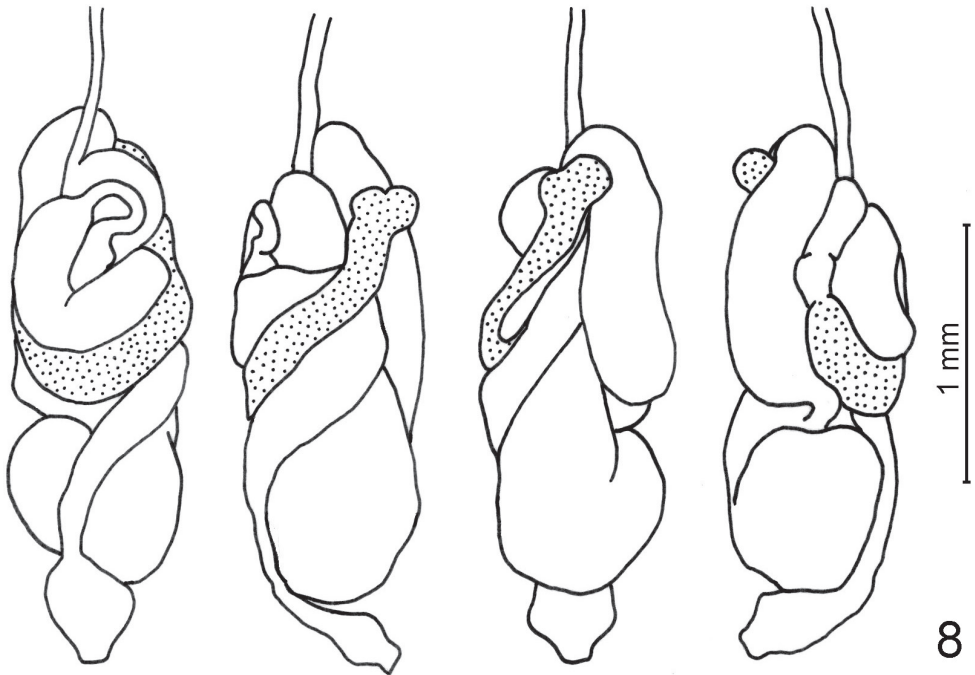


Figure 8. *Schievitermes globicornis* sp. nov.: camera lucida drawings of worker gut *in situ*. From left to right: viewed from above, right, below, left. Mesenteron stippled.

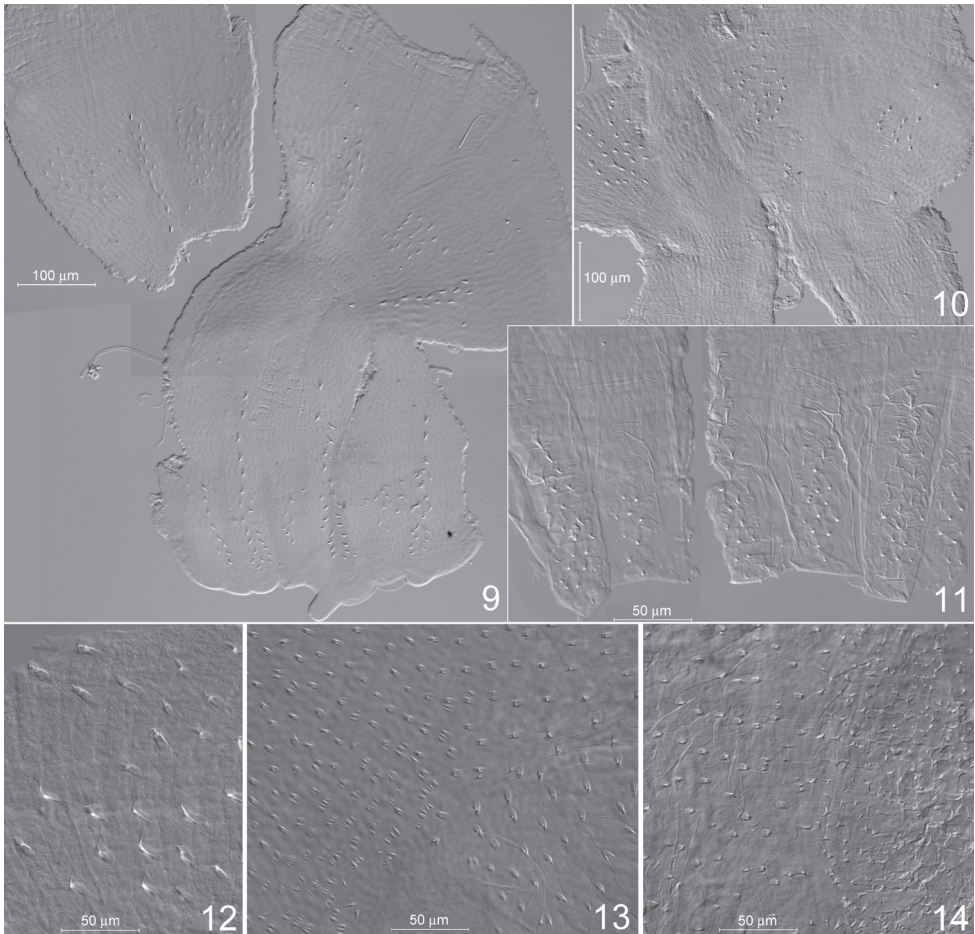
(Figs 10, 11), apart from minor differences in the ornamentation of spiny areas. Cuticular differentiations within P3 of *Schievitermes* are intermediate between the long spines and filaments observed in *Neocapritermes* (Noirot 2001) and the tiny spines present in *Planicapritermes* (Noirot 2001; Fig. 14).

Most workers show signs of dehiscence between metanotum and first abdominal tergite, ranging from a short slit-like aperture bordered by brown sclerotic marks (Fig. 15) to a broad opening through which the whole anterior part of the gut protrudes (Figs 16, 17).

***Schievitermes globicornis* sp. nov.**

<https://zoobank.org/6D760044-34C4-47E0-8FB9-C3542473928B>

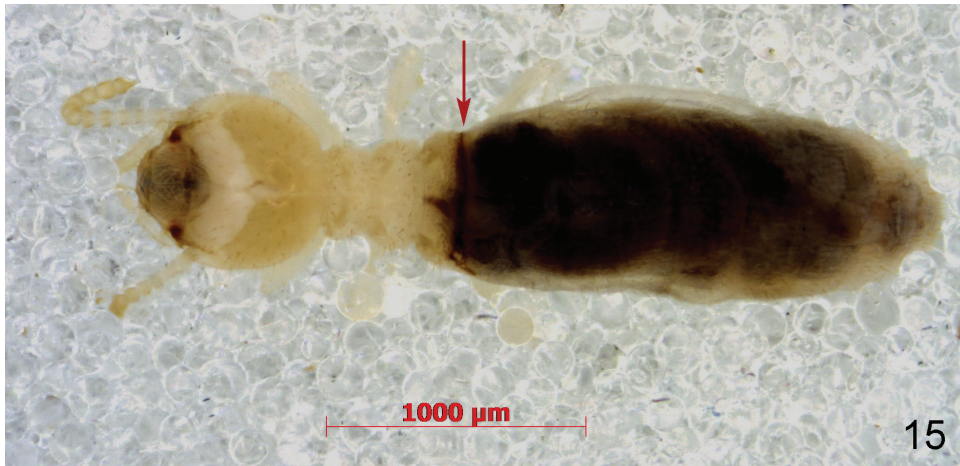
Material examined. *Holotype*: soldier. French Guiana, Petit Saut Dam Road, Carbet Maman Léazard, 05.0672°N, 52.9992°W, from nest among tree roots, 20.i.2012 (coll. Y. Roisin – accession G683). *Paratypes*: soldiers and workers from same colony as holotype. Worker's mtDNA sequence deposited in GenBank under label *Neocapritermes* sp. H TB-2017 isolate G683, accession (Bourguignon et al. 2017). From other colonies than holotype: French Guiana, Laussat (N1 road, PK194), forest on white



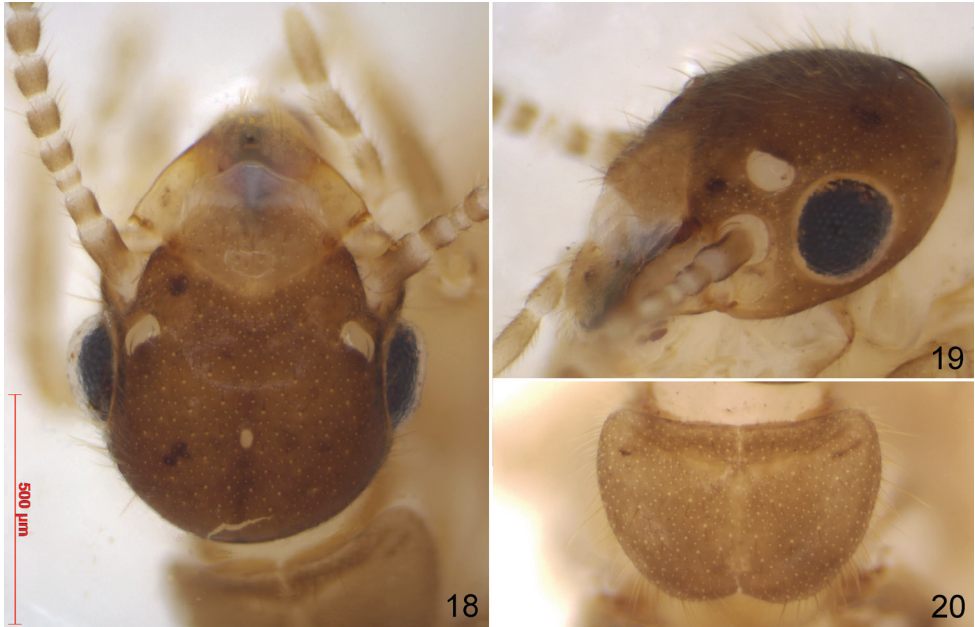
Figures 9–14. Proctodeal wall ornaments under phase-contrast illumination **9** *Schievitermes globicornis* sp. nov., worker enteric valve, spread on slide **10**, **11** *Planicapritermes planiceps* (Emerson, 1925), worker enteric valve, spread on slide; proximal spiny areas and detail of distal spiny ridges, respectively **12**, **13** *Schievitermes globicornis* sp. nov., ornamentation of worker paunch wall, in bulbous posterior part and narrower anterior section, respectively **14** *Planicapritermes planiceps*, ornamentation of worker paunch wall.

sands, 05.4698°N, 53.5748°W, small nest in rotten stump, with queen, soldiers and workers, 27.i.2020 (coll. Y. Roisin, N. Fontaine, A. Dumortier – accession G20-12); Mana Road (D8, PK1-2), forest on white sands, 05.5125°N, 53.5504°W, soldiers and workers in dead wood on the ground, 27.x.2021 (coll. Y. Roisin, N. Fontaine, J. Timmermans – accession G21-54). Type material to be deposited in the Royal Belgian Institute for Natural Sciences, Brussels, Belgium.

Description. Imago (Figs 18–20): caste only known from single queen from colony G20-12. This individual was physogastric, with partly depigmented eyes indicating a long underground life. Other body parts were probably of paler pigmentation than



Figures 15–17. Workers of *Schievitermes globicornis* sp. nov. fixed at various stages of abdominal dehiscence **15** linear crack (*arrow*) behind rear margin of metanotum **16** gut protruding through crack **17** anterior part of the gut completely extruded.



Figures 18–20. Queen of *Schievitermes globicornis* sp. nov. **18** head from above **19** oblique view of head **20** pronotum. The three figures are at the same scale.

in swarming alates as well. Head capsule medium brown, postclypeus, pronotum and other tergites lighter. Antennae broken, 9–11 articles remaining, article 3 narrower and shorter than 2 and 4. Fontanelle hyaline, ovoid, about 45 µm long by 30 µm wide. Head capsule regularly rounded behind. Compound eyes medium-sized, ocelli large, separated from eyes by less than their own width. Pronotum rounded laterally and posteriorly, with a distinct notch behind. Measurements (in mm; numbers between brackets refer to list of measurements proposed by Roonwal 1969): Head length to anterior margin of postclypeus [8]: 0.770; head width, with eyes [17]: 0.810; head width, between eyes [52]: 0.595; eye maximum diameter [48]: 0.260; ocellus maximum diameter [55]: 0.115; ocellus-eye distance [57]: 0.035; pronotum length [65]: 0.425; pronotum width [68]: 0.635; hind tibia length [85]: 0.820.

Soldier (Figs 1–4): Head capsule yellow-brown. Mandibles black, turning brown near base. Antennae yellow-brown. Tibial spurs 3:2:2, anterior spur of fore leg about half the length of the other two.

Measurements of 10 soldiers from three colonies (in mm; numbers between brackets refer to list of measurements proposed by Roonwal 1969): Total head length, including mandibles (held straight forward in measured individuals) [4]: 2.535–2.775; length of head to lateral base of mandibles [5]: 1.320–1.470; head width [17]: 0.700–0.755; length of left mandible [37]: 1.255–1.330; length of right mandible [37]: 1.205–1.295; length of postmentum along median line [61]: 0.800–0.930; maximum width of postmentum [62]: 0.235–0.280; minimum width of postmentum [63]: 0.145–0.175; pronotum width [68]: 0.470–0.510; length of hind tibia [85]: 0.575–0.635.

Worker (Figs 5–9, 12–13, 15–17): Antennae of 13 articles. Tibial spurs 2:2:2. Head width of 20 workers from three colonies: 0.640–0.700 mm.

Etymology. from Latin *globus* = globe, sphere, and *cornu* = horn, antenna; the specific epithet refers to the globular shape of the third antennal article of the soldier.

Discussion

Morphologically, *Schievitermes* appears closest to either *Planicapritermes* or *Neocapritermes*. The three genera share asymmetrical snapping mandibles and absence of a frontal projection in the soldier, and worker mandibles revealing wood- or soil-wood interface-feeding habits. *Schievitermes* soldier head and mandible shape appears plesiomorphic with respect to the conspicuously asymmetrical mandibles of *Planicapritermes* and *Neocapritermes*, and the flattened head and body of the former. In the worker, *Schievitermes* is very similar to *Planicapritermes* by its long mixed segment, but the mesenteric lobes at the end of the mixed segment appear intermediate between *Planicapritermes* and *Neocapritermes*. The well-separated lobes of *Neocapritermes* probably represent a derived condition, but the partially bilobed mesenteric tongue of *Schievitermes* might be plesiomorphic, as it appears similar to the condition observed in *Microcerotermes* (Roisin and Pasteels 2000). The enteric valve armature is also very similar in *Schievitermes* and *Planicapritermes*, whereas distal cushions in *Neocapritermes* species are swollen and heavily armed with spines, which probably constitutes a derived trait. The three genera share the presence of numerous spines on the internal wall of P3, although this armature is more complex and comprises longer spines in *Neocapritermes* (Noirot 2001).

Complete mitochondrial DNA sequences have now confirmed the close relationship between *Neocapritermes* and *Planicapritermes* (Bourguignon et al. 2017), as proposed by earlier authors (Krishna 1968; Constantino 1998) but in contrast with the preferred tree of Inward et al. (2007), in which *Planicapritermes* joined a morphologically and zoogeographically improbable lineage including *Orthognathotermes* and *Globitermes*; however, several nodes among the Termitinae were weakly supported, and Inward et al. (2007) did not discard the possible monophyly of *Neocapritermes* + *Planicapritermes*. This new genus *Schievitermes* clearly belongs in the *Neocapritermes* + *Planicapritermes* clade, in which it seems to come closer to *Planicapritermes* in accordance with morphological and anatomical characters.

Acknowledgements

I thank the staff of the HYDRECO lab at Petit Saut (R. Vigouroux and the late P. Cerdan) for logistic help in French Guiana. G. Josens (ULB) and P. Martin (RBINS) helped with microphotography. Funding was provided by the F.R.S.-FNRS, Belgium (grants 2.4594.12 and J.0180.20).

References

- Almeida-Azevedo R, Azevedo RA, Sobral R, Morais JW (2021) First description of the worker of *Planicapritermes longilabrum* with notes on the nest of *Planicapritermes planiceps* (Blattaria: Isoptera: Termitidae). *Acta Amazonica* 51(1): 63–66. <https://doi.org/10.1590/1809-4392202000841>
- Bandeira AG, Canello EM (1992) Four new species of termites (Isoptera, Termitidae) from the island of Maracá, Roraima, Brazil. *Revista Brasileira de Entomologia* 36: 423–435.
- Bourguignon T, Lo N, Šobotník J, Ho SYW, Iqbal N, Coissac É, Lee M, Jendryka MM, Sillam-Dussès D, Křížková B, Roisin Y, Evans TA (2017) Mitochondrial phylogenomics resolves the global spread of higher termites, ecosystem engineers of tropics. *Molecular Biology and Evolution* 34: 589–597. <https://doi.org/10.1093/molbev/msw253>
- Constantino R (1991) Notes on *Neocapritermes* Holmgren, with description of two new species from the Amazon Basin (Isoptera, Termitidae, Termitinae). *Goeldiana Zoologia* 7: 1–13. <https://repositorio.museu-goeldi.br/handle/mgoeldi/346>
- Constantino R (1998) Description of a new *Planicapritermes* from Central Amazonia, with notes on the morphology of the digestive tube of the *Neocapritermes–Planicapritermes* group (Isoptera: Termitidae: Termitinae). *Sociobiology* 32: 109–118. [Correction (1999). *Sociobiology* 33: 144.]
- Deligne J (1971) Mécanique du comportement de combat chez les soldats de termites (Insectes Isoptères). *Forma et Functio* 4: 176–187.
- Deligne J (1999) Functional morphology and evolution of a carpenter's plane-like tool in the mandibles of termite workers (Insecta Isoptera). *Belgian Journal of Zoology* 129: 201–218. https://biblio.naturalsciences.be/associated_publications/bjz/129-1/bjz_129_deligne_201-218.pdf
- Inward DJG, Vogler AP, Eggleton P (2007) A comprehensive phylogenetic analysis of termites (Isoptera) illuminates key aspects of their evolutionary biology. *Molecular Phylogenetics and Evolution* 44(3): 953–967. <https://doi.org/10.1016/j.ympev.2007.05.014>
- Krishna K (1968) Phylogeny and generic reclassification of the *Capritermes* complex (Isoptera, Termitidae, Termitinae). *Bulletin of the American Museum of Natural History* 138: 261–324. <https://digitallibrary.amnh.org/handle/2246/1673>
- Krishna K, Araujo RL (1968) A revision of the neotropical termite genus *Neocapritermes* (Isoptera, Termitidae, Termitinae). *Bulletin of the American Museum of Natural History* 138: 83–130. <https://digitallibrary.amnh.org/handle/2246/1107>
- Noirot C (1995) The gut of termites (Isoptera). Comparative anatomy, systematics, phylogeny. I. Lower termites. *Annales de la Société entomologique de France (Nouvelle Série)* 31: 197–226.
- Noirot C (2001) The gut of termites (Isoptera). Comparative anatomy, systematics, phylogeny. II. Higher termites (Termitidae). *Annales de la Société entomologique de France (Nouvelle Série)* 37: 431–471.
- Roisin Y, Pasteels JM (2000) The genus *Microcerotermes* (Isoptera: Termitidae) in New Guinea and the Solomon Islands. *Invertebrate Taxonomy* 14(2): 137–174. <https://doi.org/10.1071/IT99005>

- Roonwal ML (1969) Measurement of termites (Isoptera) for taxonomic purposes. *Journal of the Zoological Society of India* 21: 9–66.
- Sands WA (1972) The soldierless termites of Africa (Isoptera: Termitidae). *Bulletin of the British Museum (Natural History) Entomology Supplement* 18: 1–244. <https://doi.org/10.5962/p.192782>
- Scheffrahn RH, Bourguignon T, Akama PD, Sillam-Dussès D, Šobotník J (2018) *Roisinitermes ebogoensis* gen. & sp. nov., an outstanding drywood termite with snapping soldiers from Cameroon (Isoptera, Kalotermitidae). *ZooKeys* 787: 91–105. <https://doi.org/10.3897/zookeys.787.28195>
- Seid MA, Scheffrahn RH, Niven JE (2008) The rapid mandible strike of a termite soldier. *Current Biology* 18(22): R1049–R1050. <https://doi.org/10.1016/j.cub.2008.09.033>

Hidden diversity of rock geckos within the *Cnemaspis siamensis* species group (Gekkonidae, Squamata): genetic and morphological data from southern Thailand reveal two new insular species and verify the phylogenetic affinities of *C. chanardi* and *C. kamolnorranathi*

Natee Ampai¹, Attapol Rujirawan², Siriporn Yodthong³, Korkhwan Termprayoon², Bryan L. Stuart⁴, Perry L. Wood Jr⁵, Anchalee Aowphol²

1 Department of Biology, Faculty of Science, Srinakharinwirot University, Bangkok, 10110 Thailand **2** Department of Zoology, Faculty of Science, Kasetsart University, Bangkok, 10900 Thailand **3** Department of Biology, Faculty of Science, Thaksin University, Pa Phayom, Phattalung, 93210 Thailand **4** Section of Research & Collections, North Carolina Museum of Natural Sciences, Raleigh, NC, USA **5** Department of Ecology and Evolutionary Biology, University of Michigan, Ann Arbor, MI, USA

Corresponding author: Anchalee Aowphol (fsciacle@ku.ac.th)

Academic editor: Thomas Ziegler | Received 25 August 2022 | Accepted 26 September 2022 | Published 21 October 2022

<https://zoobank.org/3A08F03D-4E26-4CAF-9017-844F841EABA6>

Citation: Ampai N, Rujirawan A, Yodthong S, Termprayoon K, Stuart BL, Wood Jr PL, Aowphol A (2022) Hidden diversity of rock geckos within the *Cnemaspis siamensis* species group (Gekkonidae, Squamata): genetic and morphological data from southern Thailand reveal two new insular species and verify the phylogenetic affinities of *C. chanardi* and *C. kamolnorranathi*. ZooKeys 1125: 115–158. <https://doi.org/10.3897/zookeys.1125.94060>

Abstract

Two new insular rock geckos in the genus *Cnemaspis* are described from Ko Samui in Surat Thani Province and Ko Similan in Phang-nga Province, southern Thailand, based on a combination of morphological and mitochondrial NADH dehydrogenase subunit 2 (ND2) data. Both new species represent divergent lineages within the *Cnemaspis siamensis* species group. *Cnemaspis samui* **sp. nov.** is distinguished from other species in the group by having eight or nine supralabial and infralabial scales; 5–8 pore-bearing preloacal scales in males, pores rounded; 25–27 paravertebral tubercles, arranged randomly; 22–25 subdigital lamellae under 4th toe; enlarged median subcaudal scale row present; gular region, abdomen, limbs and subcaudal region yellowish only in males, and uncorrected pairwise divergences of 8.86–26.83% from all other species in the *C. siamensis* species group. *Cnemaspis similan* **sp. nov.** is distinguished from other species in the group by having eight or nine supralabial and seven or eight infralabial scales; one pore-bearing preloacal scale in males, pore rounded; 24 or 25 paravertebral tubercles, arranged randomly; 23 or 24

subdigital lamellae under 4th toe; no enlarged median subcaudal scale row; pale yellow reticulum on head, neck, flanks, belly and limbs in male only, and uncorrected pairwise divergences of 9.34–27.11% from all other species in the *C. siamensis* species group. *Cnemaspis samui* **sp. nov.** is found along granitic rocky stream outcrops of Hin Lad Waterfall, Ko Samui, Gulf of Thailand, while *Cnemaspis similan* **sp. nov.** occurs in granitic rocky outcrops near Ao Nguang Chang Bay, Ko Similan, Andaman Sea. The phylogenetic analyses confirmed that *C. chanardi* and *C. kamolnorrnanathi* are also nested within the *C. siamensis* species group, as previously hypothesized from morphology and color pattern characters.

Keywords

Cnemaspis, integrative taxonomy, Island, phylogeny, Thailand

Introduction

The rock gecko genus *Cnemaspis* Strauch, 1887 is one of the most diverse reptile genera, with 192 recognized species known to date (Uetz et al. 2022). The genus has a geographically widespread distribution, ranging from South Asia to Southeast Asia, and is composed of two separate clades based on multi-locus phylogenetic analyses (Gamble et al. 2012, 2015; Pyron et al. 2013; Karunarathna et al. 2019; Malonza and Bauer 2022). The 64 currently described Southeast Asian species of *Cnemaspis* represent a monophyletic group, include many species with specializations for various rocky habitats (Grismer et al. 2010, 2014; Nguyen et al. 2020), and are distributed in Myanmar, Thailand, Laos, Cambodia, Vietnam, Malaysia and Indonesia (Bauer and Das 1998; Das 2005; Grismer and Ngo 2007; Grismer et al. 2010, 2014, 2020; Kurita et al. 2017; Riyanto et al. 2017; Wood et al. 2017; Ampai et al. 2019, 2020; Lee et al. 2019; Nashriq et al. 2022). In Thailand, 19 named species of Southeast Asian *Cnemaspis* (Grismer et al. 2010, 2014, 2020; Wood et al. 2017; Ampai et al. 2019, 2020; Uetz et al. 2022) occur throughout much of the country's mainland and adjacent offshore islands (Grismer et al. 2014, 2020; Wood et al. 2017; Ampai et al. 2019, 2020; Lee et al. 2019).

Historically, the taxonomy and systematics of Thai *Cnemaspis* depended solely on data from morphology and color pattern characteristics (e.g., Smith 1925; Taylor 1963; Bauer and Das 1998; Grismer et al. 2010). During the past decade, integrative taxonomic approaches that included morphological characteristics, ecological data, and molecular genetics (e.g., Grismer et al. 2014, 2020; Wood et al. 2017; Ampai et al. 2019, 2020; Lee et al. 2019) have been used to address and resolve previous taxonomic issues (Wood et al. 2017). Thai *Cnemaspis* species are assigned to four species groups based on morphological character state differences and genetics (Grismer et al. 2014; Ampai et al. 2019, 2020), these being the *affinis* group, the *chanthaburiensis* group, the *kumpoli* group, and the *siamensis* group. Of these, the *siamensis* group shows the highest species richness with 12 recognized species in Thailand, including *C. adangrawi* Ampai et al. 2019, *C. chanardi* Grismer et al. 2010, *C. huaseesom* Grismer et al. 2010, *C. kamolnorrnanathi* Grismer et al. 2010, *C. lineatubercularis* Ampai et al. 2020, *C. omari* Grismer et al. 2014, *C. phangngaensis* Wood et al. 2017; *C. punctatonuchalis*

Grismer et al. 2010, *C. selenolagus* Grismer et al. 2020, *C. siamensis* (Smith, 1925), *C. thachanaensis* Wood et al. 2017, and *C. vandeventeri* Grismer et al. 2010. Only one member of the *siamensis* group, *C. roticanai* Grismer & Chan, 2010, occurs outside of Thailand, where it occurs on Langkawi Island, Malaysia. Within the *siamensis* group, *C. chanardi* and *C. kamolnorrnanathi* remain the least known species, in part due to a lack of genetic data from their type localities.

We conducted field surveys for *Cnemaspis* during 2015–2020 at five localities in southern Thailand. Morphological and mitochondrial DNA data analyses revealed that the *Cnemaspis* samples from Ko (= island) Samui in the Gulf of Thailand and Ko Similan in the Andaman Sea differed from all known congeners of Thai *Cnemaspis*. In addition, we obtained samples from the type localities of *C. chanardi* and *C. kamolnorrnanathi*. Herein, the two distinct insular populations of *Cnemaspis* are described as new species and genetic data are used to verify the phylogenetic placements of *C. chanardi* and *C. kamolnorrnanathi* within the *C. siamensis* group.

Materials and methods

Taxon sampling and specimen collection

Fieldwork was conducted at five different localities in southern Thailand including (1) Pathio District, Chumphon Province in June 2017, (2) Kanchanadit District, Surat Thani Province in January 2019, (3) Nayong District, Trang Province in May 2016, December 2017, and July 2019, (4) Ko Samui, Surat Thani Province in September 2015, July 2018, and August 2020, and (5) Ko Similan, Mu Ko Similan National Park, Phang-nga Province in March 2018. Sampling was conducted by using visual encounter surveys both during the day (1000–1800 h) and at night (1900–2200 h). Ecological data (air temperature and relative humidity) were collected using a Kestrel 4000 Weather Meter. Habitat preferences (e.g., microhabitat, substrate type and habitat use) were also recorded. Geographical coordinates and elevation were taken using a Garmin GPSMAP 64s. At each locality, specimens were photographed and euthanized by cardiac injection of tricaine methane sulfonate (MS-222) solution (Simmons 2015). Liver samples were removed from euthanized specimens for molecular analysis, preserved in 95% ethanol, and stored at -20 °C. Voucher specimens were then fixed in 10% formalin and later transferred to 70% ethanol for long-term storage. Specimens and tissue samples were deposited in the herpetological collection at the Zoological Museum of Kasetsart University, Bangkok, Thailand (ZMKU). All specimens of the *C. siamensis* group, including the type specimens of *C. adangrawi*, *C. chanardi*, *C. huaseesom*, *C. lineatubercularis*, *C. niyomwanae*, *C. punctatonuchalis*, and *C. vandeventeri*, were examined as comparative material (Appendix I) in the holdings of ZMKU and the Thailand Natural History Museum, Pathum Thani, Thailand (THNHM). Additional data were obtained from the original species descriptions of Thai *Cnemaspis* (Smith, 1925; Grismer et al. 2010, 2014, 2020; Wood et al. 2017; Ampai et al. 2019, 2020).

Molecular genetic study and phylogenetic analyses

Genomic DNA from 21 individuals of *Cnemaspis* (*C. adangrawi*, $N = 2$; *C. chanardi*, $N = 4$; *C. kamolnorrnanathi*, $N = 5$; *C. siamensis*, $N = 2$; Ko Samui samples, $N = 4$; and Ko Similan samples, $N = 4$) was extracted from liver tissue (Table 1) using the Qiagen DNAeasy™ Blood & Tissue Kit (Valencia, CA, USA). A fragment of mitochondrial (mt) DNA encoding the NADH dehydrogenase subunit 2 (ND2) gene and parts of its flanking tRNAs Trp, Ala, Asn and Cys was amplified by polymerase chain reaction (PCR) with an initial denaturation (95 °C, 2 min) followed by 33 cycles of denaturation (95 °C, 35s), annealing (52 °C, 35s), and extension (72 °C, 35s) and the light strand primer MetF1(L4437b; 5'-AAGCAGTTGGGCCCATACC-3'; Macey et al. 1997) and heavy strand primer CO1R1 (H5934; 5'-AGRGTGCCAATGTCTTTGTGRTT-3'; Macey et al. 1997). PCR products were purified by the NucleoSpin Gel and PCR Clean-up Kit (Machery-Nagel Inc.) and sequenced using the amplifying primers on an ABI 3730XL automatic sequencer (Sango Biotech Inc, Shanghai, China). The generated DNA sequences were edited and aligned using Geneious R11 (Biomatters, Ltd, Auckland, New Zealand). The newly generated sequences were deposited in GenBank under accession numbers – (Table 1).

Homologous sequences of 68 *Cnemaspis* and the seven outgroups *Cyrtodactylus bokorensis* Murdoch, Grismer, Wood, Neang, Poyarkov, Tri, Nazarov, Aowphol, Pauwels, Nguyen & Grismer, 2019, *Dixonius melanostictus* (Taylor, 1962), *Dixonius siamensis* (Boulenger, 1898), *Gehyra mutilata* Wiegmann, 1834, *Gekko gecko* (Linnaeus, 1758), *Hemidactylus frenatus* Duméril & Bibron, 1836 and *Hemidactylus garnotii* Duméril & Bibron, 1836 (following Wood et al. 2017; Ampai et al. 2020) were downloaded from GenBank. These were aligned to the 21 newly generated sequences of *Cnemaspis* using the MUSCLE plug-in as implemented in Geneious R11 (Biomatters, Ltd, Auckland, New Zealand). The aligned dataset was partitioned into four partitions consisting of ND2 codon positions and the flanking tRNAs. Molecular phylogenetic relationships were estimated using Bayesian inference (BI) and maximum likelihood (ML). The BI was implemented in MrBayes v3.2.7a (Ronquist et al. 2012) on XSEDE (CIPRES; Miller et al. 2010). The best-fit model of sequence evolution for each partition was estimated using the Bayesian Information Criterion (BIC) as implemented in PartitionFinder2 on XSEDE (Lanfear et al. 2016). The selected models were GTR+I+ Γ for each ND2 codon partition and HKY+I+ Γ for tRNAs. The BI analysis was performed as two simultaneous runs, each with four Markov chains (three heated and one cold chain), using the default priors and chain temperature set to 0.1 for 20,000,000 generations, with trees sampled every 2,000 generations from the Markov Chain Monte Carlo (MCMC). The first 25% of each run was discarded as burn-in using the “sumt” command. The convergence of the two simultaneous runs, stationary state of each parameter, and the effective sample sizes were evaluated by visualizing the log file in Tracer v1.6 (Rambaut et al. 2014). Nodes with Bayesian posterior probabilities support (BPP) of ≥ 0.95 were considered well-supported (Huelsenbeck and Ronquist 2001; Wilcox et al. 2002).

Table 1. Voucher information, including locality, collection numbers, GenBank accession numbers and reference for the specimens used in the phylogenetic analyses. Voucher abbreviations are as follows: Monte L. Bean Life Science Museum at Brigham Young University (**BYU**), California Academy of Sciences (**CAS**), the Field Museum of Natural History, Chicago, Illinois, USA (**FMNH**), La Sierra University Herpetological Collection (**LSUHC**), the Thailand Natural History Museum, Pathum Thani, Thailand (**THNHM**), Universiti Sains Malaysia Herpetological Collection at the Universiti Sains Malaysia, Penang, Malaysia (**USMHC**), and Zoological Museum of Kasetsart University (**ZMKU**).

Species	Locality	Collection number	GenBank accession number	Reference
Outgroup				
<i>Cyrtodactylus bokorensis</i>	Cambodia, Kampot	FMNH 263228		Grismer et al. 2015b
<i>Dixonius melanostictus</i>	Thailand (captive)	No number		Ziegler et al. 2016
<i>Dixonius siamensis</i>	Cambodia, Pursat Province, Phnom Aural	LSUHC 7328		Ziegler et al. 2016
<i>Gekko gekko</i>	Myanmar, Aycyarwady Division, Myaungmya District	CAS 204952		Rösler et al. 2011
<i>Gehyra mutilata</i>	Cambodia, Pursat Province, Phnom Aural	LSUHC 7379		Wood et al. 2017
<i>Hemidactylus frenatus</i>	Myanmar, Tanintharyi Division, Kaw Thauung District	CAS 229633		Bauer et al. 2010
<i>Hemidactylus garnotii</i>	Myanmar, Mon State, Kyait Hti Yo Wildlife Sanctuary	CAS 222276		Bauer et al. 2010
Ca Mau Clade				
<i>Cnemaspis boulengerii</i>	Vietnam, Ca Mau Province, Con Dao Archipelago	LSUHC 9278 LSUHC 9279		Grismer et al. 2014
<i>Cnemaspis psychedelica</i>	Vietnam, Ca Mau Province, Hon Khoai Island	LSUHC 9243 LSUHC 9244		Wood et al. 2017
chanthaburiensis group				
<i>Cnemaspis aurantiacopes</i>	Vietnam, Kien Giang Province, Hon Dar Hill	LSUHC 8610 LSUHC 8611		Grismer et al. 2014
<i>Cnemaspis caudanivea</i>	Vietnam, Kien Giang Province, Hon Tre Island	LSUHC 8582		Grismer et al. 2014
<i>Cnemaspis chanthaburiensis</i>	Cambodia, Pursat Province, Phnom Dalai	LSUHC 9338		Grismer et al. 2014
<i>Cnemaspis lineogularis</i>	Thailand, Prachuap Khiri Khan Province, Kui Buri District, Wat Khao Daeng	BYU 62535 ZMKU R 00728		Wood et al. 2017
<i>Cnemaspis neangthyi</i>	Cambodia, Pursat Province, O'Lakmeas	LSUHC 8515 LSUHC 8516		Grismer et al. 2014
<i>Cnemaspis nuicamensis</i>	Vietnam, An Giang Province, Nui Cam Hill	LSUHC 8646 LSUHC 8647 LSUHC 8648		Grismer et al. 2014
kumpoli group				
<i>Cnemaspis biocellata</i>	Malaysia, Perlis, Kuala Perlis	LSUHC 8789 LSUHC 8817		Grismer et al. 2014
	Malaysia, Perlis, Gua Kelam	LSUHC 8818		
<i>Cnemaspis kumpoli</i>	Malaysia, Perlis, Perlis State Park	LSUHC 8847 LSUHC 8848		Grismer et al. 2014
<i>Cnemaspis monachorum</i>	Malaysia, Kedah, Langkawi Archipelago, Pulau Langkawi	LSUHC 9114 LSUHC 10807		Grismer et al. 2014
<i>Cnemaspis niyomwanee</i>	Thailand, Trang Province, Thum Khao Ting	LSUHC 9568 LSUHC 9571		Grismer et al. 2014
<i>Cnemaspis tarutaoensis</i>	Thailand, Satun Province, Mueang Satun District, Ko Tarutao	ZMKU R 00761 ZMKU R 00763 ZMKU R 00764		Ampai et al. 2019
argus group				
<i>Cnemaspis argus</i>	Malaysia, Terengganu, Gunung Lawit	LSUHC 8304 LSUHC 10834		Grismer et al. 2014

Species	Locality	Collection number	GenBank accession number	Reference
<i>Cnemaspis karsticola</i>	Malaysia, Kelantan, Gunung Reng	LSUHC 9054 LSUHC 9055		Grismer et al. 2014
affinis group				
<i>Cnemaspis affinis</i>	Malaysia, Penang, Pulau Pinang	LSUHC 6787		Grismer et al. 2014
<i>Cnemaspis griseri</i>	Malaysia, Perak, Lenggong	LSUHC 9969		Grismer et al. 2014
<i>Cnemaspis bangus</i>	Malaysia, Pahang, Bukit H Angus	LSUHC 9358b		Grismer et al. 2014
<i>Cnemaspis barimau</i>	Malaysia, Kedah, Gunung Jeri	LSUHC 9665		Grismer et al. 2014
<i>Cnemaspis mahsuriae</i>	Malaysia, Kedah, Pulau Langkawi, Gunung Raya	LSUHC 11829		Grismer et al. 2015a
<i>Cnemaspis mcguirei</i>	Malaysia, Perak, Bukit Larut	LSUHC 8853		Grismer et al. 2014
<i>Cnemaspis narathiwatensis</i>	Malaysia, Perak, Belum-Temengor, Sungai Enam	USMHC 1347 USMHC 1348		Grismer et al. 2014
siamensis group				
<i>Cnemaspis adangrawi</i>	Thailand, Satun Province, Mueang Satun District, Ko Adang	ZMKU R 00767		Ampai et al. 2019
		ZMKU R 00768		This study
	Thailand, Satun Province, Mueang Satun District, Ko Rawi	THNHM 28207		Ampai et al. 2019
		ZMKU R 00770 ZMKU R 00774 ZMKU R 00775 ZMKU R 00776		This study Ampai et al. 2019
<i>Cnemaspis chanardi</i>	Thailand, Trang Province, Nayong District	ZMKU R 00988 ZMKU R 00989 ZMKU R 00990 ZMKU R 00991		This study
<i>Cnemaspis buasesom</i>	Thailand, Kanchanaburi Province, Sai Yok National Park	LSUHC 9455 LSUHC 9457 LSUHC 9458		Grismer et al. 2014
<i>Cnemaspis kamolnorranathi</i>	Thailand, Surat Thani Province, Kanchanadit District, Tai Rom Yen National Park	ZMKU R 00992 ZMKU R 00993 ZMKU R 00994 ZMKU R 00995 ZMKU R 00996		This study
<i>Cnemaspis lineatubercularis</i>	Thailand, Nakhon Si Thammarat Province, Lan Saka District, Wang Mai Pak Waterfall	ZMKU R 00825 ZMKU R 00828 ZMKU R 00829 ZMKU R 00830		Ampai et al. 2020
<i>Cnemaspis omari</i>	Thailand, Satun Province, Phuphaphet Cave Malaysia, Perlis, Perlis State Park	LSUHC 9565 LSUHC 9978		Grismer et al. 2014
<i>Cnemaspis phangngaensis</i>	Thailand, Phang-nga Province, Mueang Phang-nga District, Khao Chang, Phung Chang Cave	BYU 62537 BYU 62538		Wood et al. 2017
<i>Cnemaspis punctatoruchalis</i>	Thailand, Prachaup Khiri Khan Province, Thap Sakae	BYU 62539 BYU 62540		Wood et al. 2017
<i>Cnemaspis roticanai</i>	Malaysia, Kedah, Pulau Langkawi, Gunung Raya	LSUHC 9430 LSUHC 9431 LSUHC 9439		Grismer et al. 2014
<i>Cnemaspis samui</i> sp. nov.	Thailand, Surat Thani Province, Ko Samui District, Ko Samui, Hin Lad Waterfall	ZMKU R 00966 ZMKU R 00967 ZMKU R 00968 ZMKU R 00974		This study
<i>Cnemaspis similan</i> sp. nov.	Thailand, Phang-nga Province, Tai Mueang District, Mu Ko Similan National Park, Ko Similan, Ao Nguang Chang	ZMKU R 00984 ZMKU R 00985 ZMKU R 00986 ZMKU R 00987		This study
<i>Cnemaspis selenolagus</i>	Thailand, Ratchaburi Province, Suan Phueng District, Khao Laem Mountain	ZMMU R 16391 AUP 00767		Grismer et al. 2020

Species	Locality	Collection number	GenBank accession number	Reference
<i>Cnemaspis siamensis</i>	Thailand, Chumpon Province, Pathio District	LSUHC 9474		Grismer et al. 2014
		LSUHC 9485		
		ZMKU R 00997		This study
<i>Cnemaspis thachanaensis</i>	Thailand, Surat Thani Province, Tha Chana District, Tham Khao Sonk Hill	BYU 62542		Wood et al. 2017
		BYU 62543		
		BYU 62544		
<i>Cnemaspis vandeventeri</i>	Thailand, Ranong Province, Suk Saran District, Naka	BYU 62541		Wood et al. 2017

The ML analysis was implemented using the IQ-TREE web server (Nguyen et al. 2015; Trifinopoulos et al. 2016). The best-fit model of evolution for each partition was estimated using IQ-TREE's ModelFinder function (Kalyaanamoorthy et al. 2017). Based on the Bayesian Information Criterion (BIC), the TIM+F+I+G4 was the best-fit model for 1st, 2nd, 3rd codon partitions and HKY+F+G4 for tRNAs. The ultrafast bootstrap analysis (UFB; Minh et al. 2013; Hoang et al. 2017) using 10,000 bootstrap pseudo-replicates was used to construct a final consensus ML tree. Nodes with ultrafast bootstrap support (UFB) of ≥ 95 were considered well-supported (Minh et al. 2013). The 50% majority-rule consensus of sampled trees from the BI analysis and the most likely tree in the ML analysis were visualized and edited in FigTree v1.4.4 (Rambaut 2018). Uncorrected pairwise sequence divergences were estimated using a *p*-distance method with the pairwise deletion option in MEGA 11.0.11 (Tamura et al. 2021).

Morphological measurement and analyses

Coloration and pattern in life was determined by examination of digital images taken of living specimens of all possible age classes prior to preservation. Morphological and meristic data were taken by the first author on the left side of preserved specimens for symmetrical characters, when possible, using digital Mitutoyo CD-6" ASX Digimatic Calipers to the nearest 0.1 mm under a Nikon SMZ745 dissecting microscope. Three body-size classes were established by snout-vent length: small size (< 35 mm), medium size (35–40 mm) and large size (> 40 mm). Only adult individuals, as determined by the presence of secondary sexual characteristics such as pore-bearing precloacal scales or hemipenes in males or visible eggs on ventral side of body or enlarged endolymphatic glands in females, were included for morphometric and meristic measurements. A total of sixteen morphological characters was scored following Grismer et al. (2020), Wood et al. (2017) and Ampai et al. (2020): snout-vent length (**SVL**, taken from tip of snout to the anterior margin of vent); tail width (**TW**, at the base of the tail immediately posterior to the postcloacal swelling); tail length (**TL**, distance from the vent to the tip of the tail, whether original or regenerated); forearm length (**FL**, taken on the dorsal surface from the posterior margin of the elbow while flexed 90° to the inflection of the flexed wrist); tibia length (**TBL**, taken on the ventral surface from the posterior

surface of the knee while flexed 90° to the base of the heel); head length (**HL**, distance from the posterior margin of the retroarticular process of the lower jaw to the tip of the snout); head width (**HW**, at the angle of the jaws); head depth (**HD**, the maximum height of head from the occiput to the throat); axilla-groin length (**AG**, taken from the posterior margin of the forelimb at its insertion point on the body to the anterior margin of the hind limb at its insertion point on the body); eye diameter (**ED**, the maximum horizontal diameter of the eyeball); eye-ear distance (**EE**, measured from the anterior margin of the ear opening to the posterior edge of the eyeball); ear length (**EL**, taken from the greatest vertical distance of the ear opening); eye-nostril distance (**EN**, measured from the anterior most margin of the eyeball to the posterior margin of the external nares); eye-snout distance (**ES**, measured from the anterior margin of the eyeball to the tip of snout); internarial distance (**IN**, measured between the medial margins of the nares across the rostrum) and inner orbital distance (**IO**, the width of the frontal bone at the level of the anterior edges of the orbit).

Meristic characters states of scales and quantitative observations of pattern and structures were evaluated under a Nikon SMZ745 dissecting microscope. Meristic characters taken were modified from Grismer et al. (2014, 2020), Wood et al. (2017) and Ampai et al. (2020) as follows: number of supralabial (**SupL**) and infralabial (**InfL**) scales, counted from below the middle of the orbit to the rostral and mental scales, respectively; texture of scales on the anterior margin of the forearm; number of paravertebral tubercles (**PVT**) between limb insertions, counted in a straight line immediately left of the vertebral column; general size (i.e., strong, moderate, weak) and arrangement (i.e., random or linear) of dorsal body and tail tuberculation; number of subdigital lamellae beneath the fourth toe (**4TL**), counted from the base of the first phalanx to the claw; and number of postcloacal tubercles on each side of tail base. Categorical character states examined were: presence or absence of dark round spots on the nape and anterior portion of the body; the presence or absence of ocelli on the shoulder region; coloration of dorsal blotching on head, body, limbs and tail; presence or absence of a row of enlarged, widely spaced, tubercles along the ventrolateral edge of the body flank between limb insertions; number, orientation and shape of pore-bearing precloacal scales; and relative size of subcaudal and subtibial scales. Descriptions refer to right (R) and left (L) sides of the body.

Statistical analyses were used to compare differences in size and shape within the *siamensis* group, including populations from Ko Samui ($N = 18$), Ko Similan ($N = 4$) and the seven described species *C. adangrawi* ($N = 8$), *C. chanardi* ($N = 7$), *C. lineatubercularis* ($N = 19$), *C. omari* ($N = 5$), *C. phangngaensis* ($N = 3$), *C. siamensis* ($N = 8$) and *C. thachanaensis* ($N = 6$). Due to lack of available measurements, six species in the *siamensis* group (*C. huaseesom*, *C. kamolnorrnanathi*, *C. punctatonuchalis*, *C. roticanai*, *C. selenolagus* and *C. vandeventeri*) were not included in the morphometric analyses. All specimens were assigned to nine putative operation taxonomic units (OTUs) based on the mtDNA results: OTU1 (= Ko Samui population), OTU2 (= Ko Similan population), OTU3 (= *C. adangrawi*), OTU4 (= *C. chanardi*), OTU5 (= *C. lineatubercularis*), OTU6 (= *C. omari*), OTU7 (= *C. phangngaensis*), OTU8 (= *C. siamensis*) and OTU9 (= *C. thachanaensis*). TL (tail length) was excluded due to their different conditions

(e.g., complete, broken, and regenerated). All morphological variables were adjusted for differences in ontogenetic composition by the allometric equation:

$$X_{\text{adj}} = \log(X) - b[\log(\text{SVL}) - \log(\text{SVL}_{\text{mean}})]$$

where X_{adj} is the corrected value of the morphometric variable; X is the unadjusted value of dependent variable; b is the within-clade coefficient of the linear regression of each original character value (X) against SVL; SVL = snout-vent length; and SVL_{mean} = overall mean of SVL of all nine OTUs (Thorpe 1975, 1983; Turan 1999; Leonart et al. 2000; Chan and Grismer 2021).

Univariate analyses were implemented in the Paleontological statistics software (PAST v4.07b; Hammer et al. 2001) using an analysis of variance (ANOVA) to compare morphological differentiation in traits among nine putative OTUs (OTU1–OTU9). Morphological characters with equal variances and having p -values less than 0.05 were subjected to a Tukey's honestly significant difference (HSD) test to identify all pairwise comparisons among sample means for significant differences ($p < 0.05$). Moreover, multivariate analyses were performed using the platform R v3.2.1 (R Core Team 2018). A principal component analysis (PCA) using the built-in R functions: "prcomp" (R Core Team, 2018) and "ggplot2" (Wickham, 2016) was performed to find the best low-dimensional space of morphological variation in data. Principal components (PCs) with eigenvalues greater than 1.0 were retained in accordance with the criterion of Kaiser (1960). A discriminant analysis of principal components (DAPC) was applied using the "adegenet" package in R (Jombart 2008) to characterize clustering and distance in the morphospace of the two new groups compared to the seven named congeners of the *siamensis* group, as delimited by the molecular phylogenetic analyses. The DAPC relied on transformed and scaled data from the PCA as a prior step to find the linear combinations of morphological variables having the greatest between-group variance and the smallest within-group variance of linear distances (Jombart et al. 2010).

Results

Molecular analyses

The aligned dataset contained 1,310 characters of 89 individuals of *Cnemaspis* and seven individuals of the outgroup species (Fig. 1A). Estimated base frequencies of the *Cnemaspis* dataset excluding outgroups were A = 30.52%, C = 34.65%, G = 12.59% and T = 22.24%. The BI and ML phylogenetic trees had similar topologies, with only minor differences in positions of unresolved branches (Fig. 1B). The maximum standard deviation of split frequencies among the two simultaneous BI runs was 0.016685. The average standard deviation of split frequencies among the two simultaneous BI runs was 0.002622 and ESS values were greater than or equal to 6,152 for all parameters. The maximum likelihood value of the best ML tree was $\ln L = -81,696.218$.

Cnemaspis samples from Ko Samui and Ko Similan represented well-supported independent lineages (100 UFB, 1.0 BPP) and were nested within the *siamensis* group (Fig. 1B). The Ko Samui samples were well-supported for ML (99 UFB) but lacked support from BI (0.56 BPP) as the sister lineage to *C. kamolnorranathi* from its type locality at Ban Nasan District, Surat Thani Province, Thailand. The Ko Samui samples had uncorrected *p*-distances of 9.10–9.73% from *C. kamolnorranathi* and 8.86–26.83% from the other species in the *siamensis* group. The Ko Similan samples were recovered as a well-supported lineage (100 UFB, 1.0 BPP) and sister to *C. phangngaensis* (Fig. 1B). The Ko Similan samples had uncorrected *p*-distances of 8.16% from *C. phangngaensis* and 9.34–27.11% from the other species in the *siamensis* group. The Ko Samui and the Ko Similan populations had within population uncorrected *p*-distances of 0.00–1.11% and 0.00%, respectively (Table 2).

Cnemaspis chanardi and *C. kamolnorranathi* samples from their type localities (Fig. 1B, C) represented well-supported independent lineages (100 UFB, 1.0 BPP). *Cnemaspis chanardi* was well-supported (100 UFB, 1.0 BPP) as sister to a clade comprised of *C. phangngaensis* and the Ko Similan population. *Cnemaspis kamolnorranathi* was recovered as the sister lineage to the Ko Samui population (99 UFB, 0.56 BPP). *Cnemaspis chanardi* and *C. kamolnorranathi* had uncorrected *p*-distances of 7.36–26.56% and 8.23–27.52% from the other species in the *siamensis* group, respectively. The within population uncorrected *p*-distances of *C. chanardi* and *C. kamolnorranathi* were 0.00–0.32% and 0.00–0.24%, respectively.

Morphological analyses

Univariate analysis of variance (ANOVA) showed significant differences ($p < 0.05$) in morphometric characters among the Ko Samui population (OTU1), the Ko Similan population (OTU2), and seven congeners (OTU3–OTU9) in the *siamensis* group (Suppl. material 1: Table S1). These were also significantly different in the Tukey's HSD pairwise tests ($p < 0.05$; Table 3). Multivariate analysis of PCA of nine species of *Cnemaspis* revealed morphological differences on a scatter plot of the first two components having eigenvalues > 1.0 (Fig. 2A). These first two components that accounted for 71.8% of the variation in the dataset showed that the Ko Samui and the Ko Similan samples clustered separately from seven congeners in the *siamensis* group (Table 4). The first principal component (PC1) accounted for 54.6% of the of variation and was most heavily loaded on five head characters (head length, head width, head depth, eye-ear distance, and eye-snout distance), two body characters (tibia length and axillar-groin length), and one tail character (tail width). The second principal components (PC2) accounted for an additional 17.2% of the variation and was heavily loaded on three head characters (internarial distance, interorbital distance, and ear length). Factor loadings of each component of 15 morphometric characteristics from nine OTUs of the *siamensis* group are provided in Table 4. The ordination of the first two components showed that the Ko Samui population overlapped with the Ko Similan population and *C. thachanaensis*. The DAPC (94.09% of cumulative variance) revealed the Ko Samui and the Ko Similan populations as distinct clusters, with general clustering of seven congeners in the *siamensis* group (Fig. 2B).

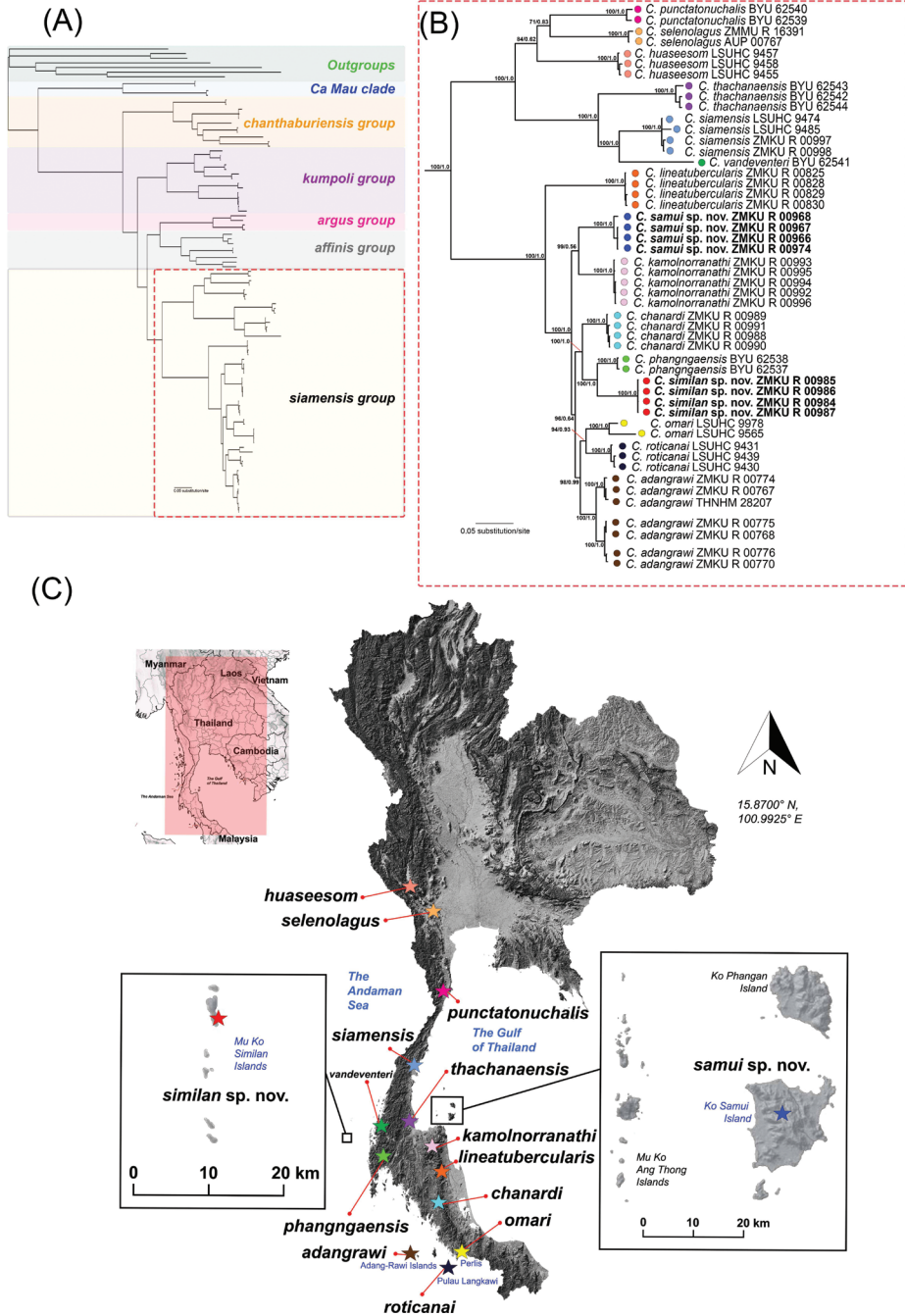


Figure 1. The single best tree from 10,000 Maximum likelihood bootstrap replicates based on 1,310 bp of the mitochondrial NADH dehydrogenase subunit 2 (ND2) and flanking tRNAs from geckos of the genera *Cnemaspis*, *Cyrtodactylus*, *Dixonius*, *Gekko*, *Hemidactylus* and *Gebyra* **A** shown in full view **B** relevant clades of *Cnemaspis siamensis* group in close-up view **C** map illustrating the type locality of all species in the *siamensis* group. Nodal support values are ultrafast bootstrap values from maximum likelihood analysis of the same dataset followed by posterior probabilities of Bayesian analysis.

Table 2. Mean (min-max) uncorrected pairwise distances (%) within the *Cnemaspis siamensis* group based on 1,310 bp of the mitochondrial ND2 gene and flanking tRNAs. Number in bold are within species divergence. *N* = number of individuals.

Species	N	1	2	3	4	5	6	7	8	9	10	11	12	13	14	15
1. <i>Cnemaspis samui</i> sp. nov.	4	0.55 (0.00– 1.11)														
2. <i>Cnemaspis similan</i> sp. nov.	4	11.50 (11.32–11.56)	0.00 (0.00 – 0.00)													
3. <i>C. adangraui</i>	9	9.32 (8.87–9.68)	11.12 (11.08–11.18)	1.58 (0.00 – 3.01)												
4. <i>C. chanardi</i>	4	8.92 (8.86–9.10)	9.40 (9.34–9.58)	7.80 (7.52–8.15)	0.26 (0.00 – 0.32)											
5. <i>C. huasecom</i>	3	23.00 (22.34–23.67)	23.19 (22.72–24.10)	22.47 (22.01–23.27)	22.63 (22.10–23.58)	0.31 (0.00 – 0.78)										
6. <i>C. kamolnornnathi</i>	5	9.55 (9.10–9.73)	11.73 (11.72–11.80)	9.08 (8.86–9.44)	8.38 (8.23–8.54)	23.48 (23.13–24.10)	0.08 (0.00 – 0.24)									
7. <i>C. lineatubercularis</i>	4	14.61 (14.10–14.96)	16.15 (15.92–16.39)	14.19 (13.63–14.77)	14.04 (13.63–14.41)	24.13 (23.02–25.41)	14.55 (14.23–14.89)	0.11 (0.00 – 0.25)								
8. <i>C. omari</i>	2	10.98 (10.17–11.81)	11.42 (10.79–12.06)	8.20 (6.77–9.40)	9.36 (8.72–9.96)	24.74 (24.00–25.60)	10.81 (10.04–11.65)	16.15 (15.07–17.04)	2.36 (0.00 – 4.72)							
9. <i>C. phuanggaensis</i>	2	9.68 (9.58–9.81)	8.16 (8.16–8.21)	9.00 (8.87–9.21)	7.48 (7.36–7.75)	21.69 (21.37–22.29)	10.23 (10.06–10.36)	15.62 (15.24–16.01)	10.50 (9.70–11.33)	0.16 (0.00 – 0.32)						
10. <i>C. punctatoneuchalis</i>	2	23.53 (21.83–24.93)	25.24 (23.67–26.82)	23.19 (21.75–24.53)	23.74 (22.46–24.93)	16.70 (15.57–17.59)	24.34 (23.02–25.62)	23.72 (21.82–25.62)	24.79 (22.75–27.82)	0.75 (0.00 – 1.5)						
11. <i>C. roitanaui</i>	3	10.57 (10.21–10.83)	11.21 (10.61–11.53)	7.69 (7.04–8.20)	8.83 (8.31–9.36)	24.15 (23.27–24.50)	10.23 (9.64–10.50)	14.94 (13.80–15.76)	8.34 (7.13–8.99)	9.00 (8.39–9.36)	0.32 (0.00 – 0.69)					

Species	N	1	2	3	4	5	6	7	8	9	10	11	12	13	14	15	
12. <i>C. selenologus</i>	2	22.75 (22.00– 23.15)	22.69 (22.48– 22.91)	21.53 (21.13– 21.88)	21.32 (20.97– 21.72)	16.08 (15.44– 17.00)	22.06 (21.84– 22.28)	22.46 (21.91– 22.99)	23.33 (23.02– 23.57)	21.35 (21.05– 21.66)	15.93 (15.29– 17.13)	22.15 (21.21– 22.89)	22.15 (21.21– 22.89)	0.28 (0.00 – 0.56)			
13. <i>C. siamensis</i>	4	22.04 (20.83– 23.59)	23.21 (21.73– 24.88)	22.20 (21.21– 23.39)	21.70 (20.64– 23.11)	19.28 (18.73– 19.59)	22.27 (21.12– 23.83)	23.00 (22.30– 24.64)	23.30 (21.21– 24.58)	21.68 (20.25– 23.29)	19.49 (18.12– 20.70)	23.26 (21.41– 24.87)	19.10 (18.72– 19.55)	0.55 (0.00 – 1.74)			
14. <i>C. thachanaensis</i>	3	23.10 (22.66– 23.29)	24.27 (24.12– 24.50)	23.43 (22.97– 23.89)	22.59 (22.35– 22.89)	20.98 (20.79– 21.11)	23.04 (22.91– 23.19)	24.08 (23.65– 24.58)	25.03 (24.88– 25.24)	23.44 (23.29– 23.71)	20.83 (20.05– 21.57)	24.79 (24.09– 25.32)	20.73 (20.49– 21.00)	14.31 (13.86– 15.21)	0.67 (0.00 – 1.74)		
15. <i>C. vanderventeri</i>	1	26.76 (26.56– 26.83)	27.11 (27.11– 27.11)	26.36 (26.15– 26.42)	26.49 (26.42– 26.56)	20.75 (20.66– 20.80)	27.52 (27.52– 27.52)	25.23 (24.65– 25.86)	27.36 (27.11– 27.60)	26.71 (26.59– 26.83)	20.89 (20.89– 20.89)	27.71 (27.66– 27.80)	23.24 (23.00– 23.48)	13.84 (13.64– 14.21)	17.45 (17.22– 17.63)	0.00 (0.00 – 0.00)	

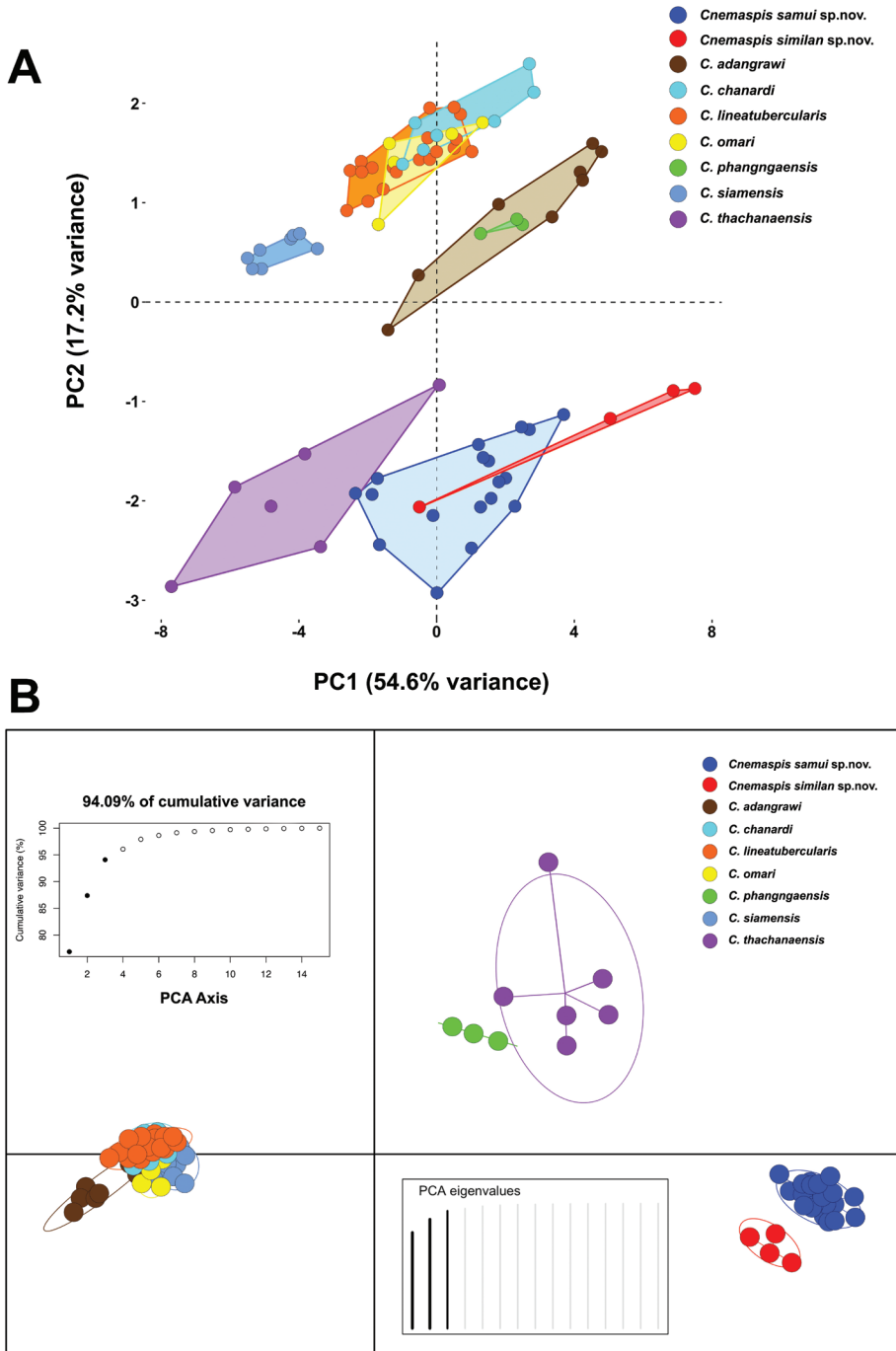


Figure 2. Multivariate analysis results of principal component analysis (PCA) and discriminant analysis of principal component (DAPC) of 14 morphological variables for nine OTUs ($N = 78$ individuals) of *Cnemaspis* in the *siamensis* group **A** PCA scatterplot showing morphospacial differentiation among nine species in the *siamensis* group **B** DAPC ordination of six PCs and discriminant eigenvalues showing morphospacial variation among nine species in the *siamensis* group.

Table 3. Pairwise significant difference matrix from 15 size-corrected morphometric measurements of *Cnemaspis samui* sp. nov. and *Cnemaspis similan* sp. nov. compared with seven congeners of the *Cnemaspis siamensis* group (Tukey’s HSD; $p < 0.05$). Measurement abbreviations are defined in the text.

No.	Species	1	2	3	4	5	6	7	8
1	<i>Cnemaspis samui</i> sp. nov.	–							
2	<i>Cnemaspis similan</i> sp. nov.	SVL, FL, TBL, AG, HL, HW, IN, IO	–						
3	<i>C. adangrawi</i>	TBL, IN, IO	HW, IN, IO	–					
4	<i>C. chanardi</i>	FL, EL, IN, IO	SVL, TW, FL, HL, HW, IN, IO	FL, EL, IO	–				
5	<i>C. lineatubercularis</i>	TBL, HL, HW, EL, IN, IO	SVL, TW, FL, TBL, HL, HW, IN, IO	SVL, FL, TBL, HL, HW, EL, IO	TBL, HL, HW	–			
6	<i>C. omari</i>	TW, FL, TBL, HL, HW, EL, IN, IO	SVL, TW, HL, HW, IN, IO	TW, FL, HL, HW, ES, EL, IO	FL, HW, IN	FL, TBL, IN	–		
7	<i>C. phangngaensis</i>	TW, TBL, IN	TW, IN	TW, IO	TW, FL	TW, FL, TBL, HL	HL, IN	–	
8	<i>C. siamensis</i>	SVL, TW, FL, TBL, HL, HW, ES, IN, IO	SVL, TW, FL, TBL, AG, HL, HW, ES, IN, IO	SVL, TW, FL, TBL, AG, HL, HW, ES, IN	SVL, TW, TBL, AG, HL, HW, ES, EL, IN, IO	SVL, TW, TBL, ES, IN, IO	SVL, FL, TBL, ES	SVL, FL, TBL, HL, ES, IN, IO	–
9	<i>C. thachanaensis</i>	SVL, TW, FL, TBL, AG, HL, HW, ES, EN, IN, IO	SVL, FL, TBL, AG, HL, HW, ES, EN, EL, IN	SVL, TW, FL, TBL, AG, HL, HW, ES, EN, IN, IO	SVL, TBL, AG, HL, HW, ES, EN, EL, IN, IO	SVL, TBL, AG, HW, ES, EN, EL, IN, IO	SVL, FL, TBL, AG, ES, EN, EL, IN	SVL, FL, TBL, AG, HL, HW, ES, EN, EL, IO	EN, EL, IN

Table 4. Summary of proportions of variance, standard deviation, eigenvalues and factor loadings from the 10 first principal components (PC) of 14 size-adjusted morphometric characters of two new insular species *Cnemaspis samui* sp. nov., *Cnemaspis similan* sp. nov. and seven congeners of the *Cnemaspis siamensis* group including *C. adangrawi*, *C. chanardi*, *C. lineatubercularis*, *C. omari*, *C. phangngaensis*, *C. siamensis* and *C. thachanaensis*. Values highlighted in bold represent those with the greatest contribution (≥ 0.30). Measurement abbreviations are defined in the text.

Character	PC1	PC2	PC3	PC4	PC5	PC6	PC7	PC8	PC9	PC10
Proportion of Variance	54.6	17.2	6.2	5.7	5.1	4.3	2.3	1.3	1.0	0.8
Standard deviation	2.77	1.55	0.93	0.89	0.84	0.78	0.57	0.42	0.37	0.33
eigenvalues	7.65	2.406	0.872	0.793	0.711	0.606	0.32	0.179	0.137	0.112
TW	-0.293	-0.083	0.266	0.296	-0.093	0.017	-0.747	0.069	-0.054	0.169
FL	-0.263	-0.125	-0.375	-0.362	0.414	-0.207	-0.317	-0.01	0.005	0.374
TBL	-0.308	0.091	-0.217	-0.171	0.401	0.182	0.021	0.123	0.217	-0.454
AG	-0.302	0.233	-0.04	-0.132	-0.093	0.247	0.069	-0.708	-0.358	0.163
HL	-0.324	-0.118	-0.063	-0.020	0.037	0.360	0.229	0.310	0.064	0.371
HW	-0.328	-0.097	-0.009	-0.030	-0.115	0.418	0.100	0.016	-0.145	-0.267
HD	-0.321	-0.073	0.332	0.211	-0.114	0.066	0.175	0.170	-0.108	0.095
ED	-0.264	0.079	0.422	-0.232	0.237	-0.518	0.161	0.132	-0.458	-0.196
EE	-0.323	-0.005	-0.032	0.422	0.145	-0.073	0.080	0.071	0.209	-0.164
ES	-0.304	0.191	0.011	0.198	-0.086	-0.370	0.098	-0.408	0.532	-0.027
EN	-0.210	0.208	-0.563	0.093	-0.500	-0.325	0.119	0.308	-0.236	0.083
EL	-0.105	0.439	0.282	-0.558	-0.364	0.087	-0.158	0.214	0.357	0.004
IN	-0.096	-0.565	0.172	-0.231	-0.137	-0.155	0.325	-0.085	0.254	0.292
IO	0.113	0.538	0.14	0.211	0.370	0.079	0.236	0.131	0.032	0.473

Taxonomic hypotheses

The Ko Samui and Ko Similan populations distinctly differed from all congeners in the *C. siamensis* group that were evaluated based on molecular analyses of mtDNA with high genetic distances, as well in the univariate analyses (ANOVA and Tukey's HSD pairwise) and the multivariate analyses (PCA and DAPC) of morphology. Based on these corroborating lines of evidence, we hypothesize that the Ko Samui and the Ko Similan populations each represent new species, as described below.

Systematics

Cnemaspis samui sp. nov.

<https://zoobank.org/F75694D-7398-4084-BA37-21D5D1B40D03>

Figs 3–6

Ko Samui Rock Gecko

Thai common name: Jing Jok Niew Yaow Ko Samui (จิ้งจกนิ้วยาวเกาะสมุย)

Holotype (Fig. 3). ZMKU R 00974, adult male from Thailand, Surat Thani Province, Ko Samui District, Ang Thong Subdistrict, Hin Lad Waterfall (9°31.151'N, 99°57.598'E; 150 m a.s.l.), collected on 19 June 2018 by Natee Ampai, Attapol Rujirawan, Siriporn Yodthong and Korkhwan Termprayoon.

Paratypes (Fig. 4). Seventeen paratypes (adult males = 14, adult females = 3). Five adult males (ZMKU R 00966–00970), same collection data as holotype except collected on 26 September 2015 by Natee Ampai, Attapol Rujirawan, Siriporn Yodthong, Korkhwan Termprayoon, and Anchalee Aowphol. Nine adult males (ZMKU R 00971–00973, ZMKU R 00975–00979 and ZMKU R 00983) and three adult females (ZMKU R 00980–00982), same data as holotype.

Diagnosis. *Cnemaspis samui* sp. nov. differs from all other members of the *C. siamensis* group by having the following combination of characters: (1) SVL 37.0–42.3 mm in adult males (mean 39.90 ± 1.98 mm; $N = 15$) and 36.4–41.6 mm in adult females (mean 39.75 ± 2.91 mm; $N = 3$); (2) eight or nine supralabial and infralabial scales; (3) ventral scales keeled (4) 5–8 pore-bearing precloacal scales in males, arranged in a chevron, separated, pore rounded in males; (5) 25–27 paravertebral tubercles, arranged randomly; (6) 4–6 small, subconical spine-like tubercles present on lower flanks; (7) 22–25 subdigital lamellae under 4th toe; (8) enlarged median subcaudal scale row present; (9) ventrolateral caudal tubercles anteriorly present; (10) one or two postcloacal tubercles on lateral surface of hemipenial swellings at the base of tail in males; and (11) gular region, abdomen, limbs and subcaudal region yellowish only in males.

Description of holotype. An adult male in good state of preservation; 42.3 mm SVL; head relatively moderate in size (HL/SVL 0.27), narrow (HW/SVL 0.16), flattened (HD/HL 0.39), depressed (HD/SVL 0.11), and head distinct from neck; snout moderate (ES/HL 0.43), in lateral profile slightly concave; loreal region slightly inflated, canthus rostralis not prominent, smoothly rounded; postnasal region constricted

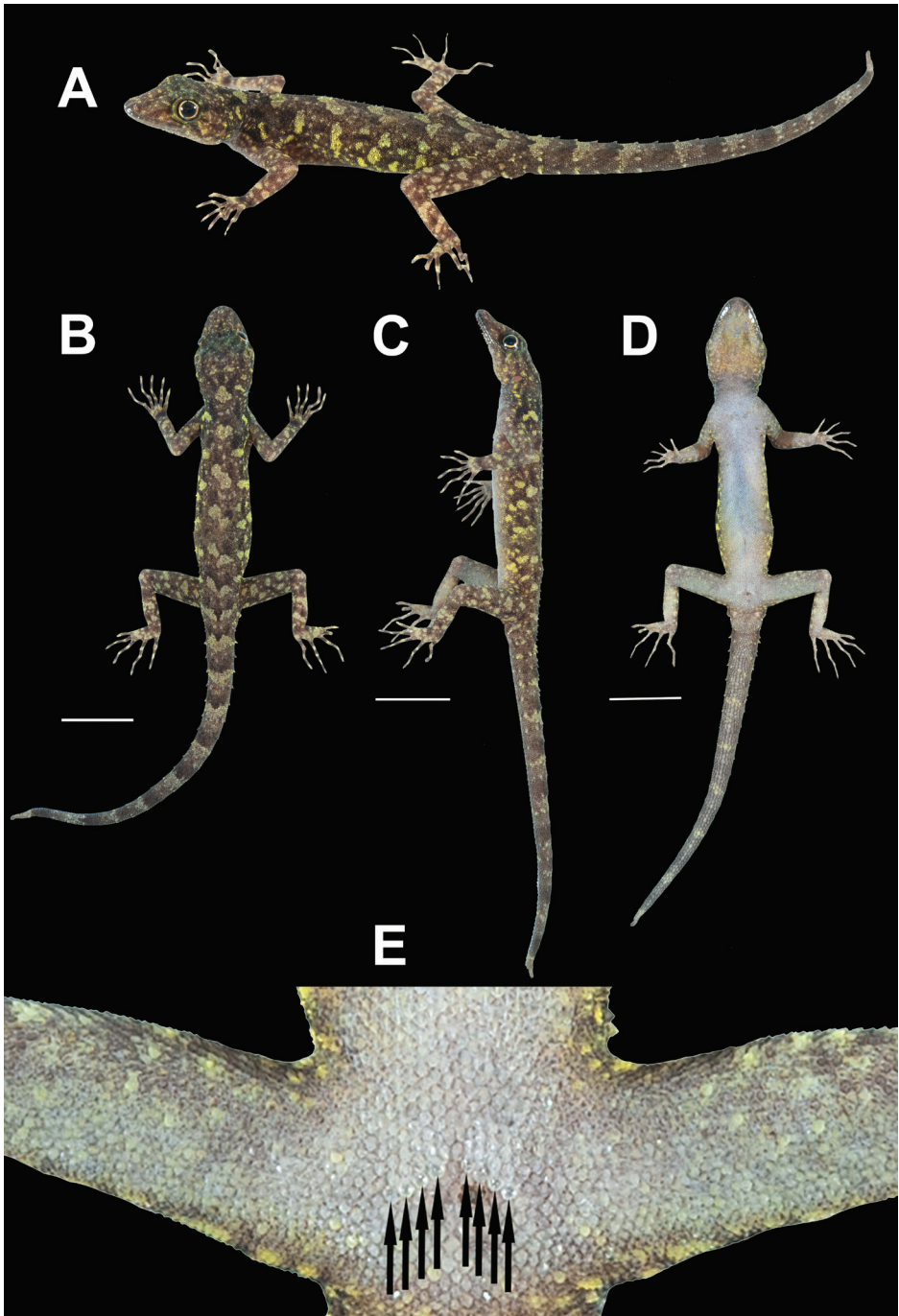


Figure 3. Adult male holotype of *Cnemaspis samui* sp. nov. (ZMKU R 00974) from Hin Lad Waterfall, Ko Samui, Ang Thong Subdistrict, Ko Samui District, Surat Thani Province, Thailand, in life **A** dorsolateral view **B** dorsal view **C** lateral view **D** ventral view **E** preloacal region showing distribution of pore-bearing scales (black arrows). Scale bars in dorsal, lateral, and ventral views: 10 mm.

medially; scales of rostrum round, juxtaposed, keeled, larger than conical scales on occiput; weak, supraorbital ridges; gular and throat scales granular, keeled and round; shallow frontorostral sulcus; eye large (ED/HL 0.21) with round pupil; orbit with extra-brillar fringe scales slightly largest anteriorly; scales on interorbitals and supercilium slightly keeled; eye to ear distance greater than eyes diameter (EE/ED 1.33); ear opening vertical, oval, taller than wide (EL/HL 0.09); rostral slightly concave; rostral bordered posteriorly by supranasals and internasal; rostral in contact laterally with first supralabials; 9R,L supralabials decreasing in size posteriorly; 8R,L infralabials decreasing in size posteriorly; nostril small, oval, oriented dorsoposteriorly, surrounded posteriorly by small postnasal scales; mental scales enlarged, subtriangular, concave, extending to level of second infralabials, bordered posteriorly by three large postmentals.

Body relatively slender, elongate (AG/SVL 0.42); small, keeled, dorsal scales equal in size throughout body intermixed with several large, keeled, scattered, conical tubercles; 26 paravertebral tubercles randomly arranged; four small, subconical spine-like tubercles on flanks; tubercles present on lower flanks; tubercles extend from occiput to tail; pectoral and abdominal scales keeled, round, flat, slightly larger than dorsal and not larger posteriorly; ventral scales of brachia smooth, raised and juxtaposed; eight separated pore-bearing precloacal scales, arranged in a chevron, with rounded pores; precloacal depression absent; femoral pores absent.

Fore and hind limbs moderately elongate, slender; scales beneath forearm slightly raised, smooth and subimbricate; subtibial scales keeled; palmar scales smooth, flat and subimbricate; digits long, slender, distinctly inflected joint with strong, slightly recurved claws; subdigital lamellae unnotched; lamellae beneath first phalanges wide; lamellae beneath phalanx immediately following inflection granular; lamellae of distal phalanges wide; lamellae beneath inflection large; interdigital webbing absent; enlarged submetatarsal scales on 1st toe present; total subdigital lamellae on fingers I–V: 18-21-22-24-23 (right manus), 18-21-22-24-23 (left manus); fingers increase in length from first to fourth with fifth nearly equal in length as fourth; relative length of fingers IV>V>III>II>I; total subdigital lamellae on toes I–V: 14-20-21-24-23 (right pes), 14-(broken)-21-24-23 (left pes); toes increase in length from first to fourth with fifth nearly equal in length as fourth; relative length of toes IV>V>III>II>I.

Tail complete, entire cylindrical, relatively slender, swollen at the base; tail length (TL) 52.2 mm; tail length longer than snout-vent length (TL/SVL 1.23); subcaudal scales keeled, juxtaposed, larger than dorsal scales of the tail; shallow, middorsal furrow; deeper lateral caudal furrow present; enlarged, transverse caudal tubercles arranged in segmented whorls, encircling tail; enlarged median subcaudal scale row present; caudal tubercles present between upper and lower of lateral furrow; 1R,L enlarged postcloacal tubercle at lateral surface of hemipenial swellings at the base of tail.

Measurements of holotype (in mm; Table 5). SVL 42.3; TL (complete tail) 52.2; TW 4.4; FL 6.5; TBL 7.9; AG 17.9; HL 11.5; HW 6.9; HD 4.5; ED 2.5; EE 3.3; ES 5.0; EN 4.0; EL 1.0; IN 1.1; IO 3.3.

Coloration in life (Figs 3, 4A). Dorsal ground color of head dark brown, top of head and snout bearing small, diffuse, finely speckled with yellowish spots; 3R,L



Figure 4. Coloration of *Cnemaspis samui* sp. nov. in dorsolateral view **A** adult male holotype ZMKU R 00974 **B** adult male paratype ZMKU R 00970 **C** adult male paratype ZMKU R 00971.

thin, and faint dark postorbital stripes extending from eye to nape; pupil black with orange streak; irregular, pale yellowish marking on nape; a single yellowish pre-capular crescent on shoulder each side, located at forelimb insertion dorsoanteriorly; dorsal ground color of body, limbs and tail brown overlain with black irregular blotches; two dark blotches form a bipartite pattern on nape; light-grey vertebral blotches extending from the nape to tail; flanks with scattered, incomplete light-grey to yellowish blotches becoming smaller posteriorly; tubercles on the whole body white or yellow; subconical spine-like yellowish tubercles on lower flanks; digits with dark brown and yellow bands; dorsum caudal bands light-grey and dark brown; ventral surfaces grayish-white intermixed with yellowish blotches on side of body; ventral pattern sexually dimorphic, gular, flanks, and caudal regions yellowish only in males; no dark markings on gular and belly; ventral side of caudal yellowish and indistinct bands.

Characters/ Museum Number	ZMKU R 00974	ZMKU R 00966	ZMKU R 00967	ZMKU R 00968	ZMKU R 00969	ZMKU R 00970	ZMKU R 00971	ZMKU R 00972	ZMKU R 00973	ZMKU R 00975	ZMKU R 00976	ZMKU R 00977	ZMKU R 00978	ZMKU R 00979	ZMKU R 00983	ZMKU R 00980	ZMKU R 00981	ZMKU R 00982
Ventral scales on thigh keeled (1) or smooth (0)	1	1	1	1	1	1	1	1	1	1	1	1	1	1	1	1	1	1
Subcaudal keeled (1) or smooth (0)	1	1	1	1	1	1	1	1	1	1	1	1	1	1	1	1	1	1
Subtibial scales keeled (1) or smooth (0)	1	1	1	1	1	1	1	1	1	1	1	1	1	1	1	1	1	1
Enlarged median subcaudal scale row (1) or not (0)	1	1	1	1	1	1	1	1	1	1	1	1	1	1	1	1	1	1
Caudal tubercles restricted to the single paravertebral row on each side (1) or not (0)	1	1	1	1	1	1	1	1	1	1	1	1	1	1	1	1	1	1

Coloration in preservative (Figs 5, 6). Dorsal ground color of head, body, limbs and tail darker brown than coloration in life; indistinct, irregular vertebral blotches; all yellowish spots and markings on head, body, limbs, and tail faded to whitish gray; banding on the tail faded and less prominent; ventral surface whitish gray with indistinct darker marking; gular, pectoral and tail regions with faint dark blotches.

Variation and additional information. Most paratypes closely resemble the holotype in all aspect of pattern and coloration. Morphometric and meristic variation within the type series is presented in Table 5. Some paratypes differ in their degree of vertebral blotches. Sexual dimorphism in color pattern was apparent, as all adult male paratypes have yellowish coloration in the gular, flanks and caudal regions but this yellowish coloration was absent in females. ZMKU R 00968, ZMKU R 00971, ZMKU R 00973 (three adult males), and ZMKU R 00981–00982 (two adult females) have regenerated tails of uniform tan coloration. ZMKU R 00969 and ZMKU R 00975 (two adult males) have broken tail tips. ZMKU R 00976 (one adult male) has approximately three-fourth of the tail broken. ZMKU R 00966–00969, ZMKU R 00971, ZMKU R 00977, ZMKU R 00980, and ZMKU R 00983 (eight adult males) have paler dorsal markings that more resemble transverse bands than paravertebral blotches. ZMKU R 00969 and ZMKU R 00983 (two adult males) have 2R, 1L enlarged post-cloacal tubercles on the lateral surface of the hemipenial swelling at the base of tail.

Distribution. *Cnemaspis samui* sp. nov. is currently only known from the type locality at Hin Lad Waterfall (9°31.151'N, 99°57.598'E; 150 m a.s.l.; Fig. 7), Ang

Thong Subdistrict, Ko Samui District, Surat Thani Province, Thailand, approximately 35 km off the mainland of Don Sak District, Surat Thani Province in the Gulf of Thailand.

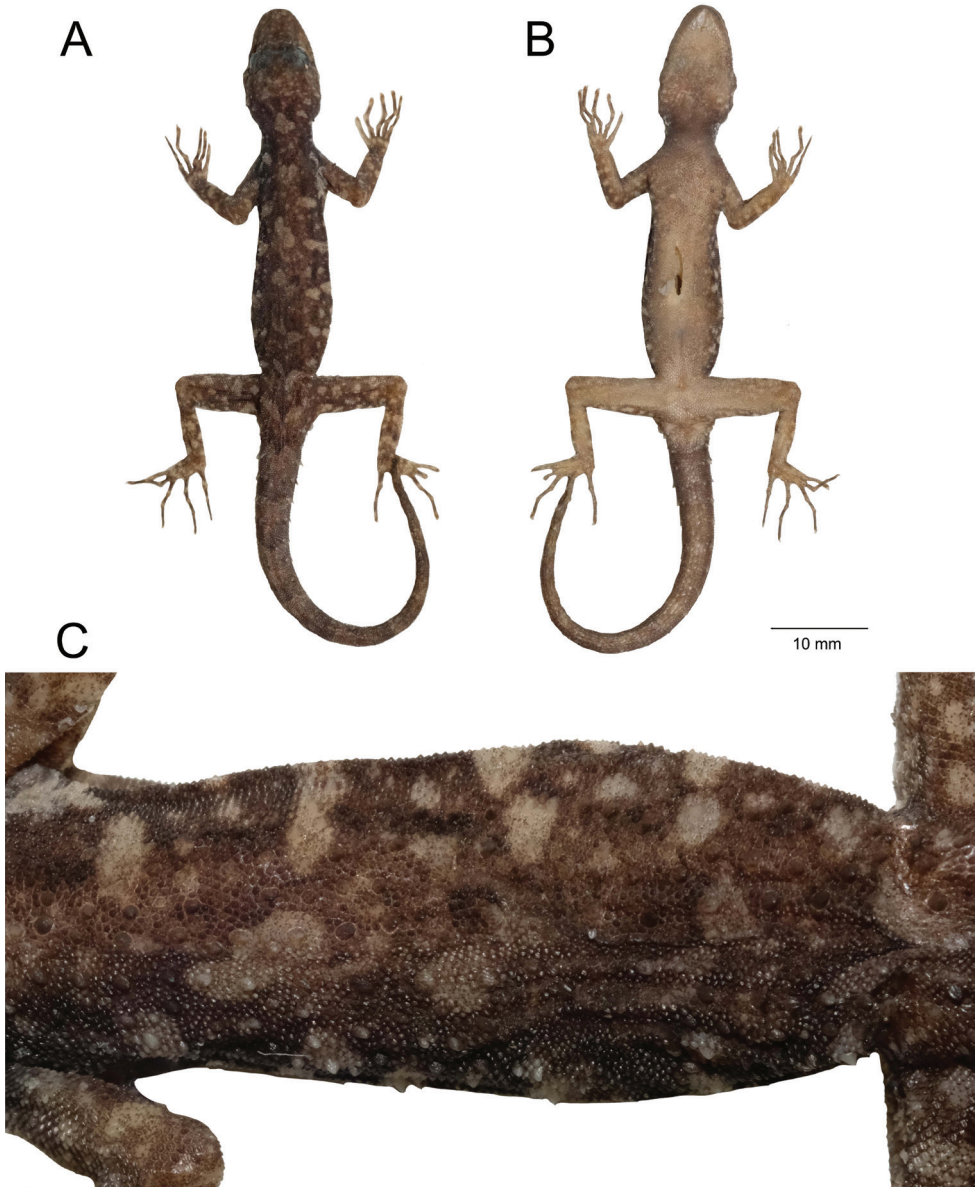


Figure 5. Adult male holotype of *Cnemaspis samui* sp. nov. (ZMKU R 00974) from Hin Lad Waterfall, Ko Samui, Ang Thong Subdistrict, Ko Samui District, Surat Thani Province, Thailand, in preservative. **A** dorsal view **B** ventral view **C** dorsal view of trunk. Scale bar in dorsal, and ventral views: 10 mm.

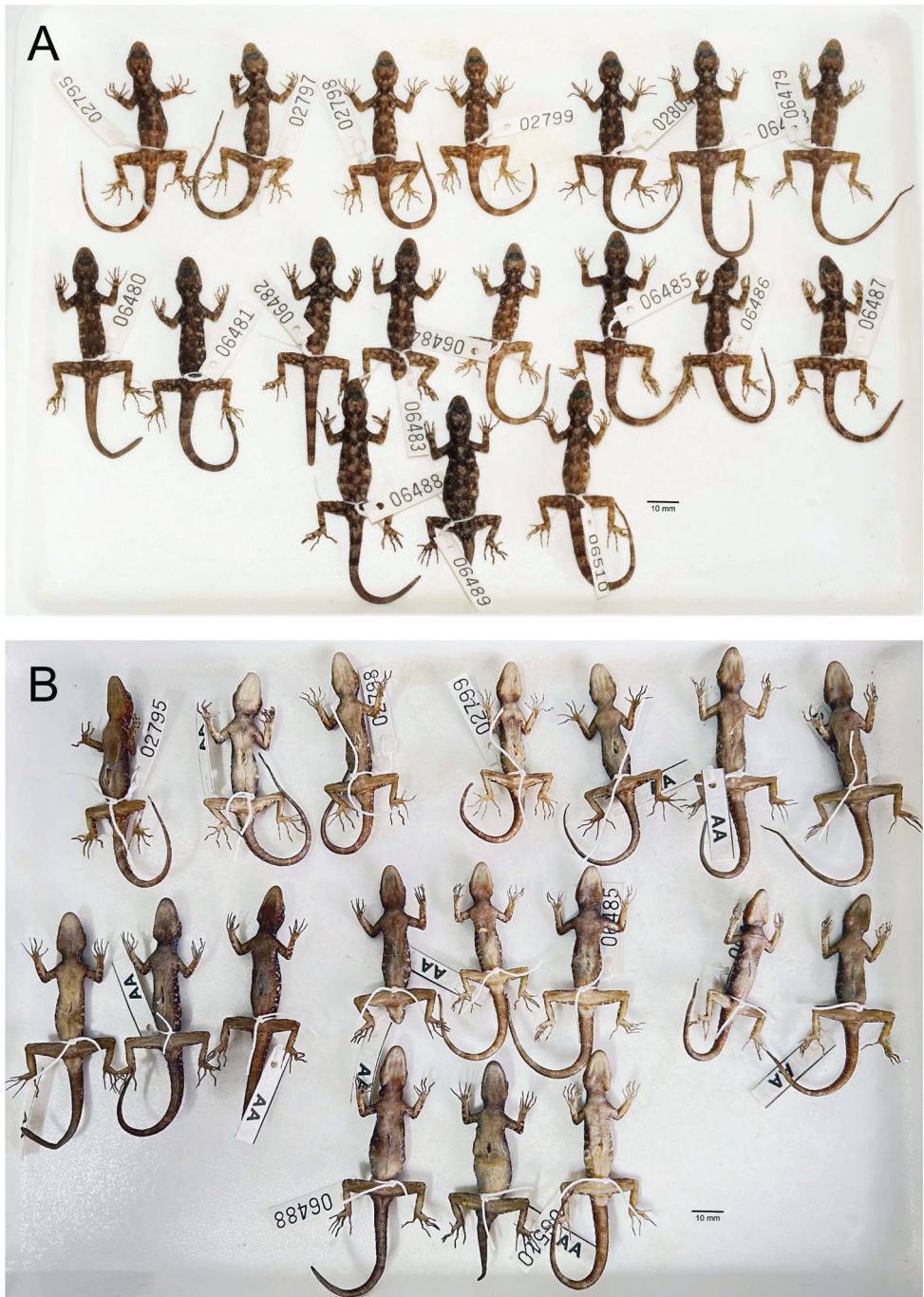


Figure 6. Paratypes of *Cnemaspis samui* sp. nov. in preservative. **A** dorsal view **B** ventral view; from left to right, top panel: ZMKU R 00966–00972; middle panel: ZMKU R 00973–00980; bottom panel: ZMKU R 00981–00983. Scale bars in dorsal and ventral views: 10 mm.

Natural history. The type locality is surrounded by lowland evergreen forest with granitic rocky outcrops along Lipa Yai Canal in the western part of Ko Samui. All specimens of *C. samui* sp. nov. were found along rocky stream outcrops of Hin Lad Waterfall during the day (1435–1752 h) and night (1800–1845 h) with air temperatures of 26.2–30.1 °C and relative humidity of 76.9–92.7%. Their microhabitats in rocky boulders were relatively dry and cool. The male holotype was found at night (1845 h) perched upside down on an overhanging surface of a granitic rock boulder near a stream. Most specimens were found on or within deep cracks or crevices of boulders, or in shaded areas of the boulder near a stream, except that ZMKU R 00969 was found on a tree trunk and ZMKU R 00977 was found in a soil hole at the base of a boulder. Two gravid females ZMKU R 00981–00982 were carrying one or two eggs in July 2018. Some juveniles (not collected) were mostly found perched on vegetation (e.g., log, vine, tree root). *Cnemaspis samui* sp. nov. is assumed to be a diurnal rock-dwelling species. During the day, geckos were found to be active, wary and fast-moving. They were most often observed clinging upside down to the undersides of rock boulders and within deep crevices. When disturbed, they would quickly move to deeper cover and hide in the shaded area between boulder and the ground. At night, they were found to be inactive, slow moving, sheltered in crevices or cracks on rock walls, or sleeping on vegetation near rock boulders, making them easier to approach than during the day. During field surveys, the larger nocturnal gekkonid *Cyrtodactylus zebraicus* (Taylor, 1962) was found in sympatry on the ground and vegetation near a stream.

Etymology. The specific epithet *samui* is a noun in apposition and refers to the type locality of Ko Samui.

Comparisons. *Cnemaspis samui* sp. nov. is distinguished from all members of the *siamensis* group (*C. adangrawi*, *C. chanardi*, *C. huaseesom*, *C. kamolnorrnanathi*, *C. lineatubercularis*, *C. omari*, *C. phangngaensis*, *C. punctatonuchalis*, *C. selenolagus*, *C. siamensis*, *C. thachanaensis*, and *C. vandeventeri*) by having a unique combination of morphological characteristics (Table 6) and uncorrected pairwise sequence divergences of mtDNA (ND2) of 8.86–26.83% (Table 2).

Cnemaspis samui sp. nov. is distinguished from *C. adangrawi* Ampai et al. 2019 by having maximum SVL of 42.3 mm (vs. 44.9 mm); eight or nine supralabial scales (vs. 10 scales); tubercles on lower flanks present (vs. absent); 22–25 lamellae under 4th toe (vs. 26–28 lamellae); enlarged median row of subcaudal scales present (vs. absent); and yellow coloration in the subcaudal region present (vs. absent).

Cnemaspis samui sp. nov. is distinguished from *C. chanardi* Grismer et al. 2010 by having maximum SVL 42.3 mm (vs. 40.9 mm); 22–25 lamellae under 4th toe (vs. 26–29 lamellae); single median row of subcaudals keeled (vs. smooth); and ventrolateral caudal tubercles anteriorly present (vs. absent).

Cnemaspis samui sp. nov. is distinguished from *C. huaseesom* Grismer et al. 2010 by having maximum SVL of 42.3 mm (vs. 43.5 mm); pore-bearing precloacal scales row separated (vs. continuous); 25–27 paravertebral tubercles (vs. 18–24 tubercles); ventral and subcaudal scales keeled (vs. smooth); single median row of subcaudals keeled (vs. smooth); enlarged median row of subcaudal scales present (vs. absent); ventrolateral caudal tubercles anteriorly present (vs. absent); and subtibial scales keeled (vs. smooth).

Table 6. Meristic character state and color pattern of species in the *Cnemaspis siamensis* group. SVL taken in millimeters and measurement abbreviations are defined in the text. – = data unavailable, w = weak.

Characters / Species	<i>Cnemaspis samui</i> sp. nov.	<i>Cnemaspis similan</i> sp. nov.	<i>C. adangravi</i>	<i>C. ebanardi</i>	<i>C. huaseeom</i>	<i>C. kamohorruathai</i>	<i>C. lineatubercularis</i>	<i>C. onari</i>	<i>C. phangngaensis</i>	<i>C. punctatomuchalis</i>	<i>C. selenolagus</i>	<i>C. siamensis</i>	<i>C. thachanaensis</i>	<i>C. vandeventeri</i>
Sample size	18	4	15	25	5	4	19	8	2	5	2	12	6	3
Maximum SVL	42.3	48.1	44.9	40.9	43.5	37.8	41.8	41.3	42.0	49.6	36.2	39.7	39.0	44.7
Supralabial scales	8 or 9	8 or 9	10	8–10	7–10	8 or 9	9	8 or 9	10	8	10 or 11	8 or 9	10 or 11	8 or 9
Infralabial scales	8 or 9	7 or 8	9	8	6–9	7 or 8	9	7 or 8	10	7 or 8	10	6–8	9–11	7–9
No. of pore-bearing precloacal scales	5–8	1	6–8	6–8	5–8	6 or 7	4–7	3–6	4	0	6 or 7	0	0	4
Pore-bearing precloacal scales row continuous (1) or separated (0)	0	–	0	0	1	1	0	0	1	–	1	–	–	0
Pore-bearing precloacal scales elongate (1) or round (0) shapes	0	0	0	0	0	1	0	0	0	–	1	–	–	0
No. of paravertebral tubercles	25–27	24 or 25	23–25	22–25	18–24	19–24	19–21	22–29	22	24–27	16–18	19–25	15–19	25–29
Paravertebral tubercles linearly arranged (1) or more random (0)	0	0	0	0	w or 0	w	1	w or 0	1	w	0	0	1	0
Tubercles present (1) or absent (0) on lower flanks	1	1	0	1	1	1	1	w or 1	0	1	0	1	1	1
No. of 4 th toe lamellae	22–25	23 or 24	26–28	26–29	21–31	24–28	27–29	25–28	29	29–31	22	24–26	24	24–28
Ventral scales keeled (1) or smooth (0)	1	1	1	1	0	w or 0	1	1	1	0	0	1	1	1
Subcaudal scales keeled (1) or smooth (0)	1	1	1	1	0	1	1	1	1	0	0	1	1	1
Single median row of keeled subcaudals (1) or smooth (0) scales	1	1	1	0	0	w	1	0	1	0	–	0	1	w
Enlarged median subcaudal scales row (1) or not (0)	1	0	0	1	0	w	0	0	0	1	0	1	0	1
Caudal tubercles restricted to a single paravertebral row on each side (1) or not (0)	0	0	0	0	0	0	1	0	1	0	–	0	1	0
Ventrolateral caudal tubercles anteriorly present (1) or not (0)	1	1	1	0	0	0	1	0	1	1	0	0	1	0
No. of postcloacal tubercles in males	1 or 2	2	1	1	1 or 2	1 or 2	1	1	2	1–3	2	1 or 2	0	1–3
Subtibial scales keeled (1) or smooth (0)	1	1	1	1	0	0 or 1	1	1	1	1	0	1	1	1
Yellow coloration in the subcaudal region present (1) or not (0)	1	0	0	1	1	0	1	1	1	0	0	0	0	0
Ventral pattern sexually dimorphic present (1) or not (0)	1	1	1	1	1	0	1	1	1	1	–	1	1	1

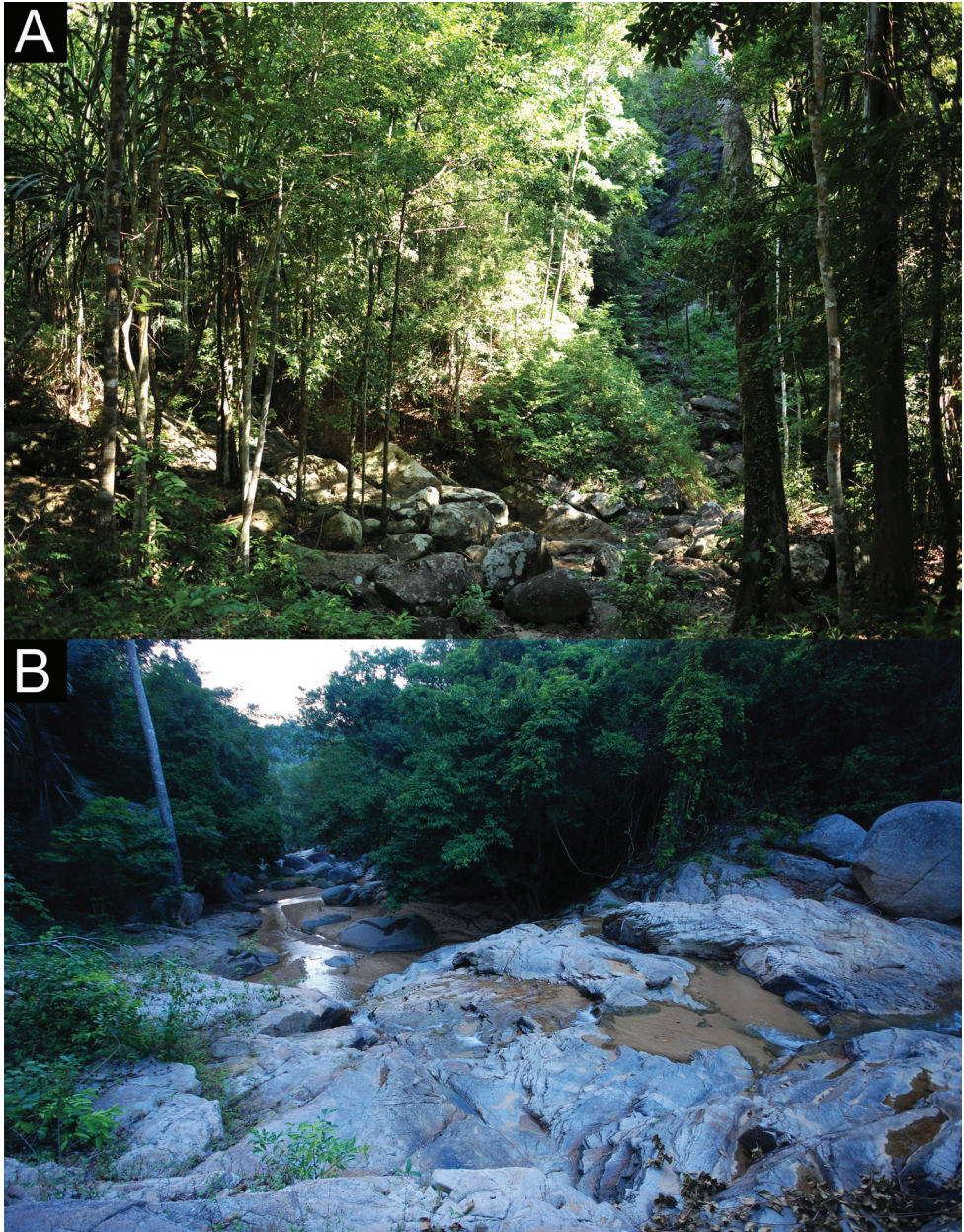


Figure 7. Habitats of *Cnemaspis samui* sp. nov. at the type locality **A** lowland evergreen forest with granitic outcrops **B** rocky stream outcrops along Lipa Yai Canal of Hin Lad Waterfall, Ko Samui, Ang Thong Subdistrict, Ko Samui District, Surat Thani Province, Thailand.

Cnemaspis samui sp. nov. is distinguished from *C. kamolnorrnanathi* Grismer et al. 2010 by having maximum SVL 42.3 mm (vs. 37.8 mm); pore-bearing precloacal scales row separated (vs. continuous); pore-bearing precloacal scales rounded (vs. elongated); 25–27 paravertebral tubercles (vs. 19–24 tubercles); enlarged median subcaudal scale

row present (vs. absent); ventrolateral caudal tubercles anteriorly present (vs. absent); yellow coloration in the subcaudal region present (vs. absent); and ventral pattern sexually dimorphism present (vs. absent).

Cnemaspis samui sp. nov. is distinguished from *C. lineatubercularis* Ampai et al. 2020 by having maximum SVL 42.3 mm (vs. 41.8 mm); 25–27 paravertebral tubercles (vs. 19–21 tubercles); paravertebral tubercles randomly arranged (vs. linearly arranged); 22–25 lamellae under 4th toe (vs. 27–29 lamellae); enlarged median row of subcaudal scales present (vs. absent); and caudal tubercles restricted to a single paravertebral row on each side absent (vs. present).

Cnemaspis samui sp. nov. is distinguished from *C. omari* Grismer et al. 2014 by having maximum SVL 42.3 mm (vs. 41.3 mm); single median row of subcaudals keeled (vs. smooth); enlarged median row of subcaudal scales present (vs. absent); and ventrolateral caudal tubercles anteriorly present (vs. absent).

Cnemaspis samui sp. nov. is distinguished from *C. phangngaensis* Wood et al. 2017 by having eight or nine supralabial scales (vs. 10 scales); eight or nine infralabial scales (vs. 10 scales); 5–8 pore-bearing precloacal scales in males (vs. four scales); pore-bearing precloacal scales row separated (vs. continuous); 25–27 paravertebral tubercles (vs. 22 tubercles); paravertebral tubercles randomly arranged (vs. linearly arranged); tubercles on lower flanks present (vs. absent); 22–25 lamellae under 4th toe (vs. 29 lamellae); enlarged median row of subcaudal scales present (vs. absent); and caudal tubercles restricted to a single paravertebral row on each side absent (vs. present).

Cnemaspis samui sp. nov. is distinguished from *C. punctatonuchalis* Grismer et al. 2010 by having maximum SVL of 42.3 mm (vs. 49.6 mm); pore-bearing precloacal scales present (vs. absent); 22–25 lamellae under 4th toe (vs. 29–31 lamellae); ventral and subcaudal scales keeled (vs. smooth); single median row of subcaudals keeled (vs. smooth); and yellow coloration in the subcaudal region present (vs. absent).

Cnemaspis samui sp. nov. is distinguished from *C. selenolagus* Grismer et al. 2020 by having maximum SVL 42.3 mm (vs. 36.2 mm); eight or nine supralabial scales (vs. 10 or 11 scales); eight or nine infralabial scales (vs. 10 scales); pore-bearing precloacal scales row separated (vs. continuous); pore-bearing precloacal scales shape rounded (vs. elongated); 25–27 paravertebral tubercles (vs. 16–18 tubercles); tubercles on lower flanks present (vs. absent); enlarged median row of subcaudal scales present (vs. absent); ventrolateral caudal tubercles anteriorly present (vs. absent); subtibial scales keeled (vs. smooth); and yellow coloration in the subcaudal region present (vs. absent).

Cnemaspis samui sp. nov. is distinguished from *C. siamensis* (Smith, 1925) by having maximum SVL 42.3 mm (vs. 39.7 mm); pore-bearing precloacal scales present (vs. absent); single median row of subcaudals keeled (vs. smooth); ventrolateral caudal tubercles anteriorly present (vs. absent); and yellow coloration in the subcaudal region present (vs. absent).

Cnemaspis samui sp. nov. is distinguished from *C. thachanaensis* Wood et al. 2017 by having maximum SVL 42.3 mm (vs. 39.0 mm); eight or nine supralabial scales (vs. 10 or 11 scales); pore-bearing precloacal scales present (vs. absent); 25–27 paravertebral tubercles (vs. 15–19 tubercles); paravertebral tubercles randomly arranged (vs. linearly arranged); enlarged median row of subcaudal scales present (vs. absent); caudal

tubercles restricted to a single paravertebral row on each side absent (vs. present); one or two postcloacal tubercles in males (vs. absent); and yellow coloration in the subcaudal region present (vs. absent).

Cnemaspis samui sp. nov. is distinguished from *C. vandeventeri* Grismer et al. 2010 by having maximum SVL of 42.3 mm (vs. 44.7 mm); 5–8 pore-bearing precloacal scales (vs. four scales); ventrolateral caudal tubercles anteriorly present (vs. absent); and having yellow coloration in the subcaudal region present (vs. absent).

***Cnemaspis similan* sp. nov.**

<https://zoobank.org/AF6821E3-D520-40D3-A076-EA96CFCAB6E3>

Figs 8–11

Ko Similan Rock Gecko

Thai common name: Jing Jok Niew Yaow Ko Similan (จิ้งจกนิ้วยาวเกาะลิ้มลิ้น)

Holotype (Fig. 8). ZMKU R 00984, adult male from Thailand, Phang-nga Province, Thai Mueang District, Lam Kaen Subdistrict, Mu Ko Similan National Park, Ko Similan, Ao Nguang Chang Bay (8°64.840'N, 97°64.834'E; 13 m a.s.l.), collected on 5 March 2018 by Natee Ampai, Attapol Rujirawan, Siriporn Yodthong and Piyawan Puanprapai.

Paratypes (Fig. 9). Three adult females paratypes. ZMKU R 00985–00986 (two adult females), same data as holotype. ZMKU R 00987 (one adult female), same data as holotype except collected on 6 March 2018 by Natee Ampai, Attapol Rujirawan, Siriporn Yodthong and Piyawan Puanprapai.

Diagnosis. *Cnemaspis similan* sp. nov. can be distinguished from all other members of the *C. siamensis* group by having the following combination of characters: (1) SVL of 47.6 mm in adult male and 38.6–48.1 mm (mean 43.6 ± 4.8 mm, $N = 3$) in adult females; (2) eight or nine supralabial and seven or eight infralabial scales; (3) ventral scales keeled (4) one pore-bearing precloacal scale, pore rounded in male; (5) 24 or 25 paravertebral tubercles, arranged randomly; (6) five small, elongated, spine-like tubercles on lower flanks; (7) 23 or 24 subdigital lamellae under the 4th toe; (8) no enlarged median subcaudal scale row; (9) ventrolateral caudal tubercles anteriorly present; (10) two postcloacal tubercles on lateral surface of hemipenial swellings at tail base in male; (11) sexual dimorphism in dorsal and ventral patterns; and (12) pale yellow reticulum on head, neck, flanks, belly and limbs only in male.

Description of holotype. An adult male in good state of preservation; 47.6 mm SVL; head moderate in size (HL/SVL 0.26), narrow (HW/SVL 0.16), flattened (HD/HL 0.39) and head distinct from neck; snout moderate (ES/HL 0.43), in lateral profile concave; loreal region marginally inflated, canthus rostralis nearly absent; postnasal region concave medially; scales of rostrum smooth, raised, larger than conical scales on occiput; weak and faint supraorbital ridges; gular scales granular, keeled, rounded, juxtaposed; throat scales granular, keeled, flat, subimbricate; shallow frontonasal sulcus; eye large (ED/HL 0.19); pupil round; extra-brillar fringe scales small in general but slightly larger anteriorly; scales on interorbitals and supercilium keeled; eye to ear distance great-

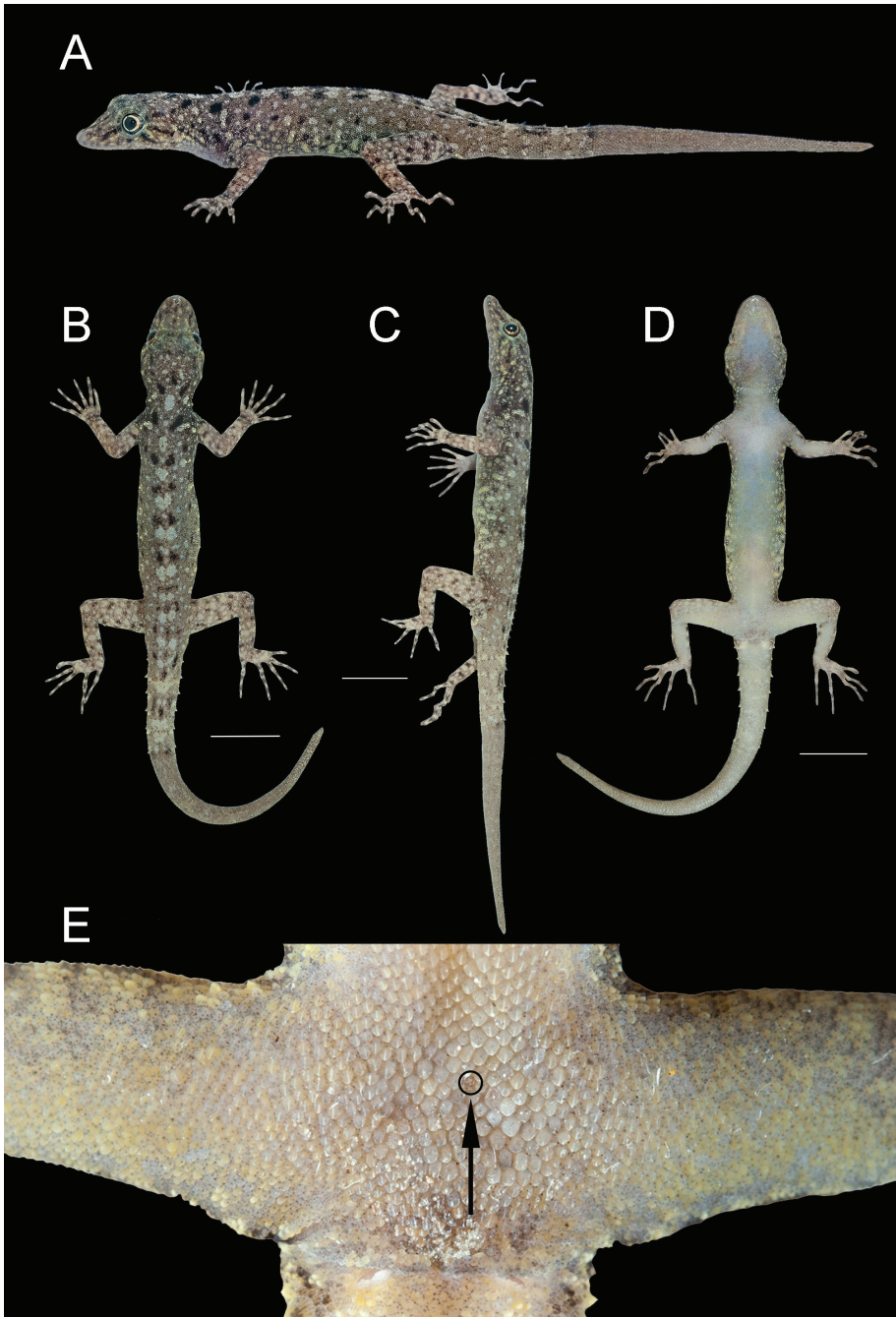


Figure 8. Adult male holotype of *Cnemaspis similan* sp. nov. (ZMKU R 00984) from Ao Nguang Chang Bay, Ko Similan, Mu Ko Similan National Park, Lam Kaen Subdistrict, Thai Mueang District, Phang-nga Province, Thailand, in life **A** dorsolateral view **B** dorsal view **C** lateral view **D** ventral view **E** preloocal region showing distribution of pore-bearing scale (black arrow). Scale bars in dorsal, lateral, and ventral views: 10 mm.

er than eyes diameter (EE/ED 1.50); ear opening elongate, much taller than wide (EL/HL 0.08); rostral concave dorsally; rostral bordered posteriorly by supranasals and laterally by first supralabials; 8R,L supralabials decreasing in size posteriorly; 7R,L infralabials decreasing in size posteriorly; nostril small, elliptical, oriented dorsoposteriorly, bordered posteriorly by small postnasal scales; mental scales large, triangular, flat, extending to level of second infralabial scales, bordered posteriorly by three large postmental scales.

Body robust, not elongate (AG/SVL 0.41); small, raised, keeled, dorsal scales equal in size throughout body intermixed with numerous large, keeled, multicarinate tubercles; 24 paravertebral tubercles randomly arranged; five small, elongated, spine-like tubercles on flanks; tubercles present on lower flanks; tubercles extend from occiput to tail; pectoral and abdominal scales keeled, round, flat, imbricate; abdominal scales larger than pectoral and dorsal scales; ventral scales of brachia smooth, raised and juxtaposed; one pore-bearing precloacal scale, with rounded pore; precloacal depression absent; femoral pores absent.

Fore and hind limbs moderately long, slender; scales beneath forearm slightly raised, smooth and subimbricate; subtibial scales keeled; palmar scales keeled, flat and subimbricate; digits long, slender with inflected joint; claws slightly recurved; subdigital lamellae unnotched; lamellae beneath first phalanges wide; lamellae beneath phalanx immediately following inflection granular; lamellae of distal phalanges wide; lamellae beneath inflection large; interdigital webbing generally absent; enlarged submetatarsal scales on 1st toe present; total subdigital lamellae on fingers I–V: 15-21-22-24-23 (right manus), 15-21-23-24-23 (left manus); fingers increase in length from first to fourth with fifth nearly equal in length as fourth; relative length of fingers IV>V>III>II>I; total subdigital lamellae on toes I–V: 17-20-22-24-23 (right pes), 17-19-22-24-23 (left pes); toes increase in length from first to fourth with fifth nearly equal in length as fourth; relative length of toes IV>V>III>II>I.

Tail regenerated, subcylindrical, relatively swollen at the base; tail length (TL) 49.6 mm; tail length longer than head and body (TL/SVL 1.04); dorsal and ventral scales at the tail base similar in size on mid-body dorsum; subcaudal scales keeled, juxtaposed, larger than dorsal scale of the tail size; shallow, middorsal furrow; lateral caudal furrow present; enlarged, transverse caudal tubercles arranged in segmented whorls, encircling tail; enlarged median subcaudal scale row absent; caudal tubercles present between upper and lower of lateral furrow; rest of the tail regenerated, slightly keeled, imbricate scales with no enlarged tubercles; scales on ventral aspect of the regenerated tail marginally larger in size than mid-body ventrals; 2R,L enlarge postcloacal tubercle at lateral surface of hemipenial swellings at the tail base.

Measurements of holotype (in mm; Table 7). SVL 47.6; TL (regenerated tail) 49.6; TW 4.6; FL 6.8; TBL 8.6; AG 19.6; HL 12.4; HW 7.8; HD 4.8; ED 2.4; EE 3.6; ES 5.3; EN 4.0; EL 1.0; IN 1.1; IO 3.1.

Coloration in life (Figs 8, 9). Dorsal ground color of head brown, top of head and snout bearing diffuse, mottled with smaller yellowish markings; 3R,L vertical, thin and fine dark stripes extending from postorbital to neck; 1R,L indistinct darker stripes runs from preorbital to supranasal; pupil black with orange streak; irregular,

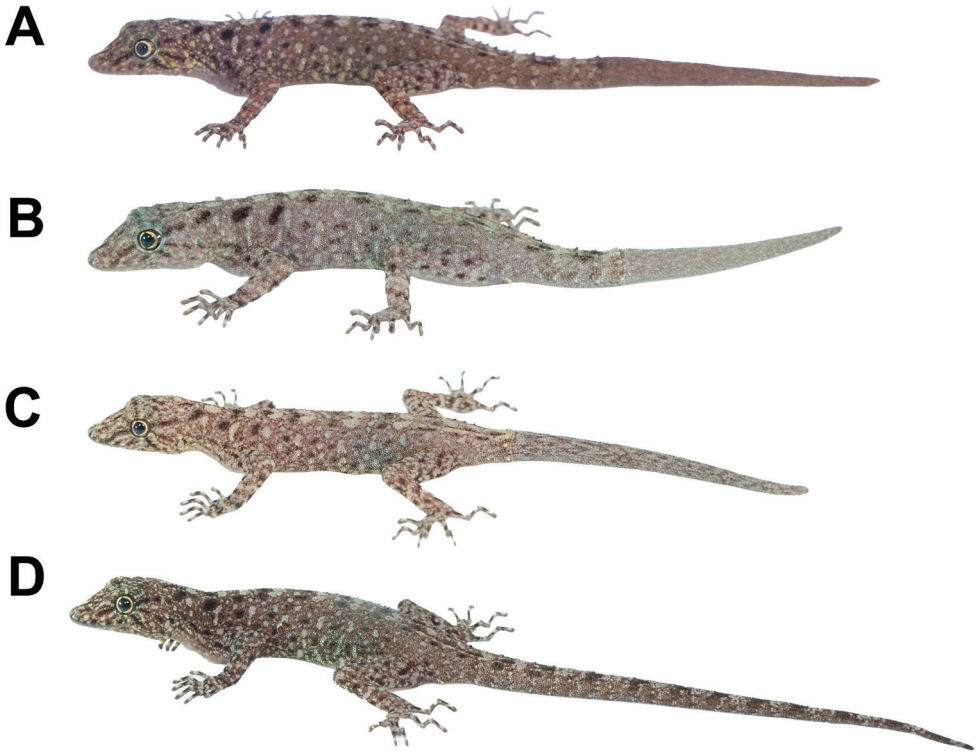


Figure 9. Coloration of adult *Cnemaspis similan* sp. nov. in dorsolateral view **A** adult male holotype ZMKU R 00986 **B** adult female paratype ZMKU R 00985 **C** adult female paratype ZMKU R 00986 **D** adult female paratype ZMKU R 00987.

faint pale yellow reticulum on lateral surface of head, neck and flanks; 1R,L light-colored prescapular crescent on shoulder, located at forelimb insertion dorsoanteriorly; two dark streaks form a bipartite pattern on neck; dorsal ground color of body and tail brown with irregular black blotches except much paler brown on limbs; pale sage vertebral blotches run from the nape to tail; flanks with smaller dark and larger pale yellow streaks; enlarged conical spine-like yellowish tubercles on lower flanks; tubercles on the whole body pale sage and pale yellow; digits with distinct dark and pale bands; dorsum of limbs pale brown with dark blotches randomly arranged; ventral surfaces pale greyish intermixed with pale yellowish blotches on gular, neck, limbs and belly; no markings on gular and belly regions; original part of the tail brown with dark streaks form a bipartite pattern; regenerated part of the tail brown without bands; ventral side of tail pale greyish with no markings.

Coloration in preservative (Figs 10, 11). Overall coloration of head, body, limbs, flanks and tail about the same as in life. Dorsal ground color of the whole-body became faded. The pale tones of limbs and tail darker than in life. Vertebral blotches run from the nape to tail became paler than in life. All pale yellowish coloration on head, limbs, flanks fade to creamy white. Ventral region of the whole-body homogeneously tan colored.

Variation and additional information. Due to having only a single adult male ($N = 1$), variation in adult males is currently unknown. Most paratypes approximate the holotype in general features of body pattern and coloration. Adult females lack pore-bearing precloacal scale. Pale yellowish markings in head, neck, limbs, flanks and caudal regions were also absent in adult females. Three adult females have paler dorsal markings than the holotype. ZMKU R 00985 and ZMKU R 00986 have regenerated tails of uniform tan colored. ZMKU R 00985 has a large calcium sac on each side of the neck. ZMKU R 00985 has also broken left 4th pes.

Distribution. *Cnemaspis similan* sp. nov. is known only from the type locality at Ao Nguang Chang Bay (8°64.840'N, 97°64.834'E; 13 m a.s.l.; Fig. 12), Ko Similan, Lam Kaen Subdistrict, Thai Mueang District, Phang-nga Province, Thailand, approximately 65 km off the mainland of Thai Mueang District, Phang-nga Province in the Andaman Sea.

Natural history. The type locality is dominated by mixed evergreen forest with shrub and beach forests. Ao Nguang Chang Bay is located at the southern part of the largest island, Ko Similan (= Ko Pad). All specimens of *C. similan* sp. nov. were found in granitic rocky outcrops near Ao Nguang Chang Bay during the day (1542 h) and night (2023–2049 h) with an air temperature of 28.4 °C and relative humidity of 86%. Granitic boulder surfaces appeared to be relatively dry and cool. The male holotype was found during the night (2023 h) on a tree near a boulder. Most paratypes (ZMKU R 00985–00986) were found during the day time on vegetation (tree trunks, roots, or vines) except ZMKU R 00987, which was perched on a rock wall. *Cnemaspis similan* sp. nov. seems to be a diurnal rock-dwelling species. During the day, geckos were generally active, quite wary and quickly retreated when approached or disturbed. At night, geckos were found inactive or sleeping on vegetation near crevices or cracks of rock boulder as high as 2 m above the ground. They were often found clinging upside down to the underside of rock boulder overhang. During field surveys, the larger, nocturnal gekkonid *Cyrtodactylus oldhami* (Theobald, 1876) was found in sympatry on the ground and vegetation near boulders.

Etymology. The specific epithet *similan* is a noun in apposition and refers to the type locality of Ko Similan.

Comparisons. *Cnemaspis similan* sp. nov. can be distinguished from 13 congeners of the *siamensis* group (*C. adangrawi*, *C. chanardi*, *C. huaseesom*, *C. kamolnorrnanathi*, *C. lineatubercularis*, *C. omari*, *C. phangngaensis*, *C. punctatonuchalis*, *C. samui* sp. nov., *C. selenolagus*, *C. siamensis*, *C. thachanaensis*, and *C. vandeventeri*) by having a unique combination of morphological characters (Table 6) and uncorrected pairwise sequence divergences in mtDNA (ND2) of 8.16–27.11% (Table 2).

Cnemaspis similan sp. nov. is distinguished from *C. adangrawi* Ampai et al. 2019 by having maximum SVL 48.1 mm (vs. 44.9 mm); seven or eight infralabial scales (vs. nine scales); one pore-bearing precloacal scale (vs. 6–8 scales); eight or nine supralabial scales (vs. 10 scales); tubercles on lower flanks present (vs. absent); 23 or 24 lamellae under 4th toe (vs. 26–28 lamellae); and two postcloacal tubercles in males (vs. one tubercle).

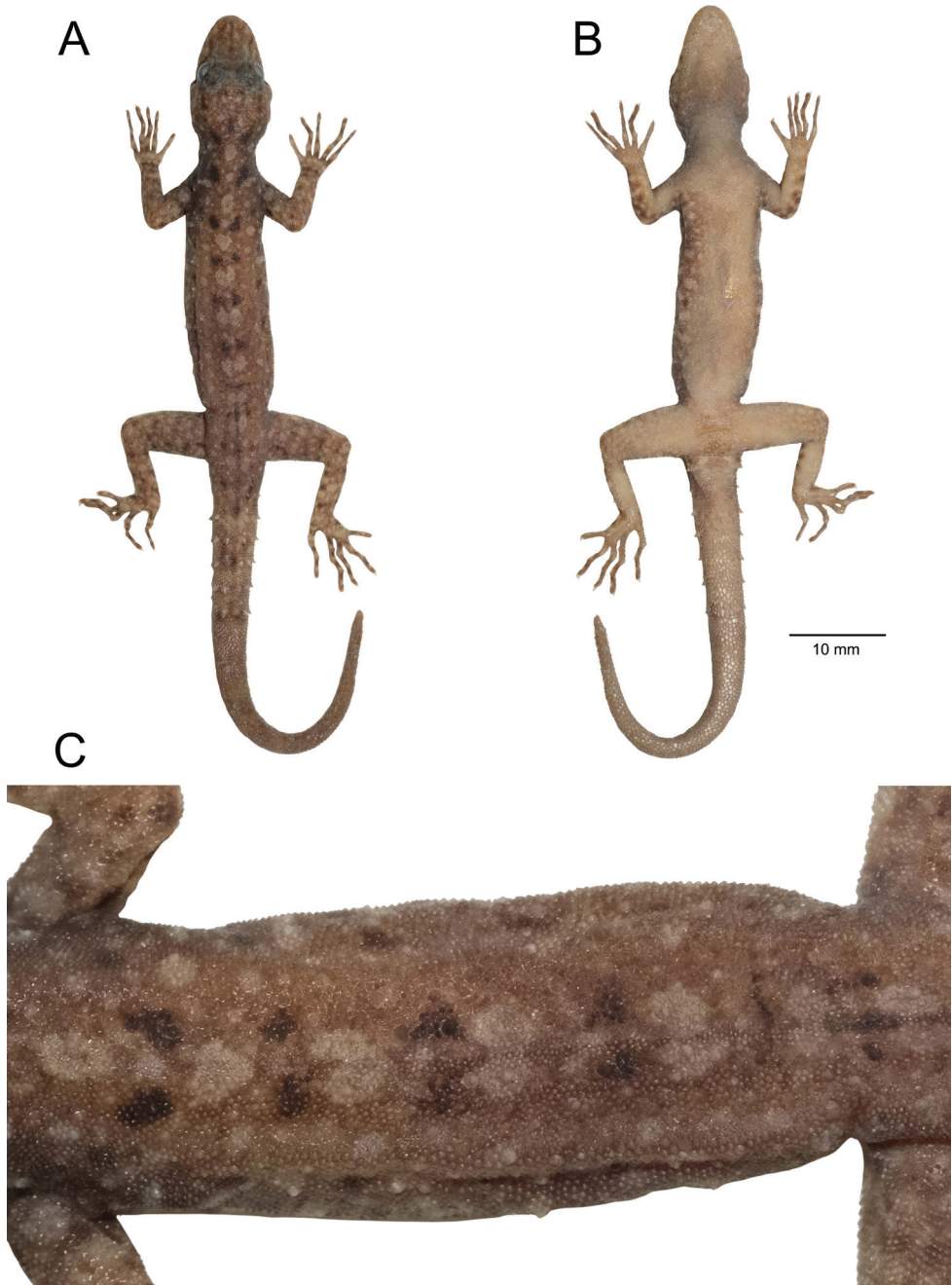


Figure 10. Adult male holotype of *Cnemaspis similan* sp. nov. (ZMKU R 00984) from Ao Nguang Chang Bay, Ko Similan, Mu Ko Similan National Park, Lam Kaen Subdistrict, Thai Mueang District, Phang-nga Province, Thailand, in preservative **A** dorsal view **B** ventral view **C** dorsal view of trunk. Scale bar in dorsal and ventral views: 10 mm.

Cnemaspis similan sp. nov. is distinguished from *C. chanardi* Grismer et al. 2010 by having maximum SVL 48.1 mm (vs. 40.9 mm); one pore-bearing precloacal scale (vs. 6–8 scales); 23 or 24 lamellae under 4th toe (vs. 26–29 lamellae); single median row of subcaudal keeled (vs. smooth); enlarged median subcaudal scales row absent (vs. present); ventrolateral caudal tubercles anteriorly present (vs. absent); two postcloacal tubercles in males (vs. one tubercle); and yellow coloration in the subcaudal region absent (vs. present).

Cnemaspis similan sp. nov. is distinguished from *C. huaseesom* Grismer et al. 2010 by having maximum SVL 48.1 mm (vs. 43.5 mm); one pore-bearing precloacal scale (vs. 5–8 scales); ventral and subcaudal scales keeled (vs. smooth); single median row of subcaudal keeled (vs. smooth); ventrolateral caudal tubercles anteriorly present (vs. absent); subtibial scales keeled (vs. smooth); yellow coloration in the subcaudal region absent (vs. present); and yellow coloration in the subcaudal region absent (vs. present).

Cnemaspis similan sp. nov. is distinguished from *C. kamolnorrnanathi* Grismer et al. 2010 by having maximum SVL 48.1 mm (vs. 37.8 mm); one pore-bearing precloacal scale (vs. six or seven scales); pore-bearing precloacal scale row absent (vs. continuous); pore-bearing precloacal scale rounded (vs. elongated); ventrolateral caudal tubercles anteriorly present (vs. absent); and ventral pattern sexually dimorphic present (vs. absent).

Cnemaspis similan sp. nov. is distinguished from *C. lineatubercularis* Ampai et al. 2020 by having maximum SVL 48.1 mm (vs. 41.8 mm); seven or eight infralabial scales (vs. nine scales); one pore-bearing precloacal scale (vs. 4–7 scales); 24 or 25 paravertebral tubercles (vs. 19–21 tubercles); paravertebral tubercles randomly arranged (vs. linearly arranged); 23 or 24 lamellae under 4th toe (vs. 27–29 lamellae); caudal tubercles restricted to a single paravertebral row on each side absent (vs. present); two postcloacal tubercles in males (vs. one tubercle); and yellow coloration in the subcaudal region absent (vs. present).

Cnemaspis similan sp. nov. is distinguished from *C. omari* Grismer et al. 2014 by having maximum SVL 48.1 mm (vs. 41.3 mm); one pore-bearing precloacal scale (vs. 3–6 scales); 23 or 24 lamellae under 4th toe (vs. 25–28 lamellae); single median row of subcaudal keeled (vs. smooth); ventrolateral caudal tubercles anteriorly present (vs. absent); two postcloacal tubercles in males (vs. one tubercle); and yellow coloration in the subcaudal region absent (vs. present).

Cnemaspis similan sp. nov. is distinguished from *C. phangngaensis* Wood et al. 2017 by having maximum SVL 48.1 mm (vs. 42.0 mm); eight or nine supralabial scales (vs. 10 scales); seven or eight infralabial scales (vs. 10 scales); one pore-bearing precloacal scale (vs. four scales); 24 or 25 paravertebral tubercles (vs. 22 tubercles); paravertebral tubercles randomly arranged (vs. linearly arranged); tubercles on lower flanks present (vs. absent); 23 or 24 lamellae under 4th toe (vs. 29 lamellae); caudal tubercles restricted to a single paravertebral row on each side absent (vs. present); and yellow coloration in the subcaudal region absent (vs. present).

Cnemaspis similan sp. nov. is distinguished from *C. punctatonuchalis* Grismer et al. 2010 by having maximum SVL of 48.1 mm (vs. 49.6 mm); one pore-bearing precloacal scale (vs. absent); 23 or 24 lamellae under 4th toe (vs. 29–31 lamellae); ventral

Table 7. Descriptive measurements in millimeters and characters of the type series of *Cnemaspis similan* sp. nov. H = holotype; P = paratype; – = data unavailable or absent; C = complete; R = regenerated. Measurement abbreviations are defined in the text.

Characters / Museum number	ZMKU R 00984	ZMKU R 00985	ZMKU R 00986	ZMKU R 00987
Sex	Male	Female	Female	Female
Type series	H	P	P	P
SVL	47.6	48.1	38.6	44.2
Tail	R	R	R	C
TL	49.6	43.2	37.6	58.2
TW	4.6	4.6	4.1	4.4
FL	6.8	6.9	6.2	6.6
TBL	8.6	8.8	7.5	8.4
AG	19.6	19.8	16.6	19.4
HL	12.4	12.6	10.4	12.1
HW	7.8	7.9	6.5	7.7
HD	4.8	4.9	4.1	4.6
ED	2.4	2.4	2.1	2.3
EE	3.6	3.7	3.0	3.4
ES	5.3	5.4	4.3	4.9
EN	4.0	4.1	3.4	3.7
EL	1.0	1.0	0.9	1.0
IO	3.1	3.2	2.6	2.6
IN	1.1	1.1	0.9	1.0
Supralabial scales	8	9	9	9
Infralabial scales	7	8	8	8
No. of preloacal pores	1	–	–	–
Preloacal pore continuous (1) or separated (0)	–	–	–	–
Preloacal pores elongate (1) or round (0)	0	–	–	–
No. of paravertebral tubercles	24	25	25	24
Tubercles linearly arranged (1) or more random (0)	0	0	0	0
Tubercles present (1) or absent (0) on lower flanks	1	1	1	1
No. of 4 th toe lamellae	24	24	23	23
Lateral caudal furrows present (1) or absent (0)	1	1	1	1
Pectoral scales keeled (1) or smooth (0)	1	1	1	1
Ventral scales on thigh keeled (1) or smooth (0)	1	1	1	1
Subcaudal keeled (1) or smooth (0)	1	1	1	1
Subtibial scales keeled (1) or smooth (0)	1	1	1	1
Enlarged median subcaudal scale row (1) or not (0)	0	0	0	0
Caudal tubercles restricted to the single paravertebral row on each side (1) or not (0)	1	1	1	1

and subcaudal scales keeled (vs. smooth); single median row of subcaudal keeled (vs. smooth); and enlarged median subcaudal scales row absent (vs. present).

Cnemaspis similan sp. nov. is distinguished from *C. samui* sp. nov. by having maximum SVL 48.1 mm (vs. 42.3 mm); one pore-bearing preloacal scale (vs. 5–8 scales); enlarged median subcaudal scales row absent (vs. present); and yellow coloration in the subcaudal region absent (vs. present).

Cnemaspis similan sp. nov. is distinguished from *C. selenolagus* Grismer et al. 2020 by having maximum SVL 48.1 mm (vs. 36.2 mm); eight or nine supralabial scales (vs. 10 or 11 scales); seven or eight infralabial scales (vs. 10 scales); one pore-bearing



Figure 11. *Cnemaspis similan* sp. nov. in preservative **A** dorsal view (top panel) **B** ventral view (bottom panel); from left to right: ZMKU R 00984–00987. Scale bar in dorsal and ventral views: 10 mm.

precloacal scale (vs. six or seven scales); pore-bearing precloacal scale shape rounded (vs. elongated); 24 or 25 paravertebral tubercles (vs. 16–18 tubercles); tubercles on lower flanks present (vs. absent); ventral and subcaudal scales keeled (vs. smooth); ventrolateral caudal tubercles anteriorly present (vs. absent); and subtibial scales keeled (vs. smooth).

Cnemaspis similan sp. nov. is distinguished from *C. siamensis* (Smith, 1925) by having maximum SVL 48.1 mm (vs. 39.7 mm); one pore-bearing precloacal scale (vs. absent); single median row of subcaudal keeled (vs. smooth); enlarged median subcaudal scales row absent (vs. present); and ventrolateral caudal tubercles anteriorly present (vs. absent).

Cnemaspis similan sp. nov. is distinguished from *C. thachanaensis* Wood et al. 2017 by having maximum SVL 48.1 mm (vs. 39.0 mm); eight or nine supralabial scales

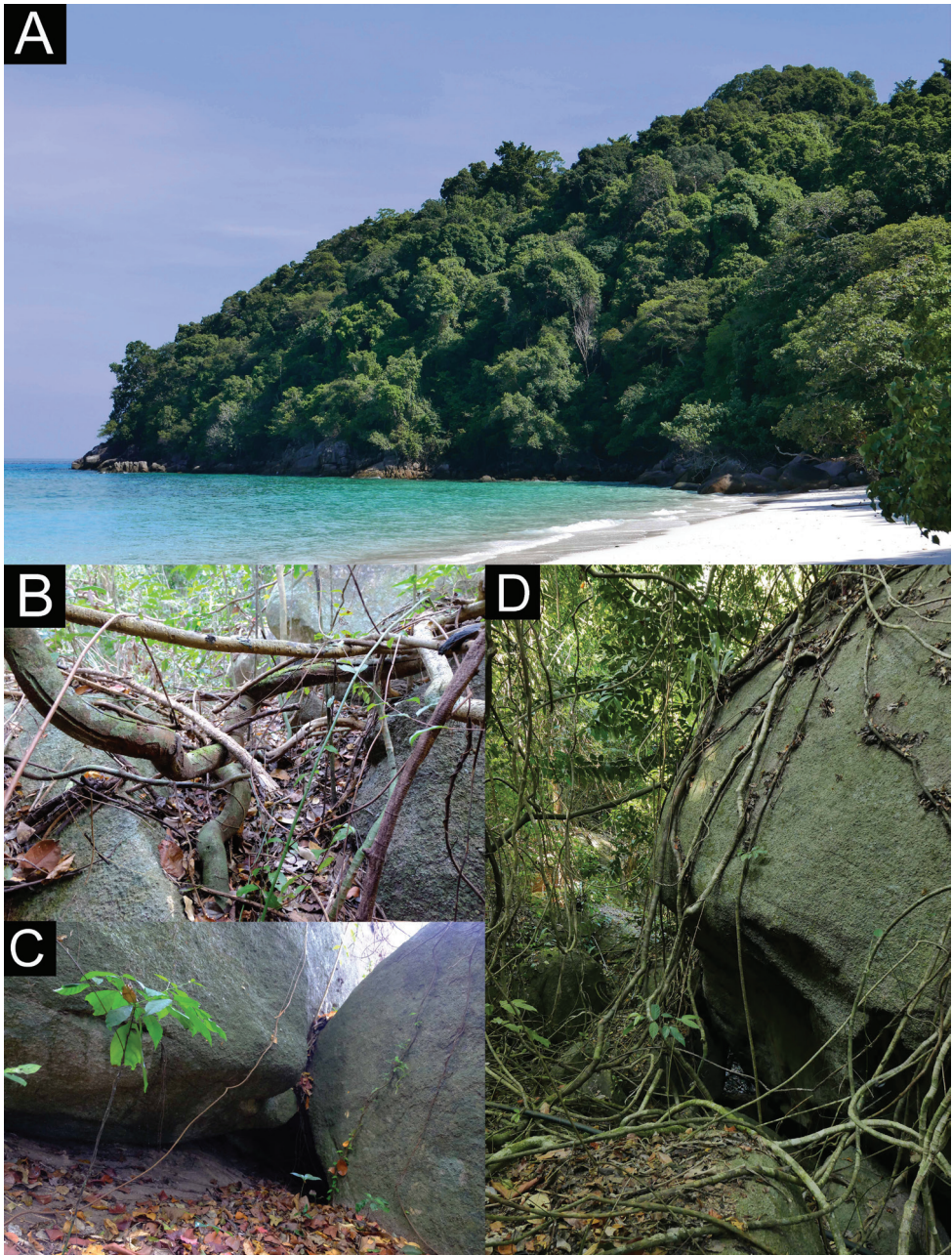


Figure 12. Habitats of *Cnemaspis similan* sp. nov. at the type locality **A** mixed evergreen forest with shrub and beach forests **B** microhabitat of holotype on tree near granitic rock boulder **C** microhabitat of paratypes in granitic rock boulder **D** microhabitat of paratypes in rock wall with vegetations (tree trunk, root or vine) of Ao Nguang Chang Bay, Ko Similan, Mu Ko Similan National Park, Lam Kaen Subdistrict, Thai Mueang District, Phang-nga Province, Thailand.

(vs. 10 or 11 scales); seven or eight infralabial scales (vs. 9–11 scales); pore-bearing precloacal scale present (vs. absent); 24 or 25 paravertebral tubercles (vs. 15–19 tubercles); paravertebral tubercles randomly arranged (vs. linearly arranged); caudal tubercles restricted to a single paravertebral row on each side absent (vs. present); and two postcloacal tubercles in males (vs. absent).

Cnemaspis similan sp. nov. is distinguished from *C. vandeventeri* Grismer et al. 2010 by having maximum SVL 48.1 mm (vs. 44.7 mm); one pore-bearing precloacal scale (vs. four scales); enlarged median subcaudal scales row absent (vs. present); and ventrolateral caudal tubercles anteriorly present (vs. absent).

Discussion

Historically, most Thai *Cnemaspis* were known from areas of limestone karsts and granitic rock formations on the mainland in western, eastern and southern Thailand (Smith 1925; Taylor 1963; Bauer and Das 1998; Grismer et al. 2010, 2020; Wood et al. 2017; Ampai et al. 2020). Only five species of Thai *Cnemaspis* have been found on offshore islands, including *C. tarutaoensis* Ampai et al. 2019 in the *kumpoli* group and four species in the *siamensis* group, *C. adangrawi* Ampai et al. 2019, *C. chanardi* Grismer et al. 2010, *C. siamensis* (Smith, 1925) and *C. vandeventeri* Grismer et al. 2010. The discoveries and descriptions of *C. samui* sp. nov. and *C. similan* sp. nov. increase the total number of Southeast Asian *Cnemaspis* to 66 species, of which 21 occur in Thailand. This also increases the number of insular species in Thailand from five to seven. Remarkably, the geographic distribution of *C. chanardi* is relatively large and discontinuous across limestone karsts and granitic formations in southern Thailand (Grismer et al. 2014). This study suggests that *C. chanardi* might actually represent a complex of species in southern Thailand. Additional data on all *C. chanardi* populations are needed to better delineate species boundaries and estimate their phylogenetic relationships within the *siamensis* group (Wood et al. in prep).

This study revealed two unrecognized species of *Cnemaspis* in granitic areas of southern Thailand, suggesting that additional sampling might reveal more species in this region. Additionally, the phylogenetic analyses of the *siamensis* group confirmed that *C. chanardi* and *C. kamolnorranathi* are strongly supported members of the *siamensis* group. Previously, Grismer et al. (2010) described *C. chanardi* and *C. kamolnorranathi* based only on a combination of morphometric and meristic characters. The phylogenetic placements shown here based on the mtDNA (ND2) of *C. chanardi* and *C. kamolnorranathi* verified the hypotheses of Grismer et al. (2010, 2014) based on morphological and color pattern characters. The phylogenetic position of *C. chanardi* is the sister species to a clade composed of *C. phangngaensis* and the new species *C. similan* sp. nov., while *C. kamolnorranathi* is the sister species to the other new species, *C. samui* sp. nov. The north-south division of the *siamensis* group shown here is concordant with previous studies (Grismer et al. 2014, 2020; Wood et al. 2017; Ampai et al. 2019, 2020; Lee et al. 2019) that revealed a northern clade of six species (*C. huaseesom*, *C. punctatonuchalis*, *C. selenolagus*, *C. siamensis*, *C. thachanaensis*, and *C. vandeventeri*) and a southern clade of nine species (*C. adangrawi*, *C. chanardi*,

C. kamolnorrnanathi, *C. lineatubercularis*, *C. omari*, *C. phangngaensis*, *C. roticanai*, *C. samui* sp. nov., and *C. similan* sp. nov.). The diversification of the *siamensis* group could be linked to the timing of sea level fluctuations that exposed the dispersal corridors between mainland and offshore islands of the Sunda Shelf (Voris, 2000; Sathiamurthy and Voris 2006; Woodruff, 2010). Additional field surveys in unexplored and overlooked areas, particularly in both limestone karst and granitic formations, are needed to better evaluate species diversity and further understand the complex biogeography of *Cnemaspis* in Thailand and adjacent areas.

Acknowledgements

This work was financially supported by Srinakharinwirot University Research Grant (No. 596/2564) and the Thailand Research Fund (DBG6080010). AR and AA were supported by Kasetsart University Research and Development Institute (KURDI), Office of the Permanent Secretary, Ministry of Higher Education, Science, Research and Innovation (No. RGNS 64-038) and the Department of Zoology, Faculty of Science, Kasetsart University. Department of National Parks, Wildlife and Plant Conservation, Thailand provided permission to conduct the research (Permit no.0907.4/20800 and 0907.4/28401). This research was approved by the Institutional Animal Care and Use Committee of Faculty of Science, Kasetsart University (project no. ACKU61-SCI-008). We thank Ruamsilp Manajongprasert (Mu Ko Similan National Park) for facilitating the fieldwork. Piyawan Puanprapai and Akrachai Aksornneam assisted with fieldwork. Lee Grismer and an anonymous reviewer improved the manuscript.

References

- Ampai N, Rujirawan A, Wood Jr PL, Stuart BL, Aowphol A (2019) Morphological and molecular analyses reveal two new species of *Cnemaspis* Strauch, 1887 (Squamata, Gekkonidae) from Satun Province, southern Thailand. *ZooKeys* 858: 127–161. <https://doi.org/10.3897/zookeys.858.34297>
- Ampai N, Wood Jr PL, Stuart BL, Aowphol A (2020) Integrative taxonomy of the rock-dwelling gecko *Cnemaspis siamensis* complex (Squamata, Gekkonidae) reveals a new species from Nakhon Si Thammarat Province, southern Thailand. *ZooKeys* 932: 129–159. <https://doi.org/10.3897/zookeys.932.50602>
- Bauer AM, Das I (1998) A new *Cnemaspis* (Reptilia: Gekkonidae) from Southeastern Thailand. *Copeia* 1998(2): 439–444. <https://doi.org/10.2307/1447438>
- Bauer AM, Jackman TR, Greenbaum E, Giri VB, de Silva A (2010) South Asia supports a major endemic radiation of *Hemidactylus* geckos. *Molecular Phylogenetics and Evolution* 57(1): 343–352. <https://doi.org/10.1016/j.ympev.2010.06.014>
- Boulenger GA (1898) Third report on additions to the lizard collection in the Natural History Museum. *Proceedings of the Zoological Society of London* 1898(4): 912–923. <https://doi.org/10.1111/j.1096-3642.1898.tb03194.x>

- Chan KO, Grismer LL (2021) Integrating spatial, phylogenetic, and threat assessment data from frogs and lizards to identify areas for conservation priorities in Peninsular Malaysia. *Global Ecology and Conservation* 28: e01650. <https://doi.org/10.1016/j.gecco.2021.e01650>
- Das I (2005) Revision of the genus *Cnemaspis* Strauch, 1887 (Sauria: Gekkonidae), from the Mentawai and Adjacent Archipelagos of Western Sumatra, Indonesia, with description of four new species. *Journal of Herpetology* 39(2): 233–247. <https://doi.org/10.1670/61-02A>
- Gamble T, Greenbaum E, Jackman TR, Russell AP, Bauer AM (2012) Repeated origin and loss of adhesive toepads in geckos. *PLoS ONE* 7(6): e39429. <https://doi.org/10.1371/journal.pone.0039429>
- Gamble T, Greenbaum E, Jackman TR, Bauer AM (2015) Into the light: Diurnality has evolved multiple times in geckos. *Biological Journal of the Linnean Society. Linnean Society of London* 115(4): 896–910. <https://doi.org/10.1111/bij.12536>
- Grismer LL, Chan KO (2010) Another new Rock Gecko (genus *Cnemaspis* Stauch 1887) from Pulau Langkawi, Kedah, Peninsular Malaysia. *Zootaxa* 2419(1): 51–62. <https://doi.org/10.11646/zootaxa.2419.1.2>
- Grismer LL, Ngo VT (2007) Four new species of the gekkonid genus *Cnemaspis* Strauch 1887 (Reptilia: Squamata) from Southern Vietnam. *Herpetologica* 63(4): 482–500. [https://doi.org/10.1655/0018-0831\(2007\)63\[482:FNSOTG\]2.0.CO;2](https://doi.org/10.1655/0018-0831(2007)63[482:FNSOTG]2.0.CO;2)
- Grismer LL, Sumontha M, Cota M, Grismer JL, Wood Jr PL, Pauwels OSG, Kunya K (2010) A revision and redescription of the rock gecko *Cnemaspis siamensis* (Taylor 1925) (Squamata: Gekkonidae) from Peninsular Thailand with descriptions of seven new species. *Zootaxa* 2576(1): 1–55. <https://doi.org/10.11646/zootaxa.2576.1.1>
- Grismer LL, Wood Jr PL, Shahrul A, Awal R, Norhayati A, Muin M, Sumontha M, Grismer J, Chan K, Quah ESH, Pauwels OSG (2014) Systematics and natural history of Southeast Asian Rock Geckos (genus *Cnemaspis* Strauch, 1887) with descriptions of eight new species from Malaysia, Thailand, and Indonesia. *Zootaxa* 3880(1): 1–147. <https://doi.org/10.11646/zootaxa.3880.1.1>
- Grismer LL, Wood Jr PL, Quah ES, Anuar S, Ngadi E, Norhayati A (2015a) A new insular species of Rock Gecko (*Cnemaspis* Boulenger) from Pulau Langkawi, Kedah, Peninsular Malaysia. *Zootaxa* 3985(2): 203–218. <https://doi.org/10.11646/zootaxa.3985.2.2>
- Grismer LL, Wood Jr PL, Tri N, Murdoch ML (2015b) The systematics and independent evolution of cave ecomorphology in distantly related clades of Bent-toed Geckos (Genus *Cyrtodactylus* Gray, 1827) from the Mekong Delta and islands in the Gulf of Thailand. *Zootaxa* 3980(1): 106–126. <https://doi.org/10.11646/zootaxa.3980.1.6>
- Grismer LL, Yushchenko PV, Pawangkhanant P, Nazarov RA, Naiduangchan M, Suwannapoom C, Poyarkov NA (2020) A new species of *Cnemaspis* Strauch (Squamata: Gekkonidae) of the *C. siamensis* group from Tenasserim Mountains, Thailand. *Zootaxa* 4852(5): 547–564. <https://doi.org/10.11646/zootaxa.4852.5.3>
- Hammer Ø, Harper DAT, Ryan PD (2001) PAST: Paleontological Statistics Software Package for Education and Data Analysis. *Palaeontologia Electronica* 4: 1–9.
- Hoang T, Akselrod G, Mikkelsen M (2017) Ultrafast room-temperature single photon source with plasmonic nanocavities. *Optics InfoBase Conference Papers, Part F42-CLEO_QELS 2017*. https://doi.org/10.1364/CLEO_QELS.2017.FF2G.4

- Huelsenbeck JP, Ronquist F (2001) MRBAYES: Bayesian inference of phylogeny. *Bioinformatics* 17(8): 754–755. <https://doi.org/10.1093/bioinformatics/17.8.754>
- Jombart T (2008) ADEGENET: A R package for the multivariate analysis of genetic markers. *Bioinformatics* 24(11): 1403–1405. <https://doi.org/10.1093/bioinformatics/btn129>
- Jombart T, Devillard S, Balloux F (2010) Discriminant analysis of principal components: A new method for the analysis of genetically structured populations. *BMC Genetics* 11(1): e94. <https://doi.org/10.1186/1471-2156-11-94>
- Kaiser HF (1960) The Application of Electronic Computers to Factor Analysis. *Educational and Psychological Measurement* 20(1): 141–151. <https://doi.org/10.1177/001316446002000116>
- Kalyaanamoorthy S, Minh BQ, Wong TK, von Haeseler A, Jermini LS (2017) ModelFinder: Fast model selection for accurate phylogenetic estimates. *Nature Methods* 14(6): 587–589. <https://doi.org/10.1038/nmeth.4285>
- Karunarathna S, Bauer A, de Silva A, Surasinghe T, Somaratna L, Madawala M, Gabadage D, Botejue M, Henkanaththegedara S, Ukuwela KDB (2019) Description of a new species of the genus *Cnemaspis* Strauch, 1887 (Reptilia: Squamata: Gekkonidae) from the Nilgala Savannah forest, Uva Province of Sri Lanka. *Zootaxa* 4545(3): 389–407. <https://doi.org/10.11646/zootaxa.4545.3.4>
- Kurita T, Nishikawa K, Matsui M, Hikida T (2017) A new species of Rock Gecko genus *Cnemaspis* (Squamata: Gekkonidae) from Western Sarawak, Malaysia. *Zootaxa* 4258(5): 525–538. <https://doi.org/10.11646/zootaxa.4258.6.2>
- Lanfear R, Frandsen PB, Wright AM, Senfeld T, Calcott B (2016) PartitionFinder 2: New methods for selecting partitioned models of evolution for molecular and morphological phylogenetic analyses. *Molecular Biology and Evolution* 34(3): 772–773. <https://doi.org/10.1093/molbev/msw260>
- Lee JL, Miller AH, Zug GR, Mulcahy DG (2019) The discovery of Rock Geckos *Cnemaspis* Strauch, 1887 (Squamata: Gekkonidae) in the Tanintharyi Region, Myanmar with the description of two new species. *Zootaxa* 4661(1): 040–064. <https://doi.org/10.11646/zootaxa.4661.1.2>
- Linnaeus C (1758) *Systema naturæ per regna tria naturæ, secundum classes, ordines, genera, species, cum characteribus, differentiis, synonymis, locis*. Tomus I. Editio decima, reformata. Laurentii Salvii, Holmiæ, 824 pp. <https://doi.org/10.5962/bhl.title.542>
- Leonart J, Salat J, Torres GJ (2000) Removing allometric effects of body size in morphological analysis. *Journal of Theoretical Biology* 205(1): 85–93. <https://doi.org/10.1006/jtbi.2000.2043>
- Macey JR, Larson A, Ananjeva NB, Papenfuss TJ (1997) Evolutionary shifts in three major structural features of the mitochondrial genome among iguanian lizards. *Journal of Molecular Evolution* 44(6): 660–674. <https://doi.org/10.1007/PL00006190>
- Malonza PK, Bauer AM (2022) Resurrection of the African gecko genus *Ancylodactylus* Müller, 1907 (Squamata: Gekkonidae) and description of six new species from Kenya. *Zootaxa* 5141(2): 101–139. <https://doi.org/10.11646/zootaxa.5141.2.1>
- Miller MA, Pfeiffer W, Schwartz T (2010) Creating the CIPRES Science Gateway for inference of large phylogenetic trees in Proceedings of the Gateway Computing Environments Workshop (GCE), 14 Nov. 2010, New Orleans, LA, 1–8. <https://doi.org/10.1109/GCE.2010.5676129>
- Minh Q, Nguyen M, von Haeseler AA (2013) Ultrafast approximation for phylogenetic bootstrap. *Molecular Biology and Evolution* 30(5): 1188–1195. <https://doi.org/10.1093/molbev/mst024>

- Nashriq I, Davis HR, Bauer AM, Das I (2022) Three New Species of *Cnemaspis* (Sauria: Gekkonidae) from Sarawak, East Malaysia, Borneo. *Zootaxa* 5120(1): 1–29. <https://doi.org/10.11646/zootaxa.5120.1.1>
- Nguyen LT, Schmidt HA, von Haeseler A, Minh BQ (2015) IQ-TREE: A fast and effective stochastic algorithm for estimating maximum-likelihood phylogenies. *Molecular Biology and Evolution* 32(1): 268–274. <https://doi.org/10.1093/molbev/msu300>
- Nguyen HN, Hung CM, Yang MY, Lin SM (2020) Sympatric competitors have driven the evolution of temporal activity patterns in *Cnemaspis* geckos in Southeast Asia. *Scientific Reports* 10(1): 1–8. <https://doi.org/10.1038/s41598-019-56549-x>
- Pyron RA, Burbrink FT, Wiens JJ (2013) A phylogeny and revised classification of Squamata, including 4161 species of lizards and snakes. *BMC Evolutionary Biology* 13(1): 1–53. <https://doi.org/10.1186/1471-2148-13-93>
- R Core Team (2018) R: A Language and Environment for Statistical Computing. R Foundation for Statistical Computing, Vienna. <https://www.R-project.org>
- Rambaut A (2018) FigTree: tree figure drawing tool (Version 1.4.4). <http://tree.bio.ed.ac.uk/software/figtree>
- Rambaut A, Suchard MA, Xie D, Drummond AJ (2014) Tracer v1.6. <http://beast.bio.ed.ac.uk/Tracer> [accessed 25 March 2022]
- Riyanto A, Hamidy A, Sidik I, Gunalen D (2017) A new species of Rock Gecko of the genus *Cnemaspis* Strauch, 1887 (Squamata: Gekkonidae) from Belitung Island, Indonesia. *Zootaxa* 4358(3): 583–597. <https://doi.org/10.11646/zootaxa.4358.3.12>
- Ronquist F, Teslenko M, Van Der Mark P, Ayres DL, Darling A, Höhna S, Larget B, Liu, L, Suchard MA, Huelsenbeck JP (2012) MrBayes 3.2: efficient Bayesian phylogenetic inference and model choice across a large model space. *Systematic biology* 61(3): 539–542. <https://doi.org/10.1093/sysbio/sys029>
- Rösler HA, Bauer AM, Heinicke MP, Greenbaum E, Jackman TR, Nguyen TQ, Ziegler T (2011) Phylogeny, taxonomy, and zoogeography of the genus *Gekko* Laurenti, 1768 with the revalidation of *G. reevesii* Gray, 1831 (Sauria: Gekkonidae). *Zootaxa* 2989(1): 1–50. <https://doi.org/10.11646/zootaxa.2989.1.1>
- Sathiamurthy E, Voris HK (2006) Maps of Holocene sea level transgression and submerged lakes on the Sunda Shelf. *The Natural History Journal of Chulalongkorn University* 2(Supplement): 1–43.
- Simmons JE (2015) *Herpetological Collecting and Collections Management*, 3rd Edn. Society for the Study of Amphibians and Reptiles Herpetological Circular No. 42. Salt Lake City, UT, 191 pp.
- Smith MA (1925) IV. Contributions to the herpetology of Borneo. *The Sarawak Museum Journal* 3(8): 15–34.
- Tamura K, Stecher G, Kumar S (2021) MEGA11: Molecular Evolutionary Genetics Analysis Version 11. *Molecular Phylogenetics and Evolution* 38: 3022–3027. <https://doi.org/10.1093/molbev/msab120>
- Taylor EH (1962) New oriental reptiles. *The University of Kansas Science Bulletin* 43: 209–263. <https://doi.org/10.5962/bhl.part.13346>
- Taylor EH (1963) The lizards of Thailand. *The University of Kansas Science Bulletin* 44: 687–1077.

- Theobald W (1876) Descriptive catalogue of the reptiles of British India. Thacker, Spink & Co., Calcutta, [xiii +] 238 pp. <https://doi.org/10.5962/bhl.title.5483>
- Thorpe RS (1975) Quantitative handling of characters useful in snake systematics with particular reference to interspecific variation in the Ringed Snake *Natrix natrix* (L.). *Biological Journal of the Linnean Society*. Linnean Society of London 7(1): 27–43. <https://doi.org/10.1111/j.1095-8312.1975.tb00732.x>
- Thorpe RS (1983) A review of the numerical methods for recognized and analysing racial differentiation. In: Felsenstein J (Ed.) *Numerical taxonomy*. Berlin Heidelberg: Springer, 404–423. https://doi.org/10.1007/978-3-642-69024-2_43
- Trifinopoulos J, Nguyen LT, von Haeseler A, Minh BQ (2016) W-IQ-TREE: A fast online phylogenetic tool for maximum likelihood analysis. *Nucleic Acids Research* 44(W1): W232–W235. <https://doi.org/10.1093/nar/gkw256>
- Turan C (1999) A note on the examination of morphometric differentiation among fish populations: The truss system. *Turkish Journal of Zoology* 23: 259–263.
- Uetz P, Freed P, Hošek J (2022) The Reptile Database. <http://www.reptile-database.org> [accessed 11 September 2022]
- Voris HK (2000) Maps of pleistocene sea levels in Southeast Asia: Shorelines, river systems and time durations. *Journal of Biogeography* 27(5): 1153–1167. <https://doi.org/10.1046/j.1365-2699.2000.00489.x>
- Wickham H (2016) *ggplot2: Elegant Graphics for Data Analysis*. Springer-Verlag New York, 216 pp. https://doi.org/10.1007/978-3-319-24277-4_9
- Wilcox TP, Zwickl DJ, Heath TA, Hillis DM (2002) Phylogenetic relationships of the dwarf boas and a comparison of Bayesian and bootstrap measures of phylogenetic support. *Molecular Phylogenetics and Evolution* 25(2): 361–371. [https://doi.org/10.1016/S1055-7903\(02\)00244-0](https://doi.org/10.1016/S1055-7903(02)00244-0)
- Wood Jr PL, Grismer LL, Aowphol A, Aguilar CA, Cota M, Grismer MS, Murdoch ML, Sites Jr JW (2017) Three new karst-dwelling *Cnemaspis* Strauch, 1887 (Squamata; Gekkonidae) from Peninsular Thailand and the phylogenetic placement of *C. punctatonuchalis* and *C. vandeventeri*. *PeerJ* 5: e2884. <https://doi.org/10.7717/peerj.2884>
- Woodruff DS (2010) Biogeography and conservation in Southeast Asia: How 2.7 million years of repeated environmental fluctuations affect today's patterns and the future of the remaining refugial-phase biodiversity. *Biodiversity and Conservation* 19(4): 919–941. <https://doi.org/10.1007/s10531-010-9783-3>
- Ziegler T, Botov A, Nguyen TT, Bauer AM, Brennan IG, Ngo HT, Nguyen TQ (2016) First molecular verification of *Dixonius vietnamensis* Das, 2004 (Squamata: Gekkonidae) with the description of a new species from Vinh Cuu Nature Reserve, Dong Nai Province, Vietnam. *Zootaxa* 4136(3): 553–566. <https://doi.org/10.11646/zootaxa.4136.3.7>

Appendix I. List of comparative specimens examined

Cnemaspis adangrawi: Thailand, Satun Province, Mueang Satun District, Ko Adang: ZMKU R 00767 (male holotype), ZMKU R 00769–70, THNHM 28206–09 (6 males), ZMKU R 00768, ZMKU R 00771 (2 females); Thailand, Satun Province,

Mueang Satun District, Ko Rawi: ZMKU R 00773, ZMKU R 00775, THNHM 28210 (3 adult males), ZMKU R 00774, THNHM 28211 (2 females).

Cnemaspis chanardi: Thailand, Trang Province, Nayong District, Ban Chong: THNHM 06983 (male holotype); Krabi Province, Klong Thom District: THNHM 012439–40 (males); Mueang Krabi District: THNHM 012436–37 (males), THNHM 012438 (female); Nakhon Si Thammarat Province, Tha Sala District: THNHM 020992 (male); Lansaka district: THNHM 014111 (immature male); Noppitam district: THNHM 013838 (male), THNHM 010705 (male); Surat Thani Province, Mu Ko Ang Thong, Mueang Surat Thani District: THNHM 016074 (female).

Cnemaspis huaseesom: Thailand, Kanchanaburi Province, Sai Yok District, Sai Yok National Park: THNHM 15909 (male holotype).

Cnemaspis lineatubercularis: Thailand, Nakhon Si Thammarat Province, Lan Saka District, Wang Mai Pak Waterfall: ZMKU R 00828 (male holotype); ZMKU R 00821–31 (males); THNHM 28694–95 (males); ZMKU R 00826 (female); THNHM 28696–97 (females); ZMKU R 00832–35 (females).

Cnemaspis niyomwanae: Thailand, Trang Province, Palean District, Thum Khao Ting: THNHM 15909 (female holotype).

Cnemaspis punctatonuchalis: Thailand, Prachuap Khiri Khan Province, Thap Sakae District, Huay Yang National Park: THNHM 02001 (male holotype).

Cnemaspis siamensis: Thailand, Nakhon Si Thammarat Province, Lan saka District: THNHM 013828 (male); Tha Sala District: THNHM 018265 (male); Chumpon Province, Mueang Chumpon District: THNHM 0372 (male); Phato District: THNHM 01086 (male); Surat Thani Province, Vibhawadee District: THNHM 01084 (female); Mu Ko Ang Thong, Mueang Surat Thani District: THNHM 015624 (female).

Cnemaspis vandeventeri: Thailand, Ranong Province, Kapur District, Klong Naka: THNHM 08261 (male holotype), THNHM 08260 (female).

Supplementary material I

Table S1

Authors: Natee Ampai, Attapol Rujirawan, Siriporn Yodthong, Korkhwan Termprayoon, Bryan L. Stuart, Perry L. Wood Jr, Anchalee Aowphol

Data type: excel file

Explanation note: Significant p -values of the ANOVA analyses (Tukey's HSD; $p < 0.05$) from 15 size-corrected morphometric measurements of nine OTUs of *Cnemaspis siamensis* species group. HD, ED and EE were not significantly different from one another. Measurement abbreviations are defined in the material and methods.

Copyright notice: This dataset is made available under the Open Database License (<http://opendatacommons.org/licenses/odbl/1.0/>). The Open Database License (ODbL) is a license agreement intended to allow users to freely share, modify, and use this Dataset while maintaining this same freedom for others, provided that the original source and author(s) are credited.

Link: <https://doi.org/10.3897/zookeys.1125.94060.suppl1>

Three new species of the leafhopper genus *Mitjaevia* Dworakowska from Karst areas in Southwest China (Hemiptera, Cicadellidae, Typhlocybinae)

Guimei Luo^{1,2}, Jinqiu Wang^{1,2}, Yuehua Song^{1,2}

1 School of Karst Science, Guizhou Normal University, Guizhou, Guiyang 550001, China **2** State Engineering Technology Institute for Karst Desertification Control, Guiyang 550001, China

Corresponding author: Yuehua Song (songyuehua@163.com)

Academic editor: J. A. Pinedo-Escatel | Received 14 February 2022 | Accepted 5 October 2022 | Published 25 October 2022

<https://zoobank.org/5394C396-88F2-4112-8BCD-980A9F4F6C81>

Citation: Luo G, Wang J, Song Y (2022) Three new species of the leafhopper genus *Mitjaevia* Dworakowska from Karst areas in Southwest China (Hemiptera, Cicadellidae, Typhlocybinae). ZooKeys 1125: 159–169. <https://doi.org/10.3897/zookeys.1125.82258>

Abstract

Three new species of the leafhopper genus *Mitjaevia* Dworakowska 1970, *M. bijiensis* **sp. nov.**, *M. solitaria* **sp. nov.**, and *M. salaxia* **sp. nov.**, are described from the Karst region of Southwest China. Specimens studied were taken by sweep net. Morphological descriptions, depictions of habitus and illustrations of male terminalia are provided. A key and checklist to known species occurring in China are given.

Keywords

Homoptera, morphology, new taxa, taxonomy

Introduction

The genus *Mitjaevia* was designated by Dworakowska in 1970 belonging to the tribe Erythroneurini of the subfamily Typhlocybinae (Hemiptera: Cicadellidae). Some members of the genus are known as important agricultural pests in the world. *Mitjaevia* Dworakowska share similar features with *Diomma* Motschulsky and *Kusala* Dworakowska such as the vertex and pronotum, usually with dark spots or stripes; the style with apex slender and curved; and connective with two strong lateral arms but can be distinguished by the combination of the following characters: (1) pygofer lobe with numerous microsetae or

microtrichia near caudal area and basal lower angle without clusters of long macrosetae; (2) abdominal apodemes small, not extending beyond hind margin of 3rd sternite; (3) forewing semitransparent, light brown or brown, often decorated with white or milky patches.

Later, Song et al. (2011) and Dmitriev (2020) supplemented features of dorsum, eyes, legs, abdomen, pygofer and pygofer dorsal appendage of *Mitjaevia* and also noted that forewings possess four apical cells, subgenital plates contains 2–4 basal macrochaetae and the aedeagus has a distal short apical processes, toothlike or absent. The species of this genus are mainly distributed in the Palearctic and Oriental regions. Until now, 19 species have been described, of which 11 species are in China (see Checklist). In the present paper, three new species of *Mitjaevia* from Guizhou Province are proposed to the Chinese fauna. A key to recognize all Chinese species is provided.

Materials and methods

Specimens for this study were collected on roadside weeds in Karst (Guizhou Province, China) by sweep net. The morphological terms used in this study followed Dietrich (2005) and Song and Li (2013). A KEYENCE VHX-5000 digital microscope was used to take pictures of male habitus. The Olympus BX53 microscope was used to dissect the male genital and the Olympus SZX16 microscope was used for viewing and drawing the male genital. Body length was measured from the apex of vertex to the tip of forewing. All specimens examined were deposited in The School of Karst Science collection, at Guizhou Normal University (GZNU).

Taxonomy

Mitjaevia Dworakowska

Mitjaevia Dworakowska, 1970: 763.

Type species. *Erythroneura amseli* Dlabola, 1961.

Type locality. Afghanistan.

Diagnosis. Yellow with brown markings; vertex usually with a pair of dark brown spots; pronotum with brown markings or completely dark; scutellum with dark basal triangles; forewing hyaline with several dark patches; abdomen ventrally and subgenital plates dark. Head distinctly narrower than pronotum.

Male genitalia. Pygofer caudally rounded or angulate, weakly sclerotized caudally; dorsal pygofer appendage movably articulated, not extended beyond pygofer apex. Style distally slender with apex foot-like; preapical lobe large. Subgenital plates extended beyond pygofer, darkly pigmented, gradually curved dorsad, with three or more macrosetae of differing length present in middle. Aedeagus with shaft tubular, straight or curved dorsad in lateral view, with or without basal processes;

preatrium developed. Connective Y- or M-shaped, with short stem and arms, central lobe well developed.

Distribution. Palaearctic and Oriental regions.

Checklist of species of *Mitjaevia* from China

- M. aurantiaca* Mitjaev, 1969: 1044 (pl. 3, figs 1, 2); Song & Li, 2014: 111, (pl. 2.71, figs D-F; I, J, M, S).
- M. bifurcata* Luo, Song & Song, 2021: 3–6, fig. 2.
- M. diana* (Distant, 1918: 100, *Typhlocyba*); Dworakowska, 1970: 765 (lectotype designated by inference); Dworakowska, 1980: 179, figs 252–262; Song & Li, 2014: 112 (pl. 2.72, figs D-F; I, J, M).
- M. dworakowskiae* Chen, Song & Webb, 2020: 34–39, figs 28–41.
- M. korolevskayae* Dworakowska, 1979: 44–45, figs 349–358; Song & Li, 2014: 113 (pl. 2.73, figs D-F; I, J, M).
- M. nanaoensis* Chiang & Knight, 1990: 223, fig. 18.
- M. protuberanta* Song, Li & Xiong, 2011: 27–29, figs 1–10.
- M. bijiensis* sp. nov.
- M. ramosa* Luo, Song & Song, 2021: 6–8, fig. 5.
- M. salixia* sp. nov.
- M. shibingensis* Chen, Song & Webb, 2020: 34, fig. 15–27.
- M. solitaria* sp. nov.
- M. tappana* Chiang & Knight, 1990: 225, fig. 19.
- M. wangwushana* Song, Li & Xiong, 2011: 29–30, figs 11–19.

Key to species of *Mitjaevia* from China (males)

- 1 Aedeagus with single or paired processes 2
- Aedeagus without processes..... 10
- 2 Aedeagal shaft with paired processes..... 3
- Aedeagal shaft with single process (Fig. 25) *M. solitaria* sp. nov.
- 3 Aedeagus with apical, subapical or basal processes, but not dorsally 4
- Aedeagus only with dorsal processes *M. bifurcata*
- 4 Aedeagal shaft with apical process 5
- Aedeagal shaft without apical process 7
- 5 Aedeagal shaft with unbifurcated apical process (Fig. 17) *M. bijiensis* sp. nov.
- Aedeagal shaft with bifurcated apical process..... 6
- 6 Aedeagal shaft with pair of asymmetric bifurcated short processes at apex
..... *M. ramosa*
- Aedeagal shaft with pair of symmetrical bifurcated short processes at apex
..... *M. diana*
- 7 Aedeagal shaft with paired processes subapically..... 8
- Aedeagal shaft without paired processes subapically 9

- 8 Aedeagal shaft with pair of small, triangle-like processes subapically.....*M. protuberanta*
 – Aedeagal shaft with pair of long, curved processes subapically.....*M. wangwushana*
 9 Aedeagal shaft with finger-like basal processes ventrally.....*M. aurantiaca*
 – Aedeagal shaft with lamellate-like basal processes ventrally (Fig. 33)*M. salaxia* sp. nov.
 10 Preatrium of aedeagus long in lateral view.....11
 – Preatrium of aedeagus short in lateral view.....*M. tappana*
 11 Aedeagal shaft cylindrical, evenly tapered from base to apex.....12
 – Aedeagal shaft laterally compressed, abruptly tapered from subapically to apex....13
 12 Aedeagus dorsal apodeme visible in lateral view*M. korolevskayae*
 – Aedeagus dorsal apodeme absent or vestigial in lateral view.....*M. nanaoensis*
 13 Aedeagal shaft with rounded apex in lateral view; preatrium expanded in ventral view*M. shibingensis*
 – Aedeagal shaft with acute apex in lateral view; preatrium narrow in ventral view.*M. dworakowskiae*

Descriptions

Mitjaevia bijiensis sp. nov.

<https://zoobank.org/77C7830A-4369-4A7E-96C6-D099579FDC07>

Figs 1–5, 16–23

Material examined. *Holotype*: ♂, CHINA: Guizhou Province, Bijie, 6.VI.2021, coll. Jia Jiang and Ni Zhang. *Paratypes*: 1 ♀, same data as holotype.

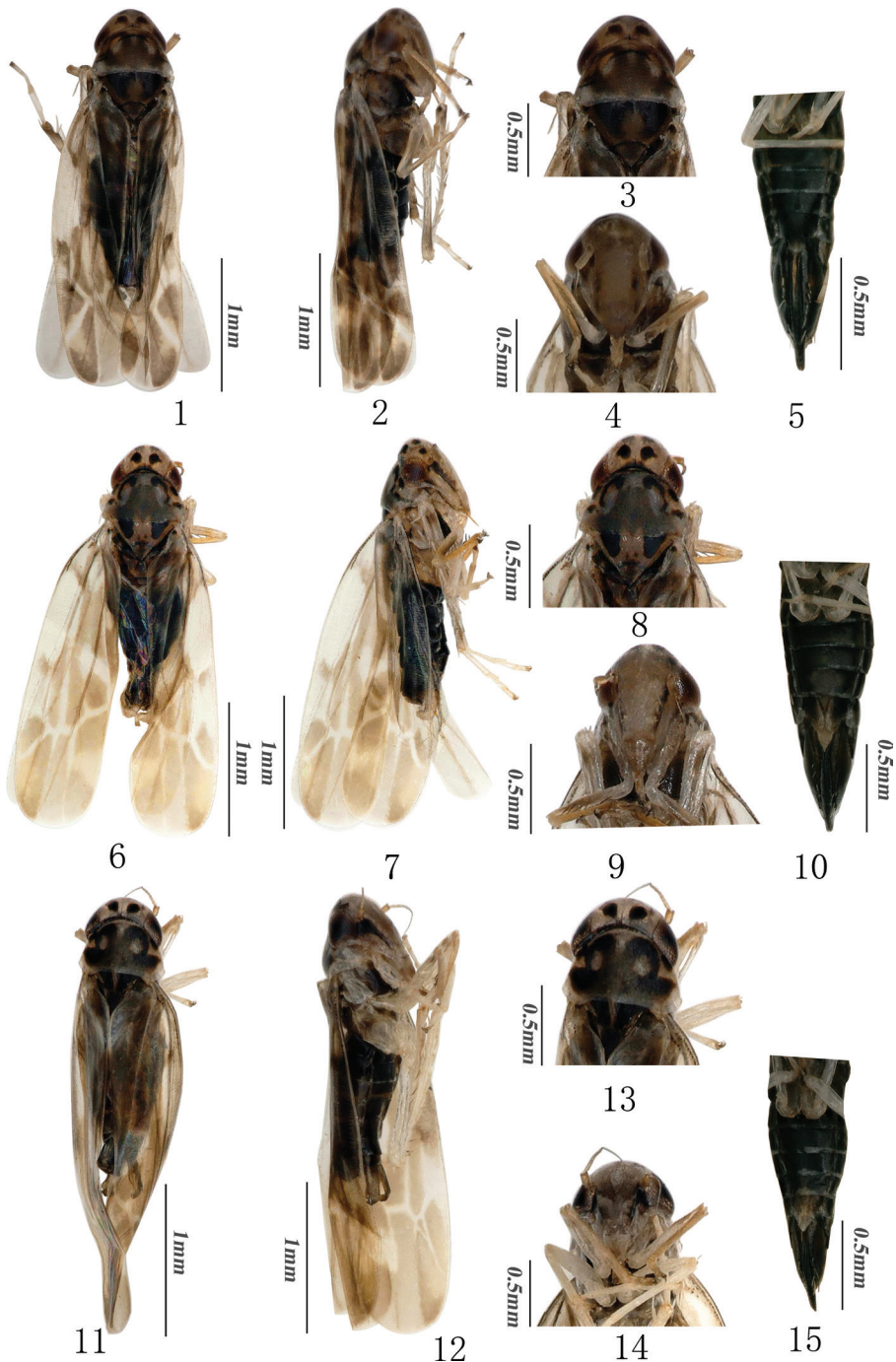
Diagnosis. The new species can be distinguished from other species by the aedeagal shaft long with two apical processes; preatrium of aedeagus with two atrial processes. The head and pronotum yellow. Pygofer dorsal appendage tapered to apex and bent back into a hook shape. Style apex slightly expanded, underpart straight and thick. Connective with large central lobe.

Description. Head and thorax yellow marked with brown; vertex with a pair of dark brown spots (Figs 1–4). Pronotum yellow, with irregularly dark brown patch medially (Figs 1, 3). Scutellum yellow, transverse impression distinct. Face brownish yellow (Fig. 1); anteclypeus with black patches at sides basally (Fig. 4). Forewing brownish, with large milky white or whitish patches.

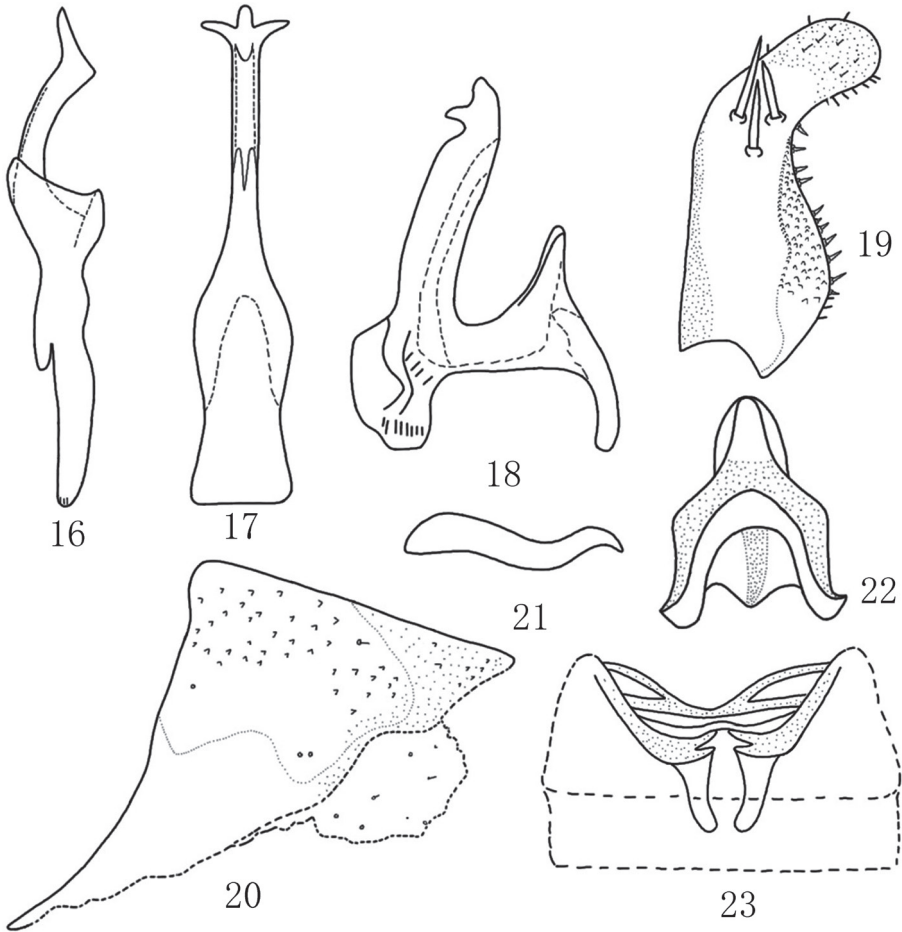
Abdominal apodemes long, exceeding posterior margin of 3rd sternite (Fig. 23).

Male genitalia. Pygofer lobe broad, with sparse fine setae on lateral surface (Fig. 20). Pygofer dorsal appendage slightly expanded at base, bends up and down and tapers gradually (Fig. 21). Subgenital plate with three macrosetae of different lengths medially (Fig. 19). Style long and strong; preapical lobe large (Fig. 16). Aedeagal shaft long, with pair of short bifurcate apical processes; preatrium also with two atrial processes (Figs 17, 18). Connective M-shaped, with distinct stem and central lobe (Fig. 22).

Body length (including wings). ♂, 2.9–3.0 mm, ♀, 2.8–2.9 mm.



Figures 1–15. External morphology of *Mitjaevia* species **1–5** *Mitjaevia bijiensis* sp. nov. **1** habitus, dorsal view **2** habitus, lateral view **3** head and thorax, dorsal view **4** face **5** female thorax and abdomen, ventral view **6–10** *Mitjaevia solitaria* sp. nov. **6** habitus, dorsal view **7** habitus, lateral view **8** head and thorax, dorsal view **9** face **10** female thorax and abdomen, ventral view **11–15** *Mitjaevia salaxia* sp. nov. **11** habitus, dorsal view **12** habitus, lateral view **13** head and thorax, dorsal view **14** face **15** female thorax and abdomen, ventral view.



Figures 16–23. *Mitjaevia bijiensis* sp. nov. **16** style **17** aedeagus, ventral view **18** aedeagus, lateral view **19** subgenital plate **20** male pygofer, lateral view **21** pygofer dorsal appendage, lateral view **22** connective **23** abdominal apodemes.

Remarks. The new species is similar to *Mitjaevia diana* (Distant, 1918) but can be distinguished by the aedeagal shaft with two apical processes and preatrium of aedeagus with two atrial processes; the style apex slightly expanded, underpart straight and thick; the connective with large central lobe.

Etymology. The new species is named after its type locality Bijie City in China.

***Mitjaevia solitaria* sp. nov.**

<https://zoobank.org/29D48CC0-BE39-4F3D-983C-53FE2CD472B3>

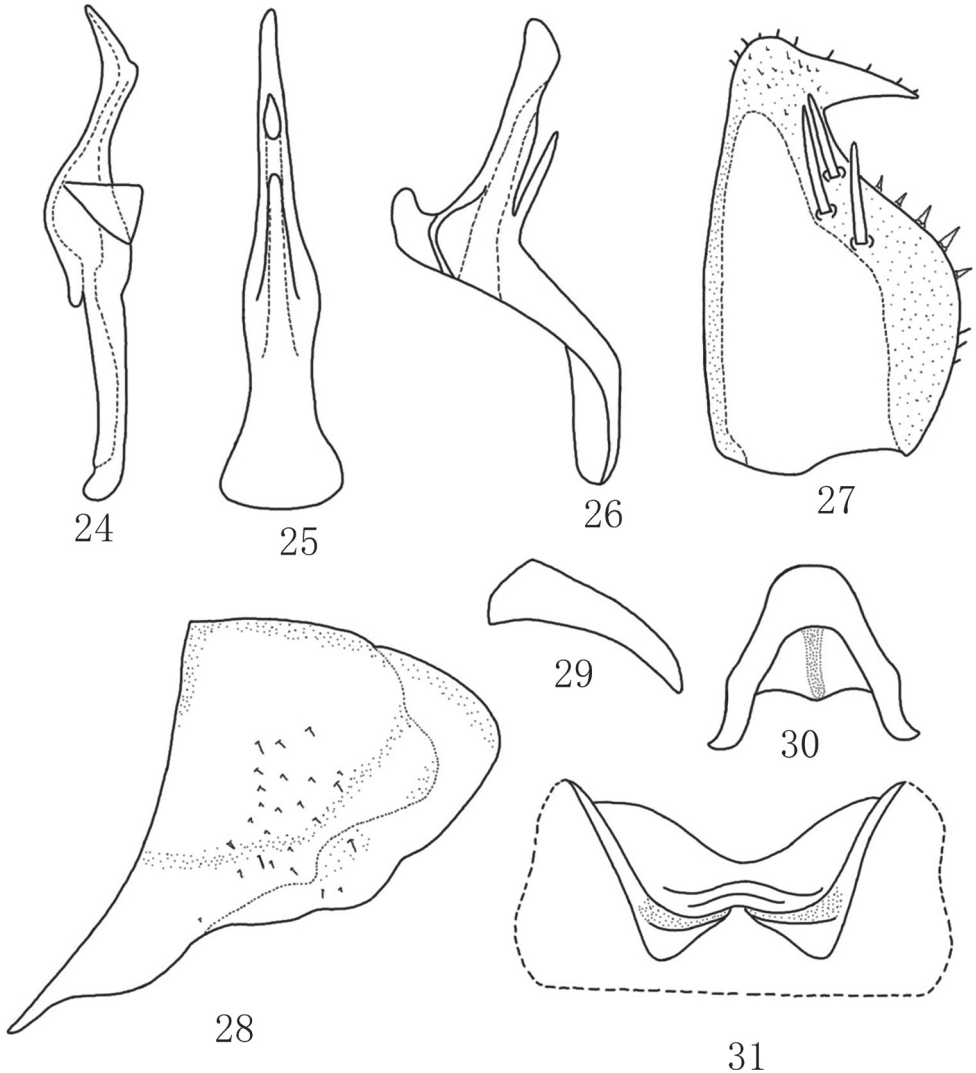
Figs 6–10, 24–31

Material examined. **Holotype:** ♂, CHINA: Guizhou Province, Bijie, 6.VI.2021, coll. Jia Jiang and Ni Zhang. **Paratypes:** 18 ♂♂, 3 ♀♀, same data as holotype.

Diagnosis. The new species can be distinguished from other species by the aedeagal shaft with only one thick finger-like process at base. Pygofer dorsal appendage not extended beyond hind margin of pygofer. Style strong; preapical lobe obvious. Subgenital plate wide and short with one hook-like process on apex.

Description. Vertex yellowish (Fig. 6). Pronotum mostly grayish black (Figs 6, 8). Scutellum yellowish, transverse impression distinct (Fig. 6). Face brownish yellow; anteclypeus brownish except lighter base (Fig. 9). Forewing brownish, with large milky white or whitish patches.

Abdominal apodemes small, located in 3rd sternite (Fig. 31).



Figures 24–31. *Mitjaevia solitaria* sp. nov. **24** style **25** aedeagus, ventral view **26** aedeagus, lateral view **27** subgenital plate **28** male pygofer, lateral view **29** pygofer dorsal appendage, lateral view **30** connective **31** abdominal apodemes.

Male genitalia. Pygofer dorsal appendage weakly expanded at base, not extended beyond hind margin of pygofer (Fig. 29). Pygofer lobe broad, with fine setae scattered outer lateral surface (Fig. 28). Subgenital plate wide and short, with three macrosetae on lateral surface, and one hook-like process on apex (Fig. 27). Style strong; preapical lobe obvious (Fig. 24). Aedeagal shaft as long as or little shorter than that of preatrium, with one finger-like process basally; dorsal apodeme small (Figs 25, 26). Connective Y-shaped; arms and central lobe slender (Fig. 30).

Body length (including wings). ♂, 3.1–3.2 mm, ♀, 3.0–3.2 mm.

Remarks. The new species is similar to *M. aurantiaca* (Mitjaev, 1969), but can be distinguished by the aedeagal shaft with only one thick finger-like process at base; the style is stronger and the subgenital plate is shorter and wider.

Etymology. The new species is named from the Latin word *solitarius*, referring to the aedeagal shaft with only one processes at the base.

Mitjaevia salaxia sp. nov.

<https://zoobank.org/278419B3-C800-4929-A7AD-6B9BBBF0056>

Figs 11–15, 32–39

Material examined. Holotype: ♂, CHINA: Guizhou Province, Bijie, 5.VI.2021, coll. Jia Jiang and Ni Zhang. **Paratypes:** 1 ♂♂, 6 ♀♀, same data as holotype.

Diagnosis. The new species can be identified by the two pairs of abdominal apodemes and the aedeagal shaft with lamellate-like processed at base. Style apex long and slender. Subgenital plate long, expanded near caudal.

Description. Vertex pale yellow (Fig. 11). Pronotum yellowish, with symmetrical brownish black impressed patches medially (Figs 11, 13). Scutellum (Fig. 11) yellow, with basal triangles black and area under transverse impression black too. Face brownish gray; anteclypeus with central area brownish (Fig. 14). Forewing brownish, with large milky white or whitish patches.

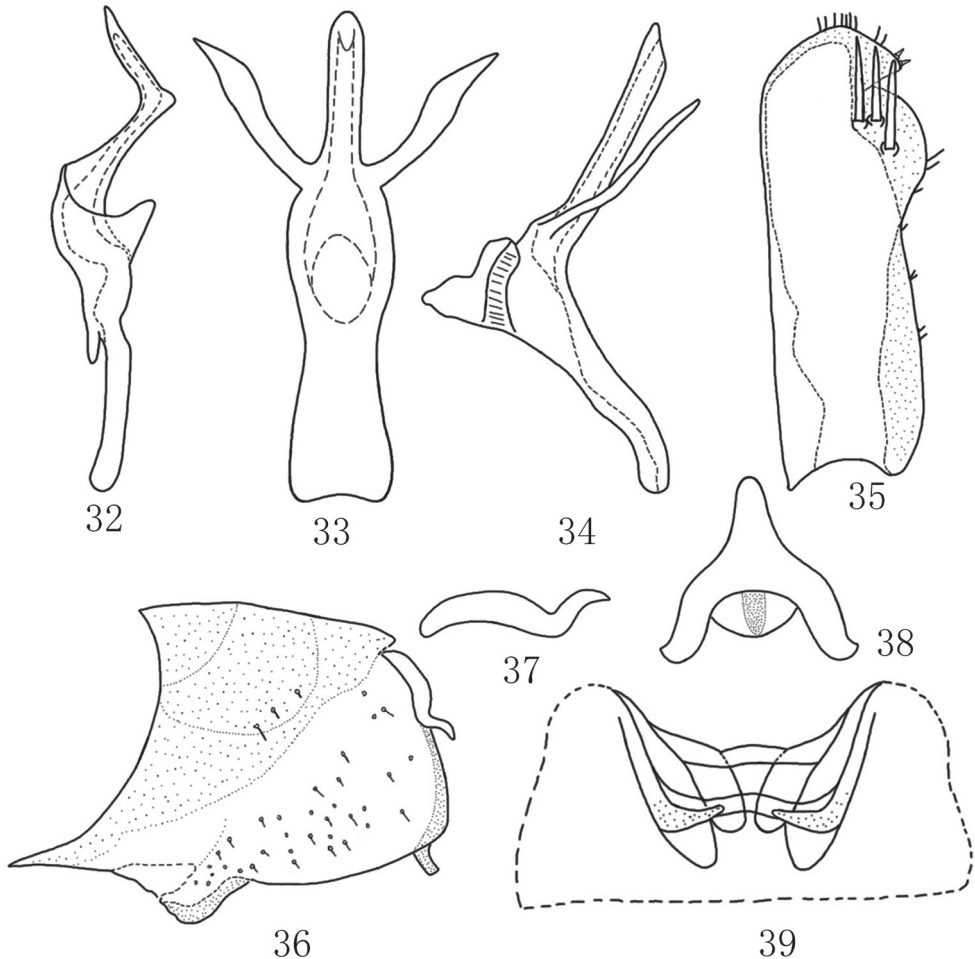
Second abdominal apodemes and third abdominal apodemes small and short, lamellate, not exceeded 3rd sternite (Fig. 39).

Male genitalia. Pygofer dorsal appendage simple, curved upward in lateral view, hook-like apically (Fig. 37). Pygofer lobe broad, with many long fine setae on lateral surface, with a small process at caudal edge ventrally (Fig. 36). Subgenital plate long, with three macrosetae near apex (Fig. 35). Style apex long and slender; preapical lobe large (Fig. 32). Aedeagal shaft slender, with pair of long processes arising from base (Figs 33, 34). Connective Y-shaped; stem slender; arms and central lobe well developed (Fig. 38).

Body length (including wings). ♂, 3.0–3.1 mm, ♀, 2.9–3.0 mm.

Remarks. The new species is similar to *M. protuberanta* Song, Li & Xiong, 2011, but differs in having the “lamellate” processed arising from base of aedeagal shaft and not branched at apex; with two pairs of abdominal apodemes.

Etymology. The new species is named after its type locality Salaxi town.



Figures 32–39. *Mitjaevia salaxia* sp. nov. **32** style **33** aedeagus, ventral view **34** aedeagus, lateral view **35** subgenital plate **36** male pygofer, lateral view **37** pygofer dorsal appendage, lateral view **38** connective **39** abdominal apodemes.

Discussion

In recent years, most research on Chinese Erythroneurine leafhoppers has been intensified and focused to enrich the taxonomic knowledge of this tribe and taxonomists have paid attention to documenting taxa using efficient descriptions, high-quality drawings, and photographs. The Guizhou province is located on the eastern slope of the Yunnan–Guizhou Plateau in southwestern China and has a particularly subtropical humid monsoon climate with four distinct seasons, abundant rainfall, seasonal temperature variations and high vegetation coverage, which is conducive to the survival and reproduction of leafhoppers. Since establishment of this genus, 19 species of *Mitjaevia* have been described worldwide, and more than half of valid species were

found in China. Here, a comparison revealed that three new species shared similarities with already known species but differences were found, for example, the aedeagal shaft of *M. bijiensis* sp. nov. and *M. diana* have apical processes, but *M. bijiensis* sp. nov. dispose processes arising from preatrium of aedeagus, while *M. diana* shows another processes at base of aedeagal shaft. *Mitjaevia. solitaria* sp. nov. and *M. aurantiaca* also have a single process at base of aedeagal shaft, not paired. Moreover, the subgenital plate is short and wide but in latter species it is long or thin. *Mitjaevia. salaxia* sp. nov. is similar to *M. protuberanta* but differs in having lamellate-like processes arising from the base of aedeagal shaft and not branched at apex.

Acknowledgements

We thank Mick Webb for checking and revising the manuscript. This study was partly funded by the World Top Discipline Program of Guizhou Province: Karst Ecoenvironment Sciences (No.125 2019 Qianjiao Keyan Fa), the Guizhou Provincial Science and Technology Foundation ([2018]1411), the Guizhou Science and Technology Support Project ([2019]2855), the Science and Technology Project of Guiyang City ([2020]7–18), the Innovation Group Project of Education Department of Guizhou Province ([2021]013) and the National Natural Science Foundation of China (32260120).

References

- Chen XX, Song YH, Webb MD (2020) Two new species of the leafhopper genus *Mitjaevia* Dworakowska from China (Hemiptera, Cicadellidae, Typhlocybinae). *ZooKeys* 964(1): 31–40. <https://doi.org/10.3897/zookeys.964.48655>
- Chiang CC, Knight WJ (1990) Studies on taiwanese Typhlocybinae (Homoptera: Cicadellidae) (IV) tribe Erythroneurini. *Bulletin of the National Museum of Natural Science* 2: 191–255.
- Dietrich CH (2005) Keys to the families of Cicadomorpha and subfamilies and tribes of Cicadellidae (Hemiptera: Auchenorrhyncha). *The Florida Entomologist* 88(4): 502–517. [https://doi.org/10.1653/0015-4040\(2005\)88\[502:KTTFOC\]2.0.CO;2](https://doi.org/10.1653/0015-4040(2005)88[502:KTTFOC]2.0.CO;2)
- Dlabola J (1961) Zikaden von Zentralasien, Dagestan und Transkaukasien (Homopt. Auchenorrhyncha). *Acta Entomologica Musei Nationalis Pragae* 34: 241–358.
- Dmitriev D (2020) An online interactive key and searchable database of Auchenorrhyncha (Hemiptera). <http://dmitriev.speciesfile.org/>
- Dworakowska I (1970) On the genera *Asianidia* Zachv. and *Singapora* Mahm. with the description of two new genera (Auchenorrhyncha, Cicadellidae, Typhlocybinae). *Bulletin de l'Académie Polonaise des Sciences, Série des Sciences Biologiques* 18(12): 759–765.
- Dworakowska I (1979) On some Erythroneurini from Vietnam (Typhlocybinae, Cicadellidae). *Annotationes Zoologicae et Botanicae* 131: 1–50.

- Dworakowska I (1980) On some Typhlocybinæ from India (Homoptera, Auchenorrhyncha, Cicadellidae). *Entomologische Abhandlungen Staatliches Museum Für Tierkunde in Dresden* 43(8): 151–201. <https://doi.org/10.1515/9783112653227-010>
- Luo GM, Song QF, Song YH (2021) Two new species of the leafhopper genus *Mitjaevia* Dworakowska from China (Hemiptera, Cicadellidae, Typhlocybinæ). *Biodiversity Data Journal* 9: e72420. <https://doi.org/10.3897/BDJ.9.e72420>
- Mitjaev ID (1969) New species of leaf-hoppers (Homoptera, Cicadinea) from Tien Shan and Karatau. *Zoologicheskii Zhurnal* 48(7): 1041–1047.
- Song YH, Li ZZ (2013) Two new species of *Empoasca* Distant (Hemiptera: Cicadellidae: Typhlocybinæ) from Yunnan Province, China. *Zootaxa* 3637(1): 089–093. <https://doi.org/10.11646/zootaxa.3637.1.11>
- Song YH, Li ZZ (2014) Erythroneurini and Zyginellini from China (Hemiptera: Cicadellidae: Typhlocybinæ). *Science and Technology Publishing House, Guiyang*, 12–209.
- Song YH, Li ZZ, Xiong KN (2011) Two new species of the genus *Mitjaevia* Dworakowska from China (Hemiptera: Cicadellidae: Typhlocybinæ). *Zootaxa* 2805(1): 26–30. <https://doi.org/10.11646/zootaxa.2805.1.2>

The genus *Japonitata* Strand (Insecta, Coleoptera, Chrysomelidae, Galerucinae) in Taiwan: a redefinition of the genus and descriptions of two new species

Chi-Feng Lee¹

¹ *Applied Zoology Division, Taiwan Agricultural Research Institute, Taichung 413, Taiwan*

Corresponding author: Chi-Feng Lee (chifeng@tari.gov.tw)

Academic editor: A. Konstantinov | Received 19 August 2022 | Accepted 6 October 2022 | Published 26 October 2022

<https://zoobank.org/1828511F-A492-4A3C-83CB-E1956E4807B4>

Citation: Lee C-F (2022) The genus *Japonitata* Strand (Insecta, Coleoptera, Chrysomelidae, Galerucinae) in Taiwan: a redefinition of the genus and descriptions of two new species. ZooKeys 1125: 171–192. <https://doi.org/10.3897/zookeys.1125.93703>

Abstract

The genus *Japonitata* is redefined based on comparison with its allied genera *Paraplotes* Laboissière, 1933 and *Shairella* Chùjò, 1962. *Japonitata quadricostata* Kimoto, 1996 and *J. caerulea* Kimoto, 1996 are transferred to *Shairella*. *Japonitata houjayi* **sp. nov.** and *J. jungchani* **sp. nov.** are described. Biological information is provided for *J. houjayi* **sp. nov.** In addition, the generic boundary of *Shairella* is redefined by including *S. quadricostata* and *S. caerulea*.

Keywords

Host plant, leaf beetles, new combination, nomenclature, *Paraplotes*, *Shairella*, taxonomy

Introduction

Weise (1922) described a new genus, *Japonia* Weise, 1922, based on the species *Phyllobrotica nigrita* Jacoby, 1886. However, *Japonia* a junior homonym of a snail genus (Gould 1859). A replacement name, *Japonitata*, was proposed by Strand (1935). This genus is composed more than 30 species in the Oriental and Palearctic regions (Nie et al. 2017). Most species (90%) were described after 1980 and 60% were described from

China (Kimoto 1970, 1996, 2004; Chen and Jiang 1981, 1986; Jiang 1989; Yang 1992; Yang et al. 1997; Medvedev and Sprecher-Uebersax 1998, 1999; Yang and Li 1998; Medvedev 2012). Although most species were described during the past 50 years, none or few morphological characters were illustrated or included in species descriptions.

In Taiwan, only two species were described by Kimoto (1996), with no additional information provided since then. The Taiwan Chrysomelid Research Team (TCRT) was founded in 2005 and is composed of ten members. All of them are amateurs interested in producing a complete inventory of chrysomelid species in Taiwan. Members of TCRT have collected sufficient material of the two Taiwanese species of *Japonitata* to allow their biology to be explored. These two species are different not only in color forms (red vs. black) and behavior (diurnal vs. nocturnal), but also in morphology. Nocturnal species shows great similarity to species of *Shairella* Chûjô, 1962. Two more species are now available for study with help from citizen scientists and loans from museums. In addition, *Japonitata* Strand is similar to *Paraplotes* Laboissière and some species of both genera have been confused. For example, *J. clavata* Yang & Wu, 1998 is a junior synonym of *P. clavicornis* Gressitt & Kimoto, 1963 and *P. rugatipennis* (Chen & Jiang, 1986) was transferred from *Japonitata* by Zhang et al. (2008); *J. indica* (Taki-zawa & Basu, 1987) was transferred from *Paraplotes* by Medvedev (2002). Diagnostic characters proposed by Zhang et al. (2008) for both genera are evaluated here. In this study, besides describing new species and redescribing known species, the taxonomic status of these is evaluated by redefining the genus *Japonitata* and its allied genera, *Paraplotes* and *Shairella*.

Materials and methods

For taxonomic study, the abdomens of adults were separated from the forebodies and boiled in 10% KOH solution, followed by washing in distilled water to prepare genitalia for illustrations. The genitalia were then dissected from the abdomens, mounted on slides in glycerin, and studied and drawn using a Leica M165 stereomicroscope. For detailed examinations a Nikon ECLIPSE 50i microscope was used.

At least three pairs from each species were examined to delimit variability of diagnostic characters. For species collected from more than one locality, at least one pair from each locality was examined. Length was measured from the anterior margin of the eye to the elytral apex, and width at the greatest width of the elytra.

Specimens studied herein are deposited at the following institutes and collections:

- NMNS** National Museum of Natural Science, Taichung, Taiwan [Jing-Fu Tsai]
- OMNH** Osaka Museum of Natural History, Osaka, Japan [Shunpei Fujie]
- SEHU** Laboratory for Systematic Entomology, Hokkaido University, Sapporo, Japan [Masahiro Ohara]
- TARI** Applied Zoology Division, Taiwan Agricultural Research Institute, Taichung Taiwan

Exact label data are cited for all type specimens of described species; a double slash (//) divides the data on different labels and a single slash (/) divides the data in different rows. Other comments and remarks are in square brackets: [p] – preceding data are printed, [h] – preceding data are handwritten, [w] – white label, [y] – yellow label, and [r] – red label.

For redefining the genus *Japonitata*, specimens of the type species, *J. nigrita*, were studied: 1♀ (OMNH), 春日山, Nara Pref., 11.VI.1968, leg. O. Tominaga; 1♀ (OMNH), Hirakura, Mie Univ. Forest, 7.VII.1954, leg. Z. Naruse.

Taxonomy

Japonitata Strand, 1935

Japonia Weise, 1922: 70 (Type species: *Phyllobrotica nigrita* Jacoby, 1885).

Japonitata Strand, 1935: 294 (replacement name for *Japonia* Weise, 1922 nec Gould, 1859).

Diagnosis. *Japonitata* can be separated from *Paraplotes* by the presence of posteriorly open anterior coxal cavities (closed in *Paraplotes*); pronotum longer, 1.5–1.7 × wider than long (pronotum short, 2.4–2.9 × wider than long in *Paraplotes*), basal border immarginate (basal border margined in *Paraplotes*); disc with lateral depressions (disc with transverse depressions in *Paraplotes*); disc of elytra with reduced punctures (disc of elytra with fine or coarse punctures in *Paraplotes*), with one more longitudinal ridge in addition to lateral ridge. Other characters proposed by Zhang et al. (2008) are not diagnostic. Antennae are variable among *Paraplotes* species. For example, ratios of length to width from antennomeres I–XI of males of *P. taiwana* Chûjô, 1963: 3.2: 1.6: 2.4: 2.8: 2.8: 2.1: 2.3: 2.2: 2.9: 3.1: 4.6; antennomeres VI–VIII much shorter than those of *J. jungchani* sp. nov., but much narrower in those of *P. cheni* Lee, 2015 (sympatric with *P. taiwana*), ratios of length to width from antennomeres I–XI of males 3.3: 1.6: 3.1: 3.3: 3.5: 3.1: 3.4: 3.7: 3.6: 3.9: 5.0. These characters are not diagnostic for either genus. The rugose or pubescent disc of the elytra occurs in some species of *Paraplotes*. Thus, it is not diagnostic. Appendiculate tarsal claws occur in both genera, with no difference between them. Some genitalic characters are diagnostic. Aedeagi of adults of *Japonitata* have a well sclerotized, elongate tectum (variable tectum with one pair of apico-lateral sclerites in *Paraplotes*), lacking endophallic spicula (with one long median spiculum, and one or two additional pairs of lateral spicula in *Paraplotes*); spermathecal receptaculum as wide as pump (spermathecal receptaculum swollen, wider than pump in *Paraplotes*).

Japonitata species are also similar to those of *Shairella* with the lateral borders of pronotum marginate but apical and basal borders unmarginated. However, *Japonitata* differs from *Shairella* by the posteriorly open anterior coxal cavities (closed in *Shairella*); robust antennae, antennomeres IV–X less than 3.5 × longer than wide (antenna slender,

Table 1. Diagnostic character states for *Japonitata*, *Paraplotes*, and *Shairella*.

Characters / Genera	<i>Japonitata</i>	<i>Paraplotes</i>	<i>Shairella</i>
Antennae	Robust, antennomeres VI–X less than 4.0 × longer than wide	Robust, antennomeres VI–X less than 4.0 × longer than wide	Slender, antennomeres VI–X less than 4.0 × longer than wide
Anterior coxal cavities	Open posteriorly	Closed	Closed
Basal border of pronotum	Unmargined	Margined	Unmargined
Depression on pronotum	Interrupted from middle	Continuous	Interrupted from middle
Shape of pronotum	1.5–1.7 × wider than long	Short, transverse, 2.4–2.9 × wider than long	1.8–2.2 × wider than long
Ridges on elytra	Lateral ridge distinct, with one more longitudinal, distinct ridge	Lateral ridge distinct, no additional longitudinal ridges	Lateral ridge weak, without additional longitudinal ridges
Punctures on elytra	Reduced	Fine or coarse	Reduced or fine
Median internal ridge on abdominal ventrite V in males	Starting from base	Reduced	Starting from apex
Tectum of aedeagus	Well sclerotized, elongate	Variable, and with one pair of apico-lateral sclerites	Membranous
Endophallic sclerites	None	One median, longitudinal spiculum without clustered short setae, and one or two pairs of lateral sclerites	Only one median, longitudinal spiculum with clustered short setae
Spermathecal receptaculum	Swollen and short, wider than pump	Narrow and short, as wide as pump	Narrow and long, as wide as pump
Behavior	Diurnal	Nocturnal or Diurnal	Nocturnal

antennomeres IV–X more than 3.5 × longer than wide in *Shairella*), with distinct lateral ridges and an additional longitudinal, distinct ridge on each elytron (with weak lateral ridge and no additional distinct ridge on each elytron in *Shairella*). Aedeagi of adults of *Japonitata* have a well sclerotized, elongate tectum (membranous tectum in *Shairella*); lack endophallic spicula (with one slender median speculum in *Shairella*); spermathecal receptaculum short, wider than pump (spermathecal receptaculum long, as wide as pump in *Shairella*). Diagnostic characters of *Japonitata*, *Paraplotes*, and *Shairella* can be summarized as follows (Table 1).

Remarks. *Japonitata quadricostata* Kimoto, 1996 and *J. caerulea* Kimoto, 1996 are transferred to *Shairella* since both species fit the redefinition of the genus. They are characterized by normal elytra. Shortened elytra and reduced hindwings occur in all other species of *Shairella*; however, reduced hindwings also occur in some populations of *S. quadricostata*.

Included species. More than 30 species are distributed in Oriental and Palaearctic regions (Nie et al. 2017) but their taxonomic status should be re-evaluated since two species are transferred to *Shairella*, and others may also require transfer.

Japonitata boujayi sp. nov.

<https://zoobank.org/68D59E89-7532-41EA-AB82-B493814CD51B>

Figs 1A–C, 2, 3

Types. *Holotype* ♂ (TARI). Taipei, Shihtzutoukeng (獅子頭坑), 300 m, 1.V.2010, leg. H.-J. Chen. *Paratypes*: 1♂, 5♀ (TARI), same data as holotype; 4♂, 1♀ (TARI), same but with “4.V.2010”; 4♂, 3♀ (TARI), same but with “8.V.2010”; 1♂, 1♀ (TARI),

same but with “26.V.2010”; 3♂, 4♀ (TARI), same but with “28.V.2010”; 3♂ (TARI), same but with “leg. H. Lee”; 1♂ (TARI), same locality, 25.IV.2012, leg. H.-J. Chen.

Description. Length 5.5–6.6 mm, width 2.7–3.4 mm. General color (Fig. 1A–C) reddish brown; antennae black; legs dark brown. Antennomeres II–XI filiform but stout in males (Fig. 2A), ratios of lengths of antennomeres I–XI 1.0: 0.4: 0.7: 0.9: 0.8: 0.8: 0.8: 0.8: 0.7: 0.7: 0.8; ratios of length to width from antennomeres I–XI 2.5: 1.5: 1.9: 2.7: 2.5: 2.5: 2.5: 2.5: 2.4: 2.4: 3.5; stout antennae in males similar in females

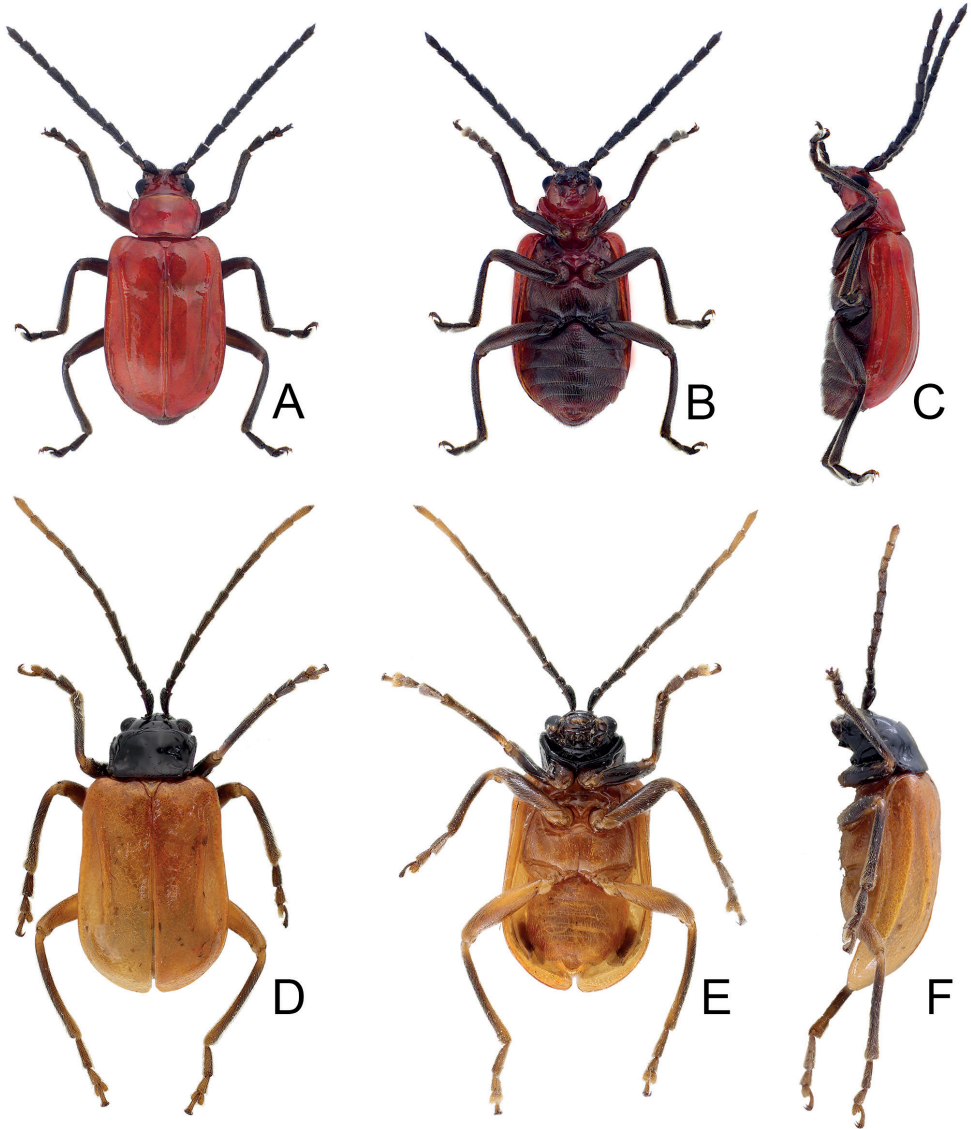


Figure 1. Habitus of *Japonitata houjayi* sp. nov. and *J. jungchani* sp. nov. **A** *J. houjayi* sp. nov., male, dorsal view **B** ditto, ventral view **C** ditto, lateral view **D** *J. jungchani* sp. nov., male, dorsal view **E** ditto, ventral view **F** ditto, lateral view.

(Fig. 2B), ratios of lengths of antennomeres I–XI 1.0: 0.4: 0.6: 0.8: 0.8: 0.7: 0.8: 0.7: 0.7: 0.6: 0.8; ratios of length to width from antennomeres I–XI 2.5: 1.5: 2.0: 2.5: 2.4: 2.3: 2.5: 2.4: 2.6: 2.3: 2.9. Pronotum 1.6–1.7 × wider than long; disc with scarce, fine punctures at sides, reduced medially, with transverse groove near base, medially

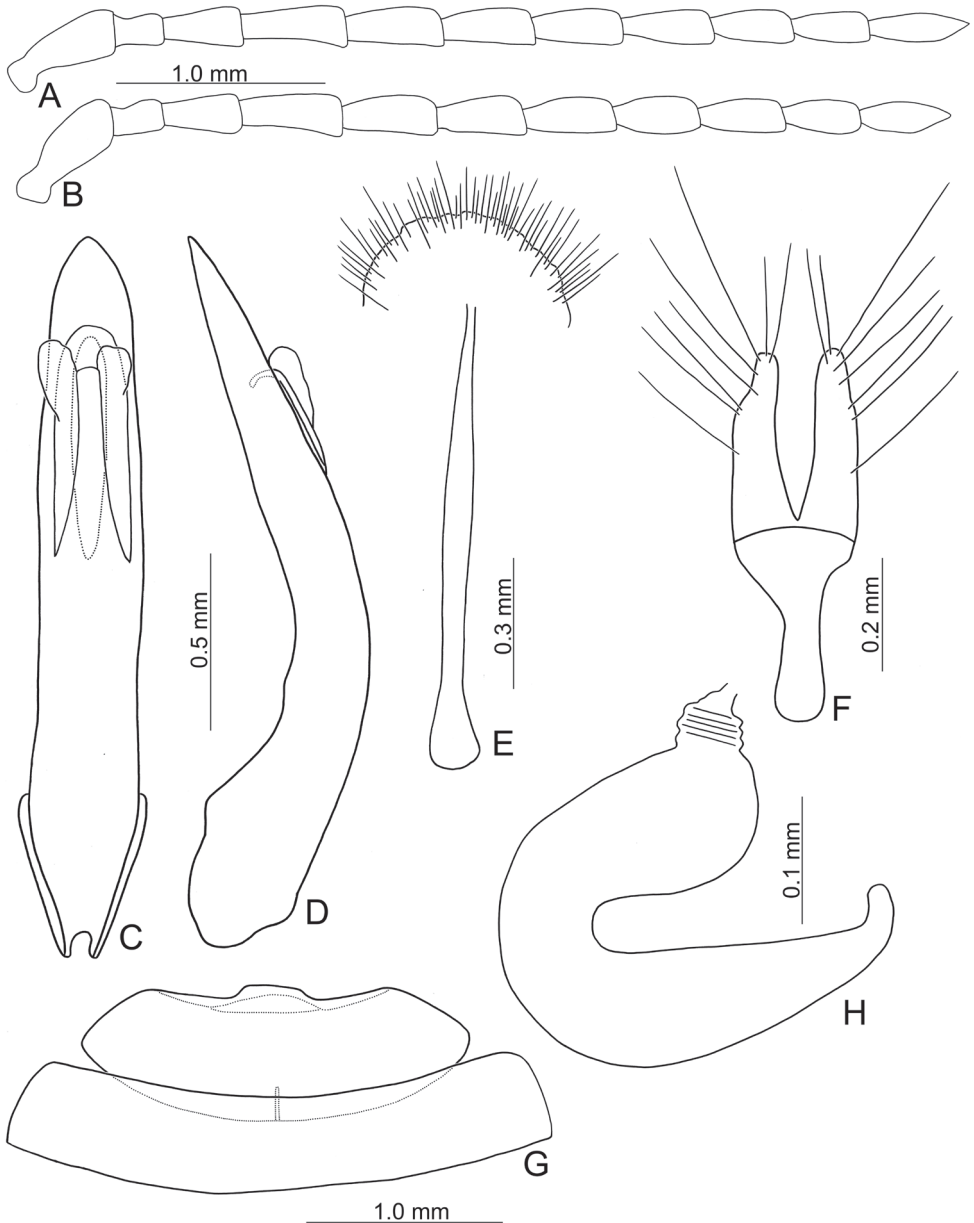


Figure 2. Diagnostic characters of *Japonitata houjayi* sp. nov. **A** antenna, male **B** antenna, female **C** aedeagus, dorsal view **D** ditto, lateral view **E** abdominal ventrite VIII **F** gonocoxae **G** abdominal ventrite IV–V, male **H** spermatheca.

abbreviated, laterally connected with short longitudinal groove on basal margin; lateral margins slightly rounded, widest behind apices; apical margin slightly concave and basal margin slightly convex. Elytra $1.5 \times$ longer than wide; disc with confused, dense, reduced punctures; with one small tubercle behind scutellum; with one distinct longitudinal ridge from humeral calli, parallel with lateral margin, abbreviated subapically; with one additional ridge also from humeral calli, distinct, directed medially; lateral margins moderately rounded, widest at apical third, apices convergent. Aedeagus (Fig. 2C, D) extremely slender, $7.5 \times$ longer than wide; parallel-sided, slightly narrowed at apical $1/4$, strongly narrowed subapically, apex narrowly rounded; moderately curved at basal $1/3$ in lateral view; tectum slender, longitudinal, apex recurved; no endophallic sclerites. Apical margin of abdominal ventrite V in males with distinct,

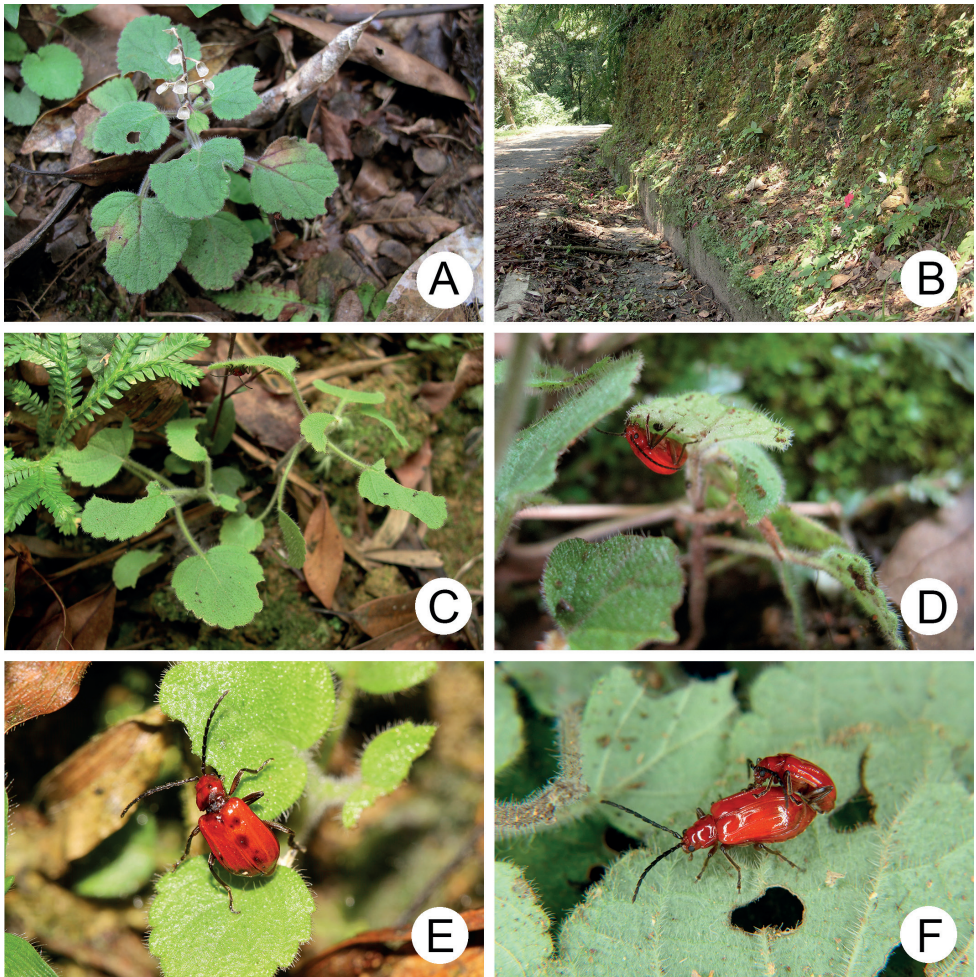


Figure 3. Field photographs of *Japonitata boujayi* sp. nov. **A** host plant, *Scutellaria indica* **B** population of *Scutellaria indica* growing on the slope along a road **C** adult resting on underside of leaf **D** close-up of adult **E** adult feeding on leaf **F** adults mating on a leaf.

narrow median lobe (Fig. 2G), apical margin slightly recurved, with short median internal ridge at middle of basal margin, from basal fourth to base; basal margin normal. Gonocoxae (Fig. 2F) longitudinal and connected basally, with narrow furrow between gonocoxae; each gonocoxa narrowed subapically, apex narrowly rounded, with eight long apical setae; base strongly sclerotized and narrow. Ventricle VIII (Fig. 2E) in females with apex weakly sclerotized, small, apical margin irregular; with dense short apical setae; spiculum extremely elongate. Spermathecal receptaculum (Fig. 2H) swollen, not delimited from pump; pump long and curved, with apical process curved; sclerotized spermathecal duct extremely short, not separated from receptaculum.

Diagnosis. Adults of *J. houjayi* sp. nov. are similar to those of *J. ruficollis* Jiang, 1989 from China (Xizang) with reddish brown bodies, but differ in possessing black antennae and dark brown legs (yellow antenna with one or two apical antennomeres black, and reddish brown legs in *J. ruficollis*).

Host plant. *Scutellaria indica* L. (Lamiaceae).

Biology. *Scutellaria indica* is a small herbaceous plant (Fig. 3A) growing on slopes along roads (Fig. 3B). Adults appear only during May, usually resting on the undersides of leaves during daytime (Fig. 3C, D). Adults feed on the leaves (Fig. 3E) and were observed mating (Fig. 3F) occasionally.

Etymology. The new species name is dedicated to Mr. Hou-Jay Chen (陳厚潔), the first team member to find the habitat and collect type specimens.

Distribution. This new species is known only from the type locality.

Japonitata jungchani sp. nov.

<https://zoobank.org/9E6F19B8-0E5B-4E46-B346-2E2F8962A2C4>

Figs 1D–F, 4

Types. *Holotype* ♂ (TARI), Pingtung, Tahanshan (大漢山), 1450 m, 12.IV.2020, leg. Y.-T. Chung. *Paratypes.* 1♀ (TARI), same locality, 4.IV.2010, leg. K.-D. Ho; 1♀ (TARI), same locality (= Jinshuiying 浸水營), 6.VI.2011, leg. J.-C. Chen; 1♂ (TARI), same but with “22.V.2012”; 1♀ (TARI), Taitung, Lichia trail (利嘉林道), 1000 m, 10.V.2018, leg. B.-X. Guo.

Description. Length 5.8–6.3 mm, width 3.1–3.3 mm. General color (Fig. 1D–F) reddish brown; head and prothorax black; legs dark brown. Antennomeres II–XI filiform but stout in males (Fig. 4A), ratios of lengths of antennomeres I–XI 1.0: 0.4: 0.6: 0.8: 0.8: 0.8: 0.8: 0.8: 0.8: 0.7: 0.8; ratios of length to width from antennomeres I–XI 2.5: 1.7: 2.1: 2.8: 2.6: 2.9: 2.9: 3.2: 3.2: 3.1: 3.9; stout antennae in males similar in females (Fig. 4B), ratios of lengths of antennomeres I–XI 1.0: 0.4: 0.5: 0.8: 0.8: 0.8: 0.8: 0.7: 0.7: 0.7: 0.8; ratios of length to width from antennomeres I–XI 2.7: 1.6: 2.0: 3.0: 3.1: 3.0: 3.1: 3.1: 3.2: 2.9: 4.0. Pronotum 1.5–1.6 × wider than long; disc with scarce, fine punctures at sides, reduced medially, with transverse groove near base, medially abbreviated, laterally connected with short longitudinal groove on basal margin; lateral margins slightly rounded, widest behind apices; apical margin slightly concave and

basal margin slightly convex. Elytra $1.4 \times$ longer than wide; disc with confused, dense, fine punctures; with one small tubercle behind scutellum; with one distinct longitudinal ridge from humeral calli, parallel with lateral margin, abbreviated subapically; with

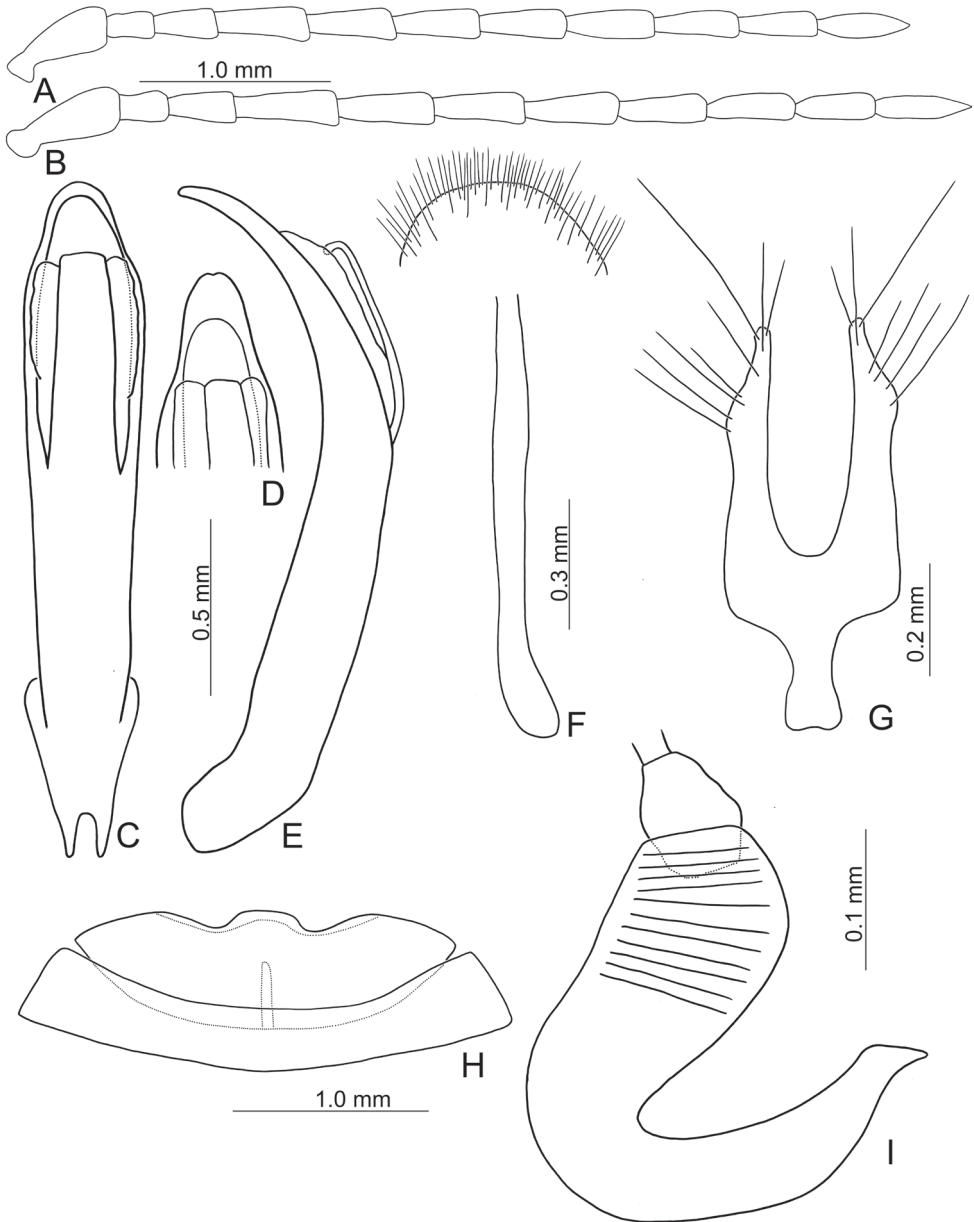


Figure 4. Diagnostic characters of *Japonitata jungchani* sp. nov. **A** antenna, male **B** antenna, female **C** aedeagus, dorsal view **D** apex of aedeagus, front view **E** aedeagus, lateral view **F** abdominal ventrite VIII **G** gonocoxae **H** abdominal ventrite IV–V, male **I** spermatheca.

one additional ridge also from humeral calli, distinct, directed medially; lateral margins moderately rounded, widest at apical third, apices divergent. Aedeagus (Fig. 4C–E) extremely slender, $6.4 \times$ longer than wide; widest at apical $1/6$, gradually narrowed toward base, moderately narrowed at apical $1/6$, apex widely rounded, slightly and medially depressed; strongly, apically curved in lateral view; tectum wide, longitudinal, apex recurved; no endophallic sclerites. Apical margin of abdominal ventrite V in males with distinct median lobe (Fig. 4H) narrow, apical margin slightly recurved, with long median internal ridge at middle of basal margin, from base to middle; basal margin normal. Gonocoxae (Fig. 4G) longitudinal and connected basally, with narrow furrow between gonocoxae; each gonocoxa narrowed subapically, apex narrowly rounded, with eight long apical setae; base weakly sclerotized and narrow. Ventrite VIII (Fig. 4F) in females with apex weakly sclerotized, small, apical margin slightly irregular; with dense short apical setae; spiculum extremely elongate. Spermathecal receptaculum (Fig. 4I) swollen, not separated from pump; pump long and curved, with apical process curved; sclerotized spermathecal duct extremely short, separated from receptaculum.

Diagnosis. This new species is similar to *J. bipartita* Chen & Jiang, 1986 from China (Shaanxi and Fujian) with reddish brown body and black head and prothorax. It differs in having black antenna with the three apical antennomeres reddish brown, and dark brown fore and middle legs.

Host plant and biology. Unknown, but one adult was collected by sweeping flowers.

Etymology. The new species name is dedicated to Mr. Jung-Chan Chen (陳榮章), the first person to collect type specimens.

Distribution. South Taiwan including Pingtung and Taitung counties.

***Shairella quadricostata* (Kimoto, 1996), comb. nov.**

Figs 5–8

Japonitata quadricostata Kimoto, 1996: 34 (Taiwan).

Type examined. Holotype ♀ (OMNH) (Fig. 5A–C): “FUNCHIIHU (奮起湖) / TAIWAN / 28.VII.1974 / Y. KIYOYAMA [p, y] // HOLOTYPE [p, r] / Japonitata / quadricostata / Kimoto, n. sp. [h] / Det. S. Kimoto, 19 [p, w] // PHOTO [p, r]”.

Specimens examined. Chiayi: 28♂, 11♀ (TARI), Erhwanping (二萬坪), 2000 m, near Alishan (阿里山), 9.VII.2014, leg. C.-F. Lee & T.-H. Lee; 1♂ (TARI), Alishan (阿里山), 17.VIII.2014, leg. B.-X. Guo; **Ilan:** 1♂ (TARI), Chiuchihtse (鳩之澤), 520 m, 2.V.2007, leg. M.-H. Tsou; 1♂ (TARI), Eboshiyama (= Tulishan 獨立山), 1900 m, 17–21.V.1933, leg. M. Chujo; **Kaohsiung:** 1♂, 1♀ (TARI), Tengchih (藤枝), 1600 m, 24.VIII.2017, leg. B.-X. Guo; 1♂ (TARI), same but with “4.IX.2017”; 1♀ (TARI), same but with “15.IX.2019”; 3♂ (TARI), same locality, 11.V.2022, leg. Y.-T. Chung; **Nantou:** 2♀ (TARI), Fenghuangshan (鳳凰山), 1700 m, near Hsitou (溪頭), 12.VIII.2010, leg. Y.-T. Wang; 1♂ (TARI), Hsitou (溪頭), 1000 m, 14.VI.2011, leg. C.-F. Lee; 4♀ (TARI), same locality, 2.VII.2011, leg. M.-H. Tsou; 1♂, 1♀ (TARI),

same but with “9.VIII.2011”; **Pingtung:** 1♂ (TARI), Peitawushan (北大武山), New Trailhead (新登山口), 1200 m, 28.IX.2017, leg. Y.-T. Chung; 1♂ (TARI), same but with “10.V.2022”; 1♂ (TARI), Shuangliu (雙流), 500 m, 6.VI.2000, leg. H.-T. Shih; **Taichung:** 1♀ (TARI), Fengyuan (豐原), 280 m, 22.V.2019, leg. C.-T. Hsu; 1♂ (TARI), Henglingshan (橫嶺山), Trailhead (登山口), 1200 m, 10.X.2020, leg. Y.-C. Hsu; **Taipei:** 1♂ (TARI), Manyuehuan (滿月圓), 300 m, 7.VI.2010, leg. C.-L. Chiang; 1♀ (TARI), Wulai (烏來), 150 m, 24.V.2007, leg. H.-J. Chen; 1♂, 1♀ (TARI), same locality (= Hsinhsien 信賢), 3.V.2014, leg. M.-H. Tsou.

Redescription. Length 6.1–7.7 mm, width 3.1–4.4 mm. General color (Fig. 5D–F) black to dark brown; abdomen yellow to dark brown; five apical antennomeres variably paler. Antennomeres II–XI filiform in males (Fig. 6A), ratios of lengths of antennomeres I–XI 1.0: 0.3: 0.7: 0.9: 0.8: 0.8: 0.8: 0.8: 0.8: 0.7: 0.9; ratios of length to width from antennomeres I–XI 2.8: 1.6: 2.8: 3.8: 4.0: 4.2: 4.5: 4.9: 4.9: 4.8: 6.3; more slender in females (Fig. 6B), ratios of lengths of antennomeres I–XI 1.0: 0.3: 0.6: 0.9: 0.8: 0.8: 0.8: 0.8: 0.8: 0.8: 0.8; ratios of length to width from antennomeres I–XI 3.4: 1.6: 2.9: 4.1: 4.1: 4.9: 5.2: 5.5: 6.1: 6.0: 6.5. Pronotum 1.8–2.0 times wider than long; disc with scarce fine punctures at sides, reduced medially, with transverse groove near base, medially abbreviated, laterally connected with short longitudinal groove on basal margin; lateral margins slightly rounded, widest behind apices; apical margin slightly concave and basal margin slightly convex. Elytra narrower, 1.3–1.4 times longer than wide; disc with confused, sparse, reduced punctures; with one small tubercle behind scutellum; with one longitudinal ridge behind tubercle, indistinct, close to suture; with one additional longitudinal ridge outside tubercle, indistinct; with one additional distinct ridge from humeral calli, parallel with lateral margin, abbreviated subapically; another additional ridge also from humeral calli, indistinct, directed medially; lateral margins moderately rounded, widest at apical third, apices convergent. Aedeagus (Fig. 6C, D) slender, 5.9 × longer than wide; lateral margins straight, widest at apical 1/10, gradually narrowed toward basal 1/3; strongly narrowed subapically, apex acute; moderately curved in lateral view; tectum membranous; one endophallic sclerite longitudinally oriented and slender, 0.6 × as long as aedeagus, base deeply bifurcate, lateral margins with clustered short setae at apical 1/3. Apical margin of abdominal ventrite V in males with distinct median lobe (Fig. 6K), narrow, apical margin slightly recurved, with median internal ridge from apex to middle; basal margin normal. Gonocoxae (Fig. 6G) longitudinal and connected basally, with wide furrow between gonocoxae; each gonocoxa narrowed subapically, apex truncate, with eight long apical setae; base weakly sclerotized. Ventrite VIII (Fig. 6E) in females with apex weakly sclerotized, dense short apical setae, reduced medially; spiculum extremely elongate. Spermathecal receptaculum (Fig. 6H) slender, as wide as pump, not separated from pump; pump long and curved, with one short, apical process; sclerotized spermathecal duct short, not separated from receptaculum.

Variations. Some distinct variation occurs in female genitalic characters among different populations. Pumps of spermathecae are larger in those of Wulai (烏來) (Fig. 6I); much slender and lacking apical process in those of Erhwanping (二萬坪) (Fig. 6J). Apices of ventrite VIII are wider and setae not reduced medially in those of

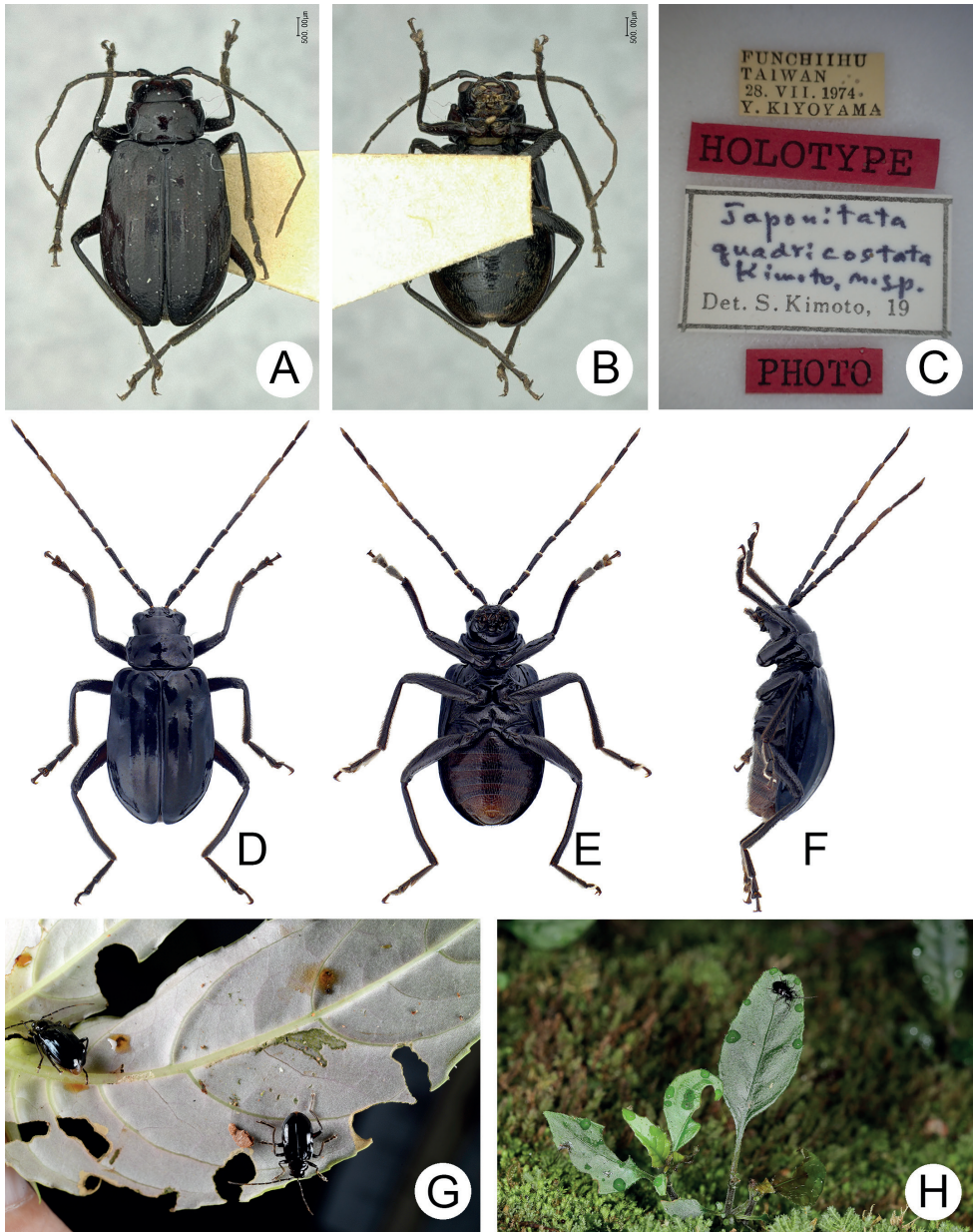


Figure 5. Habitus and field photographs of *Shairella quadricostata* (Kimoto) **A** holotype, female, dorsal view **B** ditto, lateral view **C** labels on the holotypes **D** nontype, male, dorsal view **E** ditto, ventral view **F** ditto, lateral view **G** two adults collected at Tengchih (藤枝) and feeding on leaves of *Hemiboea bicornuta* **H** adult resting on leaves of *Hemiboea bicornuta* in Erhwanping (二萬坪).

Wulai (烏來). Hindwings are normal in northern and central Taiwan and low-elevations of southern Taiwan (Fig. 7A), but they are reduced in different degrees between different populations of mid-elevations of southern Taiwan. Degree of reduction of

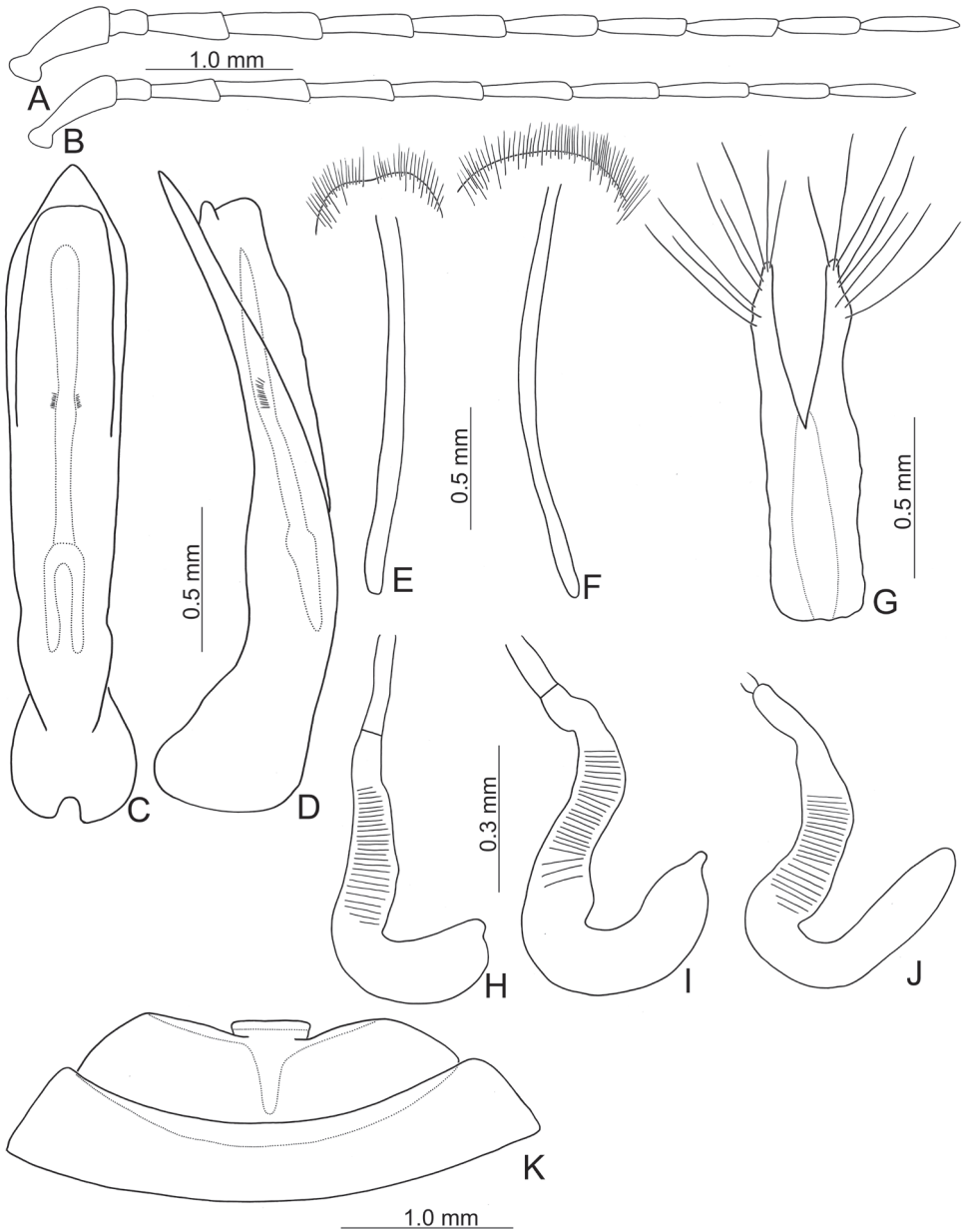


Figure 6. Diagnostic characters of *Shairella quadricostata* (Kimoto) **A** antenna, male **B** antenna, female **C** aedeagus, dorsal view **D** ditto, lateral view **E** abdominal ventrite VIII, from Erhwanping (二萬坪) **F** same, from Wulai (烏來) **G** gonocoxae **H** spermatheca, from Tengchih (藤枝) **I** same from Wulai (烏來) **J** same from Erhwanping (二萬坪) **K** abdominal ventrite IV-V, male.

hind wings is similar between individuals of both sexes of the same populations. Those in Tengchih (藤枝) are less reduced, ~ 57% with normal hind wings (Fig. 7B). Those in Hsito (溪頭) are reduced moderately, ~ 50% with normal hind wings (Fig. 7D).

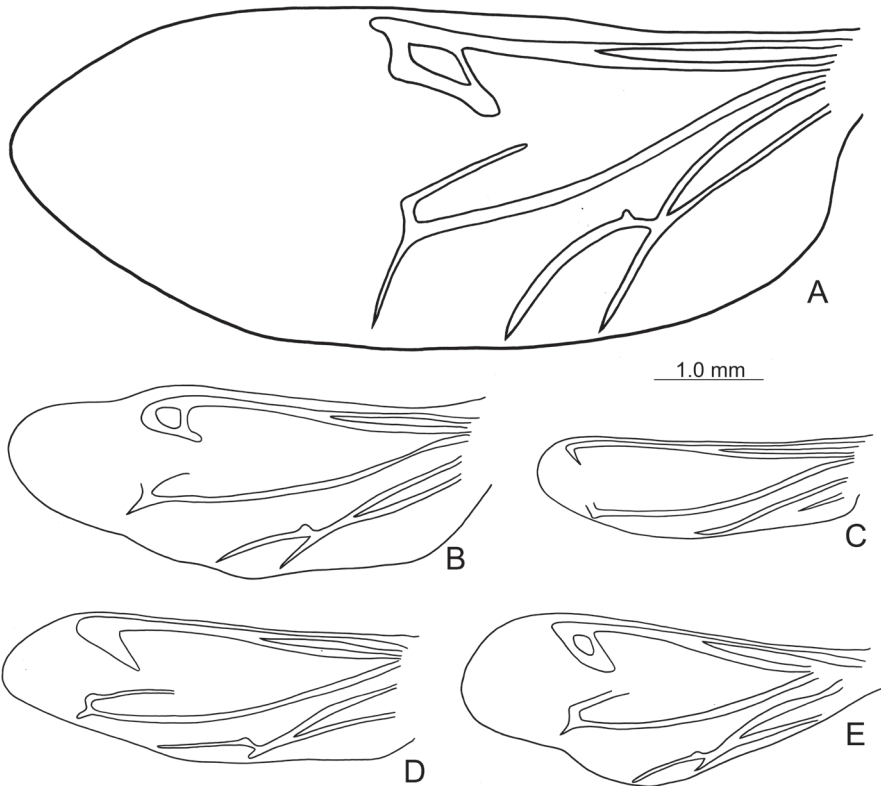


Figure 7. Hindwings of *Shairella quadricostata* (Kimoto) **A** female, from Wulai (烏來) **B** female, from Tengchih (藤枝) **C** female, from Erhwanping (二萬坪) **D** female, from Hsito (溪頭) **E** male, from Peitawushan (北大武山).

Those in Peitawushan (北大武山) have the same length of hind wings as those in Hsito but wider (Fig. 7E). Those in Erhwanping (二萬坪) are reduced strongly, ~ 40% with normal hind wings (Fig. 7C).

Diagnosis. Adults of *Shairella quadricostata* (Kimoto, 1996), comb. nov. and *S. caerulea* (Kimoto, 1996), comb. nov. are characterized by normal elytra and functional hindwings (shortened elytra and reduced hindwings in other *Shairella*; Lee and Beenen 2017) although individuals in some populations of *S. quadricostata* have more or less reduced hindwings. *Shairella quadricostata* is distinguished from *S. caerulea* by possessing black elytra with three pairs of weak longitudinal ridges (Fig. 5A–F) (bluish black elytra without longitudinal ridges besides lateral ridge in *S. caerulea*; Fig. 9); median internal ridge of abdominal ventrite V in males expanded from apex, abbreviated before base (Fig. 6K) (median internal ridge of abdominal ventrite in males expanded from apex to base in *S. caerulea*; Fig. 10G); apically narrowed apex of aedeagus (Fig. 6C) (bifurcate apex of aedeagus in *S. caerulea*; Fig. 10C); apex of spermatheca rounded with or without small process (Fig. 6H–J) (apex of spermatheca swollen, bifurcate in frontal view in *S. caerulea*; Fig. 10H, I).

Host plant. *Hemiboea bicornuta* (Hayata) Ohwi (Gesneriaceae).

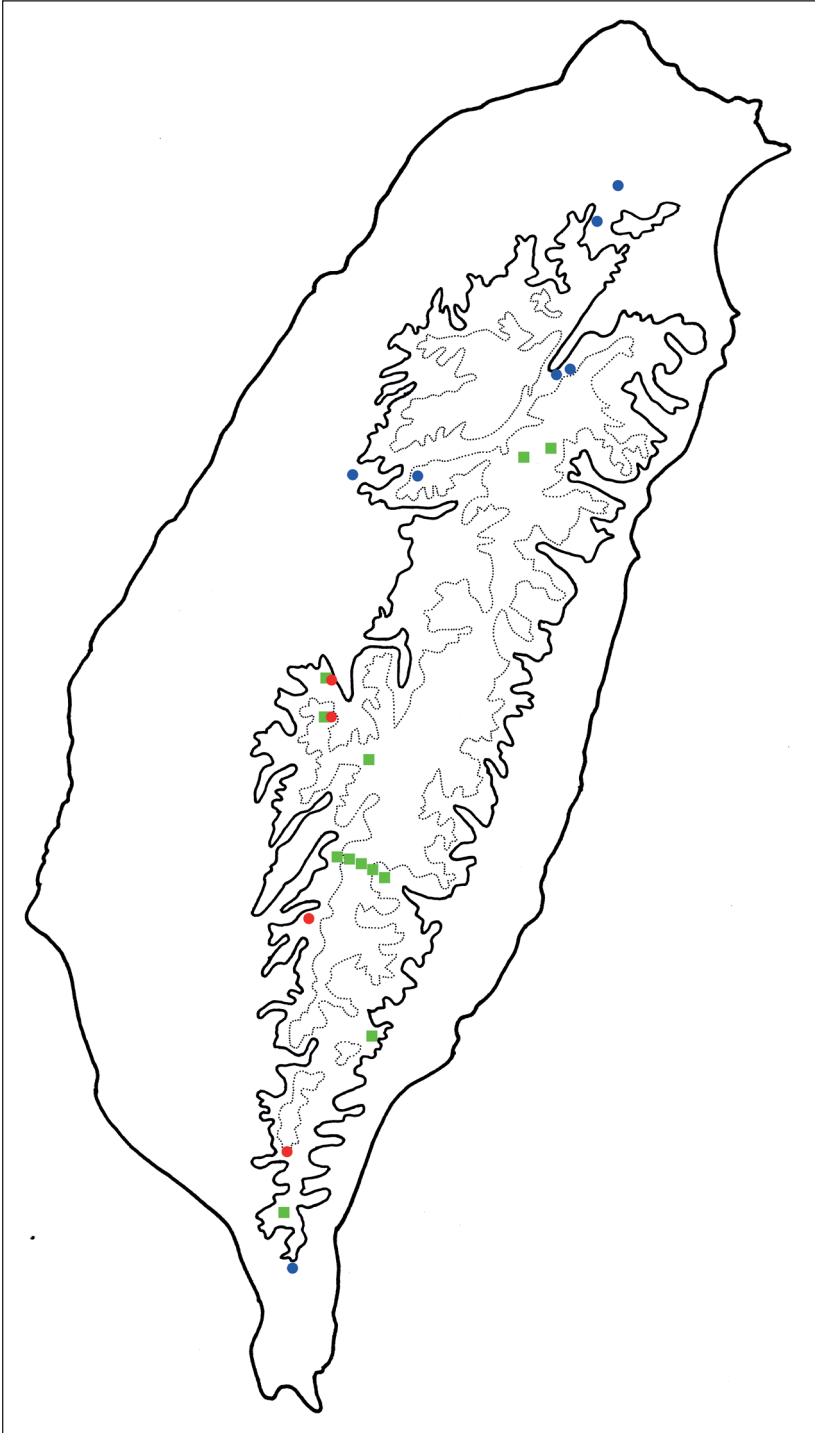


Figure 8. Distribution map of *Shairella quadricostata* (Kimoto) and brachelytrous *Shairella* species, solid line: 1000 m, broken line: 2000 m. Key: green squares – brachelytrous species, blue circles – adults of *S. quadricostata* with normal hindwings, red circles – adults of *S. quadricostata* with reduced hindwings.

Biology. Adults of *Shairella quadricostata* were observed active at night and feeding on leaves of *Hemiboea bicornuta*. However, adults were hard to find with the exception of a single event. Three adults were collected on 11 May 2022 in Tengchih (藤枝) (Fig. 5G). We collected 39 adults on 9 July 2014 in Erhwanping (二萬坪). Many host plants were growing on a steep slope and numerous adults were feeding on leaves (Fig. 5H).

Distribution. The flighted populations are widespread in low-elevations of Taiwan and mid-elevations of northern and central Taiwan, and flightless populations are restricted to mid-elevations of southern Taiwan (Fig. 8).

***Shairella caerulea* (Kimoto, 1996), comb. nov.**

Figs 9, 10

Japonitata caerulea Kimoto, 1996: 33 (Taiwan).

Type examined. Holotype ♂ (SEHU) (Fig. 9A–C): “Pilu (碧綠), Hualien / Taiwan / 10.VII.1983 / H. Takizawa [p, w] // HOLOTYPE [p, r] // Japonitata / caerulea / Kimoto, n. sp. [h] / Det. S. Kimoto, 19[p]95[h, w] // Euliroetis [h] / Det. H. Takizawa [p, w] // 0000000172 / Sys. Ent / Hokkaido Univ. / Japan [SEHU] [p, w]”.

Specimens examined. Hualien: 1♀ (NMNS), Hualuhsi (華祿溪), 1300 m, 28.VII.–25.IX.2011, leg. W.-T. Yang & K.-W. Huang; 1♀ (NMNS), Biyu Sacred Tree (碧綠神木), 2150 m, 1.VI.–28.VII.2011, leg. W.-T. Yang & K.-W. Huang; 1♂ (NMNS), same but with “28.VII.–5.IX.2011”; 1♂, 1♀ (NMNS), same but with “28.V.–24.VII.2012”; 2♂ (NMNS), same but with “24.VII.–10.IX.2012”; **Kaohsiung:** 1♀ (TARI), Chungchihkuan (中之關), 1930 m, 10.VI.2015, leg. T.-H. Lee; **Nantou:** 1♂ (TARI), Tunyuan (屯原), 1900 m, 21.VI.2019, leg. B.-X. Guo. All specimens from Hualien were collected using Malaise traps.

Redescription. Length 6.8–6.9 mm, width 3.7–3.9 mm. General color (Fig. 9D–F) black to blackish brown; abdomen yellow; elytra bluish black. Antennomeres II–XI filiform in males (Fig. 10A), ratios of lengths of antennomeres I–XI 1.0: 0.3: 0.9: 1.0: 1.1: 1.1: 1.1: 0.9: 0.9: 0.8: 1.0; ratios of length to width from antennomeres I–XI 3.0: 1.4: 2.9: 3.6: 3.9: 4.2: 4.3: 4.2: 4.6: 4.3: 6.1; more slender in females (Fig. 10B), ratios of lengths of antennomeres I–XI 1.0: 0.4: 0.9: 1.0: 1.0: 1.0: 1.0: 0.9: 0.9: 0.8: 0.9; ratios of length to width from antennomeres I–XI 3.0: 1.6: 3.4: 3.9: 4.3: 4.6: 4.8: 5.5: 6.1: 5.3: 6.1. Pronotum 2.2 times wider than long; disc with scarce fine punctures at sides, reduced medially, with transverse groove near base, medially abbreviated, laterally connected with short longitudinal groove on basal margin; lateral margins slightly rounded, widest behind apices; apical margin slightly concave and basal margin slightly convex. Elytra 1.4 × longer than wide; disc with confused, dense, fine punctures; with one small tubercle behind scutellum, with one deep depression behind tubercle; with one indistinct longitudinal ridge from humeral calli, parallel with lateral margin, abbreviated subapically; with one additional, deep depression at middle, above longitudinal ridge; lateral margins moderately rounded, widest at apical third, apices divergent.

Aedeagus (Fig. 10C, D) wide, $4.4 \times$ longer than wide; lateral margins straight, widest at apex, gradually narrowed towards base; apex with deep notch; moderately curved in lateral view; tectum membranous; one endophallic sclerite longitudinal and slender, $0.7 \times$ as long as aedeagus, base shallowly bifurcate, lateral margins with clustered short setae at apical third; with short membranous area near apex. Apical margin of abdominal ventrite V in males with distinct median lobe (Fig. 10G), narrow, apical margin slightly recurved, with median internal ridge from apex to base, with narrow furrow between gonocoxae; basal margin expanding posteriorly. Gonocoxae (Fig. 10F) longitudinal and connected basally; each gonocoxa narrowed subapically, apex truncate, with eight long apical setae; base weakly sclerotized but strongly sclerotized medially. Ventrite VIII (Fig. 10E) in females with apex weakly sclerotized, small, depressed medially; with dense short apical setae; spiculum extremely elongate. Spermathecal

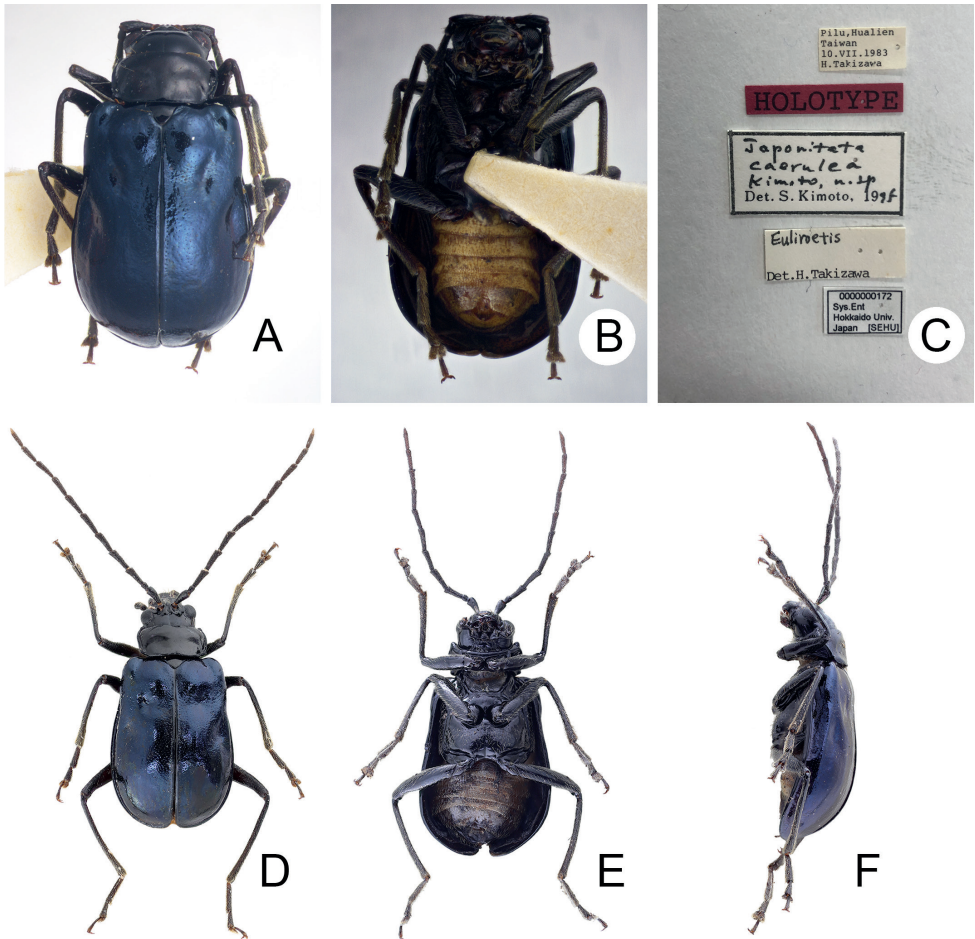


Figure 9. Habitus of *Shairella caerulea* (Kimoto) **A** holotype, male, dorsal view **B** ditto, lateral view **C** labels on the holotypes **D** nontype, male, dorsal view **E** ditto, ventral view **F** ditto, lateral view.

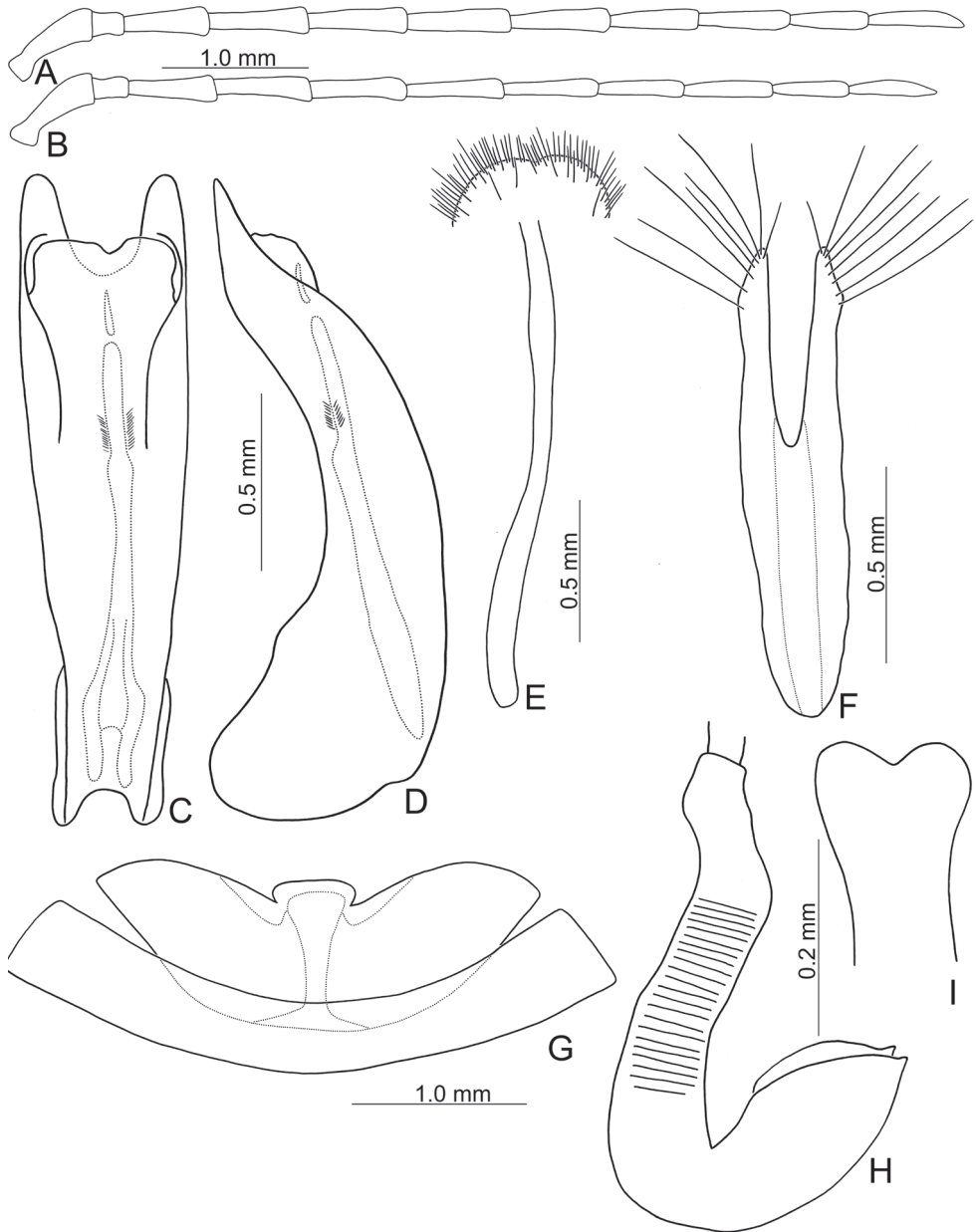


Figure 10. Diagnostic characters of *Shairella caerulea* (Kimoto) **A** antenna, male **B** antenna, female **C** aedeagus, dorsal view **D** ditto, lateral view **E** abdominal ventrite VIII **F** gonocoxae **G** abdominal ventrite IV–V, male **H** spermatheca **I** apex of spermatheca, front view.

receptaculum (Fig. 10H, I) slender, as wide as pump, not separated from pump; pump long and curved, apex slightly swollen, dorso-ventrally bifurcate; sclerotized spermathecal duct short, not separated from receptaculum.

Diagnosis. *Shairella caerulea* (Kimoto, 1996), comb. nov. and *S. quadricostata* (Kimoto, 1996), comb. nov. are characterized by having normal elytra and functional hindwings (shortened elytra and reduced hindwings in other species; Lee and Beenen 2017) although some populations of *S. quadricostata* have variably reduced hindwings. *Shairella caerulea* is distinguished easily from *S. quadricostata* by its bluish black elytra without longitudinal ridges other than the lateral ridge (Fig. 9) (black elytra with three pairs of weak longitudinal ridges in *S. quadricostata*; Fig. 5); median internal ridge of abdominal ventrite in males expending from apex into base (Fig. 10G) (median internal ridge of abdominal ventrite V in males expanding from apex, abbreviated before base in *S. quadricostata*; Fig. 6K); bifurcate apex of aedeagus (Fig. 10C) (apically narrowed apex of aedeagus in *S. quadricostata*; Fig. 6C); apex of spermatheca swollen, bifurcate in frontal view (Fig. 10H, I) (apex of spermatheca rounded with small process in *S. quadricostata*; Fig. 6H–J).

Host plant and biology. Unknown.

Remarks. All specimens deposited at the National Museum of Natural Science, Taichung were collected using Malaise traps. Many flightless, nocturnal galerucines have been collected in Malaise traps, including *Taiwanoshaira chujoi* (Kimoto, 1982) (Lee and Beenen 2020), *Paraplotes taiwana* Chûjô, 1963 (Lee 2015), and *Lochmaea lesagei* Kimoto, 1996 (Lee 2019). Moreover, two specimens were collected during the night by Ta-Hsiang Lee (李大翔) and Bo-Xin Guo (郭泊鑫), respectively; they are members of TCRT. These events suggest that adults of *Shairella caerulea* are nocturnal.

Distribution. This species is probably widespread in Taiwan although few specimens are available for study.

Discussion

The former studies have confused the taxonomic boundaries between *Japonitata* and *Paraplotes* (Chen and Jiang 1986; Medvedev 2002; Zhang et al. 2008). This confusion is probably due to overlooking detailed structures of the aedeagus and female genitalic characters. Shapes and structures of the tectum and endophallic sclerites of the aedeagus, and spermatheca in *S. quadricostata* and *S. caerulea* indicate great similarity among both species and species of *Shairella*. Diagnostic characters between *Japonitata*, *Paraplotes*, and *Shairella* are reevaluated and proposed in this study. Transfer of *S. quadricostata* and *S. caerulea* to *Shairella* is supported based on these diagnostic characters. This study also emphasizes the importance of detailed studies and illustrations of male and female genitalic characters.

Presence or absence of hindwings and elytral calli, or shortened elytra are not key characters for generic diagnoses. For example, females of Taiwanese species of *Paraplotes* have reduced hindwings and shortened elytra (Lee 2015). Taiwanese species of *Sikkimia* (Lee and Bezděk 2016) and some species of *Lochmaea* (Lee 2019) have reduced elytral calli and hindwings. The brachelytrous *Shairella* is redefined here by including *S. quadricostata* and *S. caerulea* with normal elytra. This implies that a number

of additional *Japonitata* species should be transferred to *Shairealla*. Specifically, species of *Japonitata* without one pair of distinct ridges on the elytra should be evaluated as possible members of *Shairella*.

Adults of *Shairella quadricostata* (Kimoto), comb. nov. are widespread and some populations have reduced hindwings in mid-elevations of southern Taiwan. They are allopatric with other members of the genus except at Erhwanping (二萬坪) and Hsitou (溪頭), where *S. aeneipennis* Chûjô, 1962 also occurs (Fig. 8). However, they are separated ecologically since both species utilize different food plants (*Hemiboea bicornuta* for *S. quadricostata* and *Clinopodium laxiflorum* var. *taiwanianum* for *S. aeneipennis*). Interestingly, adults and larvae of *S. chungi* Lee & Beenen, 2017 in southern Taiwan also feed on leaves of *Hemiboea bicornuta*. This species is allopatric with *S. quadricostata*, although the flightless populations are more northern in distribution and the winged populations are southern. A previous hypothesis for brachelytry in leaf beetles of tropical forest habitats is different from Lee's proposal for *Paraplotes* (Lee 2015): "Reduction of hind wings may result from the production of physogastric females. Nocturnal behavior increases survival since natural enemies are less of a threat. Males actively search for mates by night. In harsh environments such as islands, deserts and alpine regions, flight is not essential to survival and energy can be diverted to egg production (Beenen and Jolivet 2008). Thus, brachelytry is a predictable evolutionary trend." The species (*S. quadricostata*) with long antennae and darker color is adapted to nocturnal activity since natural enemies are less of a threat. Some populations have reduced hindwings as an adaptation to stable microhabitats (mid-altitudes in southern Taiwan). Elytra are reduced further due to allopatric speciation (*S. chungi* Lee & Beenen, 2017). Host plant shifts cause adaptive radiation in these circumstance (*S. aeneipennis*, *S. guoi* Lee & Beenen, 2017, *S. motienensis* Lee & Beenen, 2017, and *S. tsoui* Lee & Beenen, 2017).

Acknowledgements

I am grateful to the Taiwan Chrysomelid Research Team (TCRT), including Jung-Chang Chen (陳榮章), Hou-Jay Chen (陳厚潔), Yi-Ting Chung (鍾奕霆), Bo-Xin Guo (郭泊鑫), Hsueh Lee (李雪), Ta-Hsiang Lee (李大翔), and Mei-Hua Tsou (曹美華), as well as two citizen scientists Yen-Cheng Hsu (徐彥承) and Chin-Li Chiang (江進利) for assistance in collecting material. I especially thank Hsing-Che Liu (劉興哲), and Hsing-Tzung Cheng (鄭興宗) for photos of specimens, Yi-Ting Chung (鍾奕霆), Hou-Jay Chen (陳厚潔), and Mei-Hua Tsou (曹美華) for field photography, and Chih-Kai Yang for identification of host plants. In addition, I thank Takuya Takemoto for taking photos of the holotype of *S. caerulea* and Shunpei Fujie for *S. quadricostata*. I especially thank Chang Chin Chen for assisting this study in various ways, Chris Carlton for reading the draft and editing for American English style, and Jan Bezděk and Viswajyothi Keezhpattillam for reviewing the manuscript.

References

- Beenen R, Jolivet P (2008) Classification and habitat of brachelytrous Chrysomelidae (Coleoptera). In: Jolivet P, Santiago-Blay J, Schmitt M (Eds) Research on Chrysomelidae. Volume 1. Brill, Leiden, 161–173. <https://doi.org/10.1163/9789047427858>
- Chen SH, Jiang SQ (1981) Coleoptera: Chrysomelidae - Galerucinae. In: Chen CH (Ed.) Insects of Xizang. Volume 1. Sciences Press, Peking, 457–489. [in Chinese with English summary]
- Chen SH, Jiang SQ (1986) On the Chinese species of the galerucine genus *Japonitata* (Coleoptera: Chrysomelidae). Acta Zootaxonomica Sinica 11: 72–79. [in Chinese with English summary]
- Gould AA (1859) Descriptions of shells collected in the North Pacific Exploring Expedition under Captains Ringgold and Rodgers. Proceedings of Boston Society of Natural History 6: 422–426.
- Jiang SQ (1989) Four new Chinese species of *Japonitata* (Coleoptera: Chrysomelidae, Galerucinae). Acta Entomologica Sinica 32: 221–225. [in Chinese with English summary]
- Kimoto S (1970) A list of the Nepalese chrysomelid specimens preserved in Zoologische Sammlung des Bayerischen Staates, München. Khumbu Himal 3: 412–421.
- Kimoto S (1996) Notes on the Chrysomelidae from Taiwan, China. XIII. Entomological Review of Japan 51: 27–51. [http://coleoptera.sakura.ne.jp/ERJ/ERJ51\(1\)1996.pdf](http://coleoptera.sakura.ne.jp/ERJ/ERJ51(1)1996.pdf)
- Kimoto S (2004) New or little known Chrysomelidae (Coleoptera) from Nepal, Bhutan and the northern territories of Indian subcontinent. Bulletin of the Kitakyushu Museum of Natural History and Human History, Series. Natural History 2: 47–63. https://www.kmnh.jp/wp-content/themes/kmnh_jp/images/pdf/A2-47-E-Kimoto.pdf
- Lee C-F (2015) The genus *Paraplotes* Laboissière, 1933 in Taiwan, a speciose group with brachelytrous emales (Coleoptera: Chrysomelidae: Galerucinae). Zootaxa 3904: 223–248. <https://doi.org/10.11646/zootaxa.3904.2.3>
- Lee C-F (2019) The genus *Lochmaea* Weise, 1883 in Taiwan: Results of taxonomic expeditions by citizen scientists (Coleoptera, Chrysomelidae, Galerucinae). ZooKeys 856: 75–100. <https://doi.org/10.3897/zookeys.856.30838>
- Lee C-F, Beenen R (2017) Revision of the genus *Shairella* Chûjô, 1962 (Coleoptera: Chrysomelidae: Galerucinae) from Taiwan, with descriptions of five new species. Zootaxa 4268(4): 489–507. <https://doi.org/10.11646/zootaxa.4268.4.2>
- Lee C-F, Beenen R (2020) *Taiwanoshaira* Lee & Beenen, a new genus and first of moss-inhabiting Galerucinae sensu stricto (Coleoptera, Chrysomelidae) from Taiwan. ZooKeys 994: 129–146. <https://doi.org/10.3897/zookeys.944.53099>
- Lee C-F, Bezděk J (2016) Revision of the wingless *Sikkimia* Duvivier (Coleoptera, Chrysomelidae, Galerucinae) from Taiwan, including a new generic synonymy and four new species descriptions. ZooKeys 553: 79–106. <https://doi.org/10.3897/zookeys.553.6576>
- Medvedev LN (2002) New and poorly known Chrysomelidae (Coleoptera) from northern India. Entomologica Basiliensia 24: 245–253.
- Medvedev LN (2012) New species of Chrysomelidae (Coleoptera) from Indochina. Euroasian Entomological Journal 11: 63–69.

- Medvedev LN, Sprecher-Uebersax E (1998) New data on Chrysomelidae of Nepal (Insecta, Coleoptera). *Spixiana* 21: 25–42. http://www.zobodat.at/pdf/Spixiana_021_0025-0042.pdf
- Medvedev LN, Sprecher-Uebersax E (1999) Taxonomical study of Chrysomelidae (Coleoptera) from Nepal. *Entomologica Basiliensia* 21: 355–370.
- Nie R-E, Bezděk J, Yang X-K (2017) How many genera and species of Galerucinae s. str. do we know? Updated statistics (Coleoptera, Chrysomelidae). *ZooKeys* 720: 91–102. <https://doi.org/10.3897/zookeys.720.13517>
- Strand E (1935) Revision von Gattungsnamen palaeaktischer Coleoptera. *Folia Zoologia et Hydrobiologia* 7: 282–299.
- Takizawa H, Basu CR (1987) Notes on chrysomelid-beetles (Coleoptera, Chrysomelidae) of India and its neighbouring areas. Part 4. *Kontyû* 55: 266–283.
- Weise J (1922) Chrysomeliden der indo-malayischen Region. *Tijdschrift voor Entomologie* 65: 39–130. <https://www.biodiversitylibrary.org/page/10857673>
- Yang XK (1992) Chrysomelidae Galerucinae. In: Peng J, Liu Y (Eds) *Iconography of forest insects in Hunan China*. Academia Sinica & Hunan Forestry Institute, Hunan, 552–589. [in Chinese with English summary]
- Yang XK, Li WZ (1998) Coleoptera: Chrysomelidae: Galerucinae. In: Wu H (Ed.) *Insects of Longwangshan Nature Reserve*. China Forestry Publishing House, Beijing, 128–135. [in Chinese with English summary]
- Yang XK, Li WZ, Zhang BQ, Xiang ZQ (1997) Coleoptera: Chrysomelidae: Galerucinae. In: Yang XK (Ed) *Insects of the Three Gorge reservoir area of Yangtze River*. Part 1. Chongqing Publishing House, Chongqing, 863–904. [in Chinese with English summary]
- Zhang LJ, Li WZ, Yang XK (2008) Taxonomic changes in the genus *Paraplotes* Laboissière, 1933 (Coleoptera: Chrysomelidae: Galerucinae). *The Pan-Pacific Entomologist* 84(1): 17–21. <https://doi.org/10.3956/2007-05.1>

A detailed comparison of two species in the genus *Potamanthus* Pictet, 1843 from China (Ephemeroptera, Potamanthidae)

Wen-Juan Li¹, Chang-Fa Zhou¹

¹ *The Key Laboratory of Jiangsu Biodiversity and Biotechnology, College of Life Sciences, Nanjing Normal University, Nanjing 210023, China*

Corresponding author: Chang-Fa Zhou (zhouchangfa@njnu.edu.cn)

Academic editor: Ben Price | Received 20 June 2022 | Accepted 5 September 2022 | Published 26 October 2022

<https://zoobank.org/DF876772-5BBC-40E9-ACD0-AABD6D910471>

Citation: Li W-J, Zhou C-F (2022) A detailed comparison of two species in the genus *Potamanthus* Pictet, 1843 from China (Ephemeroptera, Potamanthidae). ZooKeys 1125: 193–205. <https://doi.org/10.3897/zookeys.1125.89219>

Abstract

Photographs and details of structures of two *Potamanthus* species, *P. huoshanensis* Wu, 1987 and *P. luteus* (Linnaeus, 1767), are presented for the first time. Here, based upon Chinese specimens of those species, all external structures are illustrated digitally and compared. The results and photos clearly show that the adults of the two species are different in wing color and genitalia shape, and that their nymphs have different mandibular tusks and forelegs. Specifically, *P. luteus* has a more colorful body and wings, longer penes and nymphal mandibular tusks but shorter foretarsi than those of *P. huoshanensis*. This comparison not only confirms the differences between these two similar species, but also supports the updated generic delineations of *Potamanthus* and *Potamanthodes*.

Keywords

China, *Potamanthus*, *P. huoshanensis*, *P. luteus*, morphology

Introduction

The Palearctic genus *Potamanthus* Pictet, 1843 comprises only two species and one subspecies (Bae and McCafferty 1991; Kluge 2004; Li and Zhou 2022). The first one, *P. luteus* (Linnaeus, 1767), is widely distributed from northern Africa and Europe to northeastern Asia, and its morphology has been described and mentioned by a long series of researchers (see Bauernfeind and Soldán 2012 and references therein). However,

only Bae and McCafferty (1991) provided photos of this species, but no comprehensive, detailed photographs had so far been presented to show its exact characters. Further, *P. luteus* was divided into two subspecies by Bae and McCafferty (1991) using few structures, such as the shape of the anterolateral corners of the nymphal pronotum, the vestigial apical spines on the forefemora and forking point of the medius anterior (MA) in the imaginal forewings.

In contrast to *P. luteus*, the second species in the genus, *P. huoshanensis* Wu, 1987, has a very narrow distribution. Up until now, it has been found only at one site in China and two sites in Japan (Wu 1987a, 1987b; Ishiwata 2001). Only the wings and a drawing of the nymphal habitus of this species had been provided so far, by Bae and McCafferty (1991). In addition, Wu (1987a) and Bae and McCafferty (1991) regarded this species as very similar to *P. luteus*, the latter authors even identifying Japanese *Potamanthus* materials as belonging to *P. luteus*. Thus, proper photographic documentation of *P. huoshanensis* would not only reveal the real characters of this species but also show differences with the similar *P. luteus*.

The generic circumscription and phylogeny of the genus *Potamanthus* has been changing. Bae and McCafferty (1991) downgraded the taxon *Potamanthodes* to a subgenus of *Potamanthus*. Differently, Kluge (2004) placed it as a member of another genus, *Rhoenanthus* Eaton, 1881. Recently, Li and Zhou (2022) reinstated the taxon *Potamanthodes* as an independent genus. With details of the two species in the genus *Potamanthus* and other recent related reports (Han et al. 2021; Kwanboon et al. 2021), differences among these three taxa will be clarified.

Here, we compare Chinese specimens of *P. luteus* to the types of *P. huoshanensis*, provide photographs of imaginal and nymphal structures of both species, document fine characters useful to differentiate these two species in the genus *Potamanthus*. The results support our proposal to reinstate this genus in a previous work (Li and Zhou 2022).

Material and methods

Material examined

Potamanthus huoshanensis Wu, 1987

1♂ imago (**Holotype**), 10 nymphs, 4♂♂ imagoes, 20♀♀ imagoes (**Paratypes**), Zhufoan Town, Huoshan county, Anhui Province, China, 31°24'59"N, 116°10'30.40"E, 1983-VI-11–13, collected by Xing-Yong WU; other materials: 2 nymphs, 15♀♀ imagoes, 1984-VI-11, other information as for the types.

Potamanthus luteus (Linnaeus, 1767)

7 nymphs, 12♀♀ imagoes, Nancha county, Heilongjiang Province, China, 47°7'48"N, 129°16'48"E, 1984-VII-26–29, collected by Xing-Yong WU; 1 nymph, Mohe county,

Heilongjiang Province, China, 52°58'12"N, 122°31'48"E, 2007-VIII-14, collected by Shi-Lei WANG, Hui XIE; 100 ♂♂ imagoes, 200 ♀♀ imagoes, 100 ♂♂ subimagoes, 100 ♀♀ subimagoes, Yanshou county, Heilongjiang Province, China, 45°27'0"N, 128°19'48"E, 2008-VII-14–15, collected by Shi-Lei WANG, Guo ZHAO; 2 nymphs, 1 ♀ imago, Songhua River, Fusong county, Jilin Province, China, 44°41'31"N, 125°57'8.82"E, 2008-VII-26, collected by Shi-Lei WANG, Guo ZHAO.

Methods

The nymphs of two species studied in the present paper were collected by hand net, whereas most adults were collected by light trap (using LED and mercury lamps). Some adults were reared from nymphs in the field. The materials are stored in ethanol (about 85%).

All specimens were examined under a stereomicroscope (MshOt MZ81) and photographed with a digital camera coupled to the microscope (Nikon Eclipse 50i). Some small structures, such as gills, mouthparts, terga and legs, were observed and photographed with a microscope camera on temporary slides. All specimens used in this study are deposited in the mayfly collection of the College of Life Sciences, Nanjing Normal University, China.

Results

Potamanthus huoshanensis Wu, 1987

Potamanthus (Potamanthus) huoshanensis Wu, 1987b: 421. figs 1–5. Types: nymph, male and female, from Anhui, China.

Potamanthus (Potamanthus) huoshanensis: Bae and McCafferty 1991: 49. figs 15, 95, 113, 126, 139 (nymph, male and female); Ishiwata 2001: 58; Zhou 2013: 202; Zhou et al. 2015: 252.

Potamanthus huoshanensis: Wu et al. 1991: 111. fig. 2 (egg); You and Gui 1995: 116. fig. 123 (male and female).

Distribution. China (Anhui Province); Japan (Yokkaichi city, Lake Biwa).

Description. see Wu (1987b) and Bae and McCafferty (1991).

Diagnosis. This species resembles *Potamanthus luteus* in the main characters of both the adults and the nymphs, which can be differentiated only by very fine structures (Table 1). In the nymph, the labrum of *P. huoshanensis* is slightly narrower than that of *P. luteus* (Fig. 3A, B); the mandibular tusks are indistinctly shorter than in *P. luteus*, and this can be seen in nymphal dorsal views (Figs 2A, B, E, F, 3E–H); the maxillary palpi of both species are similar but different in their length ratio: the ratio in the former species is 1.0: 0.6: 1.0, whereas that of the latter species is 1.0: 0.7: 1.3 (Fig. 3I–L). The two species have a very similar hypopharynx and labia (Fig. 3C, D, M, N). Although the color pattern of examined *P. huoshanensis* has faded and is pale, the leg lengths are different

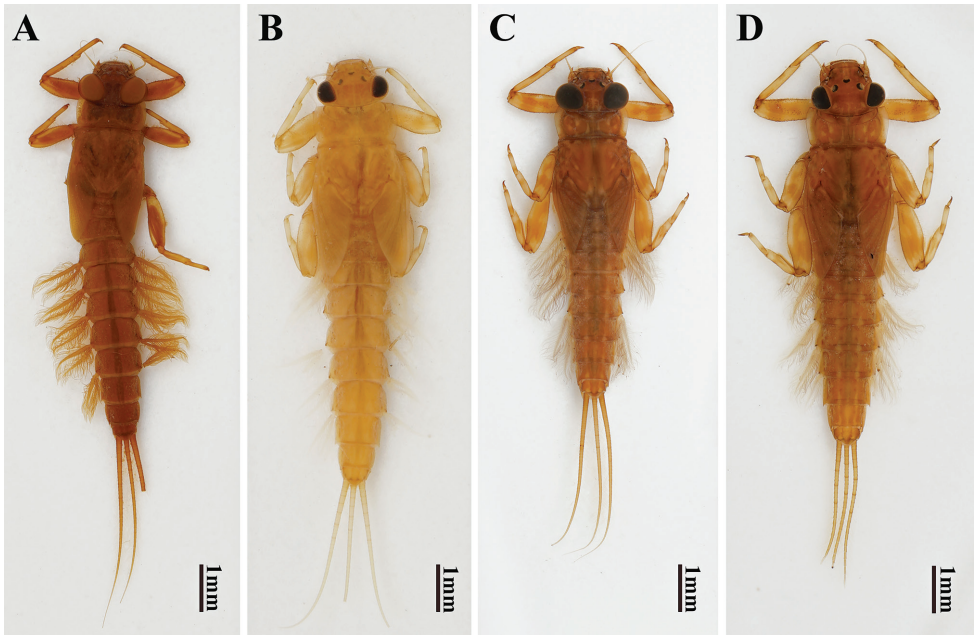


Figure 1. Male and female nymph habitus of two *Potamanthus* species: **A, B** *P. huoshanensis* and **C, D** *P. luteus*.

in the two species: ratio of forefemora: tibiae: tarsi = 1.0: 0.7: 0.6 in *P. huoshanensis* and 1.0: 0.8: 0.6 in *P. luteus*, the former having slightly shorter forelegs and tibiae (Fig. 2I, L). But the midlegs, hindlegs and their claws are very similar (Fig. 2D, H, J, K, M, N).

Males of the two species can be easily separated: (1) the pigments of the cross-veins of the forewings of *P. huoshanensis* are almost invisible, but they are clear on the forewings of *P. luteus* (Figs 4A, C, 5E, G); (2) the costal projection of the hindwings are slightly blunter in *P. huoshanensis* than in *P. luteus* (Fig. 5F, H); (3) the compound eyes of *P. huoshanensis* are almost contiguous but they are clearly separated in *P. luteus* (Fig. 5A, C); (4) both the lateral and inner extended lobes of the penis of *P. huoshanensis* are slightly smaller than those of *P. luteus* (Fig. 6C–E, H–J); (5) the penes of *P. huoshanensis* are slightly shorter than those of *P. luteus*: the subgenital plate of *P. huoshanensis* almost covers the base of the penial lobes but the penes of *P. luteus* are longer, with the whole penes completely visible in ventral view (Fig. 6A, B, F, G); (6) the subgenital plate of *P. huoshanensis* has a shallow median emargination, whereas that of *P. luteus* has a clear V-shaped cleft (Fig. 6A–D, F–I); (7) the forking point of the MA in the *P. huoshanensis* forewings is more distal than that of *P. luteus*, with the ratio of MA: MA₁ = 1.0: 0.7 in the former species and 1.0: 0.9 in the latter (Fig. 5E, G); (8) the foretibiae of *P. huoshanensis* are shorter than in *P. luteus*, with the ratio forefemora: tibiae: tarsi = 1.0: 1.3: 1.6 in *P. huoshanensis* and 1.0: 1.6: 1.5 in *P. luteus* (Fig. 4A, C).

The females of the two species can be differentiated by their wing color and the shape of the hindwings, like in the males (Fig. 4B, D). The compound eyes of female *P. luteus*

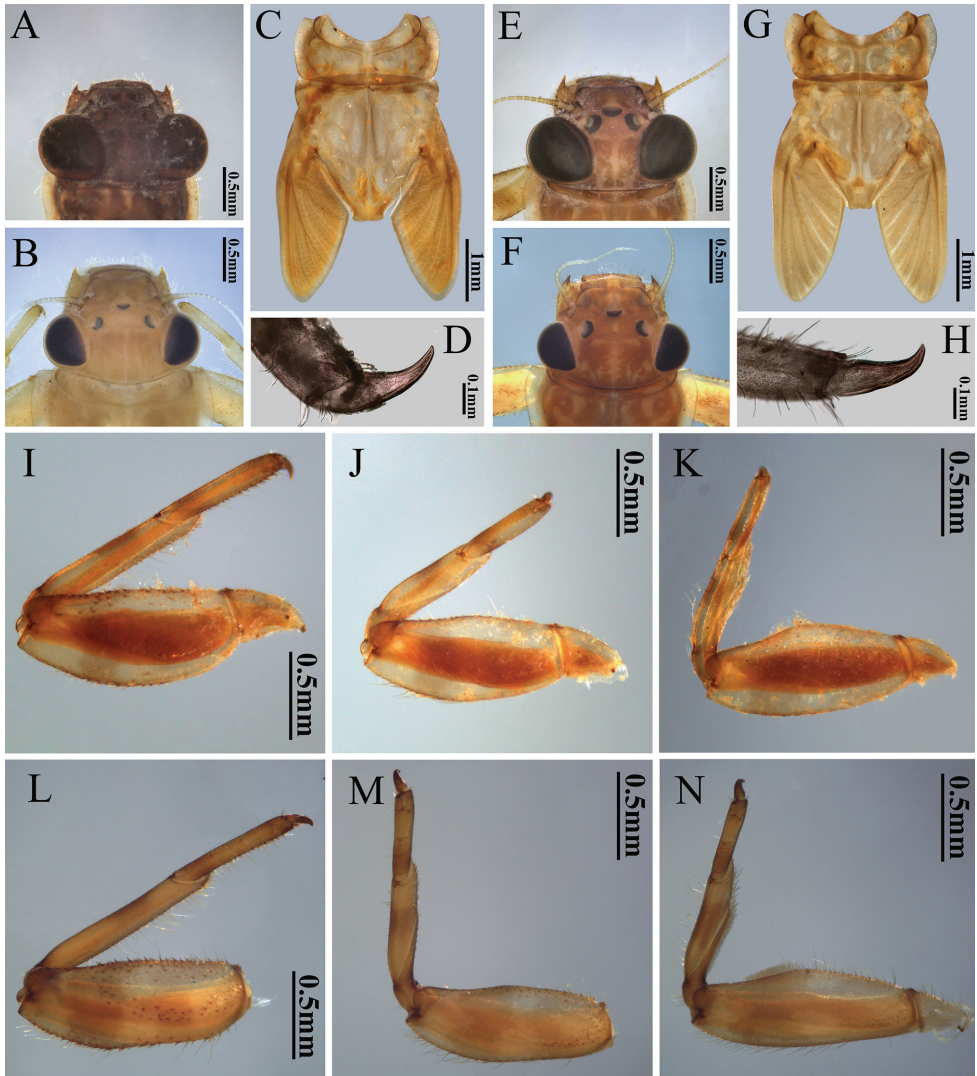


Figure 2. Male and female head, thorax, foreleg claw, foreleg, midleg and hindleg of nymph of two *Potamanthus* species: **A–D, I–K** *P. huoshanensis* and **E–H, L–N** *P. luteus*.

are slightly smaller than those of *P. huoshanensis* (Fig. 5B, D), but the subgenital plates are very similar (Fig. 7).

Although the color of the *P. huoshanensis* material is not clear, the original description of Wu (1987b) and our specimens clearly show that the males, females and nymphs of this species do not have dots on their abdominal terga. In contrast, all stages of *P. luteus* have a pair of dark dots on the abdominal terga (Fig. 4C–D). In addition, *P. luteus* has a longitudinal median reddish band on the abdomen (Fig. 4C–D).

The differences between the two species are listed in Table 1.

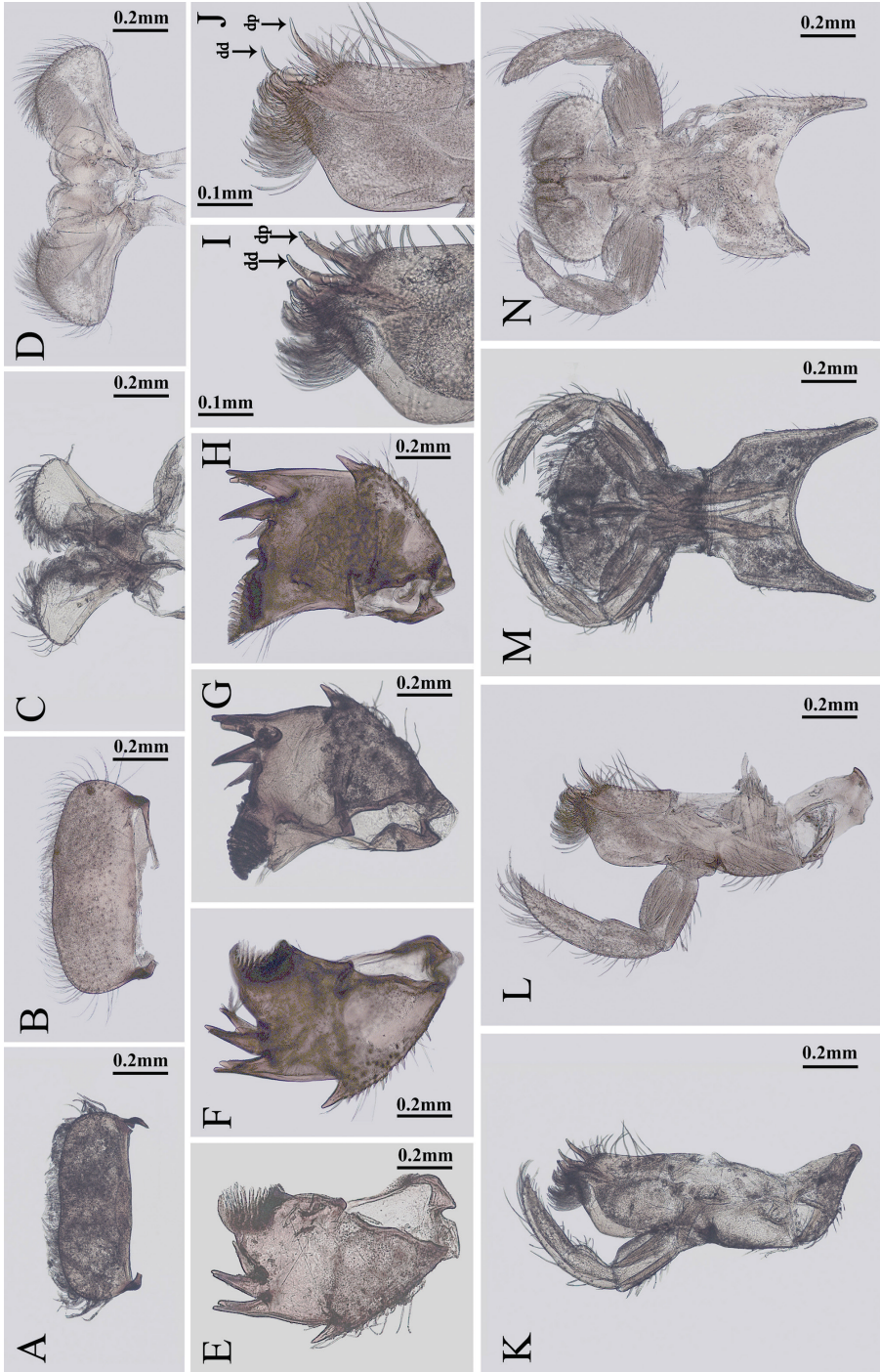
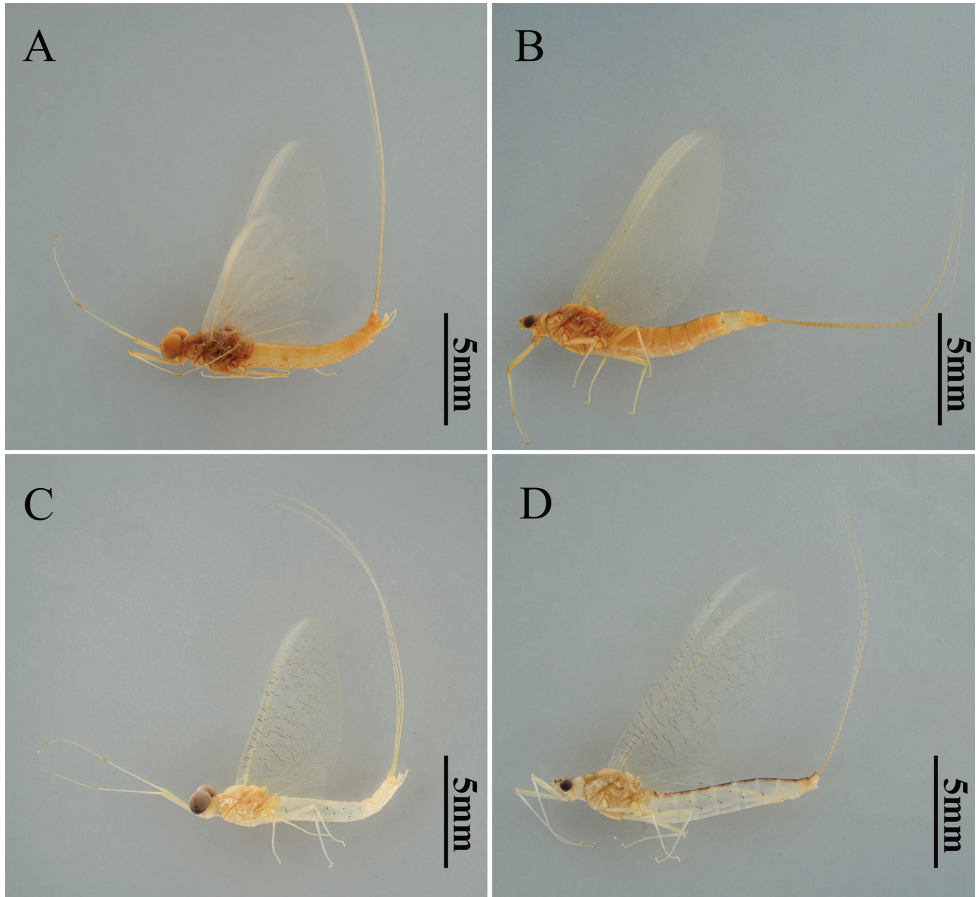


Figure 3. Labrum, hypopharynx, left mandible, right mandible, maxilla and labium of nymph mouthparts of two *Potamanthus* species: **A, C, E, G, I, K, M** *P. huoshanensis* and **B, D, F, H, J, L, N** *P. luteus*. dd: distal dentisetae; dp: proximal dentisetae.

Table 1. Comparison of characteristics of the two *Potamanthus* species.

	Characters Species	<i>P. huoshanensis</i>	<i>P. luteus</i>
Nymph	mandibular tusks	not protruding the labrum	protruding the labrum
	ratio of maxillary palpi from base to apex	1.0: 0.6: 1.0	1.0: 0.7: 1.3
	ratio of forefemora: tibiae: tarsi	1.0: 0.7: 0.6	1.0: 0.8: 0.6
	Pairs of lateral dots on abdominal terga	without	with
Male imago	pigments of crossveins in forewings	vague	clear
	MA: MA ₁	1.0: 0.7	1.0: 0.9
	costal projection of hindwings	blunt	sharp
	distance between two compound eyes	no or very short	half of median ocellus
	Pairs of lateral dots on abdominal terga	without	with
	Penial lobes covered by subgenital plate	partially	no
	Posterior emargination of subgenital plate	shallow	V-shaped cleft
ratio of forefemora: tibiae: tarsi	1.0: 1.3: 1.6	1.0: 1.6: 1.5	
Female imago	pigments of crossveins in forewings	vague	clear
	MA: MA ₁	1.0: 1.0	1.0: 0.9
	Pairs of lateral dots on abdominal terga	without	with

**Figure 4.** Male and female adult morphology of two *Potamanthus* species: **A, B** *P. huoshanensis* and **C, D** *P. luteus*.

***Potamanthus luteus* (Linnaeus, 1767)**

Ephemera luteus Linnaeus, 1767: 906. Type: England.

Ephemera reticulata Fourcroy, 1785: 351. Synonymized by Eaton (1871: 76).

Baetis mellea Curtis, 1834: 121. Types: subimago. Synonymized by Eaton (1871: 76).

Baetis marginalis Burmeister, 1839: 801. Types: male and female. Synonymized by Eaton (1871: 76).

Ephemera flavicans Rambur, 1842: 296. Types: male and female, from Paris, France. Synonymized by Eaton (1871: 76).

Ephemera chlorotica Rambur, 1842: 296. Types: male and female subimagoes, from Paris, France. Synonymized by Walker (1853: 539).

Potamanthus luteus (Linnaeus): Pictet 1843: 205; Eaton 1884: 79.

Potamanthus ferreri Pictet, 1843: 203. Types: male, from Italy. Synonymized by Bae and McCafferty (1991: 51).

Eucharidis reaumurii Joly & Joly, 1876: 314. Types: nymph. Synonymized by Eaton (1884: 79).

Potamanthus na Imanishi, 1940: 180, fig. 2 (nymph). Synonymized by Bae and McCafferty (1991: 54).

Potamanthus naa Imanishi, 1940: 181 (nymph). Synonymized by Bae and McCafferty (1991: 54).

Potamanthus luteus: Wu 1987a: 336 (female, first record from China); You and Gui 1995: 115, fig. 122 (male); Bauernfeind and Soldán 2012: 634 (adult, nymph, egg).

Potamanthus (*Patamanthus*) *luteus oriens*: Bae and McCafferty 1991: 54, fig. 4, 125 (subspecies established); Bae 1997: 408; Zhou 2013: 202; Zhou et al. 2015: 252.

Potamanthus luteus oriens: Quan et al. 2002: 257.

Distribution. China (Heilongjiang and Jilin Province); Palearctic and Oriental. From England east through Europe and Asia Minor, south to North Africa.

Description. see Bae and McCafferty (1991) or Bauernfeind and Soldán (2012).

Diagnosis. see diagnosis of *P. huoshanensis*. Males of this species can be identified by the more distinct color of the wings and penial lobes (Figs 5E–H, 6) and the foretibiae longer than the tarsi (Fig. 4A, C). The nymphs can be distinguished by the slightly larger mandibular tusks, longer foretibiae (Figs 2I, L, 3E–H) and apical segment of the maxillary palpi (Fig. 3K, L).

Remarks. Bae and McCafferty (1991) mentioned that the nymphs of the subspecies *Potamanthus luteus oriens* have very pointed anterolateral projections of the pronotal and vestigial spine-row on the forefemora. In our material, the former character is distinct, and the transverse spine-row was not recognizable, which is consistent with the description of European *P. luteus* provided by Bauernfeind and Soldán (2012). However, we do not know whether this variation is just at the population level or representative of different subspecies or geographical populations, because we have no material from abroad for comparison.

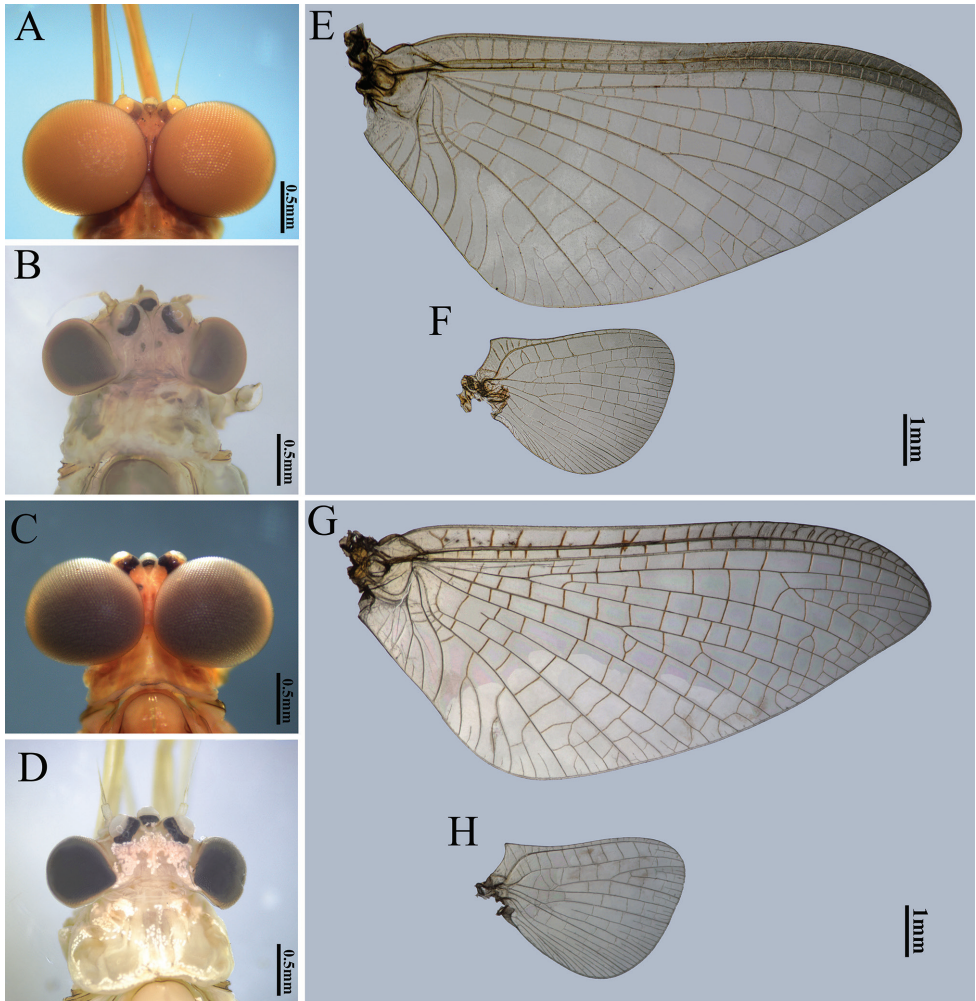


Figure 5. Male head, female head, forewing and hindwing of two *Potamanthus* species: **A, B, E, F** *P. huoshanensis* and **C, D, G, H** *P. luteus*.

In the present comparison and photos, we can see clearly that *P. huoshanensis* and *P. luteus oriens* are extremely similar in both nymphal and imaginal structures. The differences between them are very slight. Therefore, it is not surprising that Bae and McCafferty (1991) recognized Japanese materials of *P. huoshanensis* as *P. luteus oriens*, which was later corrected by Ishiwata (2001).

The distribution of *P. luteus* is wide, from Africa to Japan. In contrast, *P. huoshanensis* was reported from three allopatric sites in Japan and China. Biogeographic and genetic studies at the population level are required for these species.

At the generic level, the definitions of the genera *Potamanthus* and *Potamanthodes* were updated by Li and Zhou (2022) and confirmed by the characters presented in this study.

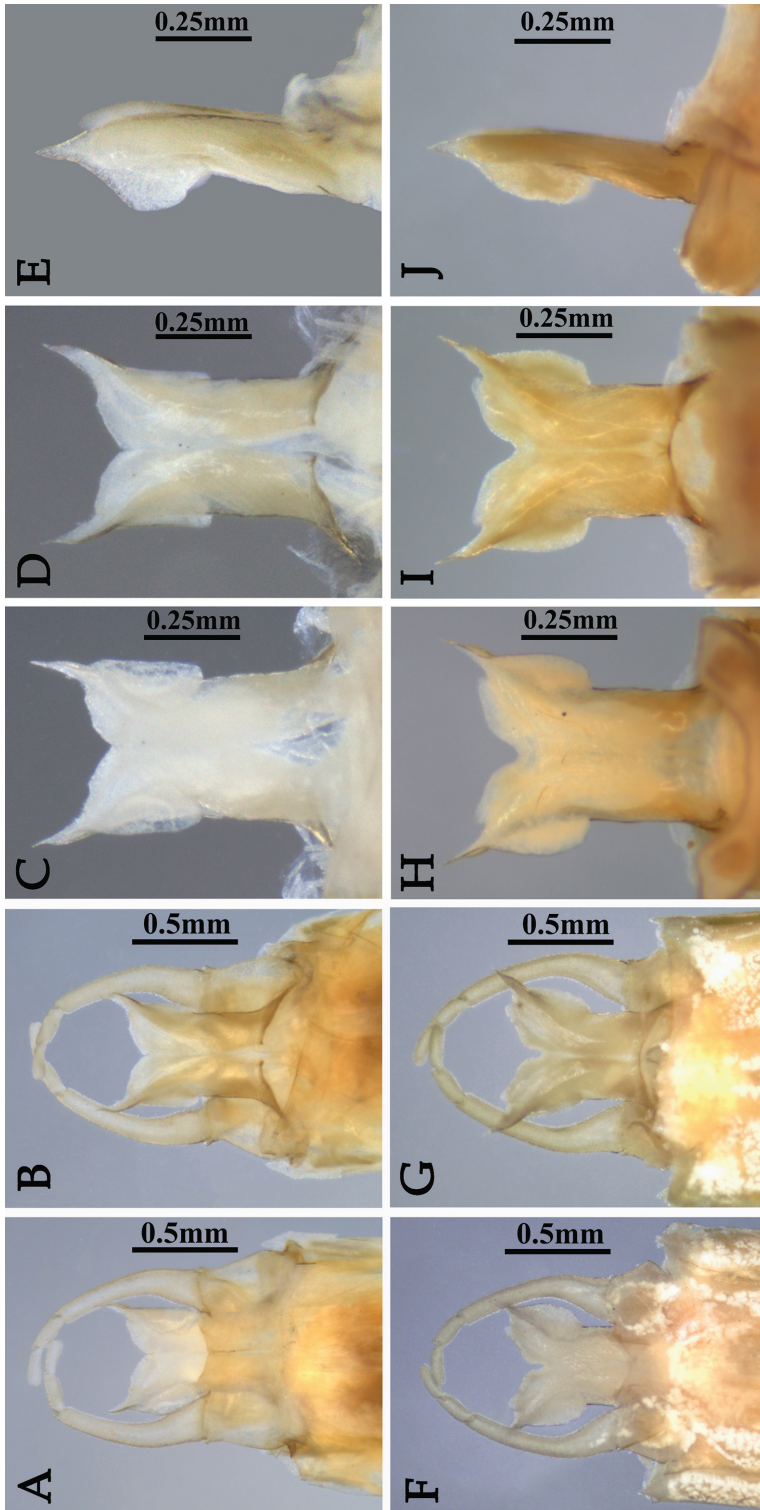


Figure 6. Genitalia (ventral and dorsal view) and penis (ventral, dorsal and lateral view) of two *Potamanthus* species: **A–E** *P. huoshanensis* and **F–J** *P. lutens*.

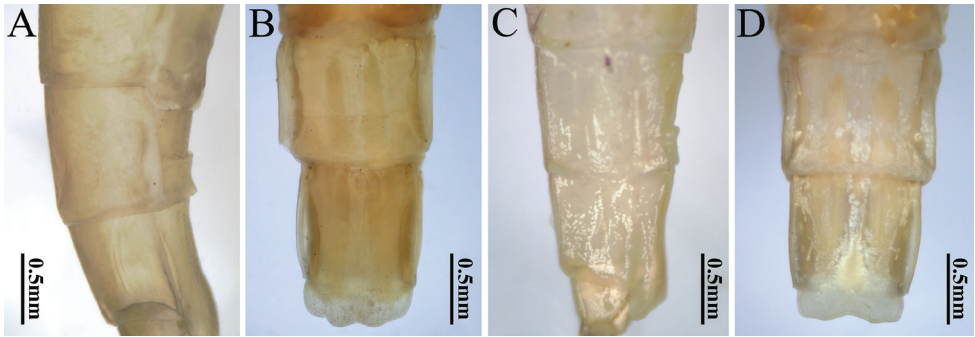


Figure 7. Abdominal segments VII–X (lateral and ventral view) of two *Potamanthus* species: **A, B** *P. huoshanensis* and **C, D** *P. luteus*.

Key to the two *Potamanthus* species

Nymph

- 1 Mandibular tusks short (not protruding beyond labrum in dorsal view) (Fig. 2A, B, 3E, G); apical segment of maxillary palpi subequal to or shorter than basal one (Fig. 3K) *P. huoshanensis*
- Mandibular tusks protruding beyond anterior margin of labrum in dorsal view or subequal (Fig. 2E, F, 3F, H); apical segment of maxillary palpi longer than basal one (Fig. 3L) *P. luteus*

Male imago

- 1 Compound eyes almost contiguous (Fig. 5A); foretibiae shorter than tarsi (Fig. 4A); penial lobes partially covered by subgenital plate in ventral view (Fig. 6A); crossveins of forewings without distinct pigments (Figs 4A, 5E) *P. huoshanensis*
- Compound eyes separated by half the width of the ocelli (Fig. 5C); foretibiae longer than tarsi (Fig. 4C); penial lobes not covered by subgenital plate, totally visible in ventral view (Fig. 6F); crossveins of forewings with reddish-brown color (Figs 4C, 5G) *P. luteus*

Female imago

- 1 Crossveins of forewings without distinct pigments; no distinct dots or markings on abdomen (Fig. 4B) *P. huoshanensis*
- Crossveins of forewings with reddish-brown color; mediolongitudinal band and lateral dark dots present on abdomen (Fig. 4D) *P. luteus*

Acknowledgements

This work was supported by the National Natural Science Foundation of China [Grant Nos. 31750002 and 32070475], funded by the Priority Academic Program Development of the Jiangsu Higher Education Institutions (PAPD), and supported by key projects of the science-technology basic condition platform of the Ministry of Science and Technology of the People's Republic of China [Grant No. 2005DKA21402]. It is also a part of the Project of Biological Resources Survey in Wuyishan National Park.

References

- Bae YJ (1997) A historical review of Ephemeroptera systematics in northeast Asia. In: Landolt P, Sartori M (Eds) Ephemeroptera & Plecoptera: Biology - Ecology - Systematics. Mauron + Tinguely & Lachat SA, Moncor, Fribourg, Switzerland, 405–417.
- Bae YJ, McCafferty WP (1991) Phylogenetic Systematics of the Potamanthidae (Ephemeroptera). Transactions of the American Entomological Society 117(3–4): 1–143.
- Bauernfeind E, Soldán T (2012) The Mayflies of Europe (Ephemeroptera). Apollo Books, Ollerup, 781 pp. <https://doi.org/10.1163/9789004260887>
- Burmeister H (1839) Handbuch der Entomologie. Fam. Ephemerina, 788–804.
- Curtis J (1834) Descriptions of some nondescript British Species of May-flies of Anglers. London and Edinburgh Philosophical Magazine and Journal of Science (3) 4(20): 120–125. <https://doi.org/10.1080/14786443408648276>
- Eaton AE (1871) A monograph on the Ephemeridae. Transactions of the Entomological Society of London, 164 pp.
- Eaton AE (1881) An announcement of new genera of the Ephemeridae. Entomologist's Monthly Magazine 17: 191–197.
- Eaton AE (1883–1888) A revisional monograph of recent Ephemeridae or mayflies. Transactions of the Linnean Society of London (2) 3: 1–352. [pl. 1–65] <https://doi.org/10.1111/j.1096-3642.1883.tb01550a.x>
- Fourcroy AF de (1785) Entomologia Parisiensis. Paris, Vol. 1–2.
- Han N, Zhang M, Zhou CF (2021) The Genus *Rhoenanthus* Eaton, 1881 in China with the re-description of *R. hunanensis* You & Gui, 1995 (Ephemeroptera: Potamanthidae). Zootaxa 4903(4): 563–577. <https://doi.org/10.11646/zootaxa.4903.4.5>
- Imanishi K (1940) Ephemeroptera of Manchoukuo, Inner Mongolia, and Chosen. Report of the Limnological Society of Kwantung and Manchoukuo, Darien, 169–263. [In Japanese]
- Ishiwata SI (2001) A checklist of Japanese Ephemeroptera. In: Bae YJ (Ed.) The 21st Century and Aquatic Entomology in East Asia. The Korean Society of Aquatic Entomology, Korea, 55–84.
- Joly N, Joly E (1876) Contributions à l'histoire naturelle et à l'anatomie des Ephémérides. Revue de l'Académie des Sciences 5: 305–330.
- Kluge NJ (2004) The phylogenetic system of Ephemeroptera. Kluwer Academic Publishers, Dordrecht, 442 pp. <https://doi.org/10.1007/978-94-007-0872-3>

- Kwanboon S, Sartori M, Boonsoong B (2021) Behningiidae and Potamanthidae (Insecta, Ephemeroptera) in Thailand. *ZooKeys* 1067: 57–82. <https://doi.org/10.3897/zookeys.1067.72779>
- Li WJ, Zhou CF (2022) The first description of the nymph of *Potamanthodes macrophthalmus* You, 1984 and reinstatements of the genera *Potamanthodes* Ulmer, 1920 and *Stygifloris* Bae, McCafferty and Edmunds, 1990 (Ephemeroptera: Potamanthidae). *Aquatic Insects*. <https://doi.org/10.1080/01650424.2022.2074043>
- Linnaeus C (1767) *Systema naturae*, Tom. I. Pars II. Editio duodecima, reformata. Holmiae. (Laurentii Salvii), 533–1327.
- Pictet FJ (1843) *Histoire naturelle générale et particulière des Insectes Névroptères—Famille des Ephemerines*. Baillière édit., Paris: Kessmann et Cherbuliez édit., aussi à Genève, 319 pp. <https://doi.org/10.5962/bhl.title.48625>
- Quan YT, Bae YJ, Jung JC, Lee JW (2002) Ephemeroptera (Insecta) fauna of Northeast China. *Insecta Koreana* 19(3, 4): 241–269.
- Rambur P (1842) *Historire naturelle des Insectes. Névroptères*. Librairie Encyclopédique de Roret, Paris, 298.
- Walker F (1853) List of the specimens of neuropterous insects in the collection of the British Museum, Part III (Termitidae – Ephemeridae): 533–585.
- Wu XY (1987a) A new generic record of the Chinese Potamanthidae – *Potamanthus* Pictet. *Acta Zootaxonomica Sinica* 12(3): 336. [In Chinese]
- Wu XY (1987b) A new species of genus *Potamanthus* (Ephemeroptera: Potamanthidae) from China. *Acta Zootaxonomica Sinica* 12(3): 421–423. [In Chinese]
- Wu XY, Xu XH, Zhang MY (1991) Observation on the chorion structure of three species of mayfly by scanning electron microscope. *Journal of Nanjing Normal University* 14(4): 110–113. [In Chinese]
- You DS, Gui H (1995) *Ephemeroptera*. Science Press, Beijing, 152 pp. [In Chinese]
- Zhou CF (2013) A species list of Chinese mayflies (Insecta: Ephemeroptera). *Inland Waters Biology*, (Proc. 1st Symp. BSA), 6: 167–225.
- Zhou CF, Su CR, Gui H (2015) *Outline of Chinese mayflies*. Science Press, Beijing, 310 pp. [In Chinese]

Corrigendum: Nozaki T, Maruyama M (2022) Taxonomy of *Homoeusa* Kraatz, 1856 (Coleoptera, Staphylinidae) from the East Palearctic: I. *Homoeusa* *rufescens* (Sharp, 1874) and a new allied species. ZooKeys 1121: 39–58. [https://doi.org/10.3897/ zookeys.1121.85489](https://doi.org/10.3897/zookeys.1121.85489)

Tsubasa Nozaki^{1,2}, Munetoshi Maruyama²

1 Entomological Laboratory, Graduate School of Bioresource and Bioenvironmental Sciences, Kyushu University, Fukuoka 819-0395, Japan **2** The Kyushu University Museum, Fukuoka 812-8581, Japan

Corresponding author: Tsubasa Nozaki (dosanko.lathrobium@gmail.com)

Academic editor: Pavel Stoev | Received 16 September 2022 | Accepted 1 October 2022 | Published 26 October 2022

<https://zoobank.org/E3A88DF6-6DB6-4435-9988-ED134D515FF9>

Citation: Nozaki T, Maruyama M (2022) Corrigendum: Nozaki T, Maruyama M (2022) Taxonomy of *Homoeusa* Kraatz, 1856 (Coleoptera, Staphylinidae) from the East Palearctic: I. *Homoeusa rufescens* (Sharp, 1874) and a new allied species. ZooKeys 1121: 39–58. <https://doi.org/10.3897/zookeys.1121.85489>. ZooKeys 1125: 207–208. <https://doi.org/10.3897/zookeys.1125.94925>

We recently published the description of a new rove beetle species *Homoeusa ovata* (Nozaki and Maruyama 2022). However, no holotype depository is indicated in the paper. This is mandatory after 1999 according to the current International Code of Zoological Nomenclature, and the new species name would be a nomen nudum and unavailable (ICZN 1999: Art. 16.4.2). In this corrigendum, we indicate the holotype depository and its etymology, which we did not include in the original paper. We thank Dr. Alfred F. Newton (Field Museum of Natural History, Chicago) for kindly pointing out this error.

***Homoeusa ovata* Nozaki & Maruyama, sp. nov.**

Type material. *Holotype.* “Mt. Maruyama / Sapporo-shi / <Hokkaido, JAPAN> / 6. VI. 1988 / M. Maruyama leg. / trail of ants” (*LFcfF*). ***Paratypes.*** See, Nozaki and Maruyama (2022).

Type depository. The holotype is deposited at the Kyushu University Museum, Fukuoka, Japan.

Etymology. The specific epithet *ovata* refers to the oval body shape of this new species.

References

- Nozaki T, Maruyama M (2022) Taxonomy of *Homoeusa* Kraatz, 1856 (Coleoptera, Staphylinidae) from the East Palearctic: I. *Homoeusa rufescens* (Sharp, 1874) and a new allied species. ZooKeys 1121: 39–58. <https://zookeys.pensoft.net/article/85489/download/pdf/>
- ICZN [International Commission on Zoological Nomenclature] (1999) International Code of Zoological Nomenclature, Fourth Edition. The International Trust for Zoological Nomenclature, London, 306 pp. <https://www.iczn.org/the-code/the-code-online/>